Brain network characteristics of pain: a network-based statistics and graph theory-based EEG analysis in healthy individuals and chronic pain patients

Wenxin Su

A thesis submitted for the degree of

Doctor of Philosophy

Department of Psychology

University of Essex

January 2026

Abstract

Traditional pain neuroimaging research has predominantly focused on regional brain activation, while emerging evidence indicates that pain perception and chronification are mediated by dynamic interactions across large-scale brain networks. Electroencephalography (EEG) is ideal for studying these interactions, yet existing studies show inconsistent findings due to lack of methodological rigour and unified framework linking experimental to clinical pain.

This thesis employs network-based statistics and graph theory to characterise the brain network organisation of pain and further validates translational applicability via machine learning. Using the debiased weighted phase lag index (dwPLI, a functional connectivity measure resistant to volume conduction artefacts) alongside multi-layer graph construction, this thesis addresses methodological discrepancies (absolute vs. relative comparisons; eyes-open/EO vs. eyes-closed/EC states) and investigates alpha-band reorganisation. Three studies are presented: (1) tonic experimental pain in healthy volunteers; (2) short-term neuroplasticity reflected by resting-state reconfigurations pre-/post-sensory stimulation; and (3) resting-state EEG dynamics between chronic pain (CP) patients and healthy controls (HC).

Global network inferences (GNIs) revealed a continuum of pain-related network reorganisation. Tonic pain shifted brain networks from segregation to adaptive integration, whereas post-stimulation rest facilitated segregation, reflecting adaptive neural plasticity. In contrast, CP was characterised by a maladaptive signature of increased integration and diminished small-worldness,

which was driven primarily by the chronic back pain subgroup. Crucially, this core signature was consistent across EO and EC states. The support vector machine classifier demonstrated the high diagnostic potential of GNIs, with classification performance yielding AUC-ROC values of 0.94 (tonic pain), 0.88 (pre-/post-stimulation), and 0.91 (CP vs. HC). Methodologically, integrating absolute and relative comparison methods with multimodal EO/EC protocols was found to optimise biomarker detection.

Overall, this thesis fosters the methodological identification and validation of GNI-based biomarkers that bridge experimental and clinical pain, establishing a network-based framework for understanding pain chronification and providing a foundation for objective subtype-specific pain diagnostics.

Acknowledgements

First and foremost, I would like to express my deepest gratitude to my supervisors, Dr. Elia Valentini from the Department of Psychology and Centre for Brain Science, and Dr. Chris G. Antonopoulos from the School of Mathematics, Statistics and Actuarial Science. Your outstanding patience, support, guidance, and understanding made my PhD journey full of possibility and joy, despite the challenges of pursuing an interdisciplinary project, especially during the global pandemic, my intermission, and the difficult period of my wrist injury. It has been a true pleasure to work under your careful supervision, and your sense of responsibility and kindness have profoundly influenced me as an academic researcher.

This thesis is dedicated to my beloved parents, Mrs. Hua Li and Mr. Gesheng Su. Their unconditional support and care, particularly during my times of greatest need, have been a constant source of courage and strength, and the solid foundation that has enabled me to explore and venture into the world with confidence. I would also like to specially thank my financial sponsor, Mrs. Yueqin Su, and her family. Thank you for your belief in my research. Although you are not here to see this day, helping people with neurological conditions like yours has always been the driving goal of my work. I am also grateful to all my relatives and friends who have supported me throughout my studies, thank you for believing in my potential and offering tangible help along the way.

Moreover, I feel incredibly fortunate to have met so many friends during my PhD who offered friendship and support. My sincere thanks go to Yiyuan

Han, Xiaoming Jiang, Yiwen Wu, Jiacheng Zhu, Huaizhi Zhang, Xuqi Zhu, and Dashuai Pei. I am especially grateful for your helping hands whenever I needed assistance. I owe particular thanks to my roommate, Amulya Hans, for the mutual support and encouragement we shared during unexpected incidents, and for caring for me when I was injured. I will always cherish our breakfasts together, starting each day with heartfelt conversation and delicious, culturally diverse food.

I am also deeply thankful for the constant companionship of my dearest friends and companions: Xiao Bai, Jingyi Cai, Tian Chong, Du Du, Yuqing Hou, Xuan Luo, Wanyi Liu, Weiwei Peng, Biyuan Wang, Haorong Zhang, Sizhuo Zhang, Lili Zhou, Barbara Runjić, and Cléa Rivera-Formaz. Thank you for your unwavering support and encouragement, for making me feel accepted and understood no matter the time or place, and for giving me the freedom and confidence to make my own decisions. I look forward to reuniting with you anywhere in the world. Finally, thank you to Jojo, though our nighttime adventures have ended, I hope we will both welcome brighter sunrises ahead. A special mention goes to the cats who came into my life: Duomi, who arrived confidently, and Fuxing, who chose me. Thank you for keeping me company through countless sleepless nights and for always offering enduring patience and trust, even when I disturbed you seeking comfort.

I would also like to extend special thanks to Karen Johnson and Trudi Day, who served as Psychology Postgraduate Research Administrators. They provided clear guidance and warm assistance when I needed it most, handled my documents with great care, and always responded to my inquiries promptly and efficiently. My gratitude also goes to my Panel Chair members, Rick

O'Gorman and Helge Gillmeister, for supporting my decisions and offering constructive feedback and understanding. I am deeply grateful for the scholarship from the University of Essex's Department of Psychology, which made this doctoral work possible.

I also wish to thank all members of Zhanglab and Dr. Jiayi Zhang from the Institutes of Brain Science at Fudan University, for giving me the opportunity to witness firsthand a successful model of interdisciplinary research and the exemplary role of an outstanding female researcher. It was a privilege to engage in cross-disciplinary exploration and practice with all of you.

I would like to express my sincere gratitude to the members of the ‘Pain and Empathy Neuroscientists’ WeChat group for their stimulating intellectual discussions and the Pain Publication Round starting from 2021, which created an empathetic environment for discussing pain-related research. The monthly sharing sessions have been deeply enlightening on my academic path.

In closing, I have never regretted embarking on this journey to explore the neuroscience of pain. I do not view any part of it as a detour; rather, every experience has been a treasure. Having lived through the pandemic, witnessed the suffering of illness in loved ones, and endured a nearly year-long chronic wrist injury myself, I have come to a deeper understanding: chronic pain is not merely a physical ailment, but a condition that carries profound implications for the brain, fostering catastrophizing, fear, anxiety, and depression. These personal experiences strengthen my hope that my research will contribute to alleviating such suffering in the future, foster a better understanding of pain, and help others live colourfully with it.

Table of Contents

List of abbreviations

Abs	Absolute comparison
ANOVA	Analysis of Variance
AR	Autoregressive
ARMA	Autoregressive moving-average
AUC-ROC	Area Under the Receiver Operating Characteristic Curve
CBP	Chronic Back Pain
Comp	Comparison
Cont	Control
CP	Chronic pain patients
CTC	Communication-Through-Coherence
Default	Default mode network
DorsAttn	Dorsal Attention
dwPLI	debiased weighted Phase Lag Index
Ebc	Edge betweenness centrality
EC	Eyes-Closed
EC-post	EC post-stimulation
EC-pre	EC pre-stimulation
EEG	Electroencephalography
EO	Eyes-Open
EO-post	EO post-stimulation
EO-pre	EO pre-stimulation
ERD	Event-Related Desynchronization

FDR	False Discover Rate
fMRI	functional Magnetic Resonance Imaging
GABAergic	Gamma-Aminobutyric acid–ergic
Gcc	Global clustering coefficient
Geff	Global efficiency
GNIs	Global network inferences
HC	Healthy controls
IASP	The International Association for the Study of Pain
ICA	Independent Component Analysis
KPSS	Kwiatkowski–Phillips–Schmidt–Schin
Lcc	Local clustering coefficient
MA	Moving-Average
MEG	Magnetoencephalography
MNI	Montreal Neurological Institute
Mod	Modularity
NBS	Network-Based Statistic
PAF	Peak Alpha Frequency
PCS	Pain Catastrophising Scale
PLV	Phase-Locking Value
PP	Phillips-Perron
PS	Pain Supersystem
Rel	Relative comparison
SalVentAttn	Salience-Ventral Attention
SomMot	Somato-motor

STAI	State-Trait Anxiety Inventory
Stim	Stimulus
SVM	Support Vector Machine
Sw	Small-worldness
tACS	transcranial Alternating Current Stimulation
ToPS	Tonic Pain Signature
TS	Trend Stationary
VAS	Visual Analogue Scale
Vis	Visual
wPLI	weighted Phase Lag Index

Chapter 1

General introduction

This chapter introduces the background and primary objectives of this research programme. It critically reviews the current landscape of chronic pain biomarker research, highlighting the promise of EEG and network neuroscience approaches while also delineating the specific methodological gaps that this thesis seeks to address. Furthermore, the foundational methodology, centred on graph theory and functional connectivity analysis of EEG data, is explained. Finally, the chapter presents the specific research questions derived from this review and provides an outline of the subsequent chapters to illustrate the structure of the empirical investigations.

1.1. Background and theoretical framework

Chronic pain is a significant public health issue, affecting over 30% of the global population (S. P. Cohen et al., 2021). Its burden is significant, encompassing not only personal suffering and diminished quality of life but also substantial socioeconomic costs through healthcare expenditure and productivity loss (Phillips, 2009). The International Association for the Study of Pain (IASP) defines chronic pain as "an unpleasant sensory and emotional experience associated with, or resembling that associated with, actual or potential tissue damage" (Raja et al., 2020). This definition underscores its dual nature as both a sensory and an emotional phenomenon, a complexity that is central to the chronic pain experience.

Converging evidence from neuroimaging and neurophysiology has firmly established the central role of the brain in the development, maintenance, and perception of chronic pain (Kucyi & Davis, 2015; Ploner et al., 2017). This recognition has catalysed the search for brain-based biomarkers, which hold the promise of revolutionising clinical practice. Such biomarkers could offer objective measures to inform diagnosis, guide personalised treatment decisions, track disease progression, and serve as robust endpoints in clinical trials (Davis et al., 2020; Tracey et al., 2019; Woo & Wager, 2015). Indeed, a growing body of research has identified various potential brain signatures of both experimental and chronic pain, with profound implications for both basic science and clinical applications (Bott et al., 2025; Eldabe et al., 2022; Tu et al., 2021; Zebhauser et al., 2023).

Despite this promise, the translation of these findings into clinically useful tools has been markedly limited. The identification of consistent, reliable biomarkers for chronic pain is fraught with challenges. A primary obstacle is the heavy reliance on subjective self-report, which is inherently variable and can be influenced by a multitude of psychological and contextual factors. Furthermore, the heterogeneity of chronic pain conditions, coupled with the involvement of multiple, distributed brain networks, complicates the identification of a unified brain signature (Eldabe et al., 2022; Van Der Miesen et al., 2019).

A significant methodological shortcoming lies in the experimental model of pain. Frequently, pain biomarkers are derived from studies of healthy individuals exposed to transient, phasic pain stimuli (e.g., brief thermal or mechanical stimuli) that are physiologically and phenomenologically detached from the persistent, complex nature of clinical chronic pain (Vigotsky et al., 2024). Consequently, there is a critical need to identify general biomarkers that bridge the translational divide between well-controlled experimental pain models and the lived experience of clinical pain populations.

Moreover, even within experimental paradigms, significant confounding variables are often inadequately controlled. For instance, the salience or unexpectedness of a stimulus is rarely disentangled from the pure nociceptive response (Hu & Iannetti, 2016; Iannetti et al., 2008). Therefore, the field requires active control conditions that match cognitive demand without inducing pain, enabling the dissociation of pain-specific effects from task-related processes (Seminowicz & Davis, 2007; K. Wang et al., 2021).

Compounding these issues is the inherent difficulty of modelling chronic pain in human experimental settings. Chronic pain persists for months or years,

a timescale that cannot be feasibly or ethically replicated in the laboratory. Furthermore, chronic pain is frequently accompanied by psychological comorbidities such as depression, anxiety, and catastrophising, which alter brain function and structure. This complex pathophysiology cannot be expected in healthy control participants, thereby limiting the generalisability of findings from experimental models in healthy volunteers.

In light of these challenges, this thesis seeks to advance the understanding of the brain's role in chronic pain by addressing specific methodological gaps in the current literature. Through a series of interconnected studies, we aim to identify brain signatures that are generalisable across both experimental and clinical chronic pain states by developing and validating novel electroencephalography (EEG)-based brain network characteristics within a generalisable framework of pain-related network dynamics.

It is hypothesised that a more nuanced, network-based approach to studying brain activity will pave the way for more robust and clinically relevant biomarkers. Ultimately, a refined understanding of the neural underpinnings of chronic pain is a critical prerequisite for developing novel, effective approaches for its diagnosis, prediction, and treatment.

1.1.1. Pain-related brain organisation

Converging evidence from neuroimaging confirms that chronic pain is a disorder of brain networks, characterised by widespread structural and functional alterations (Apkarian et al., 2011; Bak et al., 2021; Baliki & Apkarian, 2015). The perception of pain activates a distributed set of brain regions, including the primary and secondary somatosensory cortices, insula, and anterior cingulate cortex, often collectively termed the "pain matrix" (Apkarian et al.,

2005). However, this so-called "pain matrix" is not pain-specific. Functional magnetic resonance imaging (fMRI) studies have shown that it can be activated in pain-free individuals (Salomons et al., 2016) as well as in healthy participants by salient stimuli from other sensory modalities (Hu & Iannetti, 2016; Iannetti & Mouraux, 2010; Mouraux et al., 2011). Specifically, the activation pattens of such nociceptive stimuli were largely overlapping with other sensory stimuli, such as non-nociceptive somatosensory, visual, and auditory ones (Mouraux et al., 2011).

Although lacking specificity, this term highlights the distributed, large-scale brain activation pattern that integrates across regions supporting somatosensation, affect, cognition, and attention during pain processing. This shift towards understanding pain through functional connectivity and global network properties has led to concepts such as the "dynamic pain connectome" (Kucyi & Davis, 2015, 2017), emphasising the spatiotemporal dynamics of pain-attention interactions. Additionally, a growing literature characterises chronic pain through alterations in functional connectivity and network topology (Baliki & Apkarian, 2015; Farmer et al., 2012; Huang et al., 2019; Kuner & Flor, 2017).

A broader conceptualisation, the "pain supersystem" (PS), proposes that nociceptive-related systems become increasingly integrated with brain regions important for attention, consciousness, memory, and affect (Zheng et al., 2020). The PS demonstrates that noxious heat induces reorganisation characterised by increased somatosensory network connectivity with frontoparietal, ventral attention, basal ganglia, and brainstem regions. Conversely, innocuous stimulation maintains organisation resembling resting-state conditions, indicating minimal network reconfiguration.

The emergence of the PS has been further validated in studies involving both healthy participants under sustained pain and individuals with chronic pain (Lee et al., 2021). This research utilising capsaicin-induced pain models demonstrates that somatomotor-dominant functional communities expand by incorporating subcortical and frontoparietal regions. This reconfiguration forms a distinct pattern of dynamic connectivity, termed the Tonic Pain Signature (ToPS). Crucially, the ToPS not only predicts subjective pain intensity in experimental settings but also successfully forecasts ongoing clinical pain in chronic pain patients and differentiates them from healthy controls. These findings illuminate the significant translational potential of tonic pain paradigms, revealing a common neural substrate that bridges transient experimental stimuli and the persistent experience of chronic pain (Ploner & Tiemann, 2021).

In summary, pain-evoked reorganisation occurs across large-scale connectivity and involves dynamic interaction between multiple brain networks (Lee et al., 2022; Mano & Seymour, 2015). Although such reorganisation has been proposed as a bridge between tonic experimental and chronic pain, detailed characterisation remains incomplete, particularly using modalities beyond fMRI. Furthermore, to quantify network-level communication more precisely, more advanced methodology must be adopted, particularly from network neuroscience (Avena-Koenigsberger et al., 2018; Barabási et al., 2023).

1.1.2. Brain organisation from a graph-theoretical perspective

Graph theory provides a powerful framework to quantify such brain network organisation. Nodes represent brain regions, and edges reflect functional connectivity, allowing computation of global network inferences (GNIs) to quantify graph properties which capture the balance between segregation (e.g.,

global clustering coefficient, Gcc) and integration (e.g., global efficiency, Geff) in brain function (Bullmore & Sporns, 2009; Sporns, 2013). In particular, the brain network represents complex properties, such as small-worldness (Sw), modularity (Mod) and highly connected hubs, which are of high relevance to its function. These graph-theory-based measurements assess global and local information transmission as well as the properties of individual nodes, clarifying the inter-relationships between different brain regions and highlighting key pain-related networks and core targets.

Studies of the PS have revealed a reduction in Sw and increased Gcc. Moreover, network hubs were reorganised (“hub disruption”), with a greater proportion of hubs located within the PS and a shift from “connector” hubs linking disparate networks to “provincial” hubs connecting regions primarily within the PS. Multicentre research on chronic pain patients (Mano et al., 2018) also supports several global network changes in chronic low back pain patients, including reduced Gcc and betweenness centrality (the incidence of “connector nodes” that link multiple networks). Together, these pain-related connectivity studies point to increased integration within large-scale functional networks and cross-talk among networks, alongside reduced functional specialisation in chronic pain.

However, a systematic review indicated that while GNI differences exist between chronic pain patients and healthy controls, the overall findings remain mixed (Lenoir et al., 2021). Some fMRI studies have reported increased Gcc and reduced Sw and Mod in chronic pain patients (Huang et al., 2019; Qi et al., 2016) and in healthy participants responding to sustained noxious stimuli (Zheng et al., 2020). In contrast, chronic low back pain patients exhibited

decreased Gcc (Mano et al., 2018). Decreased Sw, along with declined Geff, has also been summarised in a review of neuropathic pain studies (Xin et al., 2024).

While fMRI studies have provided a rich but mixed set of results from a graph-theoretical perspective, corresponding EEG studies are rare and have also yielded controversial or negative findings (Pinheiro et al., 2016; Zebhauser et al., 2023). One cross-sectional study found a decrease in Geff in gamma frequencies in patients with chronic pain compared with healthy controls (Ta Dinh et al., 2019). In a longitudinal study examining changes in brain activity following multimodal pain therapy, a correlation between pain decrease and an increase in theta band Geff was observed (Heitmann et al., 2022). Inconsistencies are also present in experimental EEG studies using different connectivity measures; for instance, even within the same dataset, no significant Gcc or Geff differences were observed when using phase-locking value, whereas significant Gcc increases during pain emerged using the debiased weighted phase lag index (dwPLI) (Nickel et al., 2020).

In summary, while graph-theoretical approaches have revealed promising but inconsistent findings across imaging technologies, there is a clear need for systematic investigation using refined EEG-based network metrics capable of capturing pain-related network dynamics.

1.1.3. EEG biomarkers in chronic pain

EEG presents a particularly appealing modality for establishing chronic pain biomarkers due to its safety, cost-effectiveness, broad availability, and potential for mobile application (Chen, 2021; J. A. Kim & Davis, 2021). Furthermore, an EEG-based marker could not only aid in diagnosis and classification

but might also serve as a direct target for novel therapeutic strategies, such as neurofeedback (Sitaram et al., 2017) or non-invasive brain stimulation techniques (Polanía et al., 2018).

Research has explored various EEG features for this purpose, including evoked responses, spontaneous oscillations, and functional connectivity (Ploner & May, 2018). A systematic review summarised 18 studies that recorded neural responses evoked by nociceptive stimuli in patients with various types of chronic pain (Lenoir et al., 2020). The authors found that abnormalities were primarily observed only in conditions with concomitant thin-fibre dysfunction, such as certain neuropathic pain syndromes and fibromyalgia, and most revealed no significant differences in the latency or amplitude of pain-evoked potentials (e.g., N2/P2 waves) in chronic pain patients compared to healthy controls.

Investigations into spontaneous oscillatory activity during resting-states have also yielded mixed results (Zebhauser et al., 2023). Spectral analysis has proposed several candidates, including frequency band-specific power and peak alpha frequency. For instance, some studies report that chronic pain is associated with higher theta and beta band power (Zebhauser et al., 2023), while others find decreased alpha and beta connectivity in conditions like migraine (Zebhauser et al., 2024). In neuropathic pain, findings include increased theta power, decreased alpha and beta power, and a slowing of the dominant peak alpha frequency (Mussigmann et al., 2022). Slower peak alpha frequency (PAF) has also been reported in patients with widespread pain (Cavaleri et al., 2025),and pancreatitis (Vries et al., 2013). However, these associations are not universal, with some studies reporting no significant differences, underscoring

the profound heterogeneity of chronic pain conditions and the challenge of identifying a unified signature (Zebhauser et al., 2023).

Measures of functional connectivity may offer a more promising avenue than local activity alone, as they are better positioned to capture the distributed network dysfunction that characterises chronic pain (Bott et al., 2025). This is supported by evidence that contextual influences on pain relate more to inter-regional communication than to local brain activity. In chronic neuropathic pain patients, reduced connectivity has been observed between key nodes like the dorsal anterior cingulate and somatosensory cortex (Vanneste & De Ridder, 2021). A large-scale machine learning study achieved above-chance classification of chronic pain patients based primarily on increased frontal theta and gamma connectivity (Ta Dinh et al., 2019). Furthermore, graph theory approaches applied to EEG data have shown that changes in global network efficiency at theta frequencies are associated with chronic pain and can be modulated by successful therapy, even in the absence of spectral power changes (Heitmann et al., 2022).

In summary, the development of EEG-based biomarkers for chronic pain is marked by high heterogeneity. This variability stems not only from the diversity of EEG features and analytical approaches but also from the inherent pathophysiological complexity and variability of chronic pain conditions themselves. This inconsistency highlights the need for more standardised methodologies and a focus on network-level properties that may provide a more robust and generalisable foundation for biomarker discovery.

1.1.4. EEG signatures in experimental tonic pain

The sustained nature of tonic pain makes it a valuable experimental model for studying the prolonged neural processing involved in chronic pain. EEG studies consistently highlight the involvement of alpha-band oscillations in tonic pain, characterised by a suppression of local power and a reorganisation of long-range connectivity (Ploner et al., 2017).

During sustained heat pain, alpha power in sensorimotor areas is suppressed (Peng et al., 2014; Ploner et al., 2017), a phenomenon known as alpha event-related desynchronization (ERD). This suppression is thought to originate from the sensorimotor cortex (Dowman et al., 2008; H. Wang et al., 2023), and often correlates negatively with subjective pain ratings (Nir et al., 2012; Peng et al., 2015). Concurrently, phase-based alpha connectivity between the sensorimotor cortex and medial prefrontal cortex increases (Nickel et al., 2020). The alpha ERD over somatomotor areas contralateral to stimulation site is thought to reflect the translation of sustained nociception into conscious pain perception. Notably, pre- and post-stimulus alpha activity influences subjective pain perception (May et al., 2012; Tu et al., 2016).

Beyond oscillatory power, functional connectivity between distributed brain areas is also altered during tonic pain. For instance, alpha-band functional connectivity in frontoparietal and frontotemporal networks has been identified as crucial for distinguishing different pain levels (Modares-Haghighi et al., 2021). Research has also explored individual differences in pain sensitivity. Individuals with high pain sensitivity have been shown to exhibit a slower central PAF in both pain-free and tonic pain states compared to those with low sensitivity (Furman et al., 2018). Building on this, Furman and colleagues (Furman et al., 2020)

demonstrated that pain-free PAF predicted individual pain sensitivity over clinically relevant timescales (weeks) and could reliably identify the most pain-sensitive participants across independent datasets. These findings suggest that resting-state PAF may serve as a trait-like biomarker of inherent pain sensitivity.

However, the validation of PAF as a robust biomarker requires cautious interpretation since inconsistencies have emerged across studies. For example, work using hot-water immersion paradigms reported that changes in PAF were not specific to pain and did not mediate the relationship between stimulus intensity and affective pain experience (Valentini et al., 2022, 2024). Such discrepancies underscore the need for rigorous methodological control, standardised analytical pipelines, and replication across research groups. They also suggest that PAF may not exert a simple or causal role in acute pain perception in healthy populations.

Extending these findings to a network level, graph theory provides a framework for quantifying large-scale reorganisation. Although evidence for consistent network-level changes in tonic pain remains limited (L. B. Zhang et al., 2024), the translational potential is significant. For instance, classification analyses combining GNIs from alpha-band EEG have achieved up to 92% accuracy in differentiating pain and no-pain states (Modares-Haghighi et al., 2021). This promising potential, however, is tempered by significant methodological sensitivities. Research demonstrates that the detection of network changes can be critically dependent on the choice of connectivity metric. In one study using the same EEG dataset, tonic heat pain did not yield significant differences in Gcc or Geff when using the phase-locking value (PLV). In contrast, a significant increase in Gcc during pain was identified when the same analysis was

conducted with the dwPLI. Furthermore, the network alterations that were observed showed notable lateralisation, for example, an increase in Sw was found exclusively in response to left-sided stimulation, with no equivalent effect on the right (Nickel et al., 2020).

In summary, tonic pain paradigms offer a functional bridge between experimental and clinical pain research by capturing sustained pain-related neural dynamics. EEG studies highlight alpha oscillations and their network reorganisation as promising candidates for tonic pain biomarkers, providing insights into both state-dependent pain processing and trait-like pain susceptibility. Future research should aim to achieve a comprehensive understanding of large-scale network reorganisation while validating these emerging biomarkers through rigorous and reproducible methodologies.

1.2. Research framework and methodological approach

Based on the previous findings, the aim of our research is to conduct a systematic investigation using refined EEG-based functional connectivity metrics capable of capturing pain-related network dynamics, using both connectivity analysis and graph analysis of tonic experimental pain in healthy participants (Study 1), pre- and post-stimulation states in healthy participants (Study 2), and chronic pain patients (Study 3).

A core analytical pipeline was implemented across all three interconnected studies. This pipeline consisted of connectivity analysis and graph analysis, which were used to systematically assess different graph types derived from both brain-wide and higher-order networks. The methodological details are

introduced in Chapter 3 for Study 1, a brief description were applied in Chapter 4 for Study 2 and Chapter 5 for Study 3, but the general methodological choices are briefly discussed below.

Notably, connectivity analysis revealed connectivity patterns for group-level contrasts. In parallel, the graph analysis was performed on individual-level connectivity matrices to compute several network inferences, which were then submitted to group-level statistical testing to identify condition-dependent alterations in graph characteristics. Although these two analytical approaches are methodologically distinct, they provide complementary insights: connectivity analysis highlights condition-contrast connectivity patterns, while graph analysis quantifies the corresponding network-level properties.

Due to the relative thorough understanding of alpha band oscillations and promising related biomarkers suggested in both tonic and chronic pain research, we focused our analytical strategy on the alpha band oscillation. First, we calculated the dwPLI to measure the functional connectivity. The advantage of this connectivity index is its ability to reduce the volume conduction effect on the signal. We then employed graph-theoretical approaches and advanced network-based statistics for connectivity matrices.

To capture network organisation at multiple scales, a multi-level graph analysis from brain-wide graphs to higher-order graphs was constructed. To eliminate the inter-subject variability in baseline neural activity, we used both absolute and relative comparisons for analysis in different contrasts. Finally, we performed a machine learning model to validate the features for their future translation potential.

The overarching research framework has been introduced above. The following subsections will present the specific rationale for each of the core methodological approaches outlined above.

1.2.1. Assessment of functional connectivity

To estimate functional connectivity, we chose to calculate the dwPLI (Ortiz et al., 2012). This index is known for its significant reduction of volume conduction effects (M. X. Cohen, 2014). The dwPLI is a debiased estimator of the squared weighted phase lag index (wPLI) which measures the contribution of phase differences weighted by the magnitude of their imaginary parts (Vinck et al., 2011) as

$$\mathrm{wPLI} = \frac{|\sum\{\Im\{x\}\}|}{\sum\{|\Im\{x\}|\}},$$

where $\Im\{x\}$ denotes the imaginary part of the phase difference between two signals. $|\ \ |$ indicates the absolute value, and $\sum$ stands for summation. wPLI weights the sign of $\Im\{x\}$ by $|\Im\{x\}|$, making the contribution of phase differences with small time lags less significant than those with larger amplitudes in the imaginary axis.

The dwPLI was developed to correct sample-size bias and is more sensitive and capable of detecting subtle phase synchronization to other phase-based connectivity measures (M. X. Cohen, 2014). It is computed by

$$\mathrm{dwPLI} = \frac{|\sum\{\Im\{x\}\}|^2 - \sum \Im\{x\}^2}{\sum\{|\Im\{x\}|\}^2 - \sum \Im\{x\}^2},$$

where $\left|\sum\{\Im\{x\}\}\right|^2$ denotes the square of the sum of the imaginary part of the phase difference between two signals, $\sum\{|\Im\{x\}|\}^2$ is the square of the sum of the absolute values of the imaginary inputs and $\sum \Im\{x\}^2$ is the sum of the

squares of the imaginary inputs. Both wPLI and dwPLI values range from 0 to 1, with higher values indicating greater phase synchronisation.

1.2.2. Multi-level graph construction

The brain-wide graph was constructed in both sensor and source spaces. The source space data were reconstructed into 100 regions of interest of the Schaefer atlas (Schaefer et al., 2018) using an atlas-based beamforming approach via the Discover EEG toolbox. Further analysis based on brain-wide graph for intra- and inter-network connections was conducted in the source space, utilising the 100-region atlas that classifies 7 networks. Intra-network connections for all 7 networks were analysed. Intra-network analysis was focused on the SomMot for the tonic pain study, and Default for the resting-states based studies. Additionally, inter-network connections were evaluated using weighted matrices, utilising NBS and graph theory.

It is worth noting that segregation in brain-wide and intra-network graphs reflects functional specialisation within a given graph, whereas integration characterises global information flow. However, when within-network connectivity is excluded, the local network inferences derived from higher-order inter-network graphs represent dynamics related to interaction with other networks. In this context, GNIs primarily capture inter-network communication.

1.2.3. Connectivity analysis using network-based statistics

Connectivity analysis was performed using the Network-Based Statistic (NBS) toolbox (Zalesky et al., 2010, 2012) to identify significant differences in brain connectivity between conditions. NBS, a non-parametric statistical approach, employs cluster-based analysis while controlling for family-wise error

rate (Zalesky et al., 2012). To capture differences in connectivity patterns between conditions, we applied the NBS tests within each comparison method to preserve spatial information of connectivity distribution. A one-sided paired-sample t-test with 5,000 permutations was used, with a significance level of 0.05. Connections that survived the permutation test formed the edges in p-graphs, as illustrated in sensor space results. For connections that were not statistically significant, t-values were visualised as t-graphs. To improve clarity, t-graphs displayed connections with t-values greater than the threshold (dependent on the critical t-value for a one-sided paired-sample t-test at 0.05 significance level by the df for each analysis) in the source space. For intra-network and inter-network comparisons, and for edge betweenness centrality (Ebc), t-graphs included connections with positive t-values ($t > 0$).

1.2.4. Graph analysis based on graph theory

Graph analysis based on graph theory consisted of 4 GNIs in graphs of this research: global clustering coefficient (Gcc), global efficiency (Geff), small-worldness (Sw), and modularity (Mod). Gcc is one of the best-known indicators of functional segregation, quantified as the average clustering coefficient of each node in the graph. Clustering coefficients at the node level indicate the fraction of the node's neighbours that are also neighbours of each other (Watts & Strogatz, 1998). A high fraction of triangles in the graph implies functional segregation, reflecting the brain's ability to use densely interconnected regions to sustain specialised brain processes. Geff is a measure of functional integration (Achard & Bullmore, 2007), facilitating the rapid exchange of information across distributed brain regions. It is computed as the average inverse shortest path length, which is the minimum number of edges required to connect any

pair of nodes in a graph (Latora & Marchiori, 2001). Sw describes how a graph is more clustered than random networks with similar characteristic path lengths (Liao et al., 2017; Watts & Strogatz, 1998). It is calculated as the ratio of the clustering coefficient to Geff compared to random networks. Small-world organisation reflects an optimal balance of functional integration and segregation (Sporns & Honey, 2006). Mod quantifies the degree to which a graph can be subdivided into clearly delineated groups (Newman, 2004). Unlike other network-structure measures, Mod relies heavily on optimisation algorithms that subdivides the graph into non-overlapping modules. We used the maximised Mod algorithm (Newman, 2006), which is an accurate and sufficiently fast approach to quantify Mod for smaller networks (Rubinov & Sporns, 2010). Higher Mod values indicate that a network has a stronger community structure, meaning there are dense connections among nodes within the same module (or group) and sparser connections between nodes in different modules. This suggests that the network is more efficiently organised into distinct subgroups, which can enhance functional specialisation and improve resilience to disruptions.

1.2.5. Comparison methods

In this research, we employed both absolute and relative comparison methods throughout the analysis, based on methodological and theoretical considerations rather than as a duplication of analyses.

The use of resting-state baseline normalisation is a well-established methodological approach in neuroimaging research, employed to enhance the detection and interpretation of condition-specific neural dynamics. This technique improves both the specificity and sensitivity of findings. For example,

Alain et al. (2001) demonstrated enhanced specificity by using baseline-referenced analyses to dissociate overlapping activations during pitch and spatial auditory tasks, revealing distinct neural pathways that were otherwise conflated. Similarly, the utility of normalisation for sensitivity is evident in clinical neurophysiology. Feng et al. (2021) showed that a normalised alpha power metric, but not the absolute power, successfully uncovered a significant correlation with clinical pain intensity in patients with chronic low back pain. Together, these examples demonstrate that relative, normalised comparisons are vital for revealing subtle, condition-specific neural associations which absolute measures may obscure, thus supporting our analytical approach.

In the present study, we implemented both absolute and relative analyses for complementary reasons. Absolute measurements of functional connectivity are widely used but can be strongly influenced by inter-subject variability in baseline neural activity. Relative comparisons help to mitigate this variability, thereby unmasking condition-specific network properties that may otherwise be obscured. This dual approach allowed us to examine network dynamics from two perspectives: an absolute measure of overall connectivity strength, and a relative measure that highlights within-subject changes relative to baseline.

Furthermore, implementing both analytical approaches allowed us to evaluate the robustness of our findings across different methodological frameworks. The convergence of patterns across the two approaches increases confidence that the observed effects reflect genuine condition-specific network reorganisation. Although this strategy adds analytical complexity, we believe it

strengthens the methodological rigour of our study and the validity of our conclusions.

1.2.6. Graph thresholding strategies

Our decision to retain weak connections in thresholding strategies may resolve conflicting reports on GNIs such as Gcc (L. Li et al., 2022; Mano et al., 2018; Nickel et al., 2020; Zheng et al., 2020). Arbitrary thresholds, such as retaining only the top 10% of strongest connections or iterating across densities (e.g., 10-30%) and then averaging Gcc values across these arbitrary cutoffs, risk conflating reorganisation of strong, hub-dominated connections and subtler reconfigurations in weak but topologically critical edges. By contrast, our inclusion of weaker connections enables capturing nuanced shifts in network topology. This align with recent evidence that thresholding strategies critically influence neuroimaging outcome (Adamovich et al., 2022), and that weak connections, often dismissed as noise, may underpin cognitive flexibility and network resilience (Santarnecchi et al., 2014).

1.2.7. Machine learning validation

GNIs were selected as features for classification, derived from individual or combined graph types including sensor space, source space, intra-network, and inter-network graphs under both absolute and relative comparison methods. Our feature inclusion was primarily theory-driven rather than performance-optimised, as the goal was to use classification to test the robustness of GNIs as potential biomarkers. We incorporated all GNIs from four graph types because each was hypothesised to capture distinct aspects of brain network organisation that may differentiate responses to hot and warm stimuli. Given the modest

sample size, we deliberately avoided data-driven feature selection methods, which could increase the risk of overfitting and compromise the validity of cross-validation. Instead, we systematically evaluated all possible combinations of the four feature sets and reported the three best-performing combinations. This strategy ensured methodological transparency and reduced the risk of overfitting by avoiding any optimisation on the test set.

To assess the predictive capacity of GNIs in distinguishing tonic pain states (hot vs. warm), we implemented a linear support vector machine (SVM) with L2 regularisation. The regularisation parameter (λ) was automatically optimised within each training fold. Input features (GNIs) were standardised using z-score normalisation based on the training set's mean and standard deviation, and the trained model was used to classify the held-out subject's data.

A leave-one-subject-out cross-validation framework was applied across all participants. For each fold, one subject's data was held out for testing, while the remaining data were used for training and normalisation. Model performance was evaluated using area under the receiver operating characteristic curve (AUC-ROC), and pooled inferences from the confusion matrix, including accuracy, sensitivity, and specificity.

To assess the significance of the classifier's discriminative performance, we conducted a permutation test with 1000 iterations. For each iteration, participant labels were randomly shuffled to disrupt the true feature-label relationship, and the entire cross-validation pipeline was repeated using these permuted labels. The null distribution of AUC-ROC values was generated from these shuffled-label iterations. The empirical p-value was computed as the proportion of permutation AUCs exceeding or matching the original model's AUC.

This approach quantifies the probability that the observed classification performance occurred by chance under the null hypothesis of no true feature-label association.

1.3. Research questions

To deepen the understanding of pain-related brain reorganisation in both tonic pain and chronic pain conditions, we systematically analysed brain-wide graphs, higher-order intra-network, and inter-network graphs. By combining functional connectivity topology with graph-theoretical analyses, we seek to provide insights into the pain-induced brain reorganisation. Given that baseline neural activity normalisation may reduce inter-subject variability, thereby unmasking condition-specific network properties, we also assess its influence by both relative and absolute comparisons. Finally, we explore the predictive utility of GNIs for classifying pain states.

By using these methodologies, we answered the following questions:

Study 1: Experimental tonic pain

Q1-1 Can functional connectivity and network topology differentiate between experimental tonic noxious hot from innocuous warm conditions?

Q1-2 What is the neuronal mechanism, as revealed by our connectivity and graph analyses, underpin these pain-states?

Q1-3 Will the network inferences from graph-theory measurements provide accurate pain-state classification?

Study 2: Resting-state changes following stimulation

Q2-1 How does functional connectivity and network topology change from pre- to post-stimulation resting-states?

Q2-2 Do these time-dependent changes differ between eyes-open and eyes-closed resting-state conditions?

Q2-3 What neuronal mechanisms underpin these post-stimulation changes?

Q2-4 Will the network inferences from graph-theory measurements validate these changes and demonstrate translational potential?

Study 3: Chronic pain patients versus healthy controls

Q3-1 How do functional connectivity and network topology differ in resting-states between chronic pain patients and healthy controls?

Q3-2 Do these group differences vary between eyes-open and eyes-closed resting-state conditions?

Q3-3 What neuronal mechanisms underpin these group differences?

Q3-4 Will the network inferences from graph-theory measurements validate for such group differences and therefore have translational potential?

1.4. Thesis structure

This thesis is structured as follows:

Chapter 1: Introduction

This chapter provides a comprehensive overview of the research background, outlining the central methodology and the series of studies undertaken. A review of the literature on both tonic experimental pain and chronic pain, with a specific focus on EEG-based research, establishes the rationale and motivates the research questions that guide this thesis.

Chapter 2: Methodological preliminaries: stationarity analysis

This chapter presents a preliminary analysis that establishes the methodological foundation for the subsequent studies. It involves stationarity tests conducted on EEG data across various epoch lengths to determine the optimal parameters for the formal connectivity and graph-theoretical analyses.

Chapter 3: Brain reorganisation evoked by tonic thermal pain

This study investigates large-scale brain network reorganisation directly evoked by tonic thermal pain in healthy participants. Using EEG, it characterises the alterations in functional connectivity and graph-theoretical properties that underpin the sustained pain experience.

Chapter 4: The neuroplasticity after sensory stimulation in resting-states

This chapter examines the after-effects of sensory stimulation, including tonic pain. It assesses time-dependent changes in EEG-based resting-state connectivity and network topology, comparing eyes-open and eyes-closed conditions before and after stimulation.

Chapter 5: Resting-state dysfunction in chronic pain

This study addresses differences in resting-state brain dynamics between chronic pain patients and healthy control participants. It aims to identify EEG-based functional connectivity and network signatures that distinguish the two groups during both eyes-open and eyes-closed resting conditions.

Chapter 6: General discussion and conclusion

This final chapter synthesises the main findings and conclusions of the thesis. It discusses the collective implications of the research, acknowledges its limitations, and proposes potential avenues for future research and clinical translation.

1.5. Publication

Su, W., Antonopoulos, C.G., & Valentini, E. (2026). EEG Network Reorganisation Reveals Somato-Motor Transition from Segregation to Integration during Tonic Pain. *PAIN*, 167(5), 1120-1136. DOI: 10.1097/j.pain.0000000000003897. (Chapter 3)

1.6. Declaration of AI tools

For the preparation of this thesis, I acknowledge the use of ChatGPT (OpenAI, https://chatgpt.com/) and DeepSeek (深度求索, https://www.deepseek.com/) to proofread the text and suggest improvements for clarity, and the use of Zotero (Corporation for Digital Scholarship, https://www.zotero.org/) to manage references and generate citations and the bibliography.

Chapter 2

Preliminary analysis: assessing stationarity in EEG signal

A fundamental prerequisite for many time-series analyses is the assumption of stationarity. This is rarely assessed and/or reported in empirical EEG research. This chapter systematically evaluates the stationarity of EEG signals across a range of epoch lengths to identify a duration that ensures statistical reliability for the methodologies employed in the following chapters.

2.1. Stationarity in EEG data

The EEG is one of the most frequently used approaches for exploring the mechanisms of brain functions, especially for its outstanding millisecond temporal resolution (O'Neill et al., 2018). The recorded neural signal represents the results of interactions over a large-scale neuronal population (Buzsáki, 2006). By observing such neural activity in well-designed, repeated experimental conditions, researchers can find stable and reliable characteristics correlated with certain dynamic brain processes (Keitel et al., 2025). The crucial assumption made before such analysis is that the data are stationary (M. X. Cohen, 2014) The stationarity of a time series means its statistical properties, such as mean, variance, frequency, and covariance, remain the same throughout the whole data (Gagniuc, 2017). Stationarity is based on a stochastic process in which the finite dimensional joint distribution function of a time series Z_t is defined as follows:

$$F\ (x_1, x_2, \dots, x_n) = P\ (Z_{t_1} \leq x_1, Z_{t_2} \leq x_2, \dots, Z_{t_n} \leq x_n)$$

Where $X = \{x_1, x_2, \dots, x_n\}$ is a real random variable, and a finite set of integers $T = \{t_1, t_2, \dots, t_n\}$ is called the index set of the process. If $T \in \mathbb{Z}$, the process is called a discrete stochastic process. If $T \in \mathbb{R}$, the process is called a continuous stochastic process.

Strong, or strict, stationarity of Z_t is satisfied only when $(Z_{t_1}, Z_{t_2}, \dots, Z_{t_n})$ and $(Z_{t_{1+h}}, Z_{t_{2+h}}, \dots, Z_{t_{n+h}})$ have the same joint distributions for all integers h and $n > 0$. Where $h \in \mathbb{Z}, n \in \mathbb{N}$. In practical application, weak stationarity is the most frequently assessed, which is satisfied if the mean value

$$E(Z_t) = \mu_z(t) = const = \mu$$

And the autocorrelation is invariant from t and every lag h has a constant covariance value associated with it, which could be presented as:

$$\gamma(h) = Cov(Z_t, Z_{t+h})$$

However, the brain itself is a non-stationary system. Modern research suggested that the neural assemblies of coupling and synchronization might provide manifested explanations of brain activities. Kaplan and colleagues (Kaplan et al., 2005) believe that the basic source of the non-stationarity in the EEG signal is not due to the impact of the external stimuli, but rather a reflection of the inherent switching of neural assemblies during brain function. Therefore, the non-stationarity of the EEG data would inevitably influence the results of statistical analyses that treat the signal as stationary data.

2.2. Non-stationarity detection methods

To detect non-stationarity in a time series, statistical parametric and non-parametric methods, which lead to strong assumptions on decisions related to the stationarity of the data, were developed in the field of econometrics. he definition of stationarity does not limit the way in which the data are generated. Hence, stationarity is a non-parametric concept. However, the widely used stationarity detection methods were primarily developed with parametric stochastic process modelling. There are three models that are most widely addressed: the autoregressive (AR) model (Brockwell & Davis, 2002), the moving-average (MA) model (Tsay, 2005), and the autoregressive moving-average (ARMA) model (Tsay, 2005).

Although all three models are generated by a linear function plus noise, the ARMA model can also deal with non-linearity. Based on their underlying

stochastic process, the formulation of all three models could be written as an autoregressive process of order p,

$$y_t = a_0 + a_1 y_{t-1} + \cdots + a_p y_{t-p} + \varepsilon_t$$

If we consider the root of its characteristic equation by setting its polynomial part equal to 0, we get the equation as:

$$m^p - m^{p-1} a_1 - \cdots - a_p = 0$$

If $m = 1$, then we can regard this process as having a unit root. It means that after differencing d times, the process could be transformed into a weakly stationary process, where d is the multiplicity of a unit root (Bhargava, 1986). On the other hand, the presence of a unit root in the autoregressive model of a given time series proves the process is non-stationary. This is the hypothesis underlying most of the unit root tests for non-stationarity detection. The family of unit root tests has two famous members: the Phillips-Perron (PP) test and the Kwiatkowski-Phillips-Schmidt-Schin (KPSS) test.

2.3. Experimental materials and methods

A secondary dataset (Valentini et al., 2022) was used to conduct stationarity tests. The study included thirty-six healthy participants who underwent sensory stimulation while their EEG was recorded. Three types of sensory stimulation each lasted five minutes were applied. Tonic pain perception was induced by asking participants to place their left hand in hot water at 45 °C. The warm condition followed the same procedure, but with the water temperature set 6 °C lower than the painful condition. A sound condition was also administered, designed to compare unpleasantness with the tonic pain condition, using auditory stimuli.

During each trial, participants were asked to sit comfortably and experience the hot, warm, and sound stimuli separately. They were instructed to rate the unpleasantness of their sensation on a visual analogue scale (VAS) whenever it appeared on the screen in front of them, from 0 (“No unpleasantness”) to 100 (“Intolerable unpleasantness”). The VAS was displayed approximately every 10 seconds, 30 times in total, with each block lasting about 6 minutes.

The EEG data were collected throughout all blocks and pre-processed with a notch filter to exclude the frequency band from 49.5 to 50.5 Hz. A high-pass filter of 0.1 Hz and a low-pass filter of 100 Hz were applied. All data were sampled at 500 Hz and re-referenced to the average of all 62 channels. Artefacts such as eye-blinks and muscle movements were removed using Independent Component Analysis (ICA).

To compare the stationarity of the recorded data, the original data were segmented using two different methods. The first method selected epochs based on the markers indicating the appearance of the VAS. The second method segmented the data based purely on epoch length, without reference to events. For the marker-based epochs, the onset was set at 10 seconds prior to the occurrence of the VAS. Epoch durations of 0.5, 1, 2, 3, 4, 6, and 10 seconds were used for both methods. Consequently, for each participant, there were approximately 30 marker-based epochs per duration. In contrast, the duration-based epochs were segmented from the entire block, resulting in a much larger number of epochs, ranging from approximately 800 (for 0.5s) to 40 (for 10s).

Stationarity was assessed using both the PP and KPSS tests for both segmentation methods. In addition to the traditional autoregressive (AR) model

used in the PP test, a Trend Stationary (TS) model was also performed. The lag values for these tests were determined by taking the square root of the number of data points in each epoch, resulting in lags of 16, 22, 32, 39, 45, 55, and 71. The group-averaged stationarity rate was calculated and reported for each experimental condition separately.

2.4. Analytical results

The results of the stationarity detection for both the marker-based and duration-based epochs are presented in Tables 2.1 and 2.2, respectively.

Table 2.1. Stationarity results for marker-based epochs

Length of epoch (s)	Sug-gested Lag value	Average stationary ratio in PP test (%)						Average stationary ratio in KPSS test (%)		
		AR model			TS model					
		pain	warm	sound	pain	warm	sound	pain	warm	sound
0.5	16	0.87	0.91	0.9	0.04	0.03	0.04	0.71	0.76	0.76
1	22	0.98	0.99	0.99	0.44	0.49	0.5	0.65	0.71	0.7
2	32	0.99	0.99	1	0.87	0.91	0.91	0.96	0.98	0.97
3	39	1	1	1	0.94	0.97	0.97	0.99	0.99	0.99
4	45	1	1	1	0.95	0.95	0.95	0.99	1	0.99
6	55	1	1	1	0.99	0.98	0.98	1	1	1
10	71	1	1	1	1	1	1	1	1	1

Although no statistical comparison with simulated surrogate data was performed, the trend towards increasing stationarity can be clearly observed. For a given epoch length, the stationarity ratios are very similar across all three experimental conditions. As epoch length increases, the proportion of epochs that pass all three stationarity tests also rises. The results indicate that for epoch lengths longer than 2 seconds, the stationarity ratio exceeds 85% across all tests. In general, the PP test with the TS model was the most stringent detection method. The KPSS test and the PP test with the AR model were comparatively

more lenient. When epochs reach 4 seconds in length, their stationarity ratio exceeds 95%.

Table 2.2. Stationarity results for duration-based epochs

Length of trial (s)	Suggested Lag value	Average stationary ratio in PP test (%)						Average stationary ratio in KPSS test (%)		
		AR model			TS model					
		pain	warm	sound	pain	warm	sound	pain	warm	sound
0.5	16	0.88	0.89	0.89	0.03	0.03	0.03	0.73	0.74	0.74
1	22	0.99	0.99	0.99	0.68	0.46	0.7	0.6	0.7	0.63
2	32	0.99	0.99	0.99	0.98	0.9	0.99	0.86	0.98	0.89
3	39	1	1	1	0.99	0.97	0.99	0.97	0.99	0.98
4	45	1	1	0.99	0.99	0.96	0.99	0.99	0.99	0.99
6	55	1	1	1	1	0.99	0.99	0.99	0.99	0.99
10	71	1	1	1	1	1	1	0.99	1	0.99

The same trend is evident in the epochs segmented by duration. For the shortest epochs (0.5 seconds), the lowest stationarity ratio was 0.03%, observed with the PP test using the TS model. The stationarity ratio increases steadily with epoch length and remains above 95% for epochs longer than 3 seconds, regardless of the experimental condition. Furthermore, the stationarity ratios do not differ substantially across the pain, warm, and sound conditions.

2.5. Conclusions

This analysis provides clear, empirical guidance for selecting epoch lengths in EEG studies where stationarity is a key assumption. The primary finding is that epoch length has a systematic and substantial impact on stationarity, with longer epochs demonstrating significantly higher stationarity ratios across all tested conditions and analysis methods.

The PP test with the TS model was consistently the most stringent criterion for stationarity, while the KPSS and PP-AR tests were more lenient. Despite these methodological differences, the overall trend was robust: stationarity increased markedly with epoch duration, plateauing at high levels for longer segments. Critically, this pattern held true for both event-related (marker-based) and continuous (duration-based) segmentation approaches, although the duration-based method achieved high stationarity ratios at slightly shorter lengths.

In practical terms, these results provide clear guidelines for epoch selection: to achieve a high likelihood (>95%) of stationarity across various tests, EEG epochs should be at least 3 to 4 seconds long. A more conservative approach, focusing on the stringent PP test with a TS model (aiming for >90% stationarity), requires epochs longer than 3 seconds for event-related data and longer than 2 seconds for continuous data.

This finding reconciles the inherent non-stationarity of brain activity with the practical need for stationary data segments in statistical analysis. Given the constraints of the available data, a 2-second epoch length will be implemented for the duration-based segmentation in all subsequent analyses throughout this thesis.

Chapter 3

From localised processing to global integration: whole-brain reconfiguration and the pivotal role of the somato-motor network in tonic pain

Building upon the methodological foundation established in Chapter 2, this chapter investigates large-scale brain network reorganisation directly evoked by tonic thermal pain in healthy participants. Using EEG-based functional connectivity and graph theory, it systematically characterises the dynamic alterations in network architecture that underpin the sustained pain experience. The findings provide crucial insights into pain-induced neuroplasticity and establish analytical approaches that will be extended to subsequent investigations of stimulation after-effects and chronic pain states.

3.1. Introduction

Previous research has established that tonic experimental pain serves as a critical translational bridge between short-lived phasic pain stimuli and the persistent nature of clinical chronic pain (Lee et al., 2021; Ploner & Tiemann, 2021). Unlike brief nociceptive challenges, tonic pain paradigms evoke sustained neural dynamics that more closely approximate the continuous brain states underlying chronic pain conditions, making them especially valuable for identifying functionally relevant network biomarkers. Functional magnetic resonance imaging (fMRI) studies have consistently implicated several large-scale brain networks in pain processing, with central roles for the somato-motor (SomMot), frontoparietal, and dorsal attention networks (Lee et al., 2021). For instance, sustained myofascial pain has been associated with a shift in contralateral primary sensorimotor connectivity toward the salience network (J. Kim et al., 2013), while capsaicin-induced pain increases crosstalk among SomMot, default mode, auditory and visual networks (Lou et al., 2024).

EEG studies further highlight the involvement of alpha band oscillations in tonic pain. During sustained heat pain, alpha power in sensorimotor areas is suppressed, while phase-based alpha connectivity between sensorimotor and medial prefrontal cortex increases (Nickel et al., 2020). These effects are thought to originate from the sensorimotor cortex (Peng et al., 2014; H. Wang et al., 2023) and have been showed to correlate negatively with pain ratings (Peng et al., 2014, 2015). Together, these findings suggest that the SomMot network contributes to both intra-network (local) and inter-network (distributed) coordination during tonic pain, possibly mediated by alpha-band dynamics.

Graph theory provides a powerful framework to quantify such brain network organisation by measuring GNIs, which capture the balance between segregation (e.g., global clustering coefficient, Gcc) and integration (e.g., global efficiency, Geff) in brain function (Barabási et al., 2023; Rubinov & Sporns, 2010).Notably, classification analyses using a combination of GNIs from alpha-band EEG have achieved up to 92% accuracy in differentiating pain and no-pain states (Modares-Haghighi et al., 2021), underscoring their translational promise.

However, a systematic review indicated that while GNI differences exist between chronic pain patients and healthy controls, the overall findings remain mixed (Lenoir et al., 2021). Similarly, experimental pain studies report conflicting results. Some fMRI studies have reported increased Gcc and reduced small-worldness (Sw) and modularity (Mod) in response to noxious stimuli (Huang et al., 2019; Qi et al., 2016; Zheng et al., 2020). In contrast, even in the same EEG dataset, no significant Gcc or Geff differences were observed when using phase-locking value, whilst significant Gcc increases during pain emerged using the debiased weighted phase lag index (dwPLI) (Nickel et al., 2020).

To address these discrepancies, we analysed brain-wide graphs, higher-order intra-SomMot, and inter-network graphs to capture both connectivity patterns and network topology. Specifically, the study had three aims: (1) to characterise tonic pain-induced reorganisation of functional connectivity and network topology; (2) to explore the neuronal mechanisms underlying pain-states; (3) to assess the predictive utility of GNIs for classifying pain states.

Here we reanalyse a secondary EEG dataset recorded in a tonic thermal pain model (Valentini et al., 2022). We hypothesised that tonic pain would determine the reorganisation of functional connectivity from intra-network segregation to inter-network integration, with the SomMot network playing a central role. In addition, we expected that combined GNIs would exhibit robust predictive power in classifying pain states.

If validated, these EEG-based biomarkers could contribute to the development of objective pain assessment tools, particularly for non-communicative individuals and chronic pain populations.

3.2. Methods

3.2.1. Participants and demographic measures

Forty-three participants volunteered for the study. Seven participants were excluded: one had taken a painkiller before the experiment, another failed the perceptual matching procedure (detail in experimental procedure), and data from the five were excluded due to technical issues with EEG recording. Therefore, only 36 were analysed and 22 of these were female, with a mean age of 25.36 years (range: 20 to 56 years). All participants had normal or corrected-to-normal vision and normal hearing. Prior to attending, the volunteers were asked to complete a questionnaire to ensure that they had no history of neurological, psychiatric, or pain disorders that could interfere with the study or jeopardise their safety. Psychological traits relevant to pain processing were also assessed using the Pain Catastrophising Scale (PCS) (Sullivan et al., 1995) and the trait component of the State-Trait Anxiety Inventory (STAI) (Spielberger et al., 2017). These measures were later included in correlational analyses.

The study received approval from the Ethics Committee of the University of Essex (EV1801).

3.2.2. Experimental procedure

We used a 30-liter water tank (RW-3025P, Medline Scientific) to deliver two out of three experimental sensory conditions. We induced an experience of tonic pain by having participants immersing their left hand in hot water at 45 °C, referred to as the hot condition. This temperature was selected based on previous studies (Granot et al., 2008; Jackman et al., 2023) which found it to induce a moderate level of pain. We induced an innocuous warm sensation by reducing the water temperature by 6 °C less than the hot condition. During the stimulation, participants were asked to rate their level of unpleasantness every 10 seconds using an onscreen VAS, with verbal anchors at 0 ('No unpleasantness') and 100 ('Intolerable unpleasantness'). In total, participants provided 30 ratings for each condition. At the beginning and end of the experimental session, both eyes-open and eyes-closed resting-state sessions were recorded, each lasting about 2.5 minutes. Hence, each condition lasted around 5 minutes. Data from the resting-state eyes-open condition only were included in this study (Fig. 3.1). The third sensory condition (i.e., tonic sound) is not included in the current study. The sequence of experimental blocks was counterbalanced for all participants.

Before the experiment, all participants were required to complete a perceptual matching procedure. This critical step ensured the subjective unpleasantness of the auditory stimulus was equivalent to that of the painful heat stimulus for each participant. This matching was a cornerstone of the original experimental design. For consistency, we did not include the single participant who failed the procedure in the seminal study within the current re-analysis.

Since the target unpleasantness rating ranged from 50 to 75 on the VAS (0 to 100), this confirmed that we successfully induced a moderate level of unpleasantness during the hot stimulation. If the unpleasantness rating for the warm stimulation was significantly lower than that for the hot stimulation, it would further support the success of the thermal manipulation. Moreover, if unpleasantness increased during the hot water immersion, it would provide additional evidence for the successful induction of tonic pain in our study.

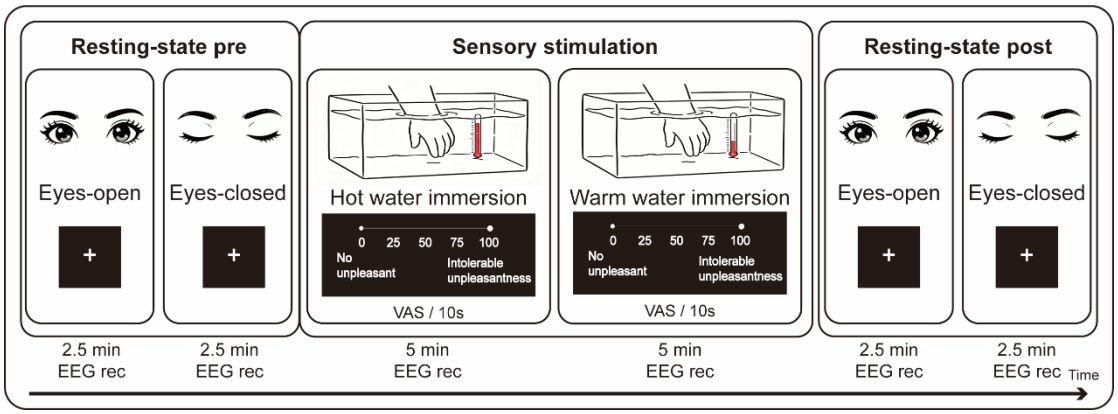

Figure 3.1. Experimental design adapted from Valentini et al. (2022). During resting-state pre and resting-state post (2.5 min each, eyes-open and eyes-closed), participants fixated on a central cross while EEG was recorded continuously. The sensory stimulation phase consisted of two 5-min blocks presented in counterbalanced order: hot water immersion and warm water immersion of the left hand. Throughout each immersion block, participants rated the unpleasantness of their sensation every 10 seconds using an on-screen Visual Analogue Scale (VAS; 0 = "No unpleasant," 100 = "Intolerable unpleasantness"; markers at 25, 50, 75). EEG was recorded continuously throughout all phases. The sequence of experimental blocks was counterbalanced for all participants. EEG rec, EEG recording.

3.2.3. EEG pre-processing

EEG data were recorded using an electrode montage of 62 channels consisting of all 10-20 system electrodes with Ag/AgCI electrodes (Easycap, BrainProducts GmbH, Gilching, Germany). The impedance of all electrodes was kept below 10 kΩ, and the EEG signal was amplified and digitised at 1000 Hz. The online reference was placed upon the left earlobe, and the ground was located at electrode position AFz.

The EEG data in hot, warm, and resting-state eyes-open conditions before stimulation were pre-processed using a high-pass value set to 0.1 Hz, and the low-pass value set to 100 Hz. All data were down sampled to 500 Hz. Artefacts such as eye-blinking and muscle movements were removed using ICA.

After ICA, the data were further denoised with a notch filter to exclude the frequency bands from 49.5 to 50.5 Hz, were re-referenced to the average of all electrodes (Goldman, 1950) and were segmented into 2-second epochs with a 25% overlapping rate and 25% baseline correction.

3.2.4. Analytical design

All analyses were performed in MATLAB using the EEGLAB toolbox (Delorme & Makeig, 2004), FieldTrip toolbox (Oostenveld et al., 2011), the Brain connectivity toolbox (Rubinov et al., 2009), the DISCOVER-EEG toolbox (Gil Ávila et al., 2023), the Network-Based Statistic toolbox V1.2 (https://www.nitrc.org/projects/nbs/), and custom-written scripts.

Pre-processed data were analysed using the pipeline showed in Fig. 3.2. The brain-wide graph (Fig. 3.2A) was constructed in both sensor and source spaces. In the sensor space, we focused on the alpha band, while exploratory

analyses were also conducted in other frequency bands. We assessed functional connectivity using dwPLI, and the thresholded matrices were binarised using one standard deviation above the median for each subject's connectivity matrix in each condition to create adjacency matrices for subsequent network-based statistics (NBS) and graph analyses. The source space data were reconstructed into 100 regions of interest of the Schaefer atlas (Schaefer et al., 2018) using an atlas-based beamforming approach via the Discover EEG toolbox. Further analysis based on brain-wide graph (Fig. 3.2B) for intra- and inter-network connections was conducted in the source space, utilising the 100-region atlas that classifies 7 networks. Intra-network connections for all 7 networks were analysed, with particular focus on the binary SomMot network. Additionally, inter-network connections were evaluated using weighted matrices, utilising NBS and graph theory.

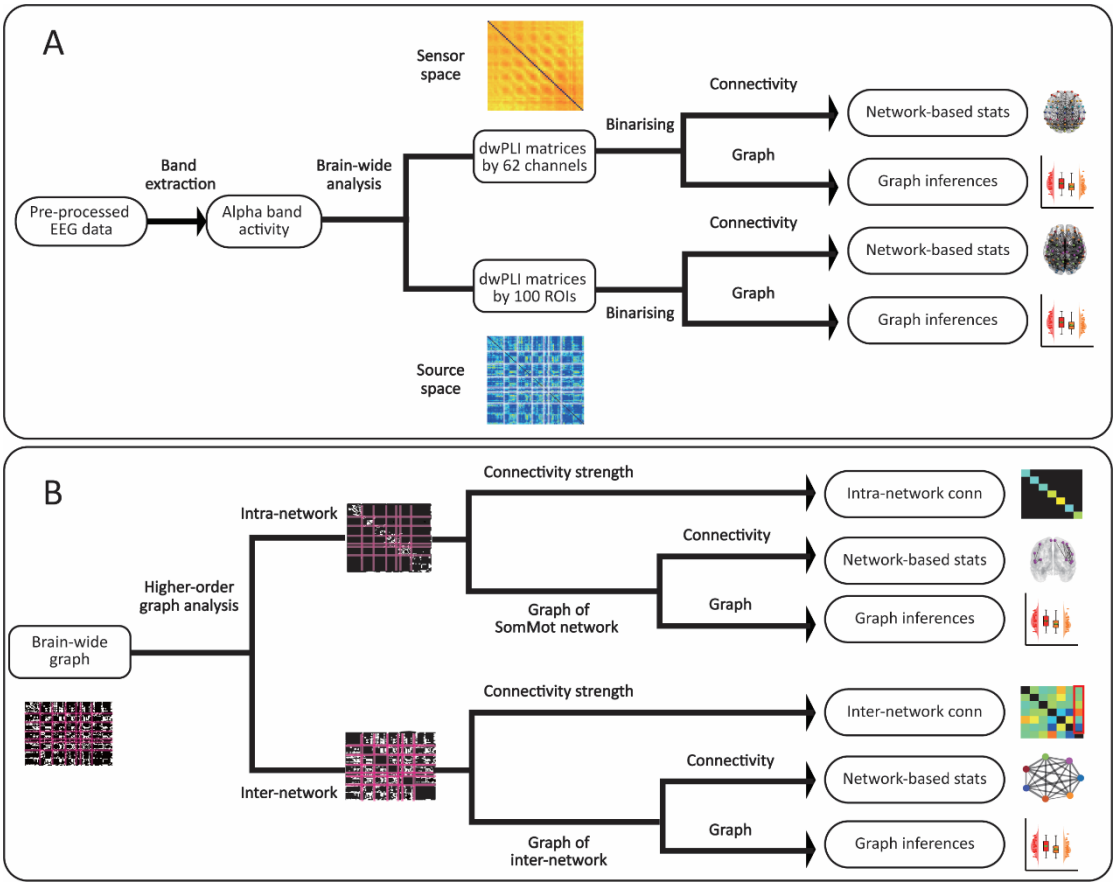

Figure 3.2. Pipeline for the analysis of EEG data. (A) The pre-processed EEG data were extracted in the alpha band and then used for the brain-wide functional connectivity assessment using dwPLI in both sensor and source spaces. The functional connectivity matrices were binarised using a threshold of one standard deviation above the median for each subject's connectivity matrix in each condition and then analysed through NBS and graph analysis. (B) The brain-wide graphs in the source space were further constructed as a higher-order graph involving 7 networks in parcellation. For intra-network analysis, statistical comparisons of the intra-network connectivity strength were conducted, and the binarised graph of the SomMot network was analysed using NBS and graph analysis. For inter-network analysis, statistical comparisons of the mean inter-network connections between each pair of networks were conducted, and inter-network connections between pairs of networks were constructed as weighted matrices and analysed through NBS, as well as both local and global graph analyses. dwPLI: debiased weighted phase lag index; ROI:

regions of interest; conn: connectivity; stats: statistics; NBS: network-based statistics.

We performed absolute and relative comparisons between the hot and warm conditions in both spaces. Specifically, the functional connectivity matrices for the relative comparisons were calculated by dividing the original dwPLI for each sensory condition by the dwPLI of the pre-stimulation resting-state eyes-open condition for each participant[1].

Notably, NBS-based graphs revealed connectivity patterns for group-level contrasts between hot and warm stimulation. In parallel, the graph-theoretical analysis was performed on individual-level connectivity matrices to compute several network inferences, which were then submitted to group-level statistical testing to identify condition-dependent alterations in graph characteristics. Although these two analytical approaches are methodologically distinct, they provide complementary insights: NBS highlights condition-contrast connectivity patterns, while graph-theoretical inferences quantify the corresponding network-level properties.

3.2.5. Brain-wide graph analysis

We conducted a brain-wide graph analysis in both sensor and source spaces (Fig. 3.2A). In the analysis of sensor space, we extracted the pre-processed EEG data in the alpha band (8-13 Hz) using the Hilbert transform. To

[1] We excluded the closed eye condition for this purpose based on the assumption that the open eyes resting state would have provided a better reference baseline for sensory-related mental states.

estimate functional connectivity in phase synchronisation, we performed further analysis using the dwPLI (M. X. Cohen, 2014) due to its significant reduction of volume conduction effects (Ortiz et al., 2012).

For each participant and condition, dwPLI values were computed for all pairs of 62 EEG channels and averaged across epochs to construct functional connectivity matrices. These matrices were then binarised using a threshold set at one standard deviation above the median of each matrix. The resulting binarised undirected adjacency matrices were used for subsequent connectivity and graph analyses.

3.2.5.1. Analysis for sensor space graphs

Connectivity analysis was performed using the Network-Based Statistic (NBS) toolbox (Zalesky et al., 2010, 2012) to identify significant differences in brain connectivity between conditions. NBS, a non-parametric statistical approach, employs cluster-based analysis while controlling for family-wise error rate (Zalesky et al., 2012). In the sensor space, we applied NBS to compare the two conditions using 62 × 62 node graphs.

3.2.5.2. Analysis for source space graphs

In the source space analysis, we projected the pre-processed sensor space data onto 100 regions of interest from the Schaefer atlas (Schaefer et al., 2018) using an atlas-based beamforming approach via the Discover EEG toolbox (Gil Ávila et al., 2023). We computed dwPLI matrices for each participant and condition, and then binarised them into adjacency matrices using the same thresholding procedure applied in the sensor space analysis. Graphs comprising 100 nodes were then constructed, and connectivity and graph-

theoretical analyses were performed following the same procedures as in the sensor space.

3.2.6. Higher-order graph analysis

Based on the binarised source space graphs, we further analysed higher-order graphs (Fig. 3.2B) which included 7 functional networks: Visual (Vis), Somato-motor (SomMot), Dorsal Attention (DorsAttn), Salience-Ventral Attention (SalVentAttn), Limbic, Control (Cont), and Default.

3.2.6.1. Intra-network analysis

For the intra-network analysis, only the intra-network connections within each of the seven networks were retained. The connectivity strength was calculated by averaging these connections and then compared between the two conditions.

Apart for the intra-network connectivity analysis, a focussed analysis was conducted on the SomMot network. Brain regions corresponding to the SomMot network were extracted, yielding a 14 × 14 binarised, undirected subgraph. Connectivity and graph-theoretical analyses were then performed using the same procedures as those applied in the sensor and source spaces.

3.2.6.2. Inter-network analysis

For the inter-network analysis, all the connections between different networks were preserved, while intra-network connections were excluded. For each network, inter-network connectivity strength was calculated as the average of its connections with the other six networks.

A 7 × 7 weighted adjacency matrix was generated for each condition, where each node represented a network, and edge weights corresponded to

the average connectivity between all pairs of brain regions across two networks. This representation was independent of the number of brain regions within each network.

We also applied connectivity and graph analysis on the resulting 7 × 7 weighted inter-network graphs. Given the limited number of nodes in the higher-order graph, two GNIs were computed: Gcc and Geff. In addition, two local inferences were assessed for each node (network) in the inter-network graph: edge betweenness centrality (Ebc), and local clustering coefficient (Lcc).

3.2.7. Graph analysis based on graph theory

Graph analysis consisted of four GNIs in the sensor space, source space and intra-network graphs: Gcc, Geff, Sw and Mod. Gcc is one of the best-known indicators of functional segregation, quantified as the average clustering coefficient of each node in the graph. Clustering coefficients at the node level indicate the fraction of the node's neighbours that are also neighbours of each other (Watts & Strogatz, 1998). A high fraction of triangles in the graph implies functional segregation, reflecting the brain's ability to use densely interconnected regions to sustain specialised brain processes. Geff is a measure of functional integration (Achard & Bullmore, 2007), facilitating the rapid exchange of information across distributed brain regions. It is computed as the average inverse shortest path length, which is the minimum number of edges required to connect any pair of nodes in a graph (Latora & Marchiori, 2001). Sw describes how a graph is more clustered than random networks with similar characteristic path lengths (Watts & Strogatz, 1998). It is calculated as the ratio of the clustering coefficient to Geff compared to random networks. Small-world organisation reflects an optimal balance of functional integration and segregation (Sporns &

Honey, 2006). Mod quantifies the degree to which a graph can be subdivided into clearly delineated groups (Newman, 2004). Unlike other network-structure measures, Mod relies heavily on optimisation algorithms that subdivides the graph into non-overlapping modules. We used the maximised Mod algorithm (Newman, 2006), which is an accurate and sufficiently fast approach to quantify Mod for smaller networks (Rubinov & Sporns, 2010). Higher Mod values indicate that a network has a stronger community structure, meaning there are dense connections among nodes within the same module (or group) and sparser connections between nodes in different modules. This suggests that the network is more efficiently organised into distinct subgroups, which can enhance functional specialisation and improve resilience to disruptions.

Graph analysis consisted of two local network inferences. The edge betweenness centrality (Brandes, 2001) represents the fraction of all shortest paths that include a specific edge; edges with high values indicate a critical role in many shortest paths. The weighted Lcc (local clustering coefficient) represents the average intensity (geometric mean) of all triangles associated with each node. Since the weighted local efficiency closely parallels the weighted Lcc (Onnela et al., 2005), we focussed solely on Lcc.

It is worth noting that segregation in brain-wide and intra-network graphs reflects functional specialisation within a given graph, whereas integration characterises global information flow. However, when within-network connectivity is excluded, the local network inferences derived from higher-order inter-network graphs represent dynamics related to interaction with other networks. In this context, GNIs primarily capture inter-network communication.

3.2.8. Statistical analysis

All statistical comparisons, except for the network-based statistics (as implemented in the NBS toolbox), were carried out using IBM SPSS (version 20; IBM Corp, Armonk, NY).

For the graph analysis, we used different statistics for global and local network inferences. For GNIs in all graphs, we applied two-way repeated measures analysis of variance (ANOVA), followed by post hoc comparisons using Bonferroni-corrected two-sided paired sample *t*-tests with an alpha level set at 0.05. Using ANOVA, we not only assessed the differences between two conditions, but also examined how these differences varied between absolute and relative comparison methods. As for the local network inferences which were conducted exclusively in higher-order inter-network graphs, we computed paired-sample *t*-tests for Lcc, with an alpha level set at 0.05 (two-tailed) with false discover rate (FDR) correction for multiple comparisons. As for Ebc, we also performed the NBS to identify significant differences in edge-level centrality. To analyse the connectivity strength within intra- and inter-network graphs we performed two-tailed paired-sample *t*-tests with an alpha level set at 0.05, with FDR correction for multiple comparisons between conditions under both absolute and relative comparison methods.

3.2.9. Visualisation

For visualisation purposes, we transferred our EEG electrode positions into the standard Montreal Neurological Institute (MNI) space via a projection of the coordinates (Koessler et al., 2009). For source space data visualisation, we transferred the centroids of 100 regions of interest from the 7-network

version of the Schaefer atlas (Schaefer et al., 2018) into the MNI space. Although the location systems in sensor space and source space differ, we aligned them by projecting both onto the ICBM152 brain template (Fonov et al., 2009). Using BrainNet Viewer (Xia et al., 2013), a high-resolution anatomical atlas, we performed grand average network visualisations from binarised matrices across participants for each condition.

To capture differences in connectivity patterns between conditions, we applied the NBS tests within each comparison method to preserve spatial information of connectivity distribution. A one-sided paired-sample t-test with 5,000 permutations was used, with a significance level of 0.05. Connections that survived the permutation test formed the edges in p-graphs, as illustrated in sensor space results (Fig. 3.3A-B bottom panel). For connections that were not statistically significant, t-values were visualised as t-graphs. To improve clarity, t-graphs displayed connections with t-values greater than 1.7 in the source space (Fig. 3.5AB bottom panel), corresponding to the critical t-value for a one-sided paired-sample t-test at 0.05 significance level with 36 participants. For intra-SomMot (Fig. 3.6A lower panel), inter-network comparisons (Fig. 3.7A bottom panel), and Ebc (Fig. 3.7B top panel), t-graphs included connections with positive t-values ($t > 0$).

3.2.10. Correlation analysis between global network inferences and individual differences

Prior to classification analyses, we quantified the correlation between GNIs and behavioural ratings for hot and warm conditions separately. To assess the potential influence of age, we conducted correlations between participant age and each GNI. We further evaluated how individual differences in pain

responsiveness modulated GNIs using partial correlations, controlling for age and gender. Individual differences were defined using four behavioural measures: pain perception was defined as the mean difference in unpleasantness ratings between hot and warm conditions for each participant; pain tolerance was operationalised as the change in average unpleasantness rating from the first third to the last third of the hot stimulation period; and pain-related psychological traits were assessed using the PCS and the STAI-T.

3.2.11. Machine learning classification

GNIs were selected as features for classification, derived from individual or combined graph types including sensor space, source space, intra-SomMot, and inter-network graphs under both absolute and relative comparison methods. Our feature inclusion was primarily theory-driven rather than performance-optimised, as the goal was to use classification to test the robustness of GNIs as potential biomarkers. We incorporated all GNIs from four graph types because each was hypothesised to capture distinct aspects of brain network organisation that may differentiate responses to hot and warm stimuli. Given the modest sample size, we deliberately avoided data-driven feature selection methods, which could increase the risk of overfitting and compromise the validity of cross-validation. Instead, we systematically evaluated all possible combinations of the four feature sets and reported the three best-performing combinations. This strategy ensured methodological transparency and reduced the risk of overfitting by avoiding any optimisation on the test set.

To assess the predictive capacity of GNIs in distinguishing tonic pain states (hot vs. warm), we implemented a linear support vector machine (SVM) with L2 regularisation. The regularisation parameter (λ) was automatically

optimised within each training fold. Input features (GNIs) were standardised using z-score normalisation based on the training set's mean and standard deviation, and the trained model was used to classify the held-out subject's data.

A leave-one-subject-out cross-validation framework was applied across all 36 participants. For each fold, one subject's data was held out for testing, while the remaining data were used for training and normalisation. Model performance was evaluated using area under the receiver operating characteristic curve (AUC-ROC), and pooled inferences from the confusion matrix, including accuracy, sensitivity, and specificity.

To assess the significance of the classifier's discriminative performance, we conducted a permutation test with 1000 iterations. For each iteration, participant labels were randomly shuffled to disrupt the true feature-label relationship, and the entire cross-validation pipeline was repeated using these permuted labels. The null distribution of AUC-ROC values was generated from these shuffled-label iterations. The empirical *p*-value was computed as the proportion of permutation AUCs exceeding or matching the original model's AUC. This approach quantifies the probability that the observed classification performance occurred by chance under the null hypothesis of no true feature-label association.

3.3. Results

3.3.1. Perception

As we already showed in a previous study (Valentini et al., 2022), the unpleasantness ratings were significantly different between tonic hot and warm stimulation ($T(35)=36.31$, $P_{FDR}<0.001$). This difference was accounted for by

greater unpleasantness during the hot condition (hot: 67.83±9.18, 95% CI = [64.73, 70.94]; warm 3.17±1.30, 95% CI = [2.23, 6.93]). These results demonstrate that the manipulation of thermal stimulation was effective in inducing distinctive affective states in healthy participants. Moreover, a paired-sample t-test comparing the average unpleasantness rating from the first third of the hot condition to the average rating from the last third revealed a significant increase ($t(35) = 5.55$, $p < 0.001$), suggesting a trend of sensitisation to the stimulus over time within the hot condition and thereby validating the successful experimental manipulation of tonic pain in our study.

3.3.2. Brain-wide graph results in sensor space

3.3.2.1. Sensor space connectivity results

In the absolute comparison (Fig. 3.3A), the group-level graph construction in the axial plane revealed that edges in the hot condition were clustered bilaterally from the central to parietal regions and within parietal areas (Fig. 3. 2A third row left panel). In contrast, the warm condition exhibited a more distributed edge pattern within brain regions, indicated by nodes of the same colour (Fig. 3.3A third row right panel). NBS revealed a significant graph with larger connectivity in the hot condition relative to warm condition (Fig. 3.3A fourth row left panel), comprising 60 nodes and 378 edges, predominantly distributed in posterior regions ($P < 0.001$). Conversely, the warm condition (Fig. 3.3A fourth row right panel) yielded a significant graph with larger connectivity relative to hot condition, consisting of 62 nodes and 410 edges, with a concentration of connections in the central region ($P < 0.001$). The relative hot and warm conditions displayed distinct differences in both the dwPLI matrices and the

adjacency matrices (Fig. 3.3B). Connections were generally distributed throughout the scalp in the group-level relative hot graph (Fig. 3.3B third row left panel), with a greater concentration in the anterior regions, whereas the relative warm condition displayed a more central distribution (Fig. 3.3B third row right panel). The relative hot condition demonstrated significantly greater connectivity pattern than the relative warm condition (Fig. 3.3B fourth row left panel) with connections predominantly extending from the frontal to parietal regions, comprising 51 nodes and 213 edges ($P < 0.001$). Conversely, the graph for the relative warm condition (Fig. 3.3B fourth row right panel), which indicated significant graph with connectivity larger than the hot condition, revealed a distribution pattern clustered from the frontal-central to central-parietal regions, maximally expressed in the central region, and comprised 58 nodes and 185 edges ($P < 0.001$).

Results from both comparison methods revealed a significant pattern of increased frontoparietal connectivity in the hot condition compared to the warm condition, while the warm condition showed a significant stronger connectivity localised in the centre of the scalp relative to the hot condition.

Although the adjacency matrices (Fig. 3.3, second row) and derived graphs (Fig. 3.3, third row) appear markedly different between the absolute and relative comparison methods, this difference reflects a key methodological point. Absolute comparison method captures overall connectivity strength, incorporating both intrinsic baseline activity and task-induced signals, whereas relative (baseline-normalised) matrices diminish shared baseline activity to isolate condition-specific neural responses. Importantly, despite these visual differences at the group level, the condition-contrasts derived from network-based statistics

(p-graphs) were more consistent across the two methods, suggesting that condition-contrast connectivity patterns were robustly identified regardless of comparison methods used.

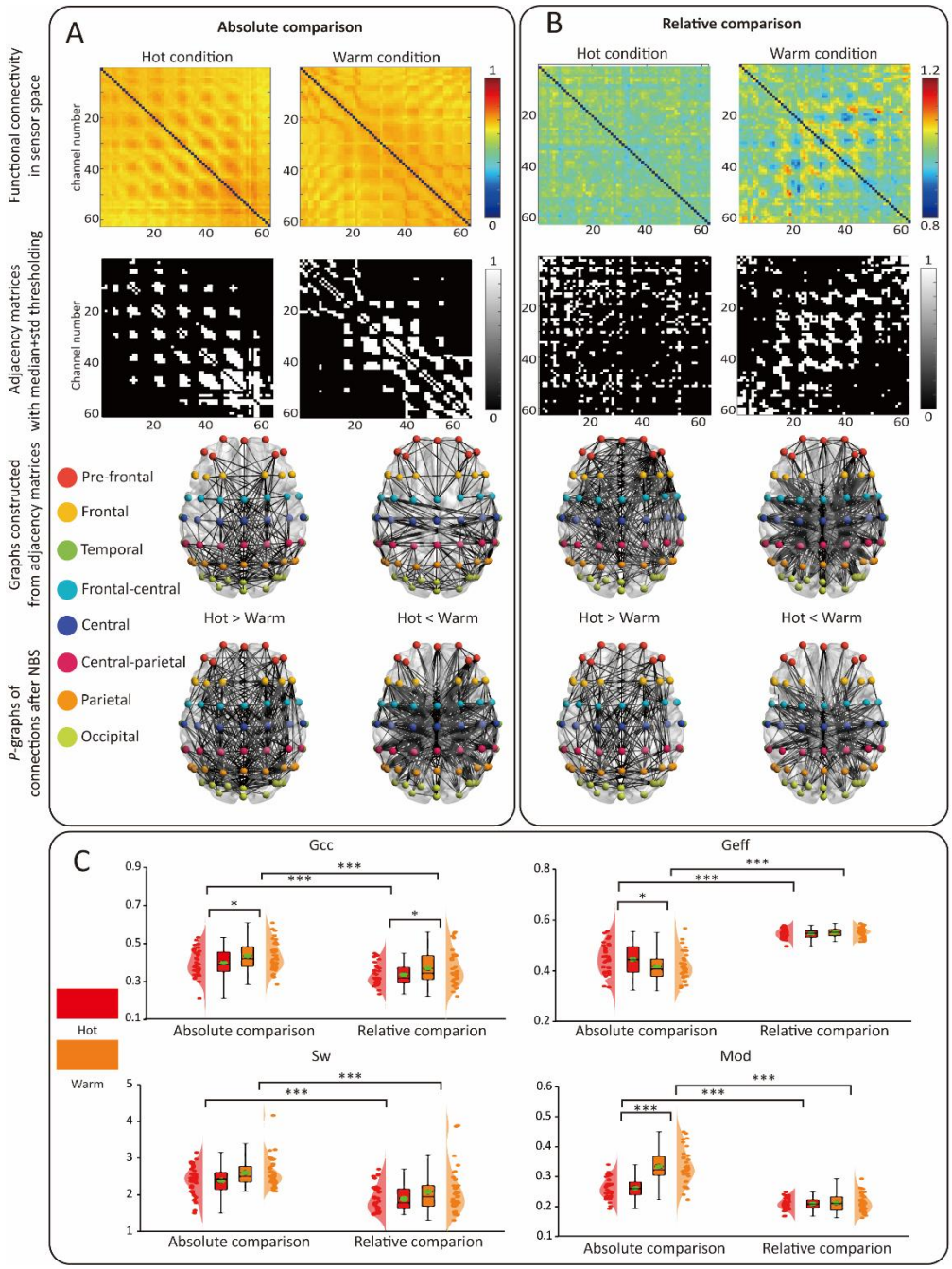

Figure 3.3. Functional graphs elicited by hot and warm stimulation using two comparison methods in sensor space. (A) Group-level functional connectivity matrices for hot and warm stimulation (first row). The corresponding

adjacency matrices (second row) were used to constructed undirected, unweighted graphs (third row). Sensors corresponding to different scalp regions (Prefrontal, Frontal, Temporal, Frontal-central, Central, Central-parietal, Parietal, and Occipital) were colour-labelled for visual distinction. Condition contrast significant connectivity patterns were identified using NBS and visualised as P-graphs (fourth row). The left panel showed hot-preferred responses, and the right panel showed warm-preferred responses. (B) Similar to (A) but using a relative comparison method in which each subject's dwPLI matrix under stimulation was normalised by their own eyes-open resting-state dwPLI matrix. (C) Violin plots with overlaid scatter and box plots show the results of repeated-measures ANOVA with Bonferroni correction for post hoc comparisons of four GNIs across the hot (red) and warm (orange) conditions and two comparison methods. A green-filled circle with a black edge denotes the mean value for each group. A significant graph emerged, characterised by increased frontoparietal connectivity for hot stimulation, whereas the warm stimulation condition showed stronger, centrally distributed connectivity. Additionally, a notably higher degree of functional segregation was observed in the graphs elicited by warm stimulation compared to those from hot stimulation, as demonstrated by both comparison methods. NBS, network-based statistics; GNIs, global network inferences; Gcc, global clustering coefficient; Geff, global efficiency; Sw, small-worldness; Mod, modularity. *P < .05, ***P < .001.

3.3.2.2. Sensor space graph analysis results

Significant main effects of stimulus condition (warm vs. hot) and comparison method (absolute vs. relative) were observed across all GNIs: functional segregation (Gcc), integration (Geff), small-worldness (Sw), and modularity (Mod) (Fig. 3.3C). Warm stimulation consistently enhanced functional segregation compared to hot stimulation under both comparison methods. Absolute comparisons amplified this effect, yielding higher Gcc than relative methods across stimuli. For functional integration (Geff), relative comparisons produced

substantially higher values than absolute methods in both conditions; notably, hot stimulation elicited greater Geff than warm stimulation only in the absolute comparisons. Both Sw and Mod were markedly elevated in the absolute versus relative comparisons, with warm stimulation further increasing Mod in absolute (but not relative) contexts. Detailed statistical results (ANOVA, post-hoc tests) are provided in Table 3.1. In summary, graphs induced by warm stimulation showed significantly greater segregation (Gcc), reduced integration (Geff), and improved information transfer into distinct modules (Mod) compared to those elicited by hot stimulation in absolute comparisons. Whilst relative comparisons only reflected increased segregation (Gcc) for warm stimuli.

Table 3.1. **Statistical results for GNIs from graphs derived from alpha band in sensor space (ANOVA and Post-hoc Comparisons).**

GNIs	Effect	$F_{1,35}$	P	η_p^2	Post-hoc Comparisons	T_{35}	$P_{Bonferroni}$	95% CI
Gcc	Stim (Main)	8.34	0.01	0.19	Warm > Hot (Abs)	2.19	0.04	[0.00, 0.07]
					Warm > Hot (Rel)	2.36	0.03	[0.00, 0.06]
Gcc	Comp (Main)	21.4	0	0.38	Abs > Rel (Hot)	3.81	< 0.001	[0.03, 0.09]
					Abs > Rel (Warm)	3.56	0.001	[0.03, 0.10]
Geff	Comp (Main)	223	<0.001	0.86	Rel > Abs (Hot)	9.09	<0.001	[0.08, 0.12]
					Rel > Abs (Warm)	13.3	<0.001	[0.11, 0.16]
Geff	Stim × Comp (Interaction)	5.73	0.02	0.14	Hot > Warm (Abs only)	2.07	0.05	[0.00, 0.06]
					Hot vs Warm (Rel): ns	1.33	0.16	[0.00, 0.01]
Sw	Stim (Main)	8.36	0.01	0.19	Hot vs Warm (Abs): ns	-1.9	0.07	[-0.45, 0.01]
					Hot vs Warm (Rel): ns	-1.85	0.07	[-0.40, 0.02]
Sw	Comp (Main)	61.3	<0.001	0.64	Abs > Rel (Hot)	5.66	<0.001	[0.32, 0.69]
					Abs > Rel (Warm)	3.56	<0.001	[0.03, 0.10]
Mod	Stim (Main)	38.5	<0.001	0.52	Warm > Hot (Abs only)	7.2	<0.001	[0.05, 0.09]
					Warm vs Hot (Rel): ns	0.5	0.62	[-0.01, 0.02]
Mod	Comp (Main)	154	<0.001	0.82	Abs > Rel (Hot)	8.83	<0.001	[0.04, 0.07]
					Abs > Rel (Warm)	10.17	<0.001	[0.10, 0.15]
Mod	Stim × Comp (Interaction)	33.3	<0.001	0.49				

Note. GNIs, global network inferences; Gcc, global clustering coefficients; Geff, global efficiency; Sw, small-worldness; Mod, modularity; Stim, Stimulus; Comp, Comparison; Abs, absolute comparison; Rel, relative comparison.

3.3.2.3. Exploratory results of graphs derived from theta, beta and gamma bands in sensor space

Aligned with the alpha band findings, condition-contrast graphs across all frequency bands exhibited greater consistency than group-level condition-specific graphs elicited by hot and warm stimulation (Fig. 3.4). Under absolute comparisons, condition-specific graphs showed predominantly occipital connectivity across all bands (Fig. 3.4 ABC, upper and left-half panel), accompanied by additional frontal connectivity in the theta band (Fig. 3.4A), central connectivity in the beta band (Fig. 3.4B), and prefrontal connectivity in the gamma band (Fig. 3.4C). In contrast, relative comparisons consistently revealed dense right-frontal to left-parietal connectivity across all frequency bands (Fig. 3.4 ABC, upper and right-half panel).

The majority of condition contrasts did not reach statistical significance, and the corresponding t-graphs consisted of sparse connectivity (Fig. 3.4 ABC, lower panel). The only statistically significant contrast was identified in the beta band under absolute comparison (Fig. 3.4B, lower panel second column), which showed greater connectivity during warm than hot stimulation ($P = 0.04$). This graph comprised 107 edges and 52 nodes, distributed within the right hemisphere (frontal to parietal regions) and included cross-hemispheric connections from left frontal to right parietal areas.

Unlike the robust findings in the alpha band, no main effect of stimulus condition was observed in other frequency bands. A post hoc difference was detected only in the theta band, with higher Mod during hot compared to warm stimulation.

Overall, the limited number of significant GNI results and the sparsity of condition-contrast t-graphs restrict the interpretability of findings outside the alpha band. Although oscillatory activity in theta, beta, and gamma bands is implicated in pain-related brain dynamics, the present results highlight alpha oscillations as the primary frequency band of interest for subsequent analyses.

The results of GNIs in other frequency bands were shown in Table 3.2.

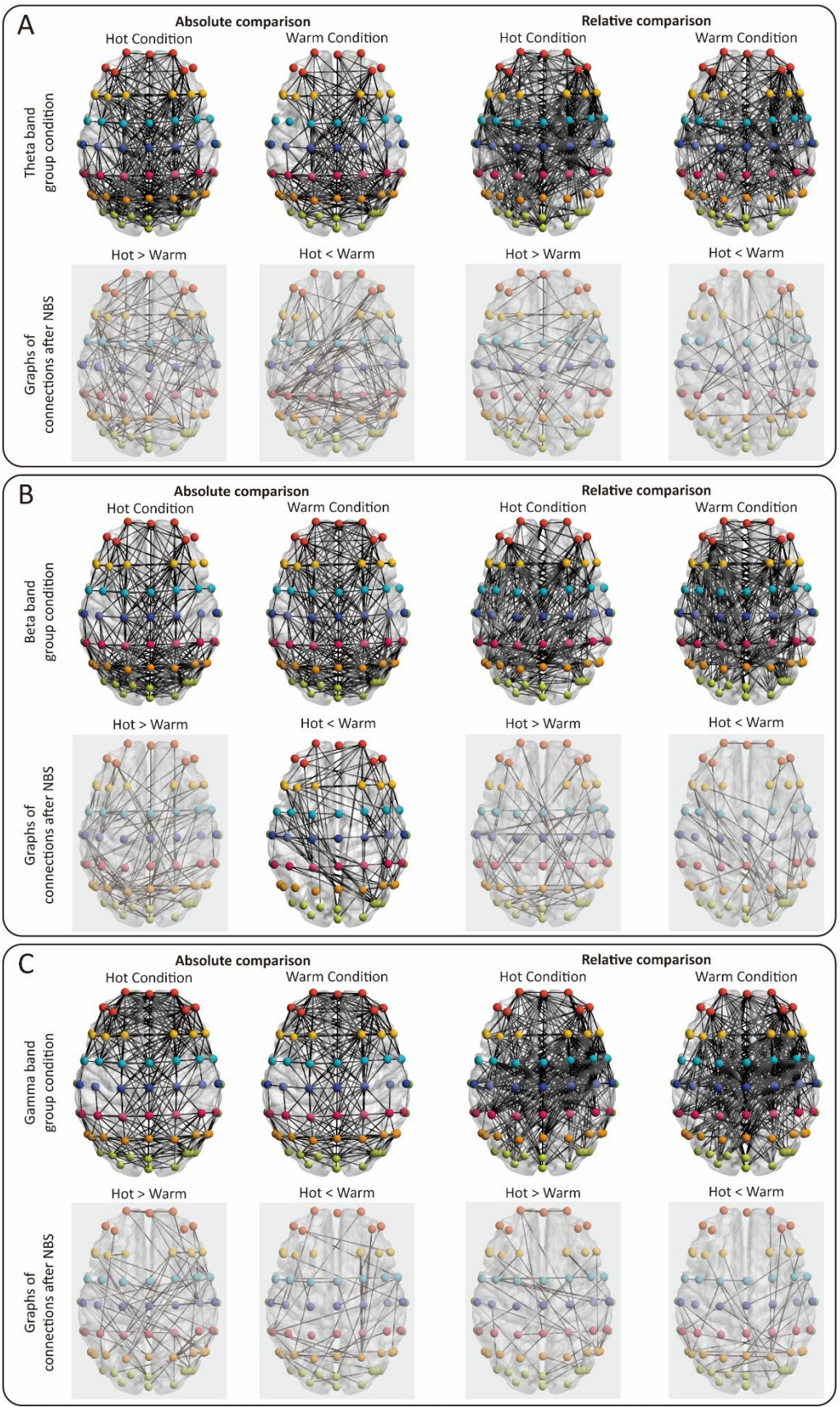
A
Absolute comparison
Relative comparison
Hot Condition
Warm Condition
Hot Condition
Warm Condition
Theta band group condition
Hot > Warm
Hot < Warm
Hot > Warm
Hot < Warm
Graphs of connections after NBS
B
Absolute comparison
Relative comparison
Hot Condition
Warm Condition
Hot Condition
Warm Condition
Beta band group condition
Hot > Warm
Hot < Warm
Hot > Warm
Hot < Warm
Graphs of connections after NBS
C
Absolute comparison
Relative comparison
Hot Condition
Warm Condition
Hot Condition
Warm Condition
Gamma band group condition
Hot > Warm
Hot < Warm
Hot > Warm
Hot < Warm
Graphs of connections after NBS

Figure 3.4 Functional graphs derived from theta, beta, and gamma bands elicited by hot and warm stimulation using two comparison methods in sensor space. (A) Group-level undirected, unweighted graphs derived from theta band (upper panel). Sensors corresponding to different scalp regions (Prefrontal, Frontal, Temporal, Frontal-central, Central, Central-parietal, Parietal, and Occipital) were colour-labelled for visual distinction. Condition contrast connectivity patterns were identified using NBS (lower panel). T-graphs are constructed from connections with a t-value greater than 1.7 from the between-condition contrast; non-significant results are shown with reduced opacity. P-graphs depicting the statistically significant connectivity contrasts are also included. The left half of each panel displays results from the absolute comparison method, while the right half displays results from the relative comparison method, in which each participant's stimulation dwPLI matrix was normalised to their own eyes-open resting-state dwPLI matrix. (B-C) Equivalent analyses for the beta and gamma bands, respectively. NBS, network-based statistics.

Table 3.2. Statistical results for GNIs graphs derived from other frequency band in sensor space (ANOVA and Post-hoc Comparisons).

Frequency bands	GNIs	Effect	$F_{1,35}$	P	η_p^2	Post-hoc Comparisons	T_{35}	$P_{Bonferroni}$	95% CI
Theta (4-8 Hz)	Gcc	Comp (Main)	32.33	< 0.001	0.48	Abs > Rel (Hot) Abs > Rel (Warm)	3.53 5.00	< 0.001 < 0.001	[0.03, 0.08] [0.04, 0.09]
Theta (4-8 Hz)	Geff	Comp (Main)	110.36	< 0.001	0.76	Rel > Abs (Hot) Rel > Abs (Warm)	8.90 9.00	<0.001 <0.001	[0.07, 0.11] [0.07, 0.11]
Theta (4-8 Hz)	Sw	Comp (Main)	45.43	< 0.001	0.57	Abs > Rel (Hot) Abs > Rel (Warm)	4.71 7.53	<0.001 <0.001	[0.29, 0.72] [0.44, 0.77]
Theta (4-8 Hz)	Mod	Comp (Main)	132.92	<0.001	0.79	Abs > Rel (Hot) Abs > Rel (Warm)	10.57 6.00	<0.001 <0.001	[0.06, 0.09] [0.03, 0.06]
Theta (4-8 Hz)	Mod	Stim × Comp (Interaction)	6.26	0.02	0.15	Hot > Warm (Abs) Warm > Hot (Rel)	2.00 1.75	0.04 0.09	[0.00, 0.04] [0.00, 0.02]
Beta (14-30 Hz)	Gcc	Comp (Main)	139.06	< 0.001	0.80	Abs > Rel (Hot) Abs > Rel (Warm)	8.94 11.85	< 0.001 < 0.001	[0.12, 0.19] [0.13, 0.18]
Beta (14-30 Hz)	Geff	Comp (Main)	132.84	< 0.001	0.79	Rel > Abs (Hot) Rel > Abs (Warm)	9.09 10.67	<0.001 <0.001	[0.08, 0.12] [0.08, 0.11]
Beta (14-30 Hz)	Sw	Comp (Main)	232.55	< 0.001	0.87	Abs > Rel (Hot) Abs > Rel (Warm)	10.89 10.67	<0.001 <0.001	[0.71, 1.03] [0.64, 0.94]
Beta (14-30 Hz)	Mod	Comp (Main)	243.63	<0.001	0.87	Abs > Rel (Hot) Abs > Rel (Warm)	11.60 11.40	<0.001 <0.001	[0.10, 0.14] [0.09, 0.13]
Gamma (60-100 Hz)	Gcc	Comp (Main)	129.25	< 0.001	0.79	Abs > Rel (Hot) Abs > Rel (Warm)	13.38 10.35	< 0.001 < 0.001	[0.13, 0.20] [0.14, 0.21]
Gamma (60-100 Hz)	Geff	Comp (Main)	108.97	< 0.001	0.76	Rel > Abs (Hot) Rel > Abs (Warm)	7.90 9.25	<0.001 <0.001	[0.06, 0.10] [0.06, 0.09]
Gamma (60-100 Hz)	Sw	Comp (Main)	75.20	< 0.001	0.68	Abs > Rel (Hot) Abs > Rel (Warm)	6.38 7.39	<0.001 <0.001	[0.47, 0.90] [0.59, 1.05]
Gamma (60-100 Hz)	Mod	Comp (Main)	223.60	<0.001	0.87	Abs > Rel (Hot) Abs > Rel (Warm)	11.60 14.33	<0.001 <0.001	[0.10, 0.14] [0.11, 0.15]

Note. GNIs, global network inferences; Gcc, global clustering coefficients; Geff, global efficiency; Sw, small-worldness; Mod, modularity; Abs, absolute comparison; Rel, relative comparison.

3.3.3. Brain-wide graph results in source space

3.3.3.1. Source space connectivity results

Across both comparison methods (Fig. 3.5A-B), the hot condition graphs displayed a more bilateral distribution (Fig. 3.5A-B third row left panel), while the warm condition graphs exhibited a connectivity pattern dominated by the right hemisphere (Fig. 3.5A third row right panel). Although no significant graphs were identified after NBS, *t*-graphs from both comparison methods consistently showed that the hot contrasts were primarily concentrated in the left frontoparietal regions (Fig. 3.5A-B, fourth row, left panel). In contrast, the warm contrasts were predominantly localised in the right hemisphere, particularly around the SomMot networks (Fig. 3.5A-B, fourth row, right panel).

Despite the lack of statistical significance, these results consistently revealed distinct ipsilateral-dominant differential connectivity patterns emerged in brain regions preferentially responsive to hot and warm stimulation consistent across comparison methods (Fig. 3.5A-B, fourth row). Furthermore, source space projections exhibited greater concordance between the absolute and relative comparison methods, particularly in the group-level condition-specific and condition-contrast graphs, than was observed in sensor space analyses.

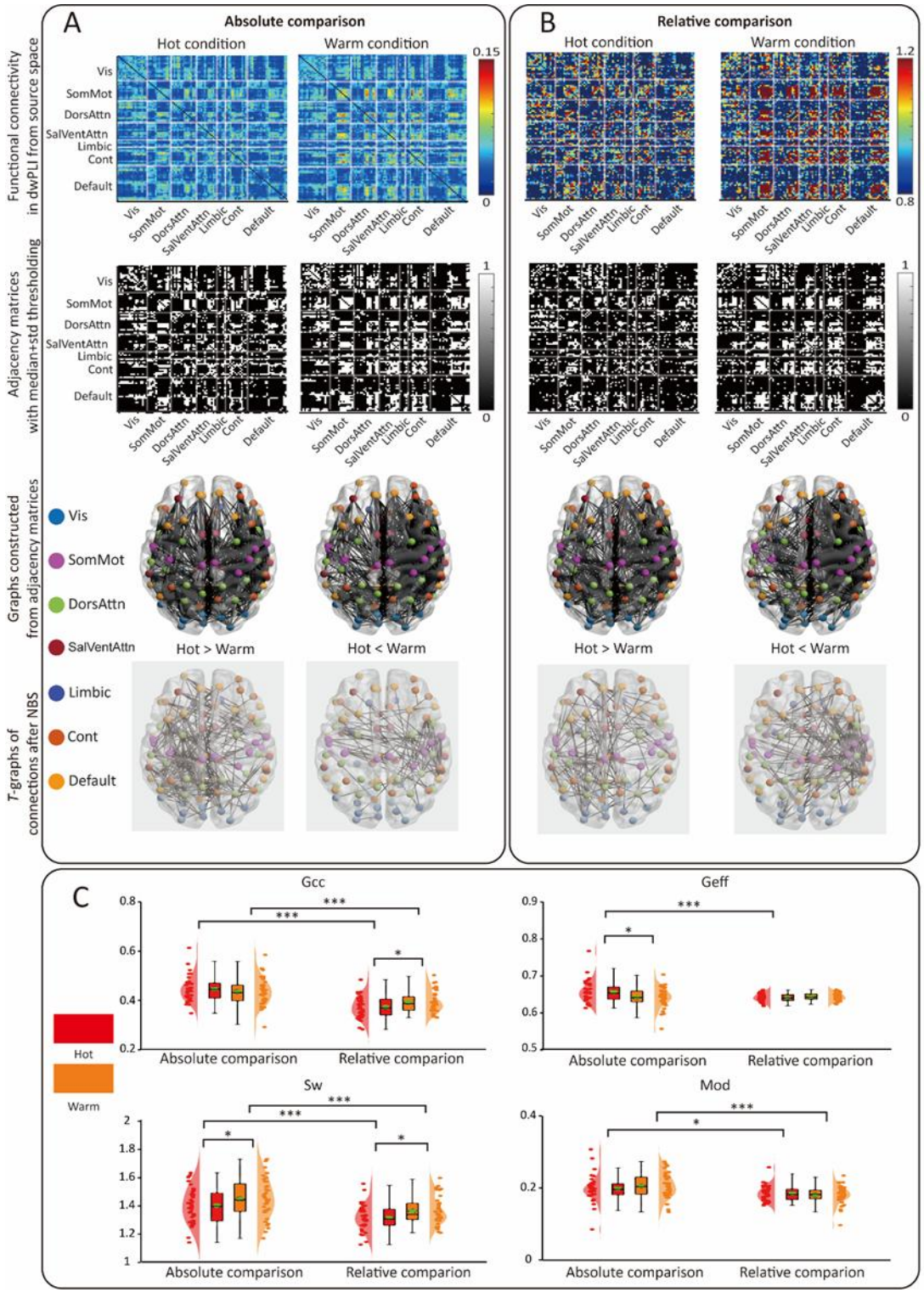

Figure 3.4. Functional graphs elicited by hot and warm stimulation using two comparison methods in source space. (A) Group-level functional connectivity matrices for hot and warm stimulation (first row) projected in source

space for 100 pairs of brain regions organised into 7 different functional networks (Visual, Somato-motor, Dorsal Attention, Salience-Ventral Attention, Limbic, Control, and Default). Adjacency matrices (second row) were constructed as absolute, unweighted graphs (third row), t-graphs (fourth row) constructed from connections with a t-value larger than 1.7 compared between conditions using NBS (shown in reduced opacity indicate non-significant results). The left panel showed hot-preferred responses, and the right panel showed warm-preferred responses. (B) Similar to (A) but using a relative comparison. (C) Violin plots with overlaid scatter, and box plots illustrate the results of repeated-measures ANOVA with Bonferroni correction for post hoc comparisons of four GNIs across the hot (red) and warm (orange) conditions and two comparison methods. A green-filled circle with a black edge denotes the mean value for each group. A stable pattern emerged across both comparison methods, with the hot condition showing a bilateral distribution of connectivity, while the warm condition exhibited a right-lateralised distribution. Notably, hot stimulation consistently elicited increased connectivity in the left frontoparietal regions, whereas the warm condition was associated with enhanced connectivity around the SomMot network. Graphs evoked by the hot stimulus exhibited a significantly lower degree of functional segregation in the relative comparison and a significantly higher degree of functional integration in the absolute comparison compared to those from warm stimulation, which were consistent with the results in sensor space. NBS, network-based statistics; GNIs, global network inferences; Gcc, global clustering coefficient; Geff, global efficiency; Sw, small-worldness; Mod, modularity. *P < .05, ***P < .001.

3.3.3.2. Source space graph analysis results

In source space, GNIs revealed significant effects of comparison method and stimulus condition (Fig. 3.5C). Absolute comparison consistently produced higher functional segregation (Gcc) than relative comparison across both stimulus conditions, while warm stimulation increased Gcc specifically in relative comparisons. For functional integration (Geff), absolute comparisons enhanced

values during hot, and hot stimulation increased Geff exclusively in absolute comparisons. Small-worldness (Sw) was elevated in absolute comparisons for both stimuli, with warm stimulation increasing Sw across methods. Modularity (Mod) was higher in absolute comparisons, with hot stimulation enhancing Mod in both methods. Detailed statistical results are in Table 3.3.

In summary, the graph analysis revealed that absolute comparisons exhibited higher functional segregation (Gcc), greater small-world properties (Sw), and enhanced information processing capabilities (Mod) compared to relative comparisons across both stimulus conditions in the source space. These results aligned with sensor-space findings, which also indicated reduced segregation for hot stimuli in relative comparisons and enhanced integration for hot stimuli in absolute comparisons.

Table 3.3. Statistical results for GNIs from graphs in source space (ANOVA and Post-hoc Comparisons).

GNIs	Effect	$F_{1,35}$	P	η_p^2	Post-hoc Comparisons	T_{35}	$P_{Bonferroni}$	95% CI
Gcc	Stim (Main)	54.8	<0.001	0.61	Abs > Rel (Hot)	7.4	<0.001	[0.05, 0.09]
					Abs > Rel (Warm)	4.3	0.001	[0.02, 0.06]
Gcc	Stim×Comp (Interaction)	6.68	0.01	0.16	Warm > Hot (Rel only)	2.5	0.01	[0.00, 0.04]
					Warm vs Hot (Abs): ns	1	0.35	[-0.03, 0.01]
Geff	Comp (Main)	5.23	0.03	0.13	Abs > Rel (Hot only)	3.2	0	[0.01, 0.03]
					Abs > Rel (Warm): ns	0.5	0.63	[-0.01, 0.01]
Geff	Stim × Comp (Interaction)	6.75	0.01	0.16	Hot > Warm (Abs only)	2.29	0.03	[0.00, 0.03]
					Hot vs Warm (Rel): ns	1	0.26	[-0.01, 0.00]
Sw	Stim (Main)	7.6	0.01	0.18	Warm > Hot (Abs)	2.07	0.04	[0.00, 0.11]
					Warm > Hot (Rel)	2.18	0.04	[0.00, 0.07]
Sw	Comp (Main)	19.2	<0.001	0.64	Abs > Rel (Hot)	3.57	0.001	[0.04, 0.13]
					Abs > Rel (Warm)	3.61	<0.001	[0.05, 0.16]
Mod	Comp (Main)	14.4	<0.001	0.29	Abs>Rel (Hot)	2.17	0.04	[0.00, 0.03]
					Abs>Rel (Warm)	4.33	<0.001	[0.01, 0.04]

Note. GNIs, global network inferences; Gcc, global clustering coefficients; Geff, global efficiency; Sw, small-worldness; Mod, modularity; Stim, Stimulus; Comp, Comparison; Abs, absolute comparison; Rel, relative comparison.

3.3.4. Higher-order intra-network and inter-network connectivity strength results

To understand better the brain-wide graph connectivity dynamics, we categorised them into intra-network and inter-network connections. Intra-network connectivity (Fig. 3.6, top) showed increased hot-stimulation connectivity in SomMot, Limbic, and Cont networks for absolute comparisons, and in Cont and SomMot (marginally) for relative comparisons. Conversely, relative comparisons exhibited increased warm-stimulation connectivity in Visual, DorsAttn, SalVentAttn, and Default networks. For inter-network connectivity (Fig. 3.6, bottom), absolute comparisons demonstrated higher hot-stimulation connectivity in Limbic and Cont networks, with no significant effects in relative comparisons. Detailed statistical results are in Table 3.4.

In summary, Limbic and Cont networks exhibited significantly higher intra-network connectivity associated with hot stimulation in both comparisons. Moreover, SomMot network showed significantly higher intra-network connectivity in absolute comparison but marginally higher intra-network connectivity for relative comparison.

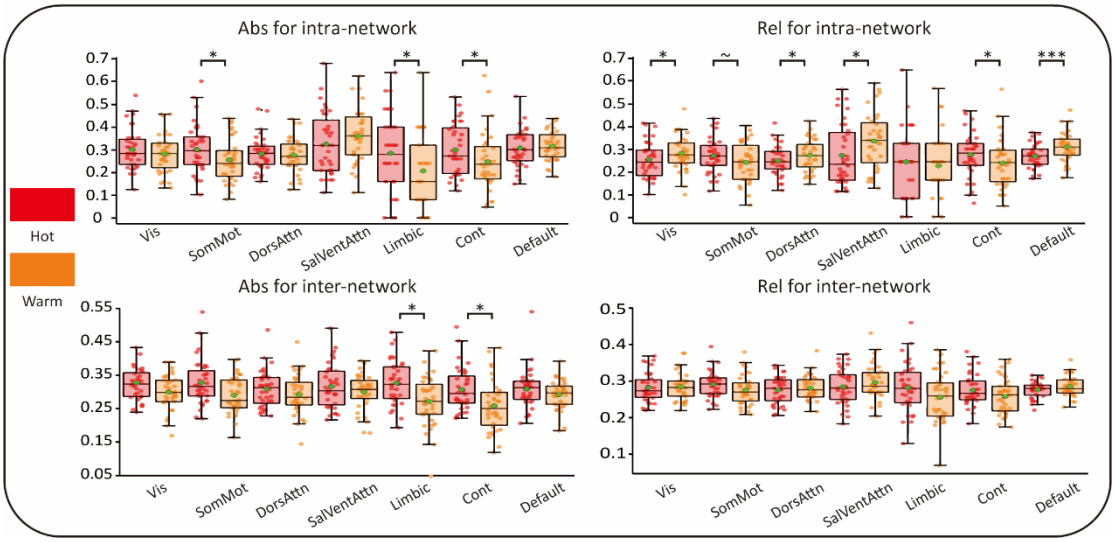

Figure 3.5. Intra-network and inter-network connectivity strength. Box plots display intra- and inter-network mean connections were performed using a paired-sample t-test with FDR correction for two comparison methods. SomMot exhibited greater intra-network connectivity in the hot condition compared to the warm condition for both comparison methods. Abs, absolute comparison; Rel, relative comparison; Vis, Visual; SomMot, Somato-Motor; DorsAttn, Dorsal Attention; SalVentAttn, Salience-Ventral Attention; Cont, Control. *P < .05, **P < .01, ***P < .001, "~" indicates the difference is marginally significant.

Table 3.4. Connectivity strength results (FDR-corrected t-tests).

Network	Connection Type	Comparison	T_{35}	P_{FDR}	95% CI	Cohen's *d*	Direction
Vis	Intra	Relative	-2.39	0.03	[-0.05, 0.00]	0.07	-2.39
SomMot	Intra	Absolute	2.62	0.03	[0.01, 0.08]	0.11	2.62
SomMot	Intra	Relative	2.07	0.05	[0.00, 0.06]	0.35	2.07
DorsAttn	Intra	Relative	-3.06	0.01	[-0.04, -0.01]	0.05	-3.06
SalVentAttn	Intra	Relative	-2.75	0.02	[-0.17, -0.11]	0.14	-2.75
Limbic	Intra	Absolute	2.69	0.03	[0.02, 0.14]	0.17	2.69
Cont	Intra	Absolute	2.74	0.03	[0.01, 0.09]	0.11	2.74
Cont	Intra	Relative	2.53	0.03	[0.01, 0.07]	0.09	2.53
Default	Intra	Relative	-3.61	0.01	[-0.06, -0.02]	0.07	-3.61
Limbic	Inter	Absolute	3.08	0.01	[0.02, 0.09]	0.43	3.08
Cont	Inter	Absolute	3.08	0.01	[0.01, 0.07]	0.43	3.08

Note. Vis, Visual; SomMot, Somato-Motor; DorsAttn, Dorsal Attention; SalVentAttn, Salience-Ventral Attention; Cont, Control

3.3.5. Higher-order intra-SomMot graph results

3.3.5.1. Intra-SomMot connectivity results

Focussing on the SomMot network (Fig. 3.7), group-level graphs exhibited distinct bilateral patterns with a concentration of connections in the right hemisphere in both comparison methods and stimulus conditions (Fig. 3.7A). Although no significant graphs were found post-NBS, *t*-graphs illustrated connections with *t*-values greater than zero. The hot contrast exhibited a bilateral pattern in the absolute comparison (Fig. 3.7A second row first column), whereas in the relative comparison, it showed a left hemisphere-dominated pattern accompanied by cross-hemispheric connections (Fig. 3.7A second row third column). In contrast, the warm contrast (Fig. 3.7A second row second and fourth columns) exhibited a right hemisphere-dominant pattern across both comparison methods.

In summary, we observed that during tonic pain, though not surviving statistical correction, the SomMot network shifted from a right hemisphere-dominant, clustered organisation (warm condition) to a more bilateral, distributed connectivity profile (hot condition) in both comparison methods (Fig. 3.7A, second row).

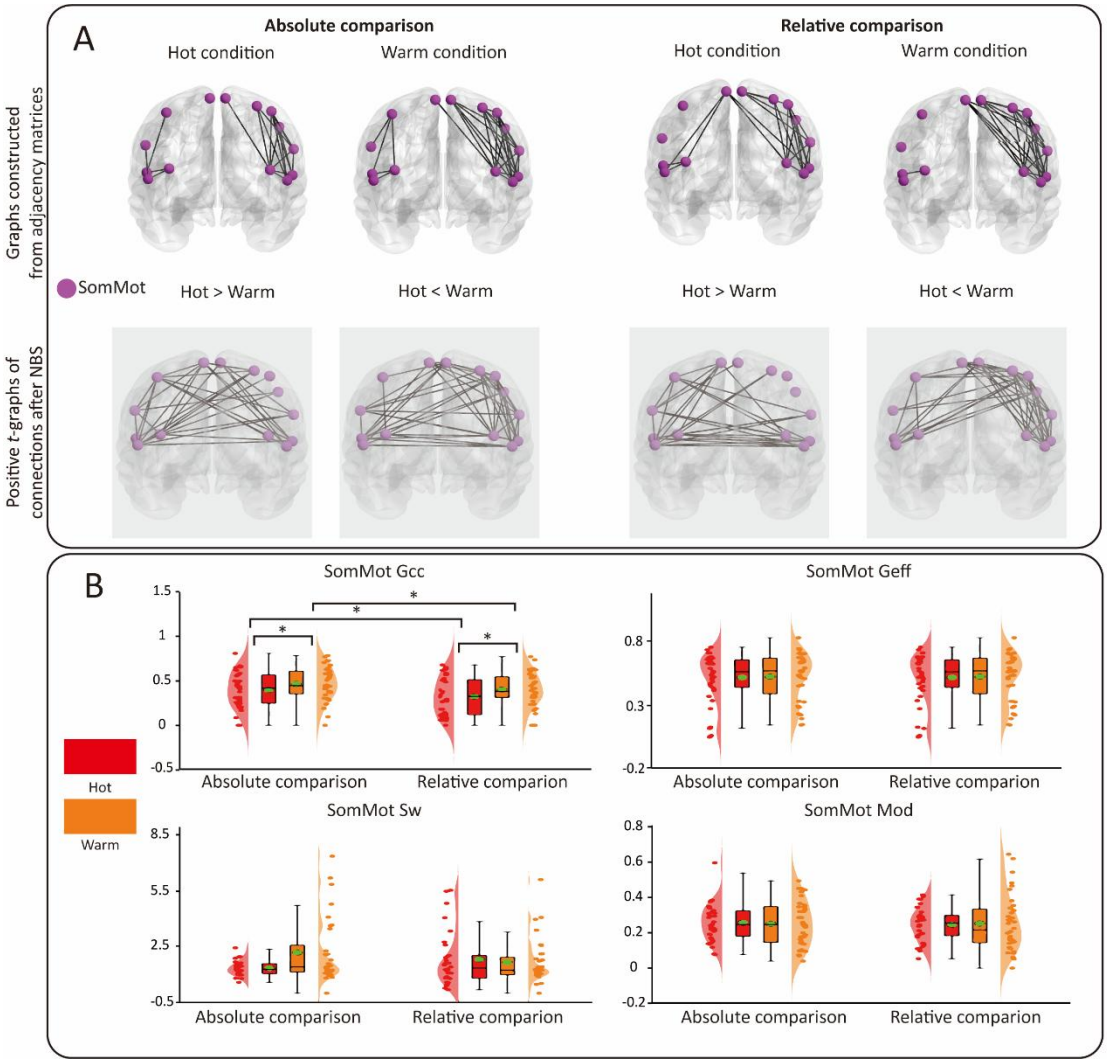

Figure 3.6: Higher-order intra-SomMot graph. (A) Group-level intra-network graphs (upper panel) for the SomMot and corresponding t-graphs (t > 0; shown in reduced opacity indicate non-significant results, in the lower panel) were generated following NBS analysis across different stimulus conditions. The left-half panel for absolute comparison and the right-half panel for relative comparison. (B) Violin plots with overlaid scatter, and box plots illustrate the results of repeated-measures ANOVA with Bonferroni correction for post hoc comparisons of four GNIs across the hot (red) and warm (orange) conditions and two comparison methods. A green-filled circle with a black edge denotes the mean value for each group. The t-graphs from both comparison methods showed less clustered edges distributed bilaterally within intra-SomMot connectivity in hot-preferred comparisons and a right hemisphere-dominated pattern with greater

clustering in the warm-preferred comparisons. The Gcc induced by warm stimulation was significantly larger than that induced by hot stimulation in both comparison methods. NBS, network-based statistics; GNIs, global network inferences; Gcc, global clustering coefficient; Geff, global efficiency; Sw, small-worldness; Mod, modularity. *P < .05, ***P < .001.

3.3.5.2. Intra-SomMot graph results

In the analysis of SomMot graph inferences, only functional segregation (Gcc) showed significant effects (Fig. 3.7B). The Absolute comparison produced higher Gcc than relative for both stimulus conditions, while warm stimulation consistently enhanced Gcc versus hot stimulation across both comparison methods. This pattern aligns with the observed right hemisphere-dominated clustering in warm condition graphs compared to the less clustered intra-SomMot connectivity in hot condition graphs (detailed statistical results are in Table 3.5).

In summary, for connections within the SomMot network across both stimulus conditions, the absolute comparison demonstrated greater functional segregation (Gcc) than relative comparison. Moreover, across both comparison methods, distinct processing dynamics were reflected in significant differences in global segregation, which may account for the contrasting connectivity patterns between conditions. Specifically, Gcc associated with warm stimulation was significantly larger than that induced by hot stimulation, likely due to the distribution of less clustered edges within intra-SomMot connectivity in the hot condition's *t*-graphs (Fig. 3.7 second row first and third columns). In contrast, right hemisphere-dominated patterns with greater clustering were observed in the warm condition's *t*-graphs (Fig. 3.7 second row second and fourth columns).

3.3.6. Higher-order inter-network graph results

3.3.6.1. Inter-network connectivity results

For the inter-network graph results (Fig. 3.8), although no statistically significant effects were observed, both comparison methods consistently indicated greater inter-network communication during hot stimulation compared to warm stimulation. Moreover, the *t*-graphs for the hot contrast in both comparison methods highlighted increased involvement of the DorsAttn and SomMot networks (Fig. 3.8A, third row, first and third columns).

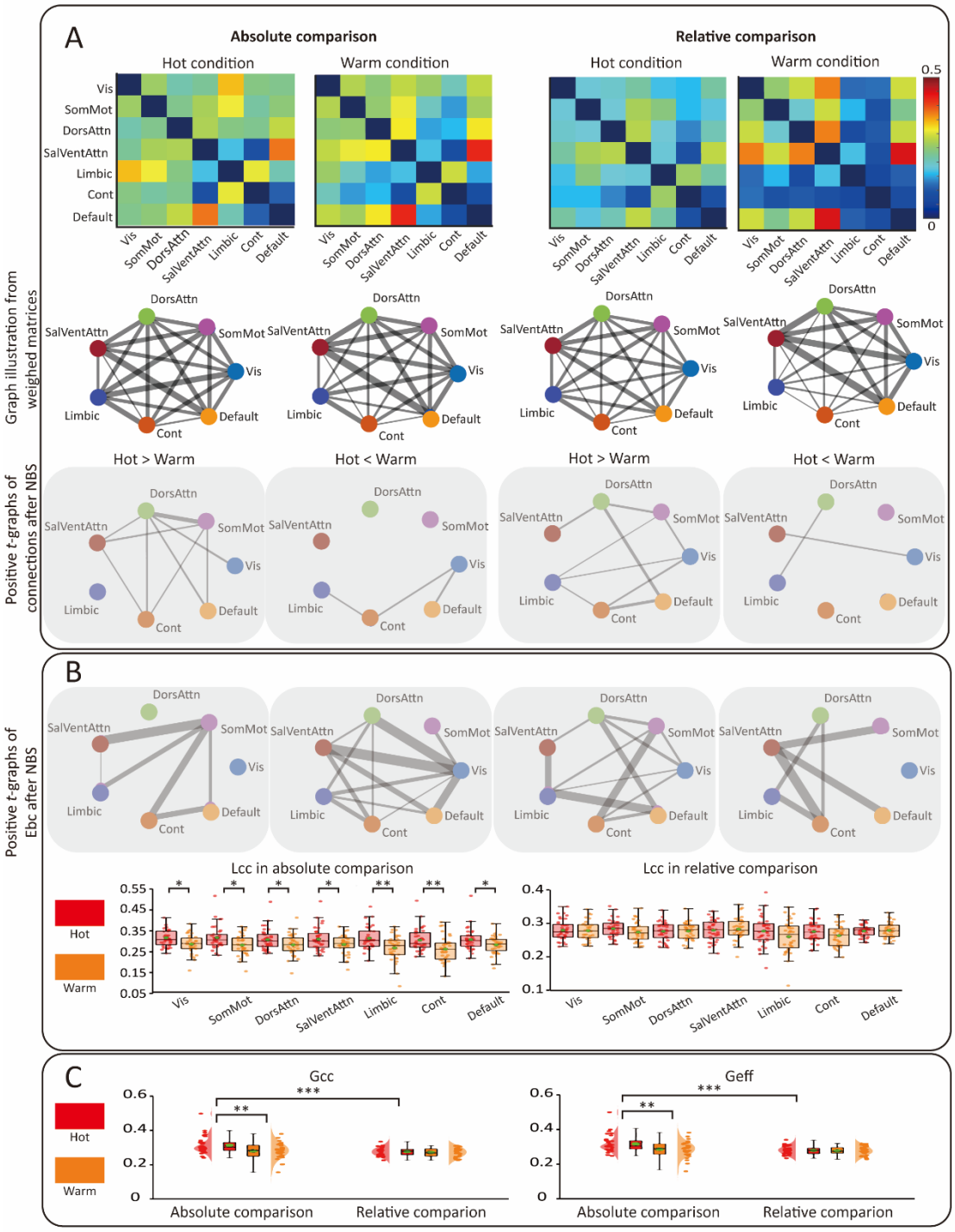

Figure 3.7. Inter-network analysis and local and global graph inferences for inter-network graph. (A) Group-level inter-network weighted matrices (first and second row) and corresponding t-graphs (t > 0; shown in reduced opacity indicate non-significant results, third row) were generated following NBS

analysis across different stimulus conditions. The left-half panel for absolute comparison and the right-half panel for relative comparison. (B) Results for local graph inferences analysis. Ebc corresponded t-graphs generated following NBS (t > 0; shown in reduced opacity, upper panel); box plots illustrate the statistical analysis for Lcc by paired-sample t-test with FDR correction between stimulus conditions for two comparison methods (lower panel). (C) Violin plots with overlaid scatter and box plots show the results of repeated-measures ANOVA with Bonferroni correction for post hoc comparisons of two GNIs across the hot (red) and warm (orange) conditions and two comparison methods. A green-filled circle with a black edge denotes the mean value for each group. The t-graphs illustrating both higher inter-network connectivity and Ebc evoked by hot stimulation emphasised the importance of edges connecting the SomMot network with other networks in both comparison methods. In absolute comparison, higher Lcc across all networks leading to significant higher Gcc in hot condition for inter-network graph. NBS, network-based statistics; GNIs, global network inferences; Gcc, global clustering coefficient; Geff, global efficiency. *P < .05, ***P < .001.

3.3.6.2. Inter-network graph results

Local graph inferences were computed using Ebc, and Lcc for each network in the weighted graph (Fig. 3.8B). Although the effects did not survive statistical correction, the *t*-graph after NBS revealed distinct edges centred on the SomMot network for the hot contrast under the absolute comparison (Fig. 3.8B, upper panel, first column). For Ebc in the hot contrast under the relative comparison, the *t*-graph shared four edges with that of the absolute comparison. Among these, two edges (SomMot–Limbic and SomMot–Cont) represented connections linking the SomMot network with other networks (Fig. 3.8B, upper panel, third column).

All seven networks exhibited significantly higher local clustering (Lcc) under hot versus warm condition in absolute comparison (Fig. 3.8B lower and left panel), while relative comparison (Fig. 3.8B lower and right panel) showed no significant differences (detailed statistics are in Table 3.5).

Table 3.5. Lcc Statistical results in absolute comparisons.

Network	T_{35}	P_{FDR}	95% CI	Cohen's *d*	Direction
Visual	2.93	0.01	[0.14, 0.83]	0.06	Hot > Warm
SomMot	2.96	0.01	[0.14, 0.84]	0.07	Hot > Warm
DorsAttn	2.23	0.03	[0.03, 0.71]	0.07	Hot > Warm
SalVen-tAttn	2.42	0.03	[0.06, 0.74]	0.06	Hot > Warm
Limbic	3.44	0.01	[0.22, 0.92]	0.08	Hot > Warm
Cont	3.47	0.01	[0.22, 0.93]	0.08	Hot > Warm
Default	2.38	0.03	[0.05, 0.73]	0.06	Hot > Warm

Note. Lcc, local clustering coefficient; Vis, Visual; SomMot, Somato-Motor; DorsAttn, Dorsal Attention; SalVentAttn, Salience-Ventral Attention; Cont, Control.

For GNIs from inter-network connections (Fig. 3.8C), both functional segregation (Gcc) and integration (Geff) showed significant stimulus and comparison method effects. Absolute comparison revealed higher Gcc and Geff for hot versus warm stimulation, while relative comparison enhanced both metrics exclusively under hot stimulation. This divergence from intra-network findings reflects hot stimulation's stronger inter-network connectivity, evidenced by greater edge density and edge betweenness centrality in t-graphs. Crucially, these patterns highlight SomMot network's crosstalk with other networks,

particularly through connections strengthened by hot stimulation (detailed statistics are in Table 3.6).

In summary, the GNIs indicated that absolute comparison demonstrates greater functional segregation (Gcc) for inter-network connections recruited by hot stimulation (Fig. 3.8C). The significantly greater Gcc in the inter-network connectivity matrix in the hot compared to the warm condition may be attributed to the significantly higher Lcc in each network from that graph (Fig. 3.8B lower and left panel), reflecting overall enhanced network communication during noxious stimulation. Although NBS-based condition-contrast t-graphs did not survive statistical correction, their spatial pattens showed qualitatively alignment with the network inferences results. Specifically, the larger number of edges in *t*-graph which represents larger inter-network connectivity evoked by hot than warm stimulation in absolute comparison (Fig. 3.8A third row, left-half panel), was consistent with the significant segregation effects captured by Gcc and Lcc.

These patterns were particularly evident in connections involving the SomMot. The *t*-graphs illustrating both higher inter-network connectivity (Fig. 3.8A third row first and third columns) and Ebc evoked by hot stimulation (Fig. 3.8B upper panel first and third columns) emphasised the importance of edges connecting the SomMot network with other networks in both comparison methods. Therefore, the higher-order inter-network graphs highlights the crosstalk of SomMot with other networks.

While these edge-level patterns should be interpreted cautiously given their non-significant status, they provide complementary spatial context to the significant network-level findings revealed by graph-theoretical analysis.

Table 3.6. Statistical results for GNIs from intra-SomMot and inter-network graphs (ANOVA and Post-hoc Comparisons).

Graphs	GNIs	Effect	$F_{1,35}$	P	η_p^2	Post-hoc Comparisons	T_{35}	$P_{Bonferroni}$	95% CI
Intra-SomMot	Gcc	Stim (Main)	7.33	0.01	0.17	Warm > Hot (Abs)	2.39	0.02	[0.01, 0.12]
						Warm > Hot (Rel)	2.55	0.02	[0.02, 0.14]
Intra-SomMot	Gcc	Comp (Main)	6.25	0.02	0.15	Abs > Rel (Hot)	2.14	0.04	[0.01, 0.15]
						Abs > Rel (Warm)	2.52	0.01	[0.01, 0.11]
Inter-network	Gcc	Stim (Main)	5.23	0.03	0.13	Hot > Warm (Abs only)	3	0.01	[0.01, 0.06]
						Hot vs Warm (Rel): ns	1.25	0.25	[-0.00, 0.01]
Inter-network	Gcc	Comp (Main)	6.75	0.01	0.16	Rel > Abs (Hot only)	4.11	<0.001	[0.02, 0.06]
						Rel vs Abs (Warm): ns	1.29	0.21	[-0.01, 0.02]
Inter-network	Gcc	Stim×Comp (Interaction)	7.6	0.01	0.18				
Inter-network	Geff	Stim (Main)	7.81	0.01	0.19	Hot > Warm (Abs only)	2.82	0.01	[0.01, 0.05]
						Hot vs Warm (Rel): ns	1	0.36	[-0.01, 0.01]
Inter-network	Geff	Comp (Main)	14.7	<0.001	0.3	Rel > Abs (Hot only)	4.11	<0.001	[0.02, 0.06]
						Rel vs Abs (Warm): ns	1.43	0.17	[-0.00, 0.02]
Inter-network	Geff	Stim×Comp (Interaction)	6.51	0.02	0.16				

Note. GNIs, global network inferences; Gcc, global clustering coefficients; Geff, global efficiency; Stim, Stimulus; Comp, Comparison; Abs, absolute comparison; Rel, relative comparison.

3.3.7. Correlation between global network inferences and individual differences

We assessed condition-specific relationships between GNIs and unpleasantness ratings for both absolute and relative comparisons (Table 3.7). Under absolute comparisons, six significant associations were identified (Fig 3.7A): inter-network Gcc and Geff positively correlated with unpleasantness during the hot condition (Gcc: $r = 0.35$, $P_{(uncorrected)} = 0.04$; Geff: $r = 0.34$, $P_{(uncorrected)} = 0.04$), while the same GNIs inversely correlated with unpleasantness during the warm condition (Gcc: $r = -0.40$, $P_{(uncorrected)} = 0.02$; Geff: $r = -0.38$, $P_{(uncorrected)} = 0.02$). For the warm condition, sensor space Geff showed a positive correlation ($r = 0.38$, $P_{(uncorrected)} = 0.02$), whereas source space Geff exhibited a negative correlation ($r = -0.40$, $P_{(uncorrected)} = 0.02$) with unpleasantness. These findings suggest that inter-network Gcc and Geff differentially encode tonic hot and warm perception, with opposing directional effects between the two conditions. In contrast, relative comparisons revealed no significant correlations between individual GNIs and unpleasantness ratings (all $P > 0.05$).

No significant correlations were observed between participant age and any GNIs. Similarly, after controlling for age and gender using partial correlation, no significant relationships were found between GNIs and individual differences in pain perception (defined as the mean unpleasantness difference between hot and warm conditions) or pain tolerance (operationalised as the change in unpleasantness from the first to last third of hot stimulation) (all $P > 0.05$).

However, significant associations emerged between GNIs and pain-related psychological traits. Pain catastrophising, as measured by the PCS, showed significant positive correlations with three GNIs derived from the hot

condition in the absolute comparison: source space Gcc (r = 0.55, $P_{(uncorrected)}$ = 0.01); Gcc and Geff from inter-network graph (both r = 0.44, $P_{(uncorrected)}$ = 0.04). Conversely, trait anxiety was negatively correlated with six GNIs under the warm condition: Gcc in absolute condition from intra-SomMot graph (r = −0.44, $P_{(uncorrected)}$ = 0.04), Gcc and Geff in relative comparison from source space graph (Gcc: r = −0.53, $P_{(uncorrected)}$ = 0.01; Geff: r = −0.50, $P_{(uncorrected)}$ = 0.02), Gcc in relative comparison from intra-SomMot graph (r = −0.48, $P_{(uncorrected)}$ = 0.02), Gcc and Geff in relative comparison from inter-network graph (both r = −0.50, $P_{(uncorrected)}$ = 0.02).

Together, these findings suggest that pain-related psychological traits (pain catastrophising and anxiety) significantly shaped functional network characteristics during noxious and innocuous thermal stimulation, even in the absence of effects related to age and gender. Pain catastrophising was associated with greater segregation and integration during noxious stimulation, whereas higher anxiety was linked to reduced network segregation and integration during innocuous warmth.

Table 3.7. Correlation coefficients between GNIs and unpleasantness ratings across graph types and comparison methods during hot and warm conditions.

Conditions	Type of graphs	Comparison method	Correlation Coefficient ($P_{[uncorrected]}$) Gcc	Geff	Sw	Mod
Hot	Sensor space	Absolute	0.09(0.60)	-0.11(0.51)	0.04(0.81)	0.17(0.33)
		Relative	0.04(0.80)	0.00(0.99)	0.05(0.78)	0.28(0.10)
	Source space	Absolute	0.20(0.25)	0.29(0.09)	-0.12(0.50)	-0.24(0.17)
		Relative	-0.12(0.47)	0.12(0.48)	-0.21(0.23)	-0.10(0.57)
	intra-SomMot	Absolute	-0.01(0.93)	0.23(0.19)	-	0.05(0.77)
		Relative	0.22(0.20)	0.14(0.42)	-	0.04(0.82)
	inter-network	Absolute	**0.35(0.04)**	**0.34(0.04)**	-	-
		Relative	0.17(0.32)	0.16(0.35)	-	-
Warm	Sensor space	Absolute	0.18(0.30)	**0.38(0.02)**	0.04(0.84)	0.21(0.21)
		Relative	0.22(0.19)	-0.14(0.43)	0.25(0.14)	-0.26(0.13)
	Source space	Absolute	-0.29(0.09)	**-0.40(0.02)**	0.06(0.74)	0.04(0.82)
		Relative	0.06(0.75)	0.07(0.68)	0.10(0.57)	-0.05(0.79)
	intra-SomMot	Absolute	-0.07(0.66)	-0.11(0.51)	-	-0.10(0.55)
		Relative	0.11(0.51)	0.04(0.80)	-	-0.11(0.51)
	inter-network	Absolute	**-0.40(0.02)**	**-0.39(0.02)**	-	-
		Relative	-0.05(0.78)	-0.03(0.89)	-	-

Note. Correlations were computed between GNIs and mean participant-level unpleasantness ratings. Statistically significant results ($P < 0.05$) are highlighted in bold. All correlations are reported using uncorrected P-values. GNIs, global network inferences; Gcc, global clustering coefficients; Geff, global efficiency; Sw, small-worldness; Mod, modularity.

3.3.8. Classification performance

The SVM classifier robustly distinguished tonic hot and warm conditions using GNIs derived from combined graph inferences, with the top three models based on absolute comparison and showed in Fig. 3.8B. The highest-performing model, integrating GNIs from sensor space, source space, and inter-network graphs, achieved an AUC-ROC of 0.94 ($P < 0.001$), with an accuracy of

86%, sensitivity of 0.78, and specificity of 0.92. The second-ranked model attained an accuracy of 85%, sensitivity of 0.75, and specificity of 0.89 (AUC-ROC = 0.93, $P < 0.001$) from GNIs in sensor space and inter-network graphs. Combining GNIs from sensor and source space graphs results in the third best-performance, with an accuracy of 83%, sensitivity of 0.78, and specificity of 0.89 (AUC-ROC = 0.92, $P < 0.001$). These results demonstrate the robust discriminative power of GNIs, particularly when combining multimodal graph features, in distinguishing between tonic hot and warm states. The high performance (accuracy above 80% and AUC-ROC above 0.90) highlights their potential as a biomarker framework for decoding tonic pain-related neurophysiological mechanisms.

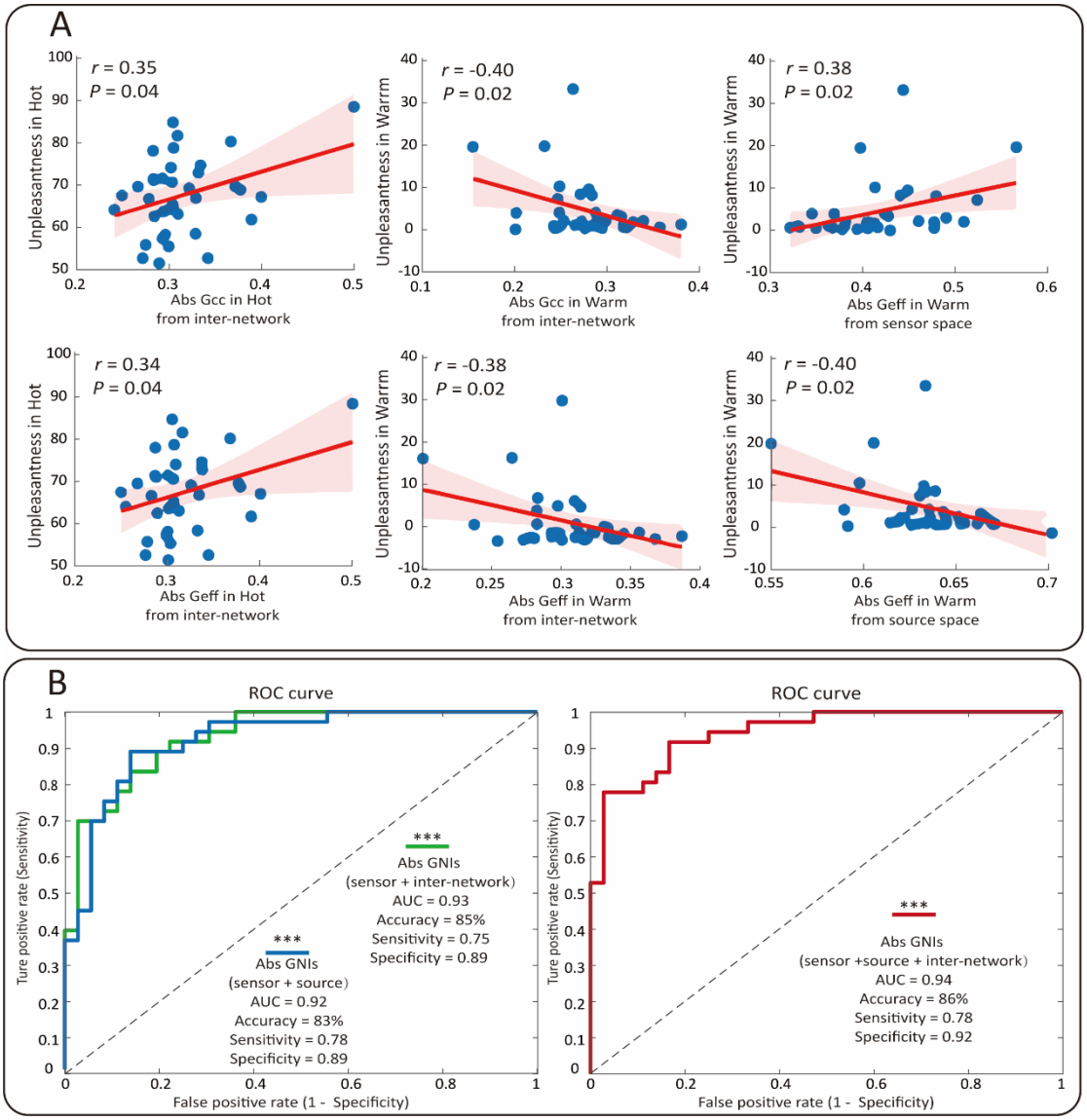

Figure 3.8. Correlation between single GNIs and behavioural ratings, and classification prediction performance. (A) Scatter plots with linear fit and 95% confidence intervals illustrating the correlations between significant individual GNIs and unpleasantness ratings within each stimulation condition. All correlations are reported using uncorrected P-values and should be interpreted with caution. (B) Classification performance was evaluated using leave-one-subject-out cross-validation with an SVM classifier. The top three performing models are presented, with the best performance highlighted in red, the second-best in green, and the third in blue. The highest classification performance was achieved using a combination of GNIs derived from sensor space, source

space, and inter-network graphs, yielding an AUC-ROC of 0.94, an accuracy of 86%, a sensitivity of 0.78, and a specificity of 0.92. Abs, absolute comparison; GNIs, global network inferences; Gcc, global clustering coefficients; Geff, global efficiency; ROC, receiver operating characteristic; AUC, area under curve. ****P* < .001.

3.4. Discussion

We systematically examined EEG functional connectivity patterns during tonic thermal pain in healthy volunteers using network-based statistics and graph theory-based analysis. Our study yielded four main findings. First, we identified a significant brain-wide reorganisation of connectivity during tonic pain, marked by a shift from functional segregation to integration. Second, contrasting segregation effects confirmed the transition from intra- to inter-network communication with enhanced SomMot-centred crosstalk. Third, we found significant correlations between pain-related psychological states and global network inferences (GNIs). Moreover, the model integrating GNIs achieved high classification performance (highest AUC-ROC of 0.94; accuracy of 86%; Fig. 3.8B), demonstrating robust discriminative power. Fourth, we highlight the critical influence of comparison methods and thresholding strategies.

3.4.1. Reorganisation of the brain-wide graph from segregation into integration

We observed a consistent and significant decline in functional segregation (specialisation) and enhanced functional integration (efficiency of global information flow) during tonic pain in both sensor and source spaces (Fig. 3.3C and 3.3C). This shift, accompanied by significantly decreased modularity (Mod,

Fig. 3.3C) and small-worldness (Sw, Fig. 3.5C), suggested a shift toward a more randomised and less cost-efficient network architecture (Liao et al., 2017). These findings aligned with alternations observed in the neuropathic pain patients (Xin et al., 2024), and a multi-centre study in chronic pain cohorts (Mano et al., 2018), indicating a fundamental and sustained characteristic shared between experimental tonic pain and clinical chronic pain, which may reflect robust nociceptive integration (Kastrati et al., 2022; Zheng et al., 2020).

This global topological alteration was underpinned by a reorganisation of brain-wide connectivity. In sensor space, we identified significantly different connectivity patterns (Fig. 3.3A-B). Although these patterns did not survive statistical correction in source space, the consistent trend supports the reliability of the topological reorganisation: a shift from contralateral functional specialised sensorimotor connectivity during warm (Fig. 3.5A-B, fourth row right panel; 3.4A, lower panel second and fourth columns) to ipsilateral integrated frontoparietal connectivity during pain (Fig. 3.5A-B, fourth row left panel). The emergent frontoparietal pattern, associated with the cognitive control network (Kong et al., 2013; Kutch et al., 2017) is implicated in attention, salience processing, and top-down modulation of pain (Corbetta & Shulman, 2002; Torta et al., 2017). Conversely, innocuous warmth was associated with strengthened contralateral sensorimotor connectivity (Fig. 3.5A-B, fourth row right panel; 3.4A, lower panel second and fourth column). The absence of the contralateral connectivity during pain might be linked to local suppression of alpha-band oscillation originating in the sensorimotor cortex (Nickel et al., 2017, 2020; Peng et al., 2014; Ploner et al., 2017; H. Wang et al., 2023). This asymmetry may reflect alpha-band event-related desynchronisation (ERD), which through thalamocortical circuits

(Hughes & Crunelli, 2005; Klimesch, 2012) and gamma-aminobutyric acid inhibition (J. A. Kim & Davis, 2021; Lőrincz et al., 2009), supporting the functional inhibition hypothesis by facilitating selective gating of information flow, suppression of irrelevant sensory input, and engagement of top-down cognitive processes for attention (Jensen & Mazaheri, 2010; Klimesch, 2012; Peng et al., 2015).

3.4.2. Transition of the SomMot network

Focused on the SomMot network, the innocuous warmth exhibited significant higher Gcc (Fig. 3.7B), reflecting higher functional specialisation. This finding aligns with prior identification of a distinct processing system overlapping with resting-state modules and subserving sensory-discriminative functions (Zheng et al., 2020), whereas the noxious hot pattern aligns with SomMot integration with control and ventral attention (salience) networks (J. Kim et al., 2013; Lee et al., 2021, 2022; Zheng et al., 2020).

This network property difference was reflected in the connectivity patten within SomMot, with the warm condition producing a right hemisphere-dominated pattern (Fig. 3.7A, lower panel second and fourth columns), while the hot condition elicited a more bilateral distribution (Fig. 3.7A, lower panel first and third columns). Although these connectivity patterns were not statistically significant, their alignment across comparison methods supports a dynamic shift in SomMot processing.

Furthermore, we found consistent, though non-significant, greater number of edges clustering around the SomMot (Fig. 3.8A, third row first and third columns) and greater edge betweenness centrality (Ebc) (Fig. 3.8B, upper panel first and third columns), highlighting the SomMot central role in between-

network communication. This adaptability may reflect rapidly increased synaptic plasticity in the primary somatosensory cortex induced by nociception (Cao et al., 2019; W. Kim et al., 2017; Kuner & Flor, 2017), mechanisms potentially disrupted in chronic pain (H. Kim et al., 2020; Pfannmöller et al., 2019; Vittersø et al., 2022). Taken together, these findings highlight the SomMot network's dual functionality: localised sensory processing for non-painful somatosensory experiences versus integrative coordination during pain.

3.4.3. Shift from intra-network to inter-network connectivity

We observed decreased segregation at the brain-wide level during tonic pain (lower Gcc; Fig. 3.3C and 3.4C) whereas inter-network connectivity exhibited increased local clustering (Lcc; Fig. 3.7B) and segregation (higher Gcc; Fig. 3.7C). This discrepancy arose from the exclusion of intra-network connections, which artificially inflated Gcc by removing interconnected local clusters. This methodological distinction explains conflicting prior results: while the community detection method found increased Gcc with reduced connectivity between an integrated "pain supersystem" and other networks during pain (Zheng et al., 2020), canonical network analysis using atlas defined parcellation (like ours) reported increased segregation (Gcc) only during the innocuous condition, with enhanced between-network connectivity (Kastrati et al., 2022).

Based on Gcc variations, intra-network connections prioritise nociceptive information, facilitating a shift from segregated to integrated brain states. This was observed in the SomMot network and aligns with reduced intra-network connectivity found in sustained myofascial pain (J. Kim et al., 2013) and Fibromyalgia patients (J. Kim et al., 2015), indicating a transition from functional

specialisation under innocuous stimulation to broader integration during pain experience.

Such integration was also reflected by overall elevation of Lcc (Fig. 3.8B, lower panel absolute comparison) and greater number of edges in the inter-network graphs (Fig. 3.8A, third row first and third columns). These results align with previous research showing that thermal pain induces a brain-wide shift from segregation to integration, with enhanced between-network connectivity (Kastrati et al., 2022). Specifically, capsaicin-induced sustained pain has been associated with the emergence of a SomMot-dominant neural community, wherein ventral primary SomMot regions showed dissociated from their original network and incorporated with subcortical and frontoparietal regions (Lee et al., 2022). A finding also replicated in patients with chronic low back pain (Zhu et al., 2024) and postherpetic neuralgia (H. Li et al., 2022).

In summary, while methodological factors explain Gcc discrepancies, our results converge to show that tonic pain induces an alteration from localised functional specialisation within intra-network to enhanced inter-network communication and global integration. This reorganisation, centred on SomMot connectivity, underscores the dynamic balance between segregation and integration in shaping pain-related brain states (Hemington et al., 2016; Kucyi & Davis, 2015).

3.4.4. Global network inferences as a potential translational biomarker

By integrating GNIs, we achieved high classification performance in distinguishing noxious hot from innocuous warm stimulation and identified significant links with pain-related psychological states. Psychological traits modulated

pain-related network reorganisation in distinct and clinically relevant ways: catastrophising predominantly influenced responses to noxious stimuli, whereas anxiety affected innocuous sensory processing.

While our findings provide a general model of pain-related network dynamics under controlled conditions, their generalisation to chronic pain populations warrants caution. Chronic pain involves neuroplastic adaptations and compensatory mechanisms that may alter functional network signatures, with psychological influences potentially amplified.

Translating GNIs into clinically useful biomarkers will require validation in large, multi-centre datasets accounting for comorbidities, medication, and pain duration. Future work should also explore the use of GNIs for real-time monitoring of psychological states and their integration into closed-loop neuromodulation, ensuring interpretability and reliability across clinical contexts.

3.5. Conclusion

Altogether, these findings provide compelling evidence that tonic experimental pain in healthy volunteers is associated with significant reorganisation of alpha EEG connectivity. The hallmark of this reorganisation is a shift from high intra-network functional segregation (especially the SomMot network) to inter-network integration via enhanced communication. Furthermore, the robust predictive performance of GNIs highlights their translational potential as biomarkers for pain states. The novel contribution of this work is the precise quantification of this network reorganisation, validated by robust classification and linked to individual psychological differences.

Chapter 4

Cross-state signatures of sensory stimulation: EEG network markers of neuroplasticity in resting-states conditions pre- and post-sensory stimulation

Following the findings in Chapter 3, where dynamic brain functional reorganisation induced by tonic noxious and innoxious sensory stimulation enabled high discrimination performance, this study extends the investigation to resting-state conditions before and after sensory stimulation, aiming to provide insights that could inform future classification of chronic pain patients.

4.1. Introduction

Resting-state brain activity has emerged as a promising biomarker for chronic pain and has been widely investigated using non-invasive neuroimaging techniques such as fMRI (Pfannmoller & Lotze, 2019), MEG, and EEG (Mussigmann et al., 2022; Zebhauser et al., 2023). Among these, EEG-derived resting-state biomarkers are particularly appealing due to their high temporal resolution, sensitivity to oscillatory synchronisation, and suitability for clinical translation. Nevertheless, findings from EEG studies remain heterogeneous, and the risk of bias is often high (Zebhauser et al., 2023).

Beyond objective pain assessment, resting-state EEG has also been deployed to evaluate non-invasive brain stimulation for pain relief (Lloyd et al., 2020; K. L. Zhang et al., 2021). For example, Ahn et al.(2019), conducted a randomised, crossover, double-blind, sham-controlled study in patients with chronic low back pain and found that targeted transcranial alternating current stimulation (tACS) in the alpha band enhanced alpha oscillations in the somatosensory cortex, which correlated with pain alleviation. Notably, although both eyes-open (EO) and eyes-closed (EC) resting-state data were collected, only EO served as the baseline. This omission not only represented a loss of potentially valuable data but also contributed to the observed heterogeneity in outcomes. This variability underscores the critical influence of context on resting-state measures, especially in clinical populations.

Resting-state activity can be strongly modulated by preceding experiences, as demonstrated in substance use disorders and phobias where anxiety-inducing tasks altered post-task resting-state patterns (Lor et al., 2023).

Within patient cohorts, EEG-based resting-state measures have also predicted acute postoperative pain (Q. Han et al., 2025). Furthermore, in healthy participants, pain-free resting-state functional networks predicted individual differences in pain sensitivity (Spisak et al., 2020), and the Default EEG connectivity at alpha band explained variance in individual pain-related vulnerability and predicted experimental peak pain intensity (Alhajri, Boudreau, Mouraux, et al., 2023).

The Default's centrality in pain processing is well-documented. Kucyi and Davis (2015) proposed that pre-task spontaneous Default activity largely reflected intrinsic physiological processes related the interaction between pain and attention, forming part of the “neural signature” of the pain connectome. This network consistently showed alterations during acute, tonic and chronic pain states (Alhajri, Boudreau, & Graven-Nielsen, 2023; Alshelh et al., 2018; Makovac et al., 2020). Crucially, a differential effect of functional connectivity has been found between EO and EC resting-state conditions: pain exposure reduced alpha connectivity in Default hubs (angular gyrus, posterior cingulate cortex, and medial prefrontal cortex) exclusively during EC (Alhajri et al., 2022). This distinct modulation underscores the role of eyes-state-dependent intrinsic functional topography in shaping pain processing.

The fundamental characteristics of EO and EC resting-states in healthy individuals have been revealed by fMRI studies showing distinct connectivity patterns. For instance, connectivity between the posterior cingulate cortex and other brain regions was greater during EO than EC, whereas connectivity between the thalamus and visual cortex, and between the posterior cingulate cortex and bilateral perisylvian regions, was reduced during EO (Jao et al., 2013).

The primary visual cortex exhibited stronger connectivity with the Default and sensorimotor networks in EC, but stronger connectivity with the salience network in EO (Costumero et al., 2020). Similarly, EC has been associated with increased connectivity of auditory and sensorimotor networks to other networks (Agcaoglu et al., 2019).

Recent work examining seven networks during resting-state condition: salience network, Default, central executive network, dorsal attention network, visual network, motor network, and auditory network and found increased connectivity between most networks during EC relative to EO, suggesting enhanced integration during EC and greater modularity during EO. Interestingly, the salience network showed increased connectivity with Default and decreased connectivity with visual network during the EO-to-EC transition, suggesting a “circuit-switch” role in modulating network relationships (J. Han et al., 2023).

While fMRI studies have provided a detailed picture of these differences, fewer EEG studies have explored EO-to-EC transitions at the level of brain dynamics. Recent EEG studies capturing the brain dynamics using the phase lag index have further shown frequency-specific changes in coupling strength and variability during EO-to-EC transitions, particularly in alpha-band connectivity within Default and central executive networks (Krukow et al., 2024).

Building on this foundation, the present study examined changes in EEG based resting-state functional connectivity in both EO and EC conditions, before and after sensory stimulation (including tonic pain). We applied brain-wide and higher-order graph measures to capture both connectivity patterns and network topology, with four aims: (1) to characterise the neuroplasticity of

functional connectivity and network topology following sensory stimulation; (2) to evaluate whether the time-dependent changes differ between EO and EC resting-state conditions; (3) to elucidate their underlying neuronal mechanisms; and (4) to assess the classification performance of global network inferences (GNIs) for distinguishing pre- versus post-stimulation resting-states for their translational potential.

We hypothesised that sensory stimulation would induce reconfiguration of functional connectivity in both EO and EC post-stimulation resting-states, detectable through both connectivity and graph-theoretical analyses, with the Default playing an essential role. We further expected that GNIs would demonstrate robust predictive power for classifying pre- versus post-stimulation states.

4.2. Methods

4.2.1. Participants

The same secondary dataset used in Study 1 (Chapter 3) was also employed in Chapter 4. However, due to the extremely short duration of the EC condition following stimulation, data from participant 19 were excluded from the analysis. This resulted in a final sample of 35 participants.

4.2.2. Experimental procedure and data analysis

Resting-state EEG recordings were collected at the beginning and end of the stimulation session. Each session included both EO and EC conditions, each lasting approximately 2.5 minutes. The data preprocessing and analysis procedures followed those described in Study 1 (Chapter 3).

Specifically, four types of connectivity graphs were constructed from the pre-processed data using dwPLI in the alpha band: sensor-graph, source-graph,

intra-network graph, and inter-network graph. Connectivity analysis was performed using the NBS, and GNIs were analysed via repeated-measures ANOVA with Bonferroni-corrected post hoc paired t-tests. Intra- and inter-network connectivity strengths and Lcc measures were examined using FDR-corrected paired t-tests. Differences in Ebc were also identified using NBS.

The analytical design of Chapter 4 was largely identical to that of Study 1 (Chapter 3), with one key difference: the intra-network analysis focused on the Default rather than the SomMot network, due to the relevance of Default to resting-state conditions.

In addition to absolute comparisons, relative comparisons between EO and EC conditions were also conducted. For relative EO connectivity, each participant's functional connectivity matrix was normalised by their corresponding EC matrix (pre- or post-stimulation), and vice versa for relative EC connectivity.

4.2.3. Machine learning classification

GNIs were extracted as features for classification tasks, derived separately from each graph type (sensor space, source space, intra-network, and inter-network) and for both absolute and relative connectivity measures. This resulted in nine GNI features per condition for evaluating classification performance in distinguishing pre- and post-stimulation states.

Given the focus on the Default, classification analyses involving intra-network features included only the intra-Default within each eyes condition. Additionally, classification was also performed using all seven intra-networks, particularly for combined EO and EC conditions.

Classification was conducted using the same procedure as in Study 1 (Chapter 3). A linear Support Vector Machine (SVM) with L2 regularisation (λ

optimised within each fold) was trained and evaluated using leave-one-subject-out cross-validation (n = 35). Features were z-score normalised within each training fold. Model performance was assessed using area under the ROC curve (AUC-ROC), accuracy, sensitivity, and specificity.

Statistical significance was evaluated via 1,000 permutation tests, where class labels were randomly shuffled to create a null distribution of AUCs. The empirical p-value was calculated as the proportion of permuted AUCs exceeding the observed AUC, reflecting the probability of achieving the result by chance.

4.3. Results for eyes-open conditions

4.3.1. Results in sensor space

4.3.1.1. Sensor space connectivity: absolute comparison

In the sensor space (Fig. 4.1), group-level graph construction in the axial plane revealed that edges in the EO pre-stimulation condition (EO-pre) were clustered from the central to occipital regions, particularly within occipital areas and predominantly in the right hemisphere for the absolute comparison (Fig. 4.1A left). In contrast, the EO post-stimulation condition (EO-post) exhibited a more widespread pattern, extending from the prefrontal to occipital regions, with dense connections still evident within the occipital area (Fig. 4.1A right).

NBS analysis revealed a significant graph showing greater connectivity in the EO-pre compared to the EO-post condition, comprising 61 nodes and 131 edges, distributed mainly across both hemispheres, with edges linking the right central and left central-parietal regions ($P = 0.03$). Conversely, a significant graph showing greater connectivity in the EO-post compared to EO-pre

condition comprised 55 nodes and 126 edges, with connections spanning within and between both hemispheres ($P < 0.04$).

4.3.1.2. Sensor space connectivity: relative comparison

The relative EO pre- and post-stimulation conditions showed distinct differences only in the P-graphs, not in the group-level graphs (Fig. 4.1B). At the group level, connections were generally distributed across anterior regions, from prefrontal to central electrodes in both pre- and post-stimulation conditions.

The NBS revealed a significant pattern of greater connectivity in the relative EO-pre condition, with connections predominantly extending across posterior regions, comprising 58 nodes and 183 edges ($P < 0.001$) in the relative EO-pre than EO-post condition. In contrast, the relative EO-post condition exhibited a significant graph with greater connectivity than EO-pre, showing a pattern clustered in anterior regions, comprising 55 nodes and 171 edges ($P < 0.001$).

From the brain-wide graphs, we observed marked differences in connectivity patterns between the two comparison methods in sensor space. In the absolute comparison, connectivity in the group-level graphs was predominantly distributed in anterior regions, whereas in the relative comparison, connections were concentrated in posterior regions.

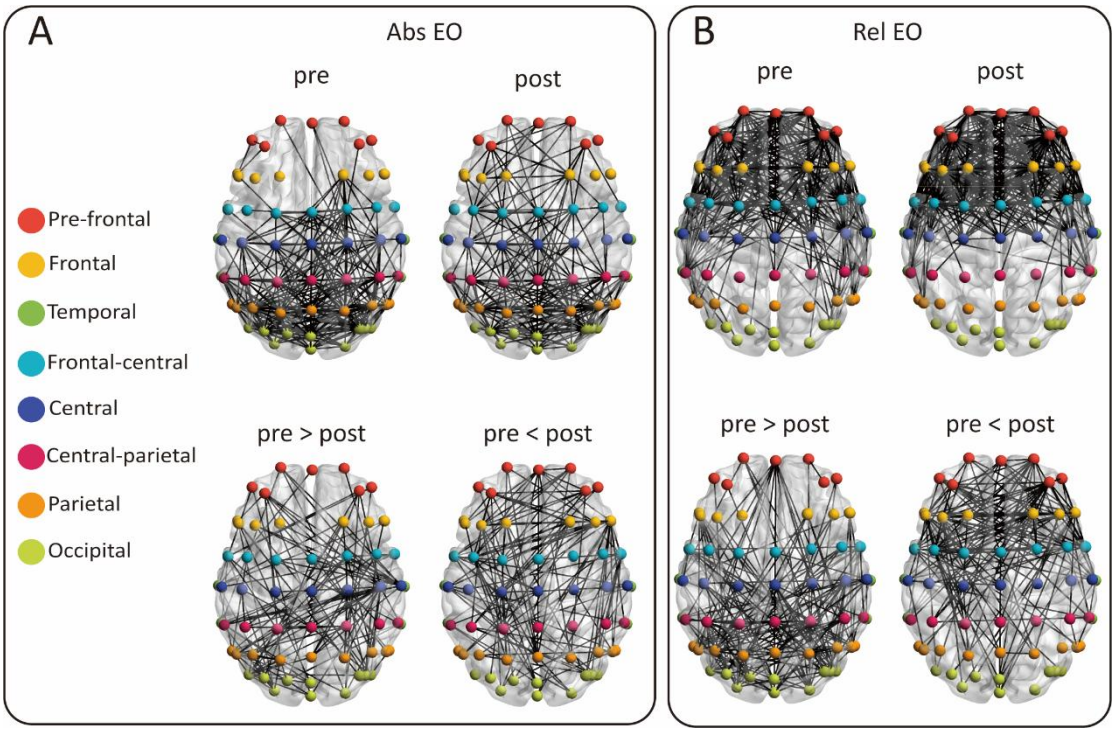

Figure 4.1. Graphs elicited by EO conditions pre- and post- stimulation using two comparison methods in sensor space. (A) Group-level functional connectivity graph for EO pre- and post-stimulation (first row). Sensors corresponding to different scalp regions (Prefrontal, Frontal, Temporal, Frontal-central, Central, Central-parietal, Parietal, and Occipital) were colour-labelled for visual distinction. State-specific significant connectivity patterns were identified using NBS and visualised as *P*-graphs (second row). (B) Similar to (A) but for relative comparison. In the absolute comparison, connectivity in the group-level graphs was predominantly distributed in anterior regions, whereas in the relative comparison, connections were concentrated in posterior regions. EO, eyes-open; NBS, network-based statistics; Abs, absolute comparison; Rel, relative comparison.

4.3.1.3. Sensor space graph analysis results

Significant main effects of comparison method (absolute vs. relative) were observed across all GNIs except small-worldness (Sw): functional segregation (Gcc), integration (Geff), and modularity (Mod) (Fig. 4.2).

Post hoc comparisons showed that the relative comparison significantly increased Gcc compared to the absolute comparison after stimulation (t (34) = 5.79, $P < 0.001$), whereas no significant difference was found at the pre-stimulation timepoint.

For Geff, a strong main effect of comparison method was detected, with significantly higher values in the relative comparison than in the absolute comparison both pre- (t (34) = 6.57, $P < 0.001$) and post-stimulation (t (34) = 8.17, $P < 0.001$).

Modularity was higher in the absolute comparison than in the relative comparison at both pre- (t (34) = 4.13, $P < 0.001$) and post-stimulation (t (34) = 9.13, $P < 0.001$). A significant interaction effect was also observed: Mod decreased from pre- to post-stimulation in the relative comparison (t (34) = 3.00, $P < 0.01$), whereas no significant change occurred in the absolute comparison.

A significant main effect of time was found only for Gcc, which was higher post-stimulation under the relative comparison (t (34) = 3.81, $P < 0.001$), while no significant change was detected in the absolute comparison.

Small-worldness exhibited a significant interaction between comparison method and time. Post hoc analysis revealed that Sw increased significantly in the relative comparison after stimulation (t (34) = 4.10, $P < 0.001$), while the absolute comparison showed no change. Furthermore, Sw was higher in the

relative than in the absolute comparison post-stimulation only (t (34) = 2.93, P < 0.01).

Detailed ANOVA statistics and post-hoc comparisons are provided in Table 4.1.

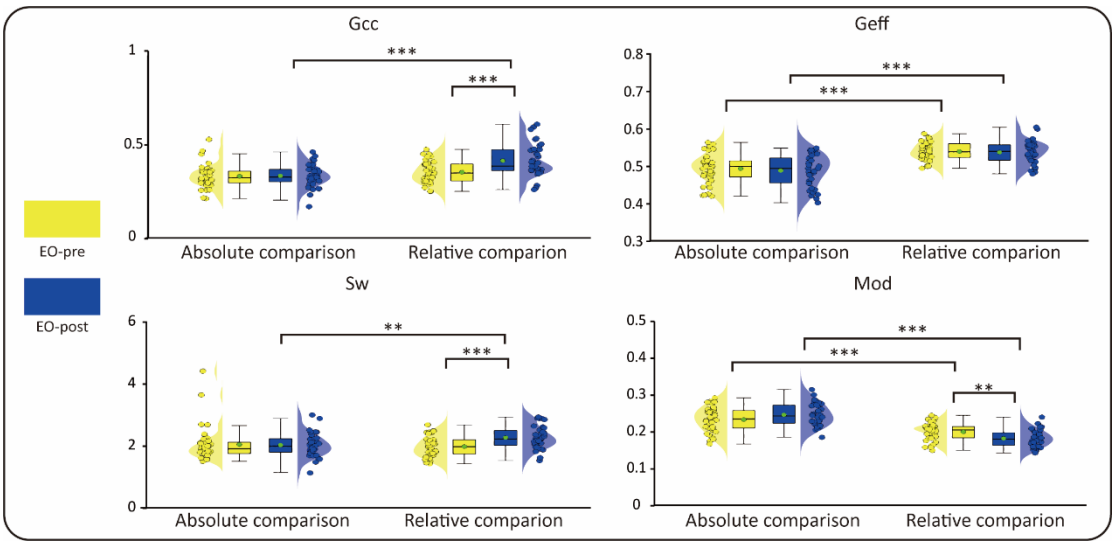

Figure 4.2. Graph analysis results for EO conditions pre- and post- stimulation using two comparison methods in sensor space. Violin plots with overlaid scatter and box plots show the results of repeated-measures ANOVA with Bonferroni correction for post hoc comparisons of four GNIs across the pre (yellow) and post (blue) conditions and two comparison methods. A green-filled circle with a black edge denotes the mean value for each group. EO, eyes-open; GNIs, global network inferences; Gcc, global clustering coefficient; Geff, global efficiency; Sw, small-worldness; Mod, modularity. *P < .05, ***P < .001.

4.3.2. Results in source space

4.3.2.1. Source space connectivity results: absolute comparison

In the source space (Fig. 4.3), the group-level graph in the EO-pre and EO-post both exhibited a predominantly left-hemisphere distribution (Fig. 4.3A). No significant graph was identified when comparing pre- and post-stimulation conditions.

The t-graphs illustrating greater connectivity in the EO-pre condition revealed clustering across both hemispheres in the central regions. In contrast, connectivity patterns with greater connections in the EO-post condition were concentrated around the central regions in the left hemisphere.

4.3.2.2. Source space connectivity results: relative comparison

For relative comparisons (Fig. 4.3B), no clear ipsilateral connectivity patterns were observed in the group-level graphs. Although no statistically significant graph was identified between conditions, the t-graph for the relative EO-pre condition showed right-hemisphere localised connectivity, whereas the relative EO-post condition demonstrated a bilateral distribution of connections.

In source space, the absolute comparison produced left-hemisphere-dominated group-level graphs. In the EO-pre condition, the absolute comparison showed bilaterally distributed larger connectivity, whereas the relative comparison emphasised inter-hemispheric connections, particularly from the right frontal to the left parietal regions. In the EO-post condition, both comparison methods displayed more bilaterally distributed patterns.

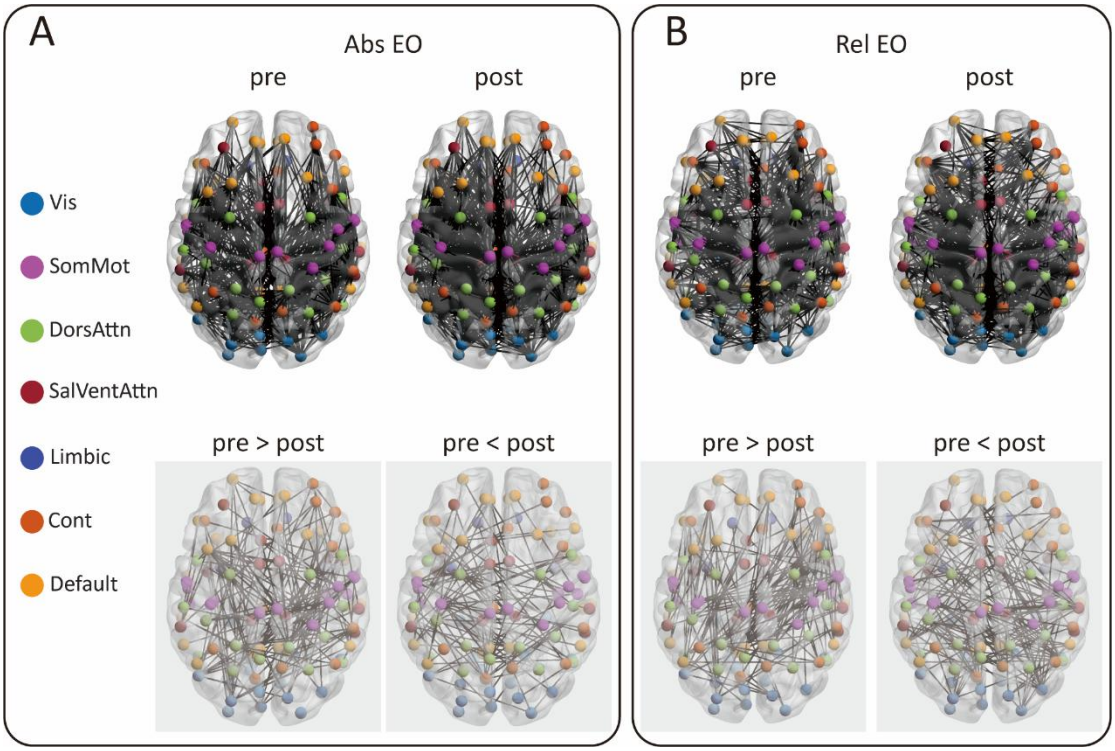

Figure 4.3. Graphs elicited by EO conditions pre- and post- stimulation using two comparison methods in source space. (A) Group-level functional connectivity matrices for hot and warm stimulation (first row) projected in source space for 100 pairs of brain regions organised into 7 different functional networks (Visual, Somato-motor, Dorsal Attention, Salience-Ventral Attention, Limbic, Control, and Default). The *t*-graphs (second row) constructed from connections with a t-value larger than 1.69 compared between conditions using NBS (shown in reduced opacity). (B) Similar to (A) but for relative comparisons. The absolute comparison produced left-hemisphere-dominated group-level graphs. In the EO-pre condition, the absolute comparison showed bilaterally distributed larger connectivity, whereas the relative comparison emphasised inter-hemispheric connections, particularly from the right frontal to the left parietal regions. In the EO-post condition, both comparison methods displayed more bilaterally distributed patterns. EO, eyes-open; NBS, network-based statistics; Abs, absolute comparison; Rel, relative comparison.

4.3.2.3. Source space graph analysis results

Significant main effects of comparison methods (absolute vs. relative) were observed only in Sw (Fig. 4.4), where post-hoc comparisons showed that the relative comparison significantly increased Sw compared to the absolute comparison both pre- (t (34) = 3.58, P < 0.001) and post-stimulation (t (34) = 2,78, P < 0.01).

A significant main effect of time was found only for Gcc, with higher values in the pre-stimulation period under the absolute comparison (t (34) = 2.50, P = 0.02), but no significant change was found post-stimulation.

Detailed ANOVA statistics and post-hoc comparisons are provided in Table 4.1.

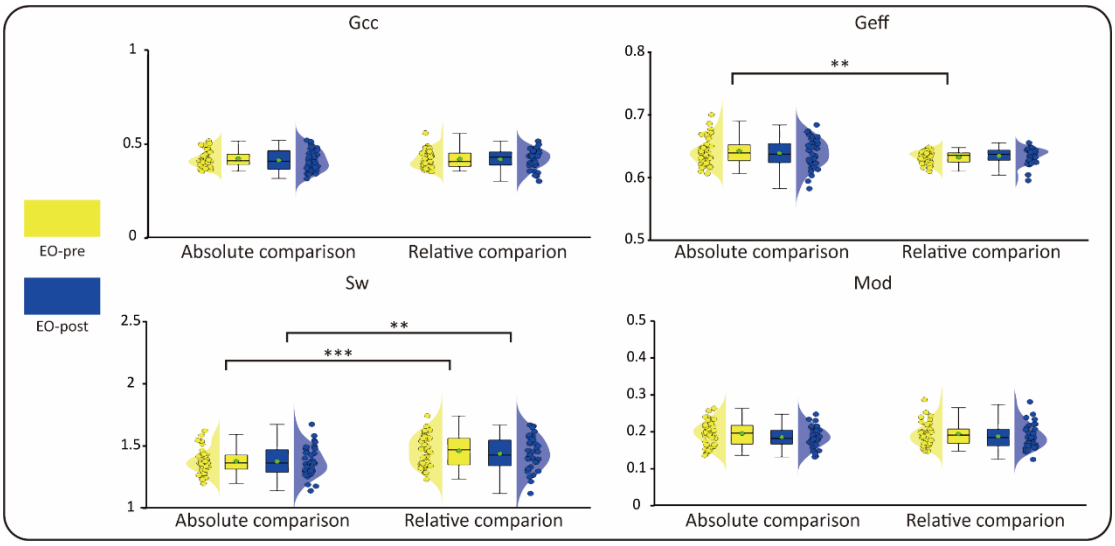

Figure 4.4. Graph analysis results for EO conditions pre- and post- stimulation using two comparison methods in source space. Violin plots with overlaid scatter and box plots show the results of repeated-measures ANOVA with Bonferroni correction for post hoc comparisons of four GNIs across the pre (yellow) and post (blue) conditions and two comparison methods. A green-filled

circle with a black edge denotes the mean value for each group. EO, eyes-open; GNIs, global network inferences; Gcc, global clustering coefficient; Geff, global efficiency; Sw, small-worldness; Mod, modularity. **P < .01, ***P < .001.

4.3.3. Intra- and inter-network connectivity strength

No significant differences were found in intra- or inter-network connectivity strength for EO conditions between pre- and post-stimulation using either comparison method in source space (Fig. 4.5).

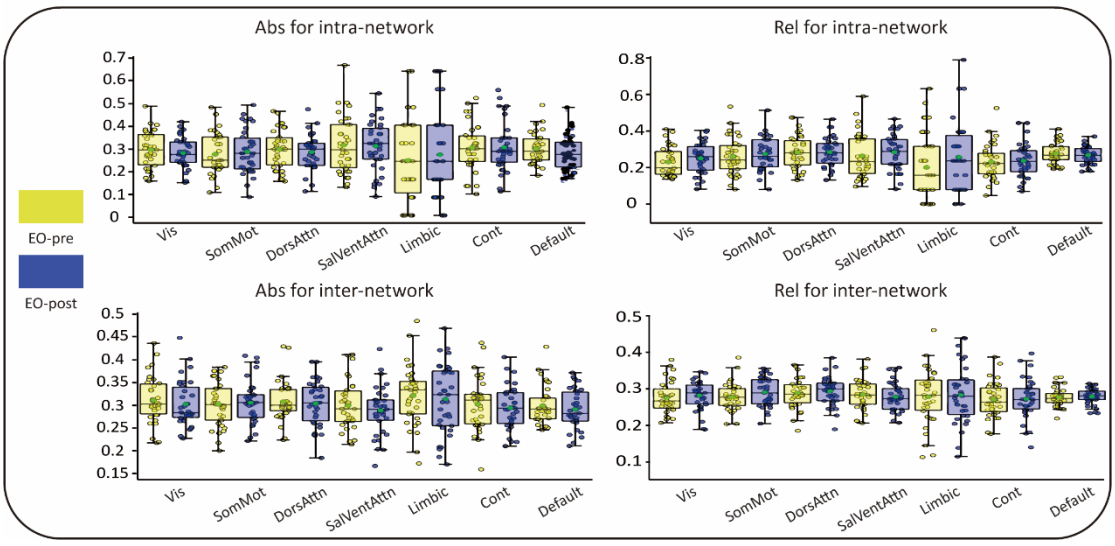

Figure 4.5. Intra-network and inter-network connectivity strength for EO conditions pre- and post- stimulation using two comparison methods in source space. Box plots display intra- and inter-network mean connections were performed using a paired-sample *t*-test with FDR correction for two comparison methods. EO, eyes-open; Abs, absolute comparison; Rel, relative comparison; Vis, Visual; SomMot, Somato-Motor; DorsAttn, Dorsal Attention; SalVentAttn, Salience-Ventral Attention; Cont, Control.

4.3.4. Higher-order graph results for intra-Default graph

4.3.4.1. Intra-Default graph connectivity results: absolute comparison

For absolute comparison (Fig. 4.6A), a greater number of connections were observed in the EO-pre condition compared to EO-post. In both conditions, connections were primarily ipsilateral, with only a few between hemispheres. The positive t-graphs showed denser connections in the EO-pre (142 edges) condition relative to EO-post (112 edges).

4.3.4.2. Intra-Default graph connectivity results: relative comparison

However, relative comparison (Fig. 4.6B) exhibited more between-hemisphere connections in both relative EO-pre and EO-post condition in the group-level graphs. The EO-pre condition showed a right-hemisphere-dominated pattern, whereas the EO-post condition showed clustering in the left hemisphere. Consistent with absolute comparisons, larger and more densely clustered connections were again observed in the EO-pre (143 edges) than EO-post (119 edges) condition.

For intra-Default graphs, the group-level patterns were consistent across pre- and post-stimulation within each comparison method. However, the absolute comparison highlighted within-hemisphere connections, whereas the relative comparison emphasised inter-hemispheric connections. In both methods, the EO-pre condition displayed more connections overall.

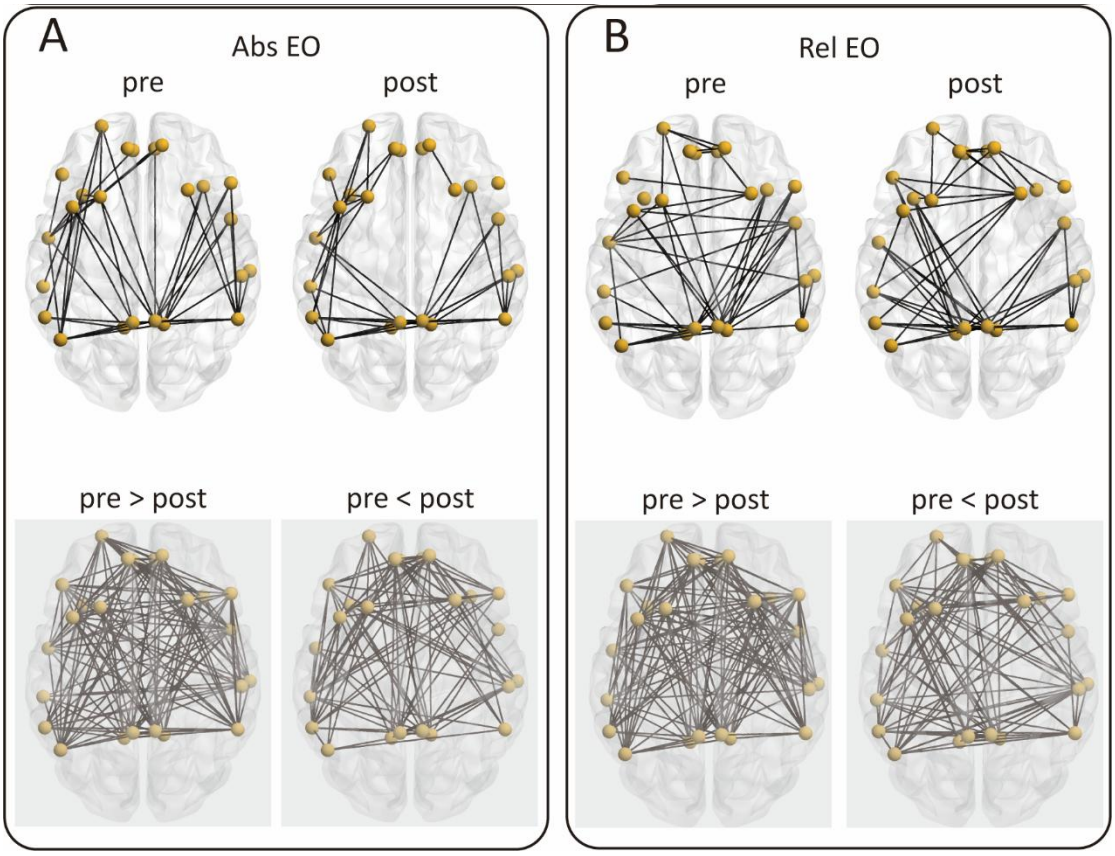

Figure 4.6. Higher-order intra- default graphs elicited by EO conditions pre- and post- stimulation using two comparison methods. (A) Group-level intra-network graphs for the default network and corresponding *t*-graphs ($t > 0$; shown in reduced opacity) were generated following NBS analysis pre- and post-stimulation. (B) Similar to (A) but for relative comparison. The group-level patterns were consistent across pre- and post-stimulation within each comparison method. However, the absolute comparison highlighted within-hemisphere connections with more connections in EO-pre condition, whereas the relative comparison emphasised inter-hemispheric connections. In both methods, the EO-pre condition displayed more connections in t-graphs. EO, eyes-open; NBS, network-based statistics; Abs, absolute comparison; Rel, relative comparison.

4.3.4.3. Graph analysis results for intra-Default graph

No significant main effects or interaction effects were found (Fig. 4.7). However, post hoc analysis revealed greater modularity in the EO-pre condition

for the absolute comparison compared to the relative comparison (t (34) = 2,78, P = 0.01).

Detailed ANOVA statistics and post-hoc comparisons are provided in Table 4.1.

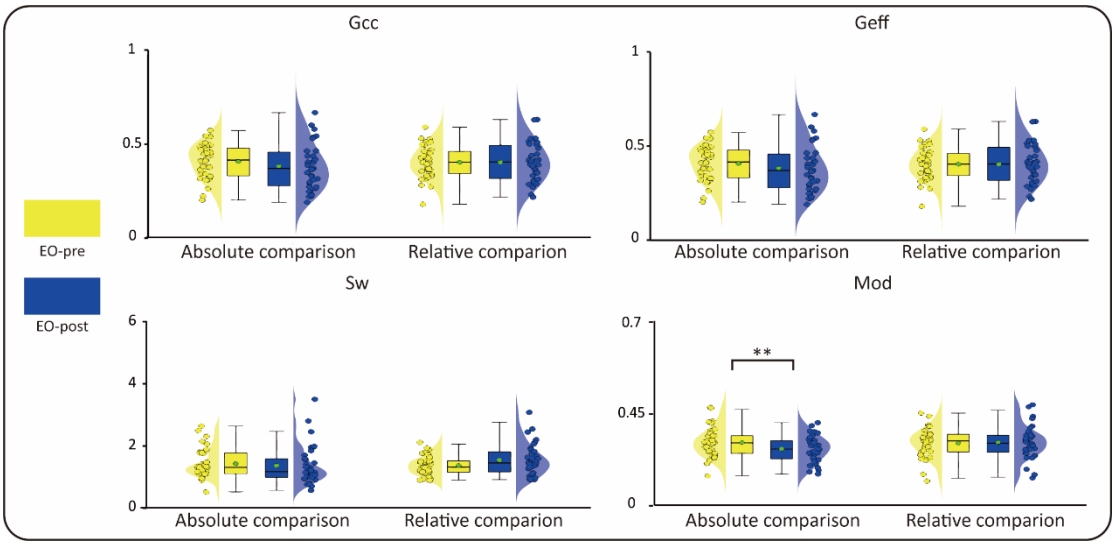

Figure 4.7. Graph analysis results for EO conditions pre- and post- stimulation using two comparison methods for intra-Default graphs. Violin plots with overlaid scatter and box plots show the results of repeated-measures ANOVA with Bonferroni correction for post hoc comparisons of four GNIs across the pre (yellow) and post (blue) conditions and two comparison methods. A green-filled circle with a black edge denotes the mean value for each group. EO, eyes-open; GNIs, global network inferences; Gcc, global clustering coefficient; Geff, global efficiency; Sw, small-worldness; Mod, modularity. **P < .01.

4.3.5. Higher-order graph results for inter-network graph

4.3.5.1. Inter-network graph connectivity results: absolute comparison

For absolute comparison (Fig. 4.8A), there were no large differences between EO-pre and EO-post inter-network connections. Specifically, four connections between SalVenAtten and SomMot, DorsAtten, Limbic and Default exhibited larger connections in EO-pre. Following stimulation, connections involving DorsAttn and SomMot increased, linking with Limbic, Default, Control, and Vis networks, respectively.

4.3.5.2. Inter-network graph connectivity results: relative comparison

Relative comparison (Fig. 4.8B) showed similar results for inter-network pattern in EO-pre. T-graphs of larger connections pre-stimulation were centred around SalVentAttn, linked with DorsAttn, Limbic, and Control, along with an additional connection to the Default network.

After stimulation, t-graphs showed that SomMot and Vis networks were central hubs, both connected with all other networks, indicating enhanced connectivity following sensory input. SalVentAttn, DorsAttn, and Limbic each had four edges, highlighting increased inter-network communication post-stimulation.

Inter-network graphs in both comparison methods emphasised the SalVentAttn network as the central hub in the EO-pre condition. Following stimulation, the relative comparison revealed that the SomMot and Vis networks established connections with all other networks.

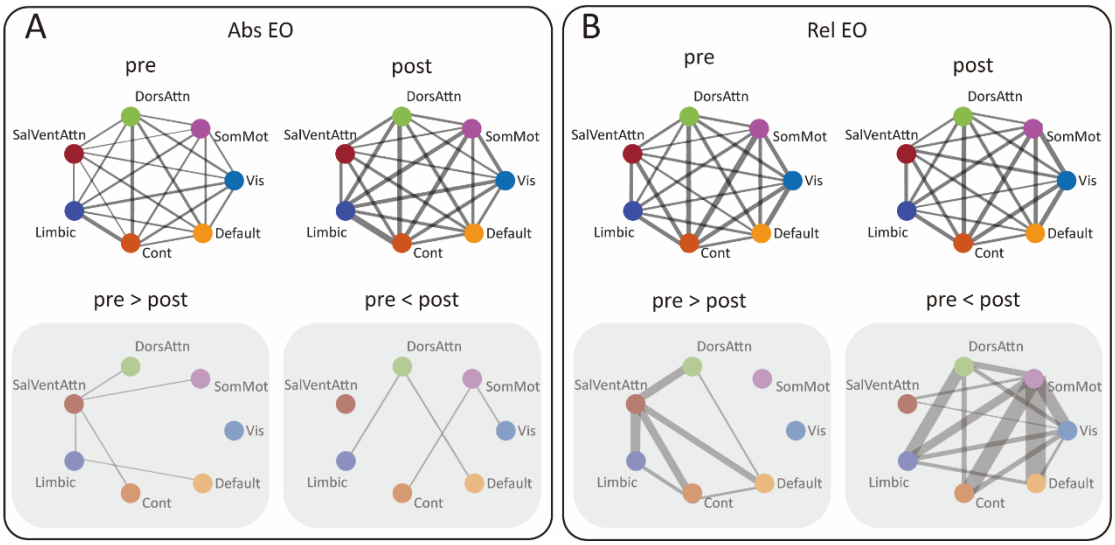

Figure 4.8. Higher-order inter-network graphs elicited by EO conditions pre- and post- stimulation using two comparison methods. (A) Group-level inter-network weighted graphs and corresponding *t*-graphs ($t > 0$; shown in reduced opacity) were generated following NBS analysis pre- and post-stimulation. (B) Similar to (A) but for relative comparison. The stroke size of each connection indicates the edge weight, representing connectivity strength in the upper panels, whereas in the lower panels it represents the corresponding t-value. Inter-network graphs in both comparison methods emphasised the SalVentAttn network as the central hub in the EO-pre condition. Following stimulation, the relative comparison revealed that the SomMot and Vis networks established connections with all other networks. EO, eyes-open; NBS, network-based statistics; Abs, absolute comparison; Rel, relative comparison.

4.3.5.3. Graph analysis results for inter-network graphs: edge betweenness centrality in absolute comparison

In the absolute comparison (Fig. 4.9A), fewer important edges were present pre-stimulation. The Ebc t-graphs showed edges linking Limbic with SalVentAttn and DorsAttn, SalVentAttn with Vis, DorsAttn with Default, and Default

with Control. The DorsAttn-Limbic, DorsAttn-Default, and SalVentAttn-Vis were three outstanding connections.

Post-stimulation, SomMot connected with all other networks, underscoring its central hub role. DorsAttn and Control each showed four connections, including links with SomMot, SalVentAttn, Vis, and other control regions. Edges expressing high centrality were SomMot-SalVentAttn, SomMot-Vis, Vis-Default, and DorsAtten-Cont.

4.3.5.4. Graph analysis results for inter-network graphs: edge betweenness centrality in relative comparison

In contrast to the absolute comparison, more important edges were found pre-stimulation in the relative comparison (Fig. 4.9B). SalVentAttn and Limbic each had five edges, connected to all networks except Default. DorsAttn and Vis both had four edges, forming a highly distributed network. Edges connected between Default and Vis, SomMot, and DorsAtten exhibited high centrality.

Post-stimulation, Cont had three important edges (to DorsAttn, Default, and Vis), with additional connections between Default-Limbic, Vis-SomMot, and SomMot-DorsAttn, totalling six prominent edges.

The Ebc-related t-graphs was further demonstrated the importance of SomMot. In the EO-post condition, the absolute comparison revealed larger Ebc values involving all other networks, with particularly strong SomMot-SalVentAttn and SomMot-Vis links. The relative comparison also highlighted strong SomMot-Vis connections.

4.3.5.5. Graph analysis results for inter-network graphs: local clustering coefficient

Only one significant result was found: higher Lcc values in the SomMot network post-stimulation in the relative comparison ($t_{(1,34)} = 1.76$, $P = 0.04$, Cohen's $d = 0.03$), indicating increased local clustering (Fig. 4.9C).

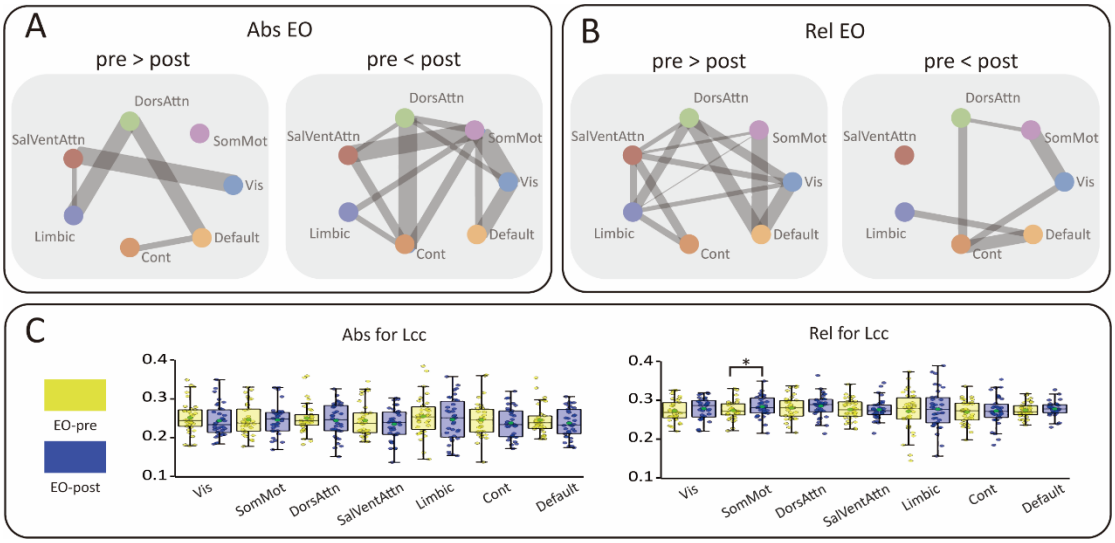

Figure 4.9. Results for local graph inferences analysis from inter-network graphs elicited by EO conditions pre- and post- stimulation using two comparison methods. (A) Ebc corresponded *t*-graphs generated following NBS ($t > 0$; shown in reduced opacity). (B) Similar to (A) but for relative comparison. The stroke size of each connection represents the corresponding t-value for the Ebc graph contrasts. (C) Box plots illustrate the statistical analysis for Lcc by paired-sample *t*-test with FDR correction between stimulus conditions for two comparison methods. The Ebc-related t-graphs further underscored the importance of SomMot. In the EO-post condition, the absolute comparison showed higher Ebc values across all networks, with particularly strong SomMot-SalVentAttn and SomMot-Vis links. The relative comparison likewise highlighted strong SomMot-Vis connections. EO, eyes-open; Ebc, Edge betweenness centrality; NBS, network-based statistics; Abs, absolute comparison; Rel, relative comparison. *$P < .05$.

4.3.5.6. Graph analysis results for inter-network graphs: global network inferences

Significant main effects of comparison methods (absolute vs. relative) were observed in both Gcc and Geff (Fig. 4.10) where post-hoc comparisons showed that the absolute comparison significantly increased Gcc and Geff compared to the relative comparison both pre- (Gcc: t (34) = 3.43, P < 0.01; Geff: t (34) = 3.14, P < 0.01) and post-stimulation (Gcc: t (34) = 2.40, P = 0.03; Geff: t (34) = 2.80, P = 0.02).

Detailed ANOVA statistics and post-hoc comparisons are provided in Table 4.1.

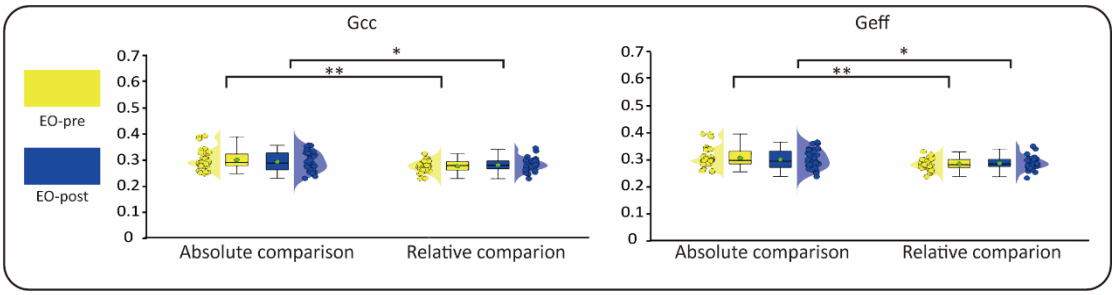

Figure 4.10. Graph analysis results for EO conditions pre- and post- stimulation using two comparison methods for inter-network graphs. Violin plots with overlaid scatter and box plots show the results of repeated-measures ANOVA with Bonferroni correction for post hoc comparisons of two GNIs across the pre (yellow) and post (blue) conditions and two comparison methods. EO, eyes-open; GNIs, global network inferences; Gcc, global clustering coefficient; Geff, global efficiency. *P < .05, **P < .01.

Table 4.1. Statistical results for GNIs from EO conditions pre- and post- stimulation using two comparison methods (ANOVA and Post-hoc Comparisons).

Graphs	GNIs	Effect	$F_{1,34}$	P	η_p^2	Post-hoc Comparisons	T_{34}	$P_{Bonferroni}$	95% CI
sensor	Gcc	Comp (Main)	19.7	<0.001	0.37	Rel > Abs (Pre): ns	1.53	0.11	[-0.07, 0.05]
						Rel > Abs (Post)	5.79	<0.001	[0.05, 0.11]
sensor	Gcc	Time (Main)	6.70	0.01	0.17	Post > Pre (Abs): ns	0.15	0.89	[-0.02, 0.03]
						Post > Pre (Rel)	3.81	<0.001	[0.03, 0.09]
sensor	Gcc	Time × Comp (Interaction)	14.61	<0.001	0.30				
sensor	Geff	Comp (Main)	136.71	<0.001	0.80	Rel > Abs (Pre)	6.57	<0.001	[0.03, 0.06]
						Rel > Abs (Post)	8.17	<0.001	[0.04, 0.06]
sensor	Geff					Post > Pre (Abs): ns	0.45	0.63	[-0.02, 0.03]
						Pre > Post (Rel): ns	0.33	0.75	[-0.01, 0.02]
sensor	Sw	Time × Comp (Interaction)	8.22	<0.01	0.20	Abs > Rel (Pre): ns	0.90	0.37	[-0.12, 0.31]
						Rel > Abs (Post)	2.93	0.006	[0.07, 0.38]
sensor	Sw					Pre > Post (Abs): ns	0.23	0.84	[-0.19, 0.23]
						Post > Pre (Rel)	4.10	<0.001	[0.15, 0.44]
sensor	Mod	Comp (Main)	86.13	<0.001	0.72	Abs > Rel (Pre)	4.13	<0.001	[0.02, 0.05]
						Abs > Rel (Post)	9.13	<0.001	[0.05, 0.08]
sensor	Mod	Time × Comp (Interaction)	7.79	<0.01	0.19	Post > Pre (Abs): ns	1.86	0.09	[-0.02, 0.03]
						Pre > Post (Rel)	3.00	0.005	[0.01, 0.03]
source	Geff	Comp (Main)	45.00	0.04	0.12	Abs > Rel (Pre)	2.50	0.02	[0.00, 0.02]
						Abs > Rel (Post): ns	1.00	0.31	[0.00, 0.01]
source	Sw	Comp (Main)	17.43	<0.001	0.34	Rel > Abs (Pre)	3.58	<0.001	[0.04, 0.13]
						Rel > Abs (Post)	2.78	0.009	[0.02, 0.11]
Intra-Default	Mod					Pre > Post (Abs)	2.78	0.01	[0.01, 0.04]
						Post > Pre (Rel): ns	0.25	0.83	[-0.02, 0.03]
Inter-network	Gcc	Comp (Main)	13.53	<0.001	0.29	Abs > Rel (Pre)	3.43	0.002	[0.01, 0.04]
						Abs > Rel (Post)	2.40	0.03	[0.00, 0.02]

Inter-network	Geff	Comp (Main)	13.43	<0.001	0.28	Abs > Rel (Pre) Abs > Rel (Post)	3.14 2.80	0.004 0.02	[0.01, 0.04] [0.00, 0.02]

Note. EO, eyes-open; GNIs, global network inferences; Gcc, global clustering coefficients; Geff, global efficiency; Sw, small-world-ness; Mod, modularity; Stim, Stimulus; Comp, Comparison; Abs, absolute comparison; Rel, relative comparison.

4.3.6. Classification performance

The top three classification performances based on GNIs derived from sensor space, source space, intra-Default and inter-network graphs for both comparison methods and their combination were showed in the Table 4.2. While permutation-based *P* values indicated statistically significant classifications, the prediction accuracies based on single comparison methods did not exceed 70%. However, when features from both absolute and relative comparisons were combined, the highest classification AUC-ROC of 0.85, with an accuracy reached 73%. These results suggest that integrating both comparison methods can enhance the predictive performance of GNIs in classifying pre- and post-stimulation EO conditions.

Table 4.2. Classification performance for pre- and post-stimulation based on GNIs across four graphs and comparison methods EO conditions.

Comp	GNIs	AUC-ROC	ACC	Sensitivity	Specificity	P_{perm}
Abs	sensor+intra-Default	0.69	57 %	0.34	0.80	<0.001
Abs	sensor+source+intra-Default	0.67	63 %	0.49	0.77	0.01
Abs	sensor+intra-Default+inter-network	0.67	59 %	0.40	0.77	0.01
Rel	sensor+inter-network	0.71	61 %	0.57	0.66	<0.001
Rel	sensor	0.70	59 %	0.49	0.69	<0.001
Rel	sensor+source	0.68	61 %	0.54	0.69	<0.001
Abs + Rel	Abs_source+Abs_intra-Default+Abs_inter-network+Rel_sensor+Rel_source+Rel_inter-network	0.85	73 %	0.63	0.83	<0.001
Abs + Rel	Abs_sensor+Abs_source+Abs_intra-Default+Abs_inter-network+Rel_sensor+Rel_source+Rel_intra-Default+Rel_inter-network	0.81	76 %	0.69	0.83	<0.001
Abs + Rel	Abs_source+Abs_intra-Default+Rel_sensor+Rel_intra-Default	0.81	74 %	0.69	0.80	<0.001

Note. EO, eyes-open; Comp, Comparison methods; Abs, absolute comparison; Rel, relative comparison; AUC-ROC., area under the receiver operating characteristic curve; ACC, accuracy; $P_{perm,}$ P value based on 1000 permutation.

4.4. Discussion for eyes-open condition

4.4.1. Representative connectivity patterns

In the EO-pre condition, the absolute comparison in sensor space revealed connections from the right central to the left parietal regions. A similar

pattern of right frontal to left parietal inter-hemispheric connectivity was also observed in source space. In the EO-post condition, both comparison methods produced more bilaterally distributed patterns.

For intra-Default graphs, the absolute comparison highlighted within-hemisphere connections, whereas the relative comparison emphasised inter-hemispheric links. Both methods showed more connections in the EO-pre condition, which aligned with the previously reported disrupted connectivity within the Default network in chronic pain patients when compared with healthy participants (Alhajri, Boudreau, & Graven-Nielsen, 2023; Alshelh et al., 2018).

4.4.2. Dynamic network reconfiguration

Distinctive network profiles emerged primarily from inter-network graphs. In both comparison methods, the SalVentAttn network functioned as the central hub in the EO-pre condition. Moreover, the central role of SalVentAttn in the EO-pre condition had also been previously identified as a characteristic of EO resting-state activity (Costumero et al., 2020; J. Han et al., 2023).

Following stimulation, the relative comparison showed that the SomMot and Vis networks became densely interconnected with all other networks, consistent with reports of increased Default-SomMot and Default-Vis connectivity after the onset of sustained pain (Lou et al., 2024). The importance of SomMot was further demonstrated in Ebc-related t-graphs: EO-post exhibited stronger SomMot-SalVentAttn and SomMot-Vis connections in absolute comparisons, while the relative comparison confirmed heightened SomMot-Vis centrality. Additionally, increased SomMot clustering post-stimulation was evidenced by elevated Lcc in the relative comparison.

4.4.3. Global network inferences and networks

GNIs showed an effect of time only in sensor space and only in the relative comparison: after stimulation, both functional segregation and small-worldness increased. Inter-network graphs revealed that pre-stimulation hub dominance (SalVentAttn) transitioned to a dual-hub architecture (SomMot and Vis) post-stimulation, aligning with increased Gcc and a higher number of edges in inter-network t-graphs in the relative comparison.

Modularity declined in sensor space graphs from the relative comparison, and in intra-Default graphs from the absolute comparison. Although brain-wide graph evidence was limited, inter-network graphs from the relative comparison demonstrated that Default-Vis, Default-SomMot, and Default-DorsAttn edges had high centrality in the EO-pre condition. Together with the reduced connections in the EO-post condition (absolute comparison), these findings suggest that pre-stimulation modularity was associated with robust Default interactions, particularly between the Default and Vis, SomMot, and DorsAttn networks.

4.4.4. Classification performance

Classification performance based on GNIs from all graphs achieved the highest AUC-ROC of 0.85 and an accuracy of 73%, although models using a single comparison method did not exceed 70% accuracy. This suggests that combining both comparison methods enhances the predictive power of GNIs for classifying pre- and post-stimulation EO conditions, especially given that significant GNI effects were limited and concentrated in sensor space graphs from the relative comparison. By capturing complementary facets of

neuroplasticity overlooked by individual methods, this integrative framework enhances the validity of GNIs as biomarkers for cross-state brain dynamics following sensory stimulation.

4.5. Results for eyes-closed conditions

4.5.1. Brain-wide graph results in sensor space

4.5.1.1. Sensor space connectivity results: absolute comparison

Both the EC pre-stimulation condition (EC-pre) and EC post-stimulation condition (EC-post) exhibited densely connected distributions, predominantly concentrated within the occipital region (Fig. 4.11A). NBS analysis revealed a significant graph showing greater connectivity in the EC-pre condition relative to the EC-post condition, comprising 55 nodes and 155 edges. These connections were primarily distributed across both hemispheres, linking frontal, central, and central-parietal regions ($P < 0.001$). In contrast, the EC-post condition yielded a significant graph with more pronounced connectivity compared to the EC-pre condition, comprising 55 nodes and 144 edges. This connectivity was predominantly distributed between the hemispheres, with a focus on central-parietal and parietal regions ($P < 0.01$).

4.5.1.2. Sensor space connectivity results: relative comparison

In the relative comparison, the group-level graphs showed an increase in connections across both the EC-pre and EC-post conditions, extending beyond the occipital region (Fig. 4.11B). Before stimulation, the connectivity was

predominantly right hemisphere-dominated in the pre-frontal and frontal areas, along with bilateral connections extending from frontal to occipital regions. After stimulation, the bilateral connections from central to occipital areas remained intact. Furthermore, the right hemisphere continued to show predominant connectivity in the frontal regions. NBS analysis identified a significant graph with larger connectivity in the EC-pre condition relative to the EC-post condition, comprising 58 nodes and 151 edges ($P < 0.01$). These connections were distributed bilaterally, spanning across both hemispheres, particularly from frontal to central-parietal regions. In contrast, the EC-post condition revealed a significant graph with increased connectivity compared to the EC-pre condition, comprising 51 nodes and 122 edges. These connections were predominantly localized from the right pre-frontal and central areas to the left parietal region ($P = 0.04$).

In sensor space, group-level graphs from both comparison methods revealed occipital connectivity patterns. The relative comparison additionally included connections from frontal-central to occipital regions, with a right-hemisphere-dominant distribution. In the EC-pre condition, both methods showed a bilateral distribution: the absolute comparison concentrated on central regions, while the relative comparison emphasised frontal and central regions. In the EC-post condition, inter-hemispheric connections were observed in both methods, with the absolute comparison focusing on parietal and occipital regions.

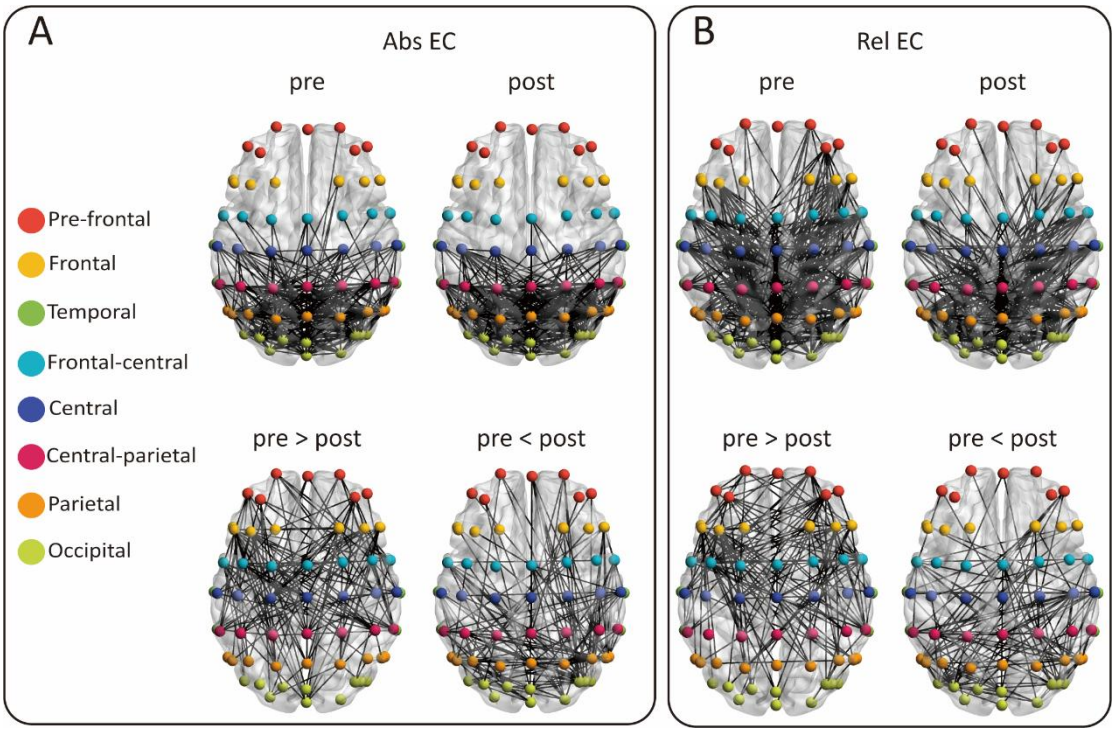

Figure 4.11. Graphs elicited by EC conditions pre- and post- stimulation using two comparison methods in sensor space. (A) Group-level functional connectivity graph for EC pre- and post-stimulation (first row). Sensors corresponding to different scalp regions (Prefrontal, Frontal, Temporal, Frontal-central, Central, Central-parietal, Parietal, and Occipital) were colour-labelled for visual distinction. State-specific significant connectivity patterns were identified using NBS and visualised as *P*-graphs (second row). (B) Similar to (A) but for relative comparison. The group-level graphs from both comparison methods revealed occipital connectivity patterns. In the EC-pre condition, a bilateral distribution was shown, and inter-hemispheric connections were observed in the EC-post condition in both methods. EC, eyes-closed; NBS, network-based statistics; Abs, absolute comparison; Rel, relative comparison.

4.5.1.3. Sensor space graph analysis results

Significant main effects of comparison methods (absolute vs. relative) and time (pre vs. post) were observed across all four GNIs (Fig. 4.12). For Gcc,

post-hoc comparisons revealed significantly higher values in the absolute comparison compared to the relative comparison in both pre- and post-stimulation conditions (Pre: t (34) = 1.50, P = 0.02; Post: t (34) = 2.73, P = 0.01). Additionally, Gcc values were significantly higher post-stimulation in the absolute comparison (t (34) = 2.70, P = 0.01), but no significant change was found in the relative comparison.

Functional integration (Geff) showed that both significant main effects were found, along with a significant interaction between comparison method and time. Geff values were significantly higher in the relative comparison both before and after stimulation (Pre: t (34) = 9.38, P < 0.001; Post: t (34) = 12.88, P < 0.001). Similar to Gcc, Geff was also significantly enhanced in the absolute comparison, but decreased in the post-stimulation condition (t (34) = 3.20, P < 0.01)

Small-worldness values were significantly higher in the absolute comparison compared to the relative comparison in both pre- and post-stimulation conditions (Pre: t (34) = 6.12, P < 0.001; Post: t (34) = 5.37, P < 0.001). Notably, Sw increased significantly in the absolute comparison after stimulation (t (34) = 2.44, P = 0.02).

Modularity showed no significant difference between the absolute and relative comparison methods in the pre-stimulation condition. However, post-stimulation Mod values were significantly higher in the relative comparison (t (34) = 7.00, P < 0.001). A significant decrease in Mod was observed from pre- to post-stimulation in the absolute condition (t (34) = 5.17, P < 0.001), whereas no change was observed in the relative condition.

Detailed ANOVA statistics and post-hoc comparisons are provided in Table 4.3.

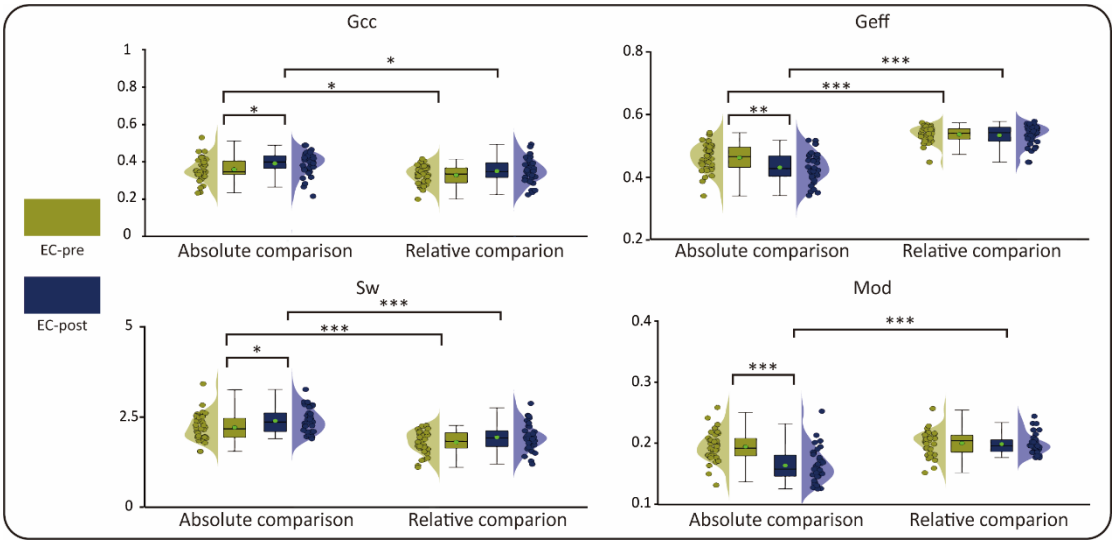

Figure 4.12. Graph analysis results for EC conditions pre- and post- stimulation using two comparison methods in sensor space. Violin plots with overlaid scatter and box plots show the results of repeated-measures ANOVA with Bonferroni correction for post hoc comparisons of four GNIs across the pre (dark yellow) and post (dark blue) conditions and two comparison methods. A green-filled circle with a black edge denotes the mean value for each group. EC, eyes-closed; GNIs, global network inferences; Gcc, global clustering coefficient; Geff, global efficiency; Sw, small-worldness; Mod, modularity. *P < .05, **P < .01, ***P < .001.

4.5.2. Brain-wide graph results in source space

4.5.2.1. Source space connectivity results: absolute comparison

Group-level graphs for the absolute comparison revealed a predominantly left hemisphere distribution in both the pre- and post-stimulation EC

conditions (Fig. 4.13A). However, the NBS analysis identified a bilateral connectivity pattern in the t-graphs, showing greater connectivity in the pre-stimulation condition. Specifically, increased connectivity between the two hemispheres was observed in regions associated with parietal regions; furthermore, those connections within each hemisphere were linked between frontal and parietal regions. In contrast, the post-stimulation condition revealed more prominent connections within the right hemisphere, particularly in the frontal regions, and between the right frontal and left parietal regions.

4.5.2.2. Source space connectivity results: relative comparison

In the relative comparison, the group-level connectivity graphs exhibited patterns that were largely consistent with those observed in the absolute comparison, but with a less pronounced left hemisphere dominance (Fig. 4.13B). The t-graphs from the pre-stimulation condition demonstrated bilateral edges linking the parietal regions, in addition to within-hemisphere connections between frontal and parietal regions. Conversely, the post-stimulation condition revealed a right hemisphere-dominated distribution, with increased connectivity between right frontal regions and left parietal regions, as well as within-hemisphere connections in the right hemisphere.

In source space, both comparison methods showed left-hemisphere dominance in pre- and post-stimulation conditions, though this dominance was less pronounced in the relative comparison. In the EC-pre condition, both methods displayed bilateral distribution with inter-hemispheric connections between parietal regions, alongside bilateral frontal-parietal connections. In the EC-post condition, both methods revealed right frontal-to-left parietal connections.

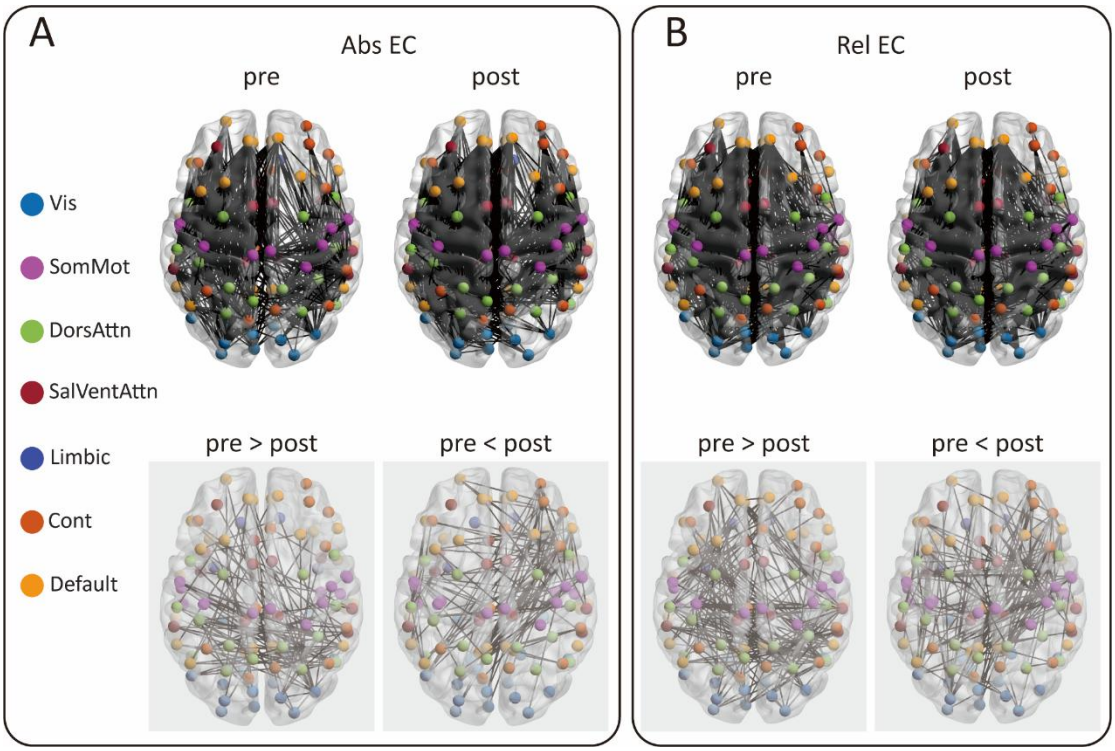

Figure 4.13. Graphs elicited by EC conditions pre- and post- stimulation using two comparison methods in source space. (A) Group-level functional connectivity matrices for hot and warm stimulation (first row) projected in source space for 100 pairs of brain regions organised into 7 different functional networks (Visual, Somato-motor, Dorsal Attention, Salience-Ventral Attention, Limbic, Control, and Default). The *t*-graphs (second row) constructed from connections with a t-value larger than 1.69 compared between conditions using NBS (shown in reduced opacity). (B) Similar to (A) but for relative comparison. The group-level graphs showed left-hemisphere dominance connectivity pattern in pre- and post-stimulation conditions in both comparison methods. In the EC-pre condition, both methods displayed bilateral distribution with inter-hemispheric connections between parietal regions, alongside bilateral frontal-parietal connections. In the EC-post condition, both methods revealed right frontal-to-left parietal connections. EC, eyes-closed; NBS, network-based statistics; Abs, absolute comparison; Rel, relative comparison.

4.5.2.3. Source space graph analysis results

Significant main effects of comparison methods (absolute vs. relative) were observed across all four GNIs in source space (Fig. 4.14). Specifically, the Gcc, Sw, and Mod all exhibited significantly larger values in the absolute comparison than the relative comparison in both pre- and post-stimulation (Gcc-pre: t (34) = 5.50, $P < 0.001$; Gcc-post: t (34) = 5.22, $P < 0.001$; Sw-pre: t (34) = 6.20, $P < 0.001$; Sw-post: t (34) = 4.03, $P < 0.001$; Mod-pre: t (34) = 5.40, $P < 0.001$; Mod-post: t (34) = 4.40, $P < 0.001$). In contrast, the relative comparison exhibited significantly higher Geff in both pre- and post-stimulation conditions (Pre: t (34) = 4.20, $P < 0.001$; Post: t (34) = 2.40, $P = 0.02$).

Detailed ANOVA statistics and post-hoc comparisons are provided in Table 4.3.

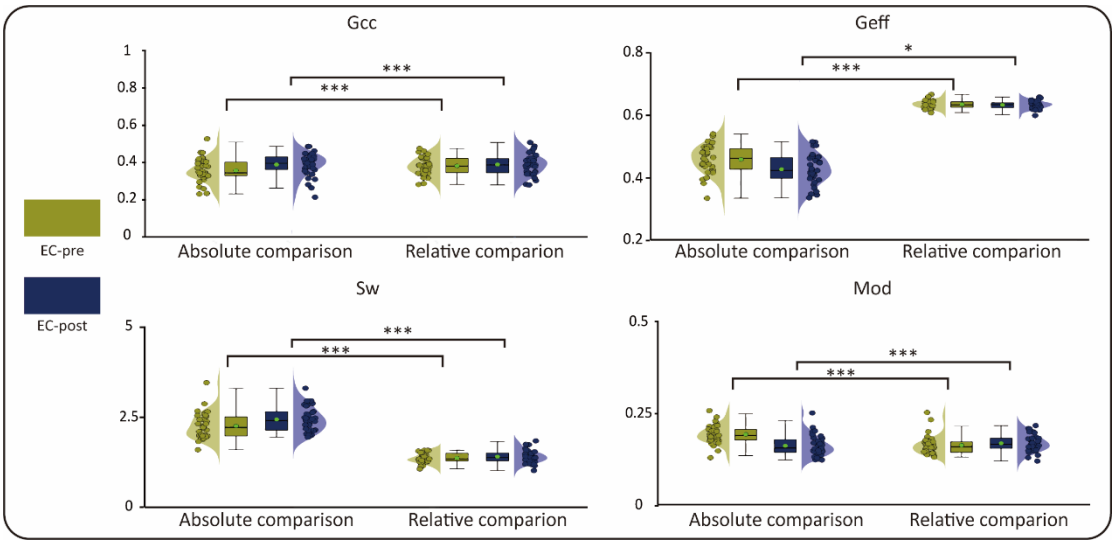

Figure 4.14. Graph analysis results for EC conditions pre- and post- stimulation using two comparison methods in source space. Violin plots with overlaid scatter and box plots show the results of repeated-measures ANOVA with Bonferroni correction for post hoc comparisons of four GNIs across the pre

(dark yellow) and post (dark blue) conditions and two comparison methods. A green-filled circle with a black edge denotes the mean value for each group. EC, eyes-closed; GNIs, global network inferences; Gcc, global clustering coefficient; Geff, global efficiency; Sw, small-worldness; Mod, modularity. *P < .05, ***P < .001.

4.5.3. Intra- and inter-network connectivity strength

No significant results were found for intra- and inter-network connectivity strength in the EC conditions for both pre- and post-stimulation using the two comparison methods in source space (Fig. 4.15).

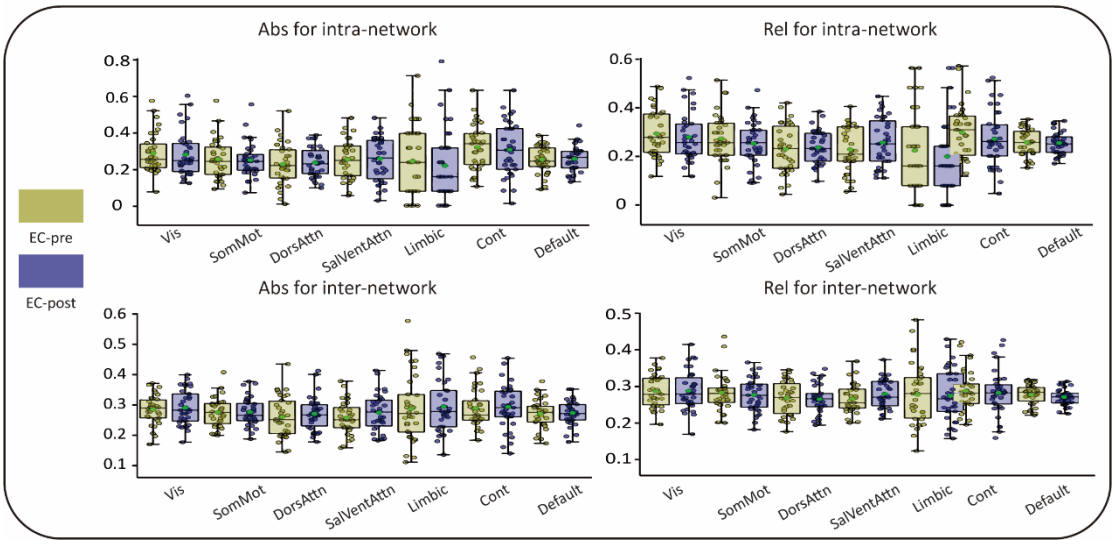

Figure 4.15. Intra-network and inter-network connectivity strength for EC conditions pre- and post- stimulation using two comparison methods in source space. Box plots display intra- and inter-network mean connections were performed using a paired-sample *t*-test with FDR correction for two comparison methods. EC, eyes-closed; Abs, absolute comparison; Rel, relative comparison; Vis, Visual; SomMot, Somato-Motor; DorsAttn, Dorsal Attention; SalVentAttn, Salience-Ventral Attention; Cont, Control.

4.5.4. Higher-order graph results for intra-Default graph

4.5.4.1. Intra-Default graph connectivity results: absolute comparison

In the absolute comparison (Fig. 4.16A), group-level intra-Default graphs exhibited a left hemisphere-dominant connectivity pattern in both the pre- and post-stimulation conditions. Positive t-graphs illustrated more dense connections in EC-post (131 edges) than in the EC-pre (115 edges) conditions.

4.5.4.2. Intra-Default graph connectivity results: relative comparison

The relative comparison (Fig. 4.16B) showed a more bilateral connectivity pattern for both pre- and post-stimulation conditions. In contrast to the absolute comparison, the relative comparison revealed more pronounced connectivity in the pre-stimulation (139 edges) condition than in the post-stimulation (121 edges) condition.

For intra-Default graphs, group-level graphs from the absolute comparison consistently showed a left-hemisphere-dominant connectivity pattern, whereas the relative comparison produced a more balanced bilateral pattern. Additionally, more connections were observed in the EC-post condition in the absolute comparison, while the relative comparison showed denser connectivity in the EC-pre condition.

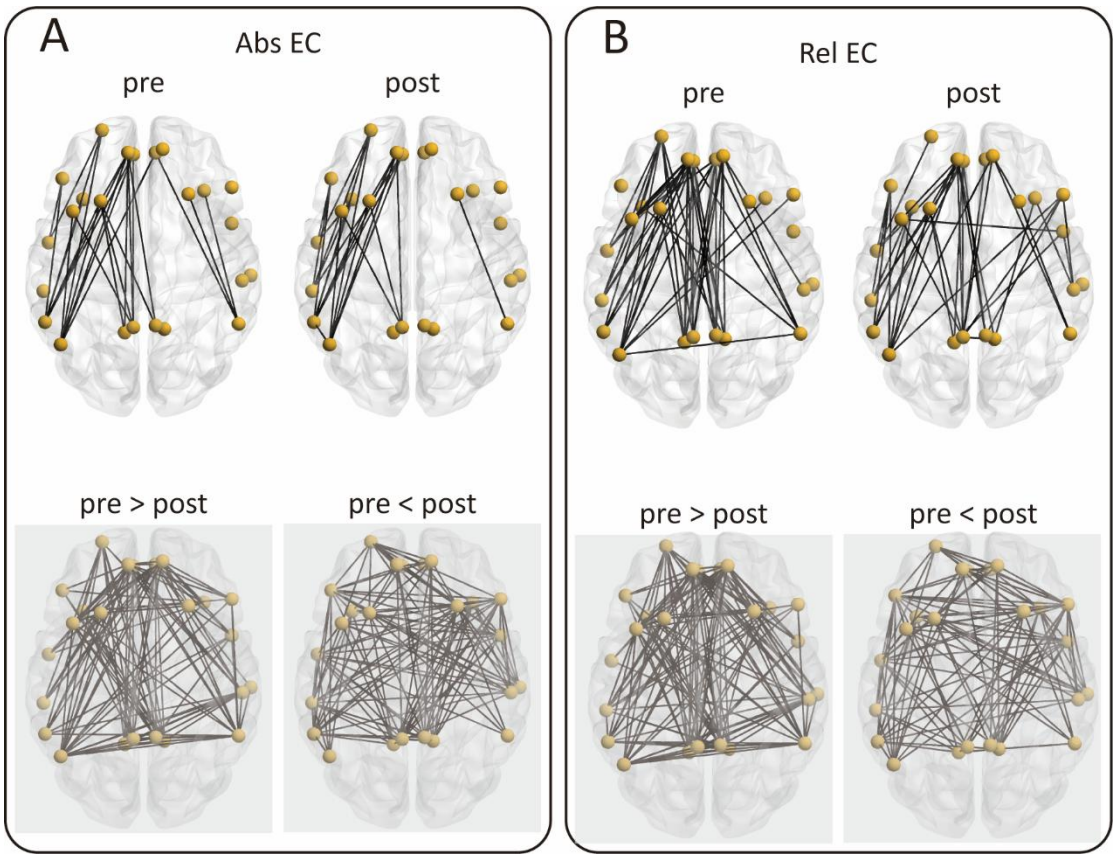

Figure 4.16. Higher-order intra- default graphs elicited by EC conditions pre- and post- stimulation using two comparison methods. (A) Group-level intra-network graphs for the default network and corresponding *t*-graphs ($t > 0$; shown in reduced opacity) were generated following NBS analysis pre- and post-stimulation. (B) Similar to (A) but for relative comparison. The group-level graphs from the absolute comparison consistently showed a left-hemisphere-dominant connectivity pattern, whereas the relative comparison produced a more balanced bilateral pattern. Additionally, more connections were observed in the EC-post condition in the absolute comparison, while the relative comparison showed denser connectivity in the EC-pre condition. EC, eyes-closed; NBS, network-based statistics; Abs, absolute comparison; Rel, relative comparison.

4.5.4.3. Graph analysis results for intra-Default graph

Significant main effects of comparison methods (absolute vs. relative) were only observed for Geff (Fig. 4.17), with the relative comparison exhibiting significantly higher Geff in both pre- and post-stimulation conditions. (Pre: t (34) = 4.71, P < 0.001; Post: t (34) = 2.91, P = 0.01). Post-hoc comparison also revealed a significantly increased Sw in the absolute comparison compared to the relative comparison in the EC-pre conditions (t (34) = 2.54, P = 0.02).

Detailed ANOVA statistics and post-hoc comparisons are provided in Table 4.3.

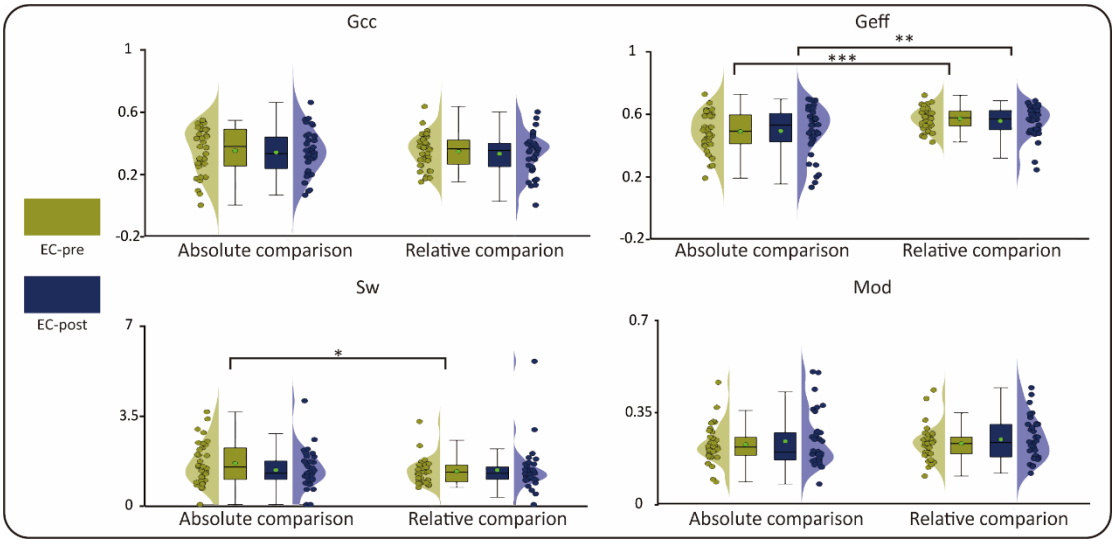

Figure 4.17. Graph analysis results for EC conditions pre- and post- stimulation using two comparison methods for intra-Default graphs. Violin plots with overlaid scatter and box plots show the results of repeated-measures ANOVA with Bonferroni correction for post hoc comparisons of four GNIs across the pre (dark yellow) and post (dark blue) conditions and two comparison methods. A green-filled circle with a black edge denotes the mean value for each group. EC, eyes-closed; GNIs, global network inferences; Gcc, global

clustering coefficient; Geff, global efficiency; Sw, small-worldness; Mod, modularity. *P < .05, **P < .01, ***P < .001.

4.5.5. Higher-order graph results for inter-network graph

4.5.5.1. Inter-network graph connectivity results: absolute comparison

In the absolute comparison (Fig. 4.18A), six edges were identified in the t-graphs for the EC-pre condition, compared to the EC-post condition. These edges were primarily associated with the Default and Limbic networks, with three connections each. The edges observed were Default-SomMot, Default-Vis, Default-Limbic, Limbic-SalVentAttn, Limbic-Cont, and Cont-SomMot. In the post-stimulation t-graph, only two edges were found, both linking SalVentAttn to DorsAttn and SomMot, respectively.

4.5.5.2. Inter-network graph connectivity results: relative comparison

The relative comparison revealed more edges in both the pre- and post-stimulation conditions than absolute comparison (Fig. 4.18B). The Default and DorsAttn networks each exhibited five edges in the t-graphs, demonstrating larger connections in the EC-pre condition compared to the EC-post condition. These connections were distributed between SomMot, Vis, Cont, and Limbic networks. In addition, each of the other three networks (Limbic, Vis, and Cont) held four connections in the t-graphs, except for the Vis-SomMot and Cont-Limbic connections. Specifically speaking, the SomMot-Cont connection was distinctive in the t-graphs pre-stimulation.

The SalVentAttn network, which showed no edges in the t-graphs in the EC-pre condition, was connected to all six other networks in the EC-post condition. Together with the missing Vis-SomMot and Cont-Limbic connections from the EC-pre condition, this resulted in a total of eight edges in the EC-post condition.

For inter-network graphs, more connections persisted in the EC-pre condition in both methods. In the relative comparison, highly active networks included DorsAttn and Default (five edges each), and SomMot, Vis, Cont, and Limbic (four edges each). The Default network had the most edges in the EC-pre condition, whereas SalVentAttn dominated in the EC-post condition in both methods. In the relative comparison for the EC-post condition, SalVentAttn connected with all other networks.

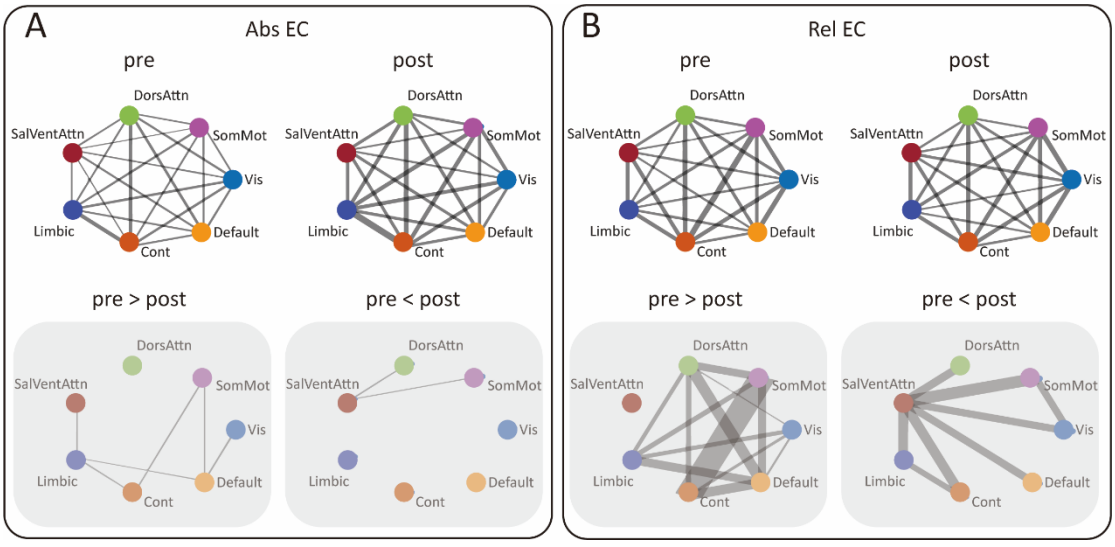

Figure 4.18. Higher-order inter-network graphs elicited by EC conditions pre- and post- stimulation using two comparison methods. (A) Group-level inter-network weighted graphs and corresponding *t*-graphs ($t > 0$; shown in reduced opacity) were generated following NBS analysis pre- and post-stimulation. (B) Similar to (A) but for relative comparison. The stroke size of each

connection indicates the edge weight, representing connectivity strength in the upper panels, whereas in the lower panels it represents the corresponding t-value. More connections persisted in the EC-pre condition in both methods. The Default network had the most edges in the EC-pre condition, whereas SalVentAttn dominated in the EC-post condition in both methods. EC, eyes-closed; NBS, network-based statistics; Abs, absolute comparison; Rel, relative comparison.

4.5.5.3. Graph analysis results for inter-network graphs: edge betweenness centrality in absolute comparison

For the absolute comparison (Fig. 4.19A), the EC-pre condition exhibited a greater number of edges in the t-graphs, particularly for large Ebc values. The SalVentAttn, Limbic, and Vis networks each displayed four edges, while the SomMot and Default networks each had three. The remaining networks, Cont and DorsAttn, each had two edges. Notable connections included Limbic-Vis, Limbic-SalVentAttn, and Cont-SomMot.

In the post-stimulation t-graphs, the primary connections involved the Cont network, which linked with the Default, Vis, SalVentAttn, and Limbic networks. Additional connections included three edges between SomMot and DorsAttn, Vis, and Default, along with two further links: DorsAttn-SalVentAttn and DorsAttn-Limbic. The most prominent edge in this condition was SalVentAttn-Cont.

4.5.5.4. Graph analysis results for inter-network graphs: edge betweenness centrality in relative comparison

As with the absolute comparison, the EC-pre condition in the relative comparison (Fig. 4.19B) showed a greater number of edges. The DorsAttn

network had the most connections, with five edges to other networks, excluding the Default network. Both the Default and SomMot networks exhibited four edges each, while Vis, Cont, and Limbic each had three. The SalVentAttn network was connected only to DorsAttn and Default. Two particularly important connections, showing the largest Ebc values, were SomMot-Limbic and SomMot-Cont.

In the EC-post condition, the SalVentAttn network was connected to four other networks in the t-graphs. The Vis, Cont, and Limbic networks each displayed three connections, maintaining links from the EC-pre condition. In contrast, the Default and SomMot networks had only two edges each, and DorsAttn had a single connection to Default. The most notable edges in this condition were SalVentAttn-Limbic and SomMot-Vis.

As for Ebc, it also revealed more edges before stimulation in both comparisons. In the absolute comparison, SalVentAttn, Limbic, and Vis each had four edges, with notable links between Limbic-Vis, Limbic-SalVentAttn, and Cont-SomMot. In the relative comparison for the same condition, DorsAttn had the most edges (five), followed by Default and SomMot (four each), and Vis, Cont, and Limbic (three each). Noteworthy edges included SomMot-Limbic and SomMot-Cont, with the latter also distinctive in the absolute comparison. In the EC-post condition, the absolute comparison highlighted the SalVentAttn-Cont edge, whereas the relative comparison emphasised the SalVentAttn-Limbic and SomMot-Vis edges, with SalVentAttn holding the most edges in this condition. The SalVentAttn network again played a prominent role in the EC-post condition, consistent with findings from the inter-network graph.

4.5.5.5. Graph analysis results for inter-network graphs: local clustering coefficient

No significant results were found in the Lcc comparison for the EC conditions pre- and post-stimulation, for both comparison methods (Fig. 4.19C).

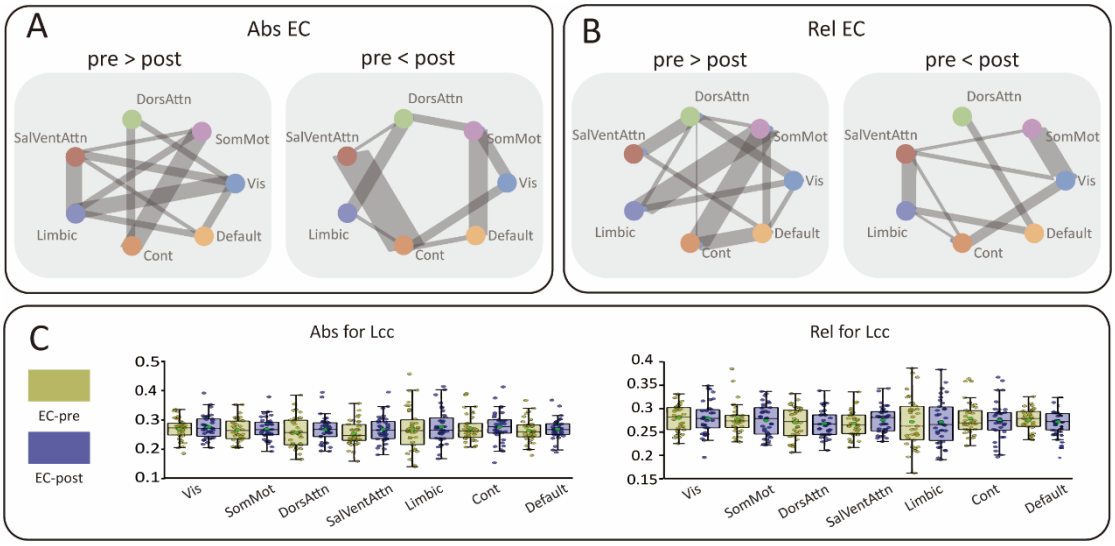

Figure 19. Results for local graph inferences analysis from inter-network graphs elicited by EC conditions pre- and post- stimulation using two comparison methods. (A) Ebc corresponded *t*-graphs generated following NBS ($t > 0$; shown in reduced opacity). (B) Similar to (A) but for relative comparison. The stroke size of each connection represents the corresponding t-value for the Ebc graph contrasts. (C) Box plots illustrate the statistical analysis for Lcc by paired-sample *t*-test with FDR correction between stimulus conditions for two comparison methods. The Ebc graphs revealed more edges before stimulation in both comparisons. In the absolute comparison, notable links included Limbic-Vis, Limbic-SalVentAttn, and Cont-SomMot. In the relative comparison for the same condition, key edges were SomMot-Limbic and SomMot-Cont, with the latter also distinctive in the absolute comparison. In the EC-post condition, the absolute comparison highlighted the SalVentAttn-Cont edge, whereas the relative comparison emphasised the SalVentAttn-Limbic and SomMot-Vis edges, with SalVentAttn holding the most edges in this condition. EC,

eyes-closed; Ebc, Edge betweenness centrality; NBS, network-based statistics; Abs, absolute comparison; Rel, relative comparison.

4.5.5.6. Graph analysis results for inter-network graphs: global network inferences

No significant main effects or post-hoc comparison results were found for the GNIs in the inter-network graphs for the EC conditions pre- and post-stimulation, using either comparison method (Fig. 4.20).

Detailed ANOVA statistics and post-hoc comparisons are provided in Table 4.3.

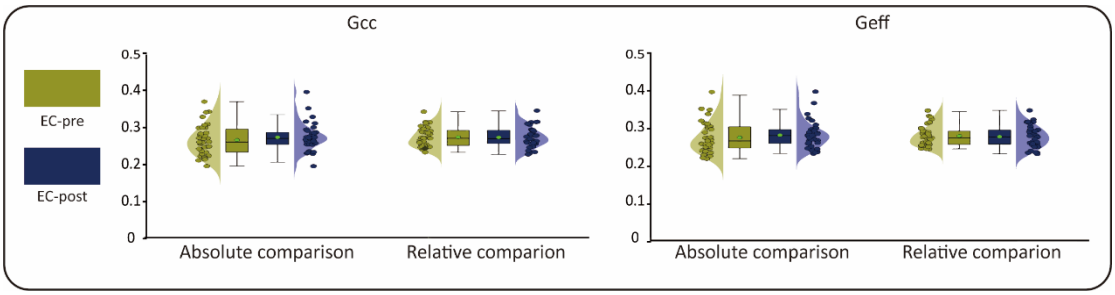

Figure 4.20. Graph analysis results for EC conditions pre- and post- stimulation using two comparison methods for inter-network graphs. Violin plots with overlaid scatter and box plots show the results of repeated-measures ANOVA with Bonferroni correction for post hoc comparisons of two GNIs across the pre (dark yellow) and post (dark blue) conditions and two comparison methods. EC, eyes-closed; GNIs, global network inferences; Gcc, global clustering coefficient; Geff, global efficiency.

Table 4.3. Statistical results for GNIs from EC conditions pre- and post- stimulation using two comparison methods (ANOVA and Post-hoc Comparisons).

Graphs	GNIs	Effect	$F_{1,34}$	P	η_p^2	Post-hoc Comparisons	T_{34}	$P_{Bonferroni}$	95% CI
sensor	Gcc	Comparison (Main)	10.75	0.002	0.24	Abs > Rel (Pre)	2.50	0.02	[0.01, 0.06]
						Abs > Rel (Post)	2.73	0.01	[0.01, 0.07]
sensor	Gcc	Time (Main)	9.14	0.005	0.21	Post > Pre (Abs)	2.70	0.01	[0.01, 0.06]
						Post > Pre (Rel): ns	1.69	0.1	[0.00, 0.05]
sensor	Geff	Comparison (Main)	204.10	<0.001	0.86	Rel > Abs (Pre)	9.38	<0.001	[0.06, 0.09]
						Rel > Abs (Post)	12.88	<0.001	[0.09, 0.12]
sensor	Geff	Time (Main)	5.33	0.03	0.14	Pre > Post (Abs)	3.20	0.004	[0.01, 0.05]
						Pre > Post (Rel): ns	0.43	0.63	[-0.01, 0.02]
sensor	Geff	Time × Comp (Interaction)	9.78	0.004	0.22				
sensor	Sw	Comparison (Main)	63.63	<0.001	0.65	Abs > Rel (Pre)	6.12	<0.001	[0.27, 0.54]
						Abs > Rel (Post)	5.37	<0.001	[0.28, 0.62]
sensor	Sw	Time (Main)	8.47	<0.001	0.20	Post > Pre (Abs)	2.44	0.02	[0.03, 0.34]
						Post > Pre (Rel): ns	1.77	0.08	[-0.02, 0.29]
sensor	Mod	Comparison (Main)	22.31	<0.001	0.40	Rel > Abs (Pre): ns	1.00	0.36	[-0.01, 0.02]
						Rel > Abs (Post)	7.00	<0.001	[0.03, 0.05]
sensor	Mod	Time (Main)	21.84	<0.001	0.39	Pre > Post (Abs)	5.17	<0.001	[0.02, 0.04]
						Pre > Post (Rel): ns	0.50	0.7	[-0.01, 0.01]
sensor	Mod	Time × Comp (Interaction)	17.23	<0.001	0.34				
source	Gcc	Comparison (Main)	43.73	<0.001	0.6	Abs > Rel (Pre)	5.50	<0.001	[0.03, 0.06]
						Abs > Rel (Post)	5.22	<0.001	[0.03, 0.07]
source	Geff	Comparison (Main)	16.06	<0.001	0.3	Rel > Abs (Pre)	4.20	<0.001	[0.01, 0.03]
						Rel > Abs (Post)	2.40	0.02	[0.00, 0.02]
source	Sw	Comparison (Main)	40.10	<0.001	0.5	Abs > Rel (Pre)	6.20	<0.001	[0.10, 0.20]
						Abs > Rel (Post)	4.03	<0.001	[0.07, 0.21]
source	Mod	Comparison (Main)	46.97	<0.001	0.6	Abs > Rel (Pre)	5.40	<0.001	[0.02, 0.04]
						Abs > Rel (Post)	4.40	<0.001	[0.01, 0.03]

Intra - Default	Geff	Comparison (Main)	25.56	<0.001	0.43	Rel > Abs (Pre)	4.71	<0.001	[0.05, 0.11]
						Rel > Abs (Post)	2.91	0.01	[0.02, 0.11]
Intra - Default	Sw					Abs > Rel (Pre)	2.54	0.02	[0.06, 0.57]
						Abs > Rel (Post): ns	0.01	0.99	[-0.42, 0.43]

Note. EC, eyes-closed; GNIs, global network inferences; Gcc, global clustering coefficients; Geff, global efficiency; Sw, small-world-ness; Mod, modularity; Comp, Comparison; Abs, absolute comparison; Rel, relative comparison.

4.5.6. Classification performance

The top three classification performances based on EC GNIs across sensor space, source space, intra-Default, and inter-network graphs, for both comparison methods and their combinations, are presented in Table 4.4. However, no significant p-value was found for GNIs based solely on the relative comparison. The highest classification performance, using GNIs from the absolute comparison and the combined comparison methods, reached an accuracy of 69% and an AUC-ROC of 0.78. These results suggest that classification performance using GNIs from the EC conditions might not provide as much information as the EO conditions, particularly for the relative comparison.

Table 4.4. Classification performance for pre- and post-stimulation based on GNIs across four graphs and comparison methods EC conditions.

Comp	GNIs	AUC-ROC	ACC	Sensitivity	Specificity	P_{perm}
Abs	Abs_sensor	0.78	69%	0.54	0.83	<0.001
Abs	Abs_sensor+Abs_inter-network	0.77	69%	0.54	0.83	<0.001
Abs	Abs_sensor+Abs_source+Abs_inter-network	0.73	69%	0.54	0.83	<0.001
Rel	Rel_sensor+Rel_intra-Default	0.58	46%	0.29	0.63	0.18
Rel	Rel_source	0.56	53%	0.46	0.60	0.21
Rel	Rel_sensor+Rel_source+Rel_intra-Default+Rel_inter-network	0.55	56%	0.43	0.69	0.32
Abs + Rel	Abs_sensor	0.78	69%	0.54	0.83	<0.001
Abs + Rel	Abs_sensor+Abs_inter-network	0.77	69%	0.54	0.83	<0.001
Abs + Rel	Abs_sensor+Abs_intra-Default+Rel_source+Rel_intra-Default+Rel_inter-network	0.77	73%	0.66	0.80	<0.001

Note. EC, eyes-closed; Comp, Comparison methods; Abs, absolute comparison; Rel, relative comparison; AUC-ROC., area under the receiver operating characteristic curve; ACC, accuracy; P_{perm}, P value based on 1000 permutation.

4.6. Discussion for eyes-closed condition

4.6.1. Representative connectivity patterns

Across both comparison methods from the brain-wide graphs, we observed a distribution of both intra-hemispheric and inter-hemispheric connectivity in the EC-pre contrasts and a predominately inter-hemispheric connectivity in the EC-post contrasts. Specifically, the EC-pre contrasts displayed bilateral frontal-parietal connections within each hemisphere, along with strong parietal-parietal links. In contrast, the EC-post contrasts were characterised by connections from the right frontal regions to the left parietal regions. This shift suggests that stimulation promoted more lateralised information transfer while reducing bilateral processing in the EC condition.

4.6.2. Dynamic network reconfiguration

In the EC-pre contrasts, both the inter-network and Ebc graphs indicated broad network engagement and increased inter-network communication across both comparison methods. The inter-network graphs highlighted strong involvement of the Default, Limbic, and SomMot networks, while the Ebc graphs identified distinctive edges such as SomMot-Cont. Notable links included Limbic-Vis and Limbic-SalVentAttn in the absolute comparison, and Limbic-SomMot in the relative comparison. This broad network communication in EC aligns with previous findings of increased connectivity between most networks, especially

Default-SomMot coupling, as well as increased connectivity from auditory and SomMot networks to other systems (Agcaoglu et al., 2019; Costumero et al., 2020; J. Han et al., 2023).

In the EC-post contrasts, SalVentAttn emerged as the dominant hub in both the inter-network and Ebc graphs. In the Ebc graphs, the absolute comparison primarily highlighted the SalVentAttn-Cont edge, while the relative comparison emphasised SalVentAttn-Limbic and SomMot-Vis. Across methods, SalVentAttn held the highest number of edges in this condition.

This transition from broadly distributed processing mode with widespread inter-network interaction to a SalVentAttn-centric communication pattern reflects prioritised attentional network recruitment after stimulation.

4.6.3. Global network inferences and networks

GNIs showed a time effect only in sensor space and only in the absolute comparison: after stimulation, global segregation increased while global functional integration decreased, resulting in higher small-worldness and lower modularity. This change corresponds to the observed shift from a bilateral intra- and inter-hemispheric pattern with extensive multi-network engagement before stimulation, to a more focused, high-segregation pattern after stimulation.

The post-stimulation network was characterised by a dominant right-frontal-to-left-parietal connection, with SalVentAttn as the central hub. The reduction in global integration, paired with increased segregation, suggests a neuroplastic response that optimised specialised processing at the expense of broader global communication.

4.6.4. Classification performance

Classification performance for EC conditions relied entirely on GNIs from the absolute comparison. The highest performance achieved an accuracy of 69% and an AUC-ROC of 0.78, highlighting the strong predictive potential of GNIs derived from the absolute comparison. The relative lack of significant effects in the relative comparison for EC conditions, suggests that the baseline normalisation approach may be less effective for classifying states under eyes-closed resting conditions, possibly due to the already high and stable alpha oscillations characteristic of EC.

4.7. Classification performance with eyes-open, eyes-closed conditions and their combination

4.7.1. Classification performance for absolute comparison

The top classification performance based on GNIs from all nine graphs from both EO, EC conditions and their combination for absolute comparison methods is presented in Table 4.5. The graphs considered include sensor space, source space, intra-Visual, intra-Somato-Motor, intra-Dorsal Attention, intra-Salience-Ventral Attention, intra-Limbic, intra-Control, intra-Default, and inter-network. The permutation p-values for all selected classifications were significant.

The first five rows in Table 4.5 show the combination of EO and EC conditions, all with AUC-ROC values above 0.87, and the highest value reaching 0.88. Accuracy values were above 74%, with the highest at 84%. This performance surpassed that of models trained on a single state.

Models based solely on EO features reached a maximum AUC-ROC of 0.72 and accuracy of 67%, while EC-only models performed better, achieving an AUC-ROC of 0.81 and accuracy of 76%.

These results indicate that combining both EO and EC conditions enhanced classification performance. A key observation was that the inclusion of multiple intra-network features, as opposed to relying on a single network like the Default network, consistently enhanced classification accuracy across all conditions. These results robustly indicate that combining information from both EO and EC states, and leveraging a diverse set of network-specific features, substantially enhances the ability to classify pre- and post-stimulation brain states using absolute connectivity metrics.

Table 4.5. Classification performance for pre- and post-stimulation based on GNIs across all nine graphs with EO, EC conditions and their combination in absolute comparison.

Eyes-condition	GNIs	AUC-ROC	ACC	Sensitivity	Specificity	P_{perm}
EO + EC	open-sensor+open-source+open-Default+open-inter+ closed-sensor+closed-Vis+closed-SalVentAttn+closed-Cont	0.88	81%	0.69	0.94	<0.001
EO + EC	open-sensor+open-source+open-Default+ closed-sensor+closed-source+closed-Vis+closed-SomMot+closed-DorsAttn+closed-Default+closed-inter	0.88	74%	0.66	0.83	<0.001
EO + EC	open-source+open-SalVentAttn+open-Default+open-inter+ closed-sensor+closed-source+closed-Vis+closed-SalVentAttn+closed-Cont+closed-inter	0.88	83%	0.74	0.91	<0.001
EO + EC	open-sensor+open-source+open-Default+open-inter+ closed-sensor+closed-Vis+closed-DorsAttn+closed-Cont	0.87	76%	0.60	0.91	<0.001
EO + EC	open-source+open-SalVentAttn+open-Default+open-inter+closed-sensor+ closed-source+closed-Vis+closed-SalVentAttn+closed-Cont+closed-inter	0.87	84%	0.77	0.91	<0.001
EO	sensor+SalVentAttn+Cont+Default	0.72	67%	0.51	0.83	<0.001
EO	sensor+source+DorsAttn+Cont+Default+inter	0.72	61%	0.51	0.71	<0.001
EO	sensor+SomMot+SalVentAttn+Default	0.72	63%	0.49	0.77	0.01
EC	sensor+DorsAttn+inter	0.81	71%	0.60	0.83	<0.001
EC	sensor+Vis+DorsAttn+SalVentAttn+Cont+inter	0.80	76%	0.66	0.86	<0.001
EC	sensor+source+Vis	0.79	71%	0.54	0.89	<0.001

Note. EO, eyes-open; EC, eyes-closed; Vis, intra-Visual network; SomMot, intra-Somato-Motor network, DorsAttn, intra-Dorsal Attention network; SalVentAttn, intra-Salience-Ventral Attention network, Limbic, intra-Limbic network; Cont, intra-Control network; Default, intra-Default network; inter, inter-network; AUC-ROC., area under the receiver operating characteristic curve; ACC, accuracy; P_{perm}, P value based on 1000 permutation.

4.7.2. Classification performance for relative comparison

A parallel analysis was conducted using the relative comparison method (Table 4.6). Mirroring the findings from the absolute comparison, the combination of EO and EC conditions yielded the strongest results, with the top models achieving an AUC-ROC of 0.83 and accuracies up to 77%.

However, this overall performance was lower than that achieved with the absolute comparison. Notably, the efficacy of the relative comparison was highly condition-dependent. For the EO condition alone, relative comparison models showed competitive performance, with a top AUC-ROC of 0.79 and accuracy of 70%. In stark contrast, models using only EC data under the relative comparison performed poorly, with a maximum AUC-ROC of 0.66 and none exceeding 70% accuracy.

This stark discrepancy highlights a fundamental limitation of the relative comparison approach when applied to the eyes-closed state, suggesting that its baseline-normalisation process may attenuate the very neural features that are most discriminative in this condition. Nevertheless, the act of combining EO and EC data still provided a clear boost in performance for the relative method, reaffirming the complementary nature of these two resting-states.

Table 4.6. Classification performance for pre- and post-stimulation based on GNIs across all nine graphs with EO, EC conditions and their combination in relative comparison.

Eyes-condition	GNIs	AUC-ROC	ACC	Sensitivity	Specificity	P_{perm}
EO+EC	Rel_open_sensor+Rel_open_source+Rel_open_SomMot+Rel_open_Default+ Rel_closed_source+Rel_closed_DorsAttn+Rel_closed_Cont+Rel_closed_Default	0.83	77%	0.69	0.86	<0.001
EO+EC	Rel_open_sensor+Rel_open_source+Rel_open_SomMot+Rel_open_Cont+Rel_open_Default+Rel_closed_SomMot +Rel_closed_DorsAttn+Rel_closed_Default	0.83	73%	0.66	0.80	<0.001
EO+EC	Rel_open_sensor+Rel_open_source+Rel_open_SomMot+Rel_open_DorsAttn+Rel_open_Cont+Rel_open_inter+ Rel_closed_SomMot+Rel_closed_DorsAttn	0.83	79%	0.66	0.91	<0.001
EO+EC	Rel_open_sensor+Rel_open_source+Rel_open_SomMot+Rel_open_inter+ Rel_closed_SomMot +Rel_closed_DorsAttn+Rel_closed_Cont	0.83	70%	0.54	0.86	<0.001
EO+EC	Rel_open_sensor+Rel_open_source+Rel_open_SomMot+Rel_open_Default+ Rel_closed_DorsAttn+Rel_closed_Cont+Rel_closed_Default+Rel_closed_inter	0.83	71%	0.60	0.83	<0.001
EO	sensor+SomMot+DorsAttn+Cont+inter	0.79	70%	0.63	0.77	<0.001
EO	sensor+SomMot+DorsAttn+SalVentAttn+Cont+inter	0.78	69%	0.57	0.80	<0.001
EO	sensor+SomMot+Cont	0.77	71%	0.60	0.83	<0.001
EC	source+Vis+DorsAttn+SalVentAttn+Cont	0.66	69%	0.57	0.80	0.01
EC	DorsAttn+SalVentAttn	0.64	56%	0.40	0.71	0.01
EC	source+DorsAttn+SalVentAttn+inter	0.63	59%	0.40	0.77	0.04

Note. EO, eyes-open; EC, eyes-closed; Vis, intra-Visual network; SomMot, intra-Somato-Motor network, DorsAttn, intra-Dorsal Attention network; SalVentAttn, intra-Salience-Ventral Attention network, Limbic, intra-Limbic network; Cont, intra-Control network; Default, intra-Default network; inter, inter-network; AUC-ROC., area under the receiver operating characteristic curve; ACC, accuracy; P_{perm}, P value based on 1000 permutation.

4.8. Discussion on combined classification on pre- and post-stimulation

The classification analyses yielded three principal findings regarding the discrimination of pre- and post-stimulation states. First, the highest classification performance was consistently achieved by integrating GNIs from both EO and EC conditions. The absolute comparison method provided the overall best result, with a peak AUC-ROC of 0.88 and accuracy of 81% when features were combined. This demonstrates that EO and EC states provide non-redundant, complementary information about the brain's functional network organisation, and their integration creates a more powerful and robust feature set for machine learning classification.

Second, the incorporation of intra-network features was critical for achieving high accuracy. Models that included GNIs from specific functional networks (e.g., SalVentAttn, SomMot, Default) consistently outperformed those relying solely on global brain-wide graphs. This indicates that stimulus-induced neuroplasticity is reflected not only in broad network-level changes but also in the distinct reconfiguration of specialised functional systems. Capturing this network-specific dynamics is therefore essential for optimal state discrimination.

Finally, the choice of comparison method was a major determinant of success. The absolute comparison method proved to be more robust and universally effective, performing well for both EO and EC conditions. In contrast, the relative comparison showed a significant conditional dependency, performing adequately for EO but poorly for EC. This suggests that the relative

method's baseline normalisation may suppress discriminative features inherent in the absolute connectivity of the eyes-closed state.

In conclusion, these findings establish an optimal strategy for classifying functional brain states using EEG-based network metrics. The most powerful predictive models are built by integrating features from both resting-state conditions (EO and EC) and multiple levels of network topology (brain-wide and intra-network), primarily using the absolute comparison method to preserve the most discriminative neural signatures. This integrative analytical framework provides a robust foundation for developing sensitive biomarkers for neurological conditions or cognitive states.

4.9. Conclusion

4.9.1. Conclusion for eyes-open condition

Our findings demonstrated that the choice of comparison method (absolute vs. relative) substantially influenced observed brain connectivity patterns in both sensor and source space. The absolute comparison highlighted anterior or within-hemisphere connections, whereas the relative comparison tended to emphasise inter-hemispheric and posterior connectivity.

Network-level analyses revealed shifts in hub structures and clustering patterns after stimulation, particularly shifting from SalVentAttn-driven integration with robust Default interactions to SomMot-Vis dual-hub segregation, reflecting altered functional organisation. This reconfiguration aligned with increased segregation and reduced modularity, suggesting that sensory stimulation enhanced specialised processing while also increasing between-network crosstalk. Our findings are consistent with previous reports of the SalVentAttn

network serving as a hub in EO and with evidence of enhanced SomMot and Vis network involvement following sustained pain, indicating the integration of sensory information into bodily self-consciousness in pain perception (Costumero et al., 2020; J. Han et al., 2023; Lou et al., 2024).

4.9.2. Conclusion for eyes-closed condition

In the EC condition, connectivity patterns and inter-network organisation were largely consistent across comparison methods. The EC-pre contrasts featured bilateral intra-hemispheric connectivity, dominated by frontal-parietal and inter-hemispheric parietal-parietal links, while the EC-post contrasts shifted to focused inter-hemispheric pathways, led by right-frontal-to-left-parietal connections.

The reconfiguration of these patterns was captured most effectively by GNIs from the absolute comparison, which also outperformed the relative comparison in classification tasks. Stimulation transformed the EC network from a high-integration, multi-network configuration into a SalVentAttn-dominated, high-segregation state, marked by increased small-worldness and reduced modularity. This transformation reflects a shift toward more specialised information processing, supported by long-distance cross-hemispheric communication. While the broad, distributed network connectivity pattern observed in the EC-pre contrasts aligned with previous research (Agcaoglu et al., 2019; Costumero et al., 2020; J. Han et al., 2023), the distinctive EC-post properties were uniquely elucidated by the present findings.

4.9.3. Similarity and uniqueness for eyes-open and eyes-closed conditions pre- and post-stimulation

The GNI analyses revealed consistent post-stimulation patterns across both EO and EC conditions, characterised by increased functional segregation and small-worldness, alongside reduced modularity, particularly in sensor space. Both conditions exhibited post-stimulation neuroplasticity with altered hub structures, though the specific connectivity pathways and network dominance differed. EO reconfiguration involved a dual-hub SomMot-Vis pattern, whereas EC reorganisation centred on a SalVentAttn-dominated architecture.

These findings highlighted both shared underlying mechanisms and state-specific adaptations to somatosensory stimulation. Furthermore, they validated the robustness of GNIs as sensitive descriptors of large-scale network organisation, supporting their potential use as discriminative features.

4.9.4. Validation and translational potential

The robust classification of pre- versus post-stimulation states, achieving an AUC-ROC of 0.88 and 81% accuracy, is a key achievement of this work. This high performance was accomplished by combining GNIs from both EO and EC conditions using the absolute comparison method. The superior predictive power of this combined model not only confirms the complementary nature of information encoded in different resting-states but also underscores the practical value of GNIs as discriminative features for machine learning. The enhanced performance gained from including intra-network features further reveals that stimulus-induced neuroplasticity is expressed through both global and network-specific reconfigurations.

4.10. Summary

This chapter systematically investigated brain network reconfiguration during eyes-open (EO) and eyes-closed (EC) resting-states before and after sensory stimulation The findings reveal a consistent stimulation-induced shift towards enhanced functional segregation across states, yet manifest through distinct, state-dependent network pathways. Under EO conditions, networks transitioned from an initial SalVentAttn-driven state characterised by robust Default network interactions toward a post-stimulation architecture dominated by dual SomMot-Visual hubs. Conversely, EC conditions shifted from a broad, multi-network integration pattern to a consolidated SalVentAttn-dominated, high-segregation state after stimulation.

These findings elucidated dynamic, state-dependent transitions triggered by sensory input including tonic pain. Critically, we achieved high-accuracy classification of pre- versus post-stimulation states (AUC-ROC = 0.88, accuracy = 81%) using global network inferences (GNIs) derived from graph-based analysis of combined both EO and EC resting-state data. This performance underscored the sensitivity of our multimodal framework in detecting stimulation-induced neuroplasticity and provided a valuable foundation for comparative studies with chronic pain cohorts.

The novel contribution of this work lies in identifying a unified yet state-dependent signature of post-stimulation neuroplasticity, optimally captured through a combined EO/EC multimodal approach.

Chapter 5

Maladaptive network persistence in chronic pain: EEG network integration in resting-states dynamics

Having established a sensitive framework in Chapter 4 for detecting stimulation-induced neuroplasticity in healthy individuals, we now apply it to characterise intrinsic resting-state networks in chronic pain patients compared with healthy controls.

5.1. Introduction

Chronic pain is increasingly understood as a disorder of brain network dysfunction rather than a localised sensory abnormality (Farmer et al., 2012; Hemington et al., 2016; Huang et al., 2019). Resting-state paradigms, which capture intrinsic brain activity in the absence of explicit task demands, have been widely used to investigate these neural correlates. Analyses of static resting-state activity consistently reveal distinct patterns of brain reorganisation that differentiate chronic pain patients (CP) from healthy controls (HC), and in some cases achieve successful group classification (Kutch et al., 2017; Ta Dinh et al., 2019; Tu et al., 2021; Zebhauser et al., 2024). Consequently, these quantifiable signatures of brain network dysfunction are increasingly regarded as highly promising objective biomarkers for chronic pain (Pfannmoller & Lotze, 2019; Zebhauser et al., 2023).

The Default mode network (Default) which plays a critical role in self-referential thought and higher-order cognition, is one of the most consistently reported networks showing disruption across various chronic pain conditions, including chronic back pain, fibromyalgia, and migraine (Alshelh et al., 2018; Baliki et al., 2014). The Default comprises a set of highly interconnected regions, including the medial prefrontal cortex (mPFC), posterior cingulate cortex, inferior parietal cortex and precuneus (Gusnard & Raichle, 2001). Critically, Default disruption is complex and not entirely uniform. Baliki et al. (2011, 2014) reported that while chronic back pain patients show enhanced high-frequency fluctuations of the mPFC, they also exhibit decreased connectivity between the mPFC and the posterior Default components. This specific decoupling is theorised to

impair the competitive inhibition between the Default and attentional networks. Collectively, this evidence suggests that the spatial reorganisation of the Default may be condition-specific, a phenomenon reflected in the unique emotional, attentional, and cognitive abnormalities observed in different clinical populations, with the mPFC effectively "losing its membership" within the canonical Default architecture (Baliki et al., 2014). This reorganisation is further evidenced by graph theoretic analyses, which reveal that the mPFC exhibits significantly higher nodal degree, efficiency, and betweenness centrality in CP patients, suggesting it assumes an altered, and potentially maladaptive, hub-like role in the pain-state brain (Tu et al., 2019).

The functional magnetic resonance imaging (fMRI) has revealed widespread dysfunction in global network architecture and altered hub connectivity in chronic pain, as quantified by graph theory (Baliki & Apkarian, 2015; Huang et al., 2019; Lee et al., 2021; Xin et al., 2024). For example, a multicentre study demonstrated alterations in global network topology in patients with chronic low back pain, including significant reductions in the clustering coefficient and betweenness centrality (Mano et al., 2018). Furthermore, chronic pain has been associated with increased network integration and reduced functional segregation, particularly involving abnormal connectivity of the Default, suggesting a dysfunction of brain state dynamics.

Electroencephalography (EEG) and magnetoencephalography (MEG) studies have also provided insight into neuronal oscillations at different frequencies (Heitmann et al., 2022; Pinheiro et al., 2016). Spectral analysis of EEG has revealed several potential biomarkers. Systematic reviews indicated that chronic pain was associated with higher theta and beta band power (Zebhauser

et al., 2023), while migraine patients showed evidence of lower alpha and beta band connectivity (Zebhauser et al., 2024). In neuropathic pain, MEG studies highlight abnormal alpha power (Kisler et al., 2020), whereas EEG studies consistently show increased theta power, decreased alpha/beta power, and slowing of the dominant peak frequency (Mussigmann et al., 2022). Slower peak alpha frequency has also been reported in patients with widespread pain (Cavaleri et al., 2025),and pancreatitis (Vries et al., 2013). However, findings can be diagnosis-specific, as some studies report no significant differences such as in peak alpha frequency between patients and controls, underscoring the heterogeneity of chronic pain (McLain et al., 2025).

From a functional connectivity perspective, which has been shown to outperform measures of brain activity alone (Bott et al., 2025), EEG and MEG studies have identified aberrant communication between key nodes of the pain connectome. In chronic neuropathic pain, reduced connectivity has been observed between the dorsal anterior cingulate cortex, somatosensory cortex, and pregenual anterior cingulate cortex, suggesting abnormal assignment of behavioural salience to pain (Vanneste & De Ridder, 2021). A large EEG study of 101 CP and 84 HC found significantly increased theta- and gamma-band connectivity in frontal areas of CP patients; machine learning models achieved above-chance classification accuracy (57%), primarily driven by frontal connectivity features (Ta Dinh et al., 2019). Furthermore, graph theory applied to EEG data has shown that changes in one of the global network inferences (GNIs), global network efficiency, at theta frequencies are associated with chronic pain and can be modulated by therapy, even in the absence of changes in spectral power (Heitmann et al., 2022).

Despite these advances, several gaps remain. First, network alterations in CP have been predominantly characterized using fMRI, and comprehensive EEG-based network biomarkers are still lacking. Second, the dynamic properties of these networks, examined through graph theory, remain underexplored in EEG. Third, the influence of the resting-state paradigm (eyes-open vs. eyes-closed) on network metrics in CP is unclear, with mixed findings and limited systematic investigation.

Addressing these gaps is critical for advancing the field of pain neuroscience. Developing robust EEG-based network biomarkers is essential for translating research findings into clinically feasible tools, given EEG's advantages in cost, portability, and temporal resolution. Furthermore, a deeper understanding of dynamic network properties and state-dependent manifestations of pain is necessary to move beyond static snapshots of brain function. This will allow us to capture the fluctuating nature of chronic pain and identify core, stable network signatures that persist across different brain states. Ultimately, bridging these knowledge gaps is a pivotal step towards establishing a unified network-based model of chronic pain that can inform the development of more objective diagnostics and targeted neuromodulatory therapies.

The primary objective of this research is to address these gaps by applying graph theory to alpha-band EEG data collected during both eyes-open (EO) and eyes-closed (EC) resting-state conditions in CP and HC, with particular focus on the Default network. Specifically, we aim to: (1) characterise the reorganisation of functional brain networks in chronic pain by comparing graph theory-based inferences between CP and HC groups across both EO and EC states; (2) evaluate whether group differences vary between EO and EC

resting-state conditions; (3) elucidate the neuronal mechanisms underlying these differences; and (4) assess the ability of GNIs to distinguish between CP and HC.

We hypothesised that chronic pain would be associated with a reconfiguration of functional network topology, manifesting as altered GNIs in the alpha band, with the Default network exhibiting alterations, and that these differences would differ between EO and EC conditions. We further expected that the derived GNIs would demonstrate robust classification performance for differentiating CP and HC groups.

5.2. Methods

5.2.1. Participants

We used an open dataset from the Technical University of Munich, collected for a large-scale study of brain dysfunction in chronic pain (https://osf.io/srpbg/). The original dataset included 96 patients and 81 healthy controls for the eyes-open (EO) condition, and 101 patients and 88 healthy controls for the eyes-closed (EC) condition, derived from three projects: chronic back pain, fibromyalgia, and mixed chronic pain. Resting-state electroencephalographic (EEG) data were recorded in EO and EC conditions; however, not all participants had recordings for both states.

Data inclusion was based on recording quality, resulting in three subgroups: participants with both EO and EC data (paired-state group), participants with only EO data, and participants with only EC data. Importantly, individuals with both EO and EC recordings were included in both the EO and EC subsets. The demographic details for each subgroup are presented in Table 5.1.

Table 5.1. **Demographics of participants**

Eye-state		CP	HC
both	Age(mean±SD)	58.40±11.88	60.38±15.94
	N_female	22	21
	N_total	35	31
	P_CBP	12	0
	P_FM	5	6
	P_NCCP	18	25
EO	Age(mean±SD)	59.22±10.92	59.22±15.45
	N_female	35	31
	N_total	54	50
	P_CBP	22	0
	P_FM	8	11
	P_NCCP	24	39
EC	Age(mean±SD)	57.72±12.07	57.47±15.40
	N_female	38	36
	N_total	54	49
	P_CBP	18	0
	P_FM	14	10
	P_NCCP	22	39

Note. CP, chronic pain patients group; HC , healthy control group matched in such project; EO, eyes-open; EC, eyes-closed; N_female, number of females in the group; N_total, total number of participants in the group; P_CBP, number of participants from chronic back pain project; P_FM, number of participants from Fibromyalgia project; P_NCCP. number of participants from mixed chronic pain conditions project.

5.2.2. Data description and processing

EEG data were recorded using 64 electrodes and a BrainAmp MR Plus amplifier (Brain Products, Munich, Germany), referenced to FCz and grounded at AFz, with a recording duration of 5 minutes. Signals were sampled at 1000 Hz with a resolution of 0.1 μV, band-pass filtered online between 0.016 and 250 Hz, and electrode impedances were kept below 20 kΩ.

Data preprocessing and analysis followed the procedures described in Chapter 4. All analyses focused on the alpha band. The analytical design and classification were largely identical to that of Chapter 4, except that adjacency matrix thresholding was based on the median rather than the median plus one standard deviation. This adjustment was necessary because the more stringent threshold resulted in an insufficient number of connections for a subset of participants, generating invalid GNIs. Most notably, this led to 21 cases of non-calculable small-worldness values across the dataset.

Relative comparisons between EO and EC conditions were conducted only in the paired-state group, where both states were available. As in Chapter 4, relative comparisons were obtained by normalizing each participant's EO connectivity matrix by their corresponding EC matrix, and vice versa for relative EC connectivity.

5.3. Results for eyes-open condition in paired-state group

5.3.1. Results in sensor space

5.3.1.1. Sensor space connectivity: absolute comparison

Sensor-space connectivity during the EO condition revealed distinct group-level patterns between HC and CP groups in absolute comparison (Fig. 5.1). The group-averaged connectivity graph for HC displayed a dense network of connections, whereas the graph for the CP group was sparsely connected (Fig. 5.1A, upper panel).

The NBS analysis revealed only identified one significant component where connectivity was stronger in the CP group compared to the HC group ($P < 0.001$). This component was bilaterally distributed but showed a right-hemispheric predominance, particularly involving prefrontal regions. It comprised 62 nodes interconnected by 822 edges. Conversely, the contrast for stronger connectivity in the HC group (t-graph) revealed a bilateral pattern characterized by sparse, long-distance connections (Fig. 5.1A, lower panel).

5.3.1.2. Sensor space connectivity: relative comparison

Group-level differences were also pronounced in the relative connectivity analysis (Fig. 5.1B). The HC group exhibited a distinctive ipsilateral, right-hemispheric pattern, while the CP group maintained a bilateral distribution (Fig. 5.1B, upper panel).

Similarly, the NBS analysis revealed only a significant connectivity pattern of larger connectivity in CP than HC, with densely connections in right hemisphere and emphasised connectivity in the prefrontal region, consisting of 61 nodes and 1021 edges ($P < 0.001$). In contrast, the t-graph which illustrated the larger connectivity in HC than CP revealed bilateral distribution with both long and short-distance connections (Fig. 5.1B, lower panel).

In summary, a marked difference in connectivity patterns was observed between the absolute and relative comparison methods, particularly within the HC group-level graphs. Despite this, both methods consistently revealed a significant network of stronger connectivity in the CP group compared to the HC group. This network was characterized by dense, bilateral connections with a notable emphasis on right prefrontal regions.

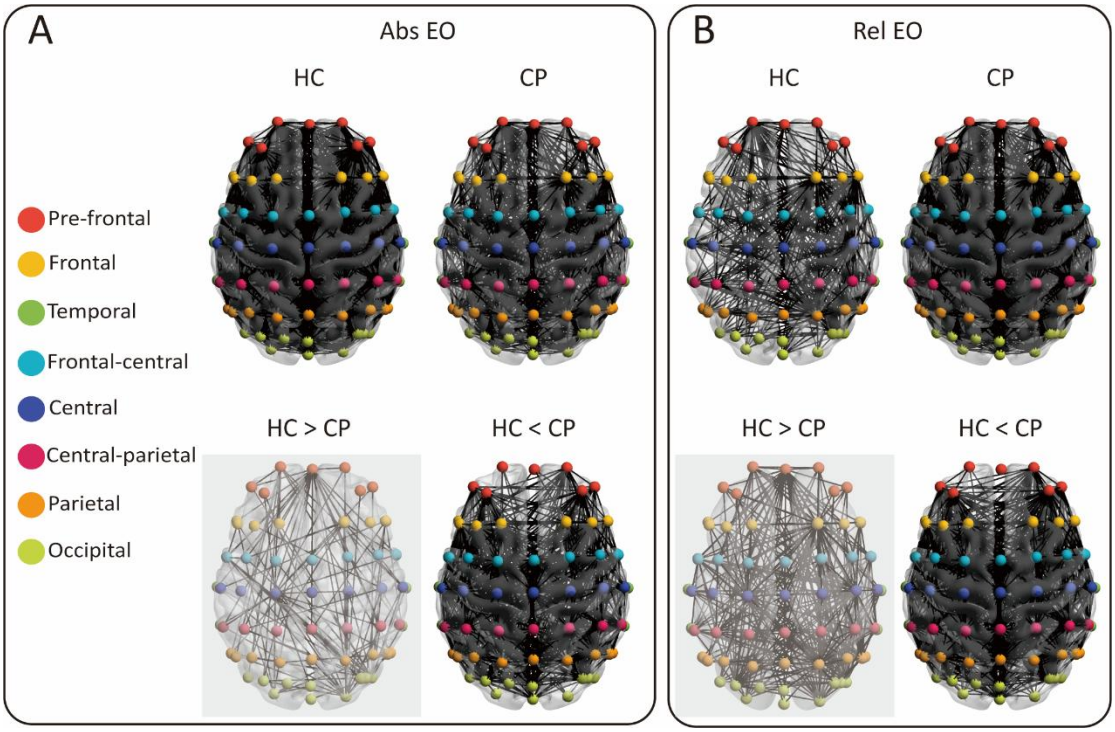

Figure 5.1. Graphs elicited by EO conditions between HC and CP groups using two comparison methods in sensor space. (A) Group-level functional connectivity graph in absolute comparison for EO in HC and CP groups (upper panel row). Sensors corresponding to different scalp regions (Prefrontal, Frontal, Temporal, Frontal-central, Central, Central-parietal, Parietal, and Occipital) were colour-labelled for visual distinction. Group contrast connectivity patterns were identified using NBS and visualised as *p*-graphs and t-graphs, the latter with reduced opacity (lower panel). (B) Similar to (A) but for relative comparison. A marked difference in HC group-level connectivity graphs was observed between the two comparison methods. Both methods, consistently identified a significant network of increased connectivity in the CP group, characterised by dense, bilateral connections with a notable emphasis on right prefrontal regions. EO, eyes-open; Abs, absolute comparison; Rel, relative comparison; HC, healthy control group; CP, chronic pain patient group; NBS, network-based statistics.

5.3.1.3. Sensor space graph analysis results

The significant main effect of comparison method (absolute vs. relative) was observed across all GNIs whereas the significant main effect of group (HC vs. CP) was found for all GNIs except Gcc (Fig. 5.2).

Post hoc comparisons revealed that the absolute comparison method yielded significantly higher Gcc values than the relative method in both the HC group (t (30) = 4.09, $P < 0.001$) and (t (34) = 2.53, $P = 0.01$).

For Geff, a strong main effect of comparison method was observed. Geff was significantly higher under the absolute comparison than the relative comparison in the HC group (t (30) = 2.86, $P = 0.01$) but not in CP group (t (34) = 1.29, $P = 0.21$). A significant main effect of group was also found, with the CP group exhibiting larger Geff values in both the absolute (t (64) = 3.17, $P < 0.01$) and relative comparison (t (64) = 3.27, $P < 0.01$).

Regarding Sw, a strong main effect of comparison method was detected. Small-worldness was significantly higher in the absolute comparison than the relative comparison for the CP group (t (34) = 2.05, $P = 0.05$) but not for the HC group (t (30) = 1.56, $P = 0.13$). A significant main effect of group was also observed, with the HC group showing larger Sw values in both the absolute (t (64) = 3.34, $P = 0.001$) and relative comparison (t (64) = 3.84, $P < 0.001$).

Modularity was significantly higher in the relative comparison than in the absolute comparison for both the HC group (t (30) = 6.08, $P < 0.001$) and the CP group (t (34) = 6.20, $P < 0.001$). Although a significant main effect of group was observed for modularity, no post hoc group comparisons survived correction for multiple comparisons in either the absolute or relative method.

Detailed ANOVA statistics and post-hoc comparisons were provided in Table 5.2.

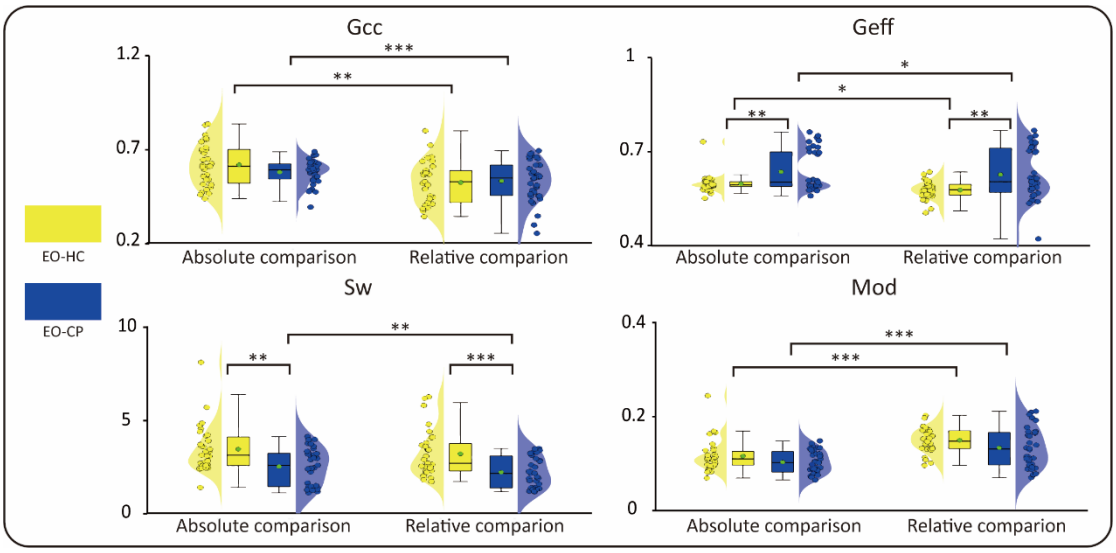

Figure 5.2. Graph analysis results for EO conditions in HC and CP groups using two comparison methods in sensor space. Violin plots with overlaid scatter and box plots show the results of two-way mixed ANOVA with Bonferroni correction for post hoc comparisons of four GNIs across the EO-HC (yellow) and EO-CP (blue) conditions and two comparison methods. A green-filled circle with a black edge denotes the mean value for each group. EO, eyes-open; HC, healthy control group; CP, chronic pain patient group; GNIs, global network inferences; Gcc, global clustering coefficient; Geff, global efficiency; Sw, small-worldness; Mod, modularity. **P* < .05, ***P* < .01, ****P* < .001.

5.3.2. Results in source space

5.3.2.1. Source space connectivity results: absolute comparison

Within the source space (Fig. 5.3), the group-level connectivity graphs for both HC and CP groups exhibited a bilateral distribution pattern (Fig. 5.3A),

and no significant graphs were identified when comparing these two groups using NBS.

The t-graphs illustrating greater connectivity in the HC group showed clusters of increased connectivity both within and across hemispheres, particularly centred in central and parietal regions. By contrast, CP group contrast was primarily localised to central-frontal regions, though also distributed within both hemispheres.

5.3.2.2. Source space connectivity results: relative comparison

For relative comparisons (Fig. 5.3B), a bilateral distribution was again observed in the group-averaged connectivity graphs for both cohorts. As with the absolute method, NBS did not detect any statistically significant networks differentiating the groups.

The t-graph for the relative HC group highlighted a left-hemisphere dominant pattern, localised to central and parietal areas, alongside interhemispheric connections between the parietal regions. For the CP group, differences were again pronounced in frontal regions, which showed connectivity to central and other areas within each hemisphere. Additional cross-hemispheric connections were observed involving frontal and central regions.

Both group-level and group contrast graphs demonstrated consistent patterns across comparison methods, while greater divergence was revealed in the spatial distribution of group differences. The absolute comparison revealed bilateral differences in the HC group, while the relative comparison showed a left-dominant posterior pattern. For the CP group, both methods

demonstrated broadly bilateral anterior patterns, though the relative comparison showed richer cross-hemispheric connectivity than the absolute contrast.

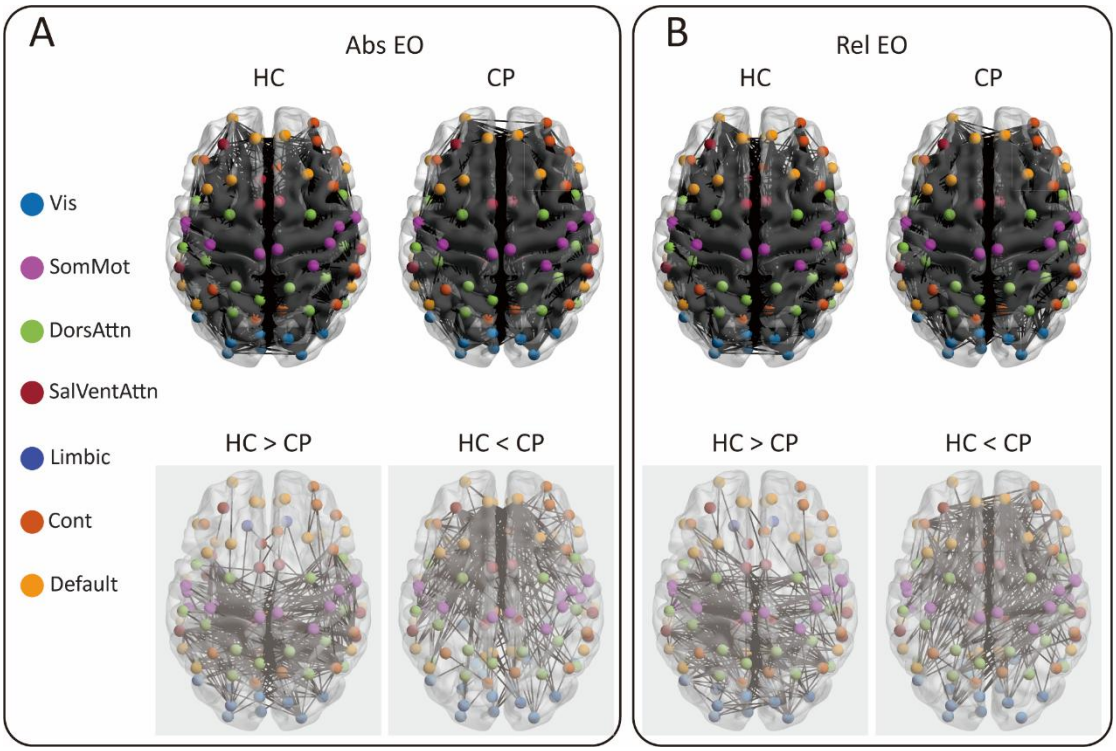

Figure 5.3. Graphs elicited by EO conditions in HC and CP groups using two comparison methods in source space. (A) Group-level functional connectivity graph in absolute comparison for EO in HC and CP groups (upper panel row) in source space for 100 pairs of brain regions organised into 7 different functional networks (Visual, Somato-motor, Dorsal Attention, Salience-Ventral Attention, Limbic, Control, and Default). The *t*-graphs (second row) constructed from connections with a t-value larger than 1.67 compared between conditions using NBS (shown in reduced opacity). (B) Similar to (A) but for relative comparison. Both group-level and contrast graphs showed consistent patterns across methods, though greater divergence emerged in the spatial patterns of these differences. The HC group showed bilaterally distributed posterior connectivity in the absolute comparison, but a left-lateralized pattern in the relative comparison. The CP group exhibited broadly bilateral anterior connectivity with both methods, though the relative comparison demonstrated

enhanced cross-hemispheric connectivity. EO, eyes-open; Abs, absolute comparison; Rel, relative comparison; HC, healthy control group; CP, chronic pain patient group; NBS, network-based statistics.

5.3.2.3. Source space graph analysis results

No significant main effect of group was identified in the source space GNIs. However, significant main effects of comparison methods (absolute vs. relative) were found for both Geff and Sw (Fig. 5.4).

Post-hoc analysis revealed that Geff was significantly higher under the relative compared to the absolute method in the CP group (t (34) = 2.75, P = 0.01) but not in the HC group (t (30) = 1.29, P = 0.20).

Similarly, Sw was significantly greater in the absolute versus relative comparison for the CP group (t (34) = 2.02, P = 0.05) with no significant difference observed in the HC group (t (30) = 1.54, P = 0.13).

Detailed ANOVA statistics and post-hoc comparisons are provided in Table 5.2.

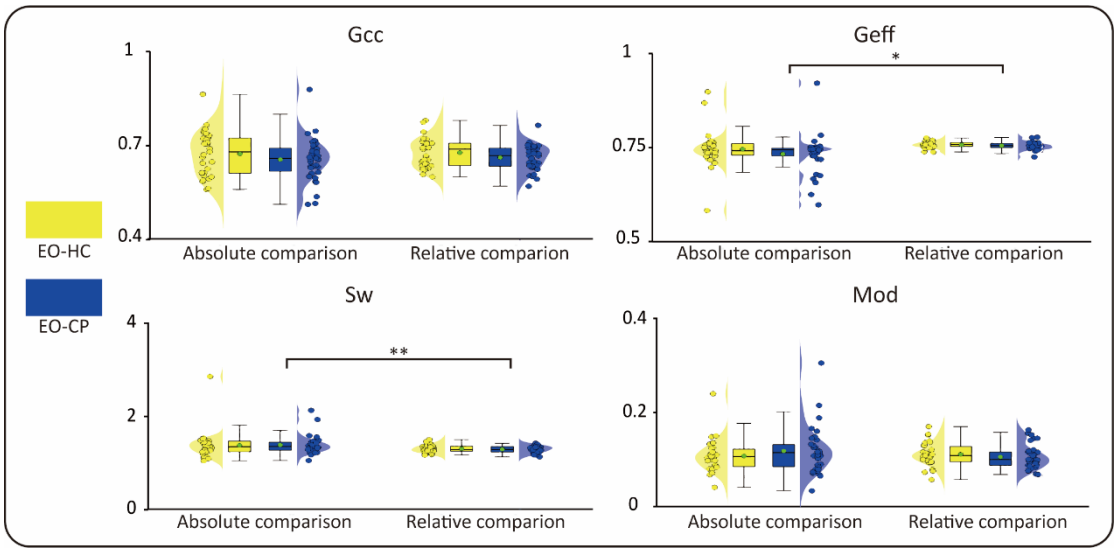

Figure 5.4. Graph analysis results for EO conditions in HC and CP groups using two comparison methods in source space. Violin plots with overlaid scatter and box plots show the results of two-way mixed ANOVA with Bonferroni correction for post hoc comparisons of four GNIs across the EO-HC (yellow) and EO-CP (blue) conditions and two comparison methods. A green-filled circle with a black edge denotes the mean value for each group. EO, eyes-open; HC, healthy control group; CP, chronic pain patient group; GNIs, global network inferences; Gcc, global clustering coefficient; Geff, global efficiency; Sw, small-worldness; Mod, modularity. ***P* < .01, ***P* < .01.

5.3.3. Intra- and inter-network connectivity strength

No significant differences were found in intra- or inter-network connectivity strength for EO conditions between HC and CP groups using either comparison method in source space (Fig. 5.5).

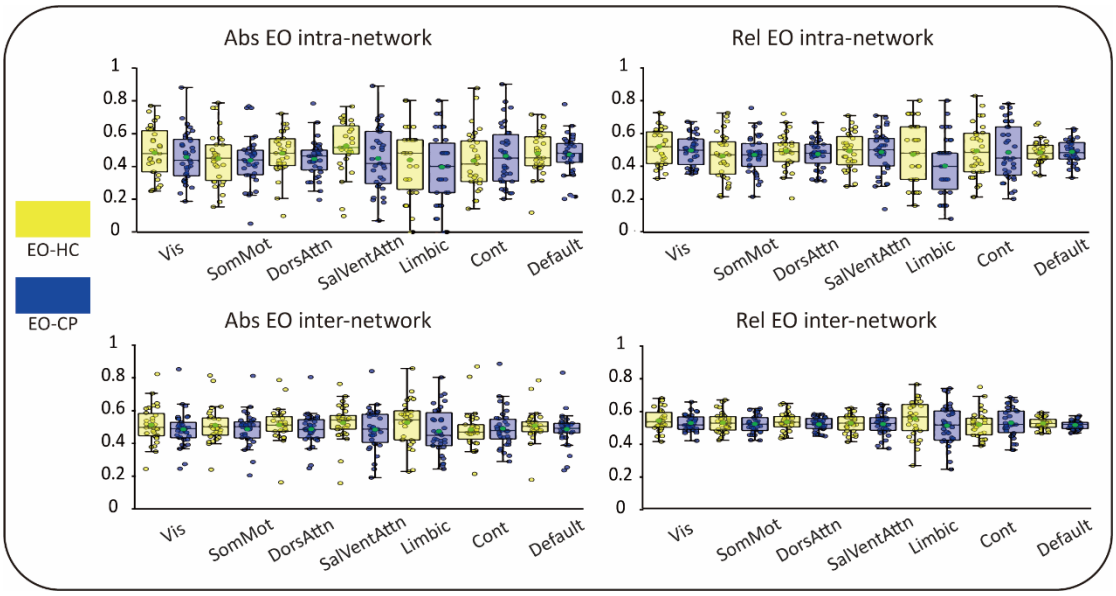

Figure 5.5. Intra-network and inter-network connectivity strength for EO conditions in HC and CP groups using two comparison methods in source space. Box plots display intra- and inter-network mean connections were

performed using a paired-sample *t*-test with FDR correction for two comparison methods. EO, eyes-open; HC, healthy control group; CP, chronic pain patient group; Abs, absolute comparison; Rel, relative comparison; Vis, Visual; Som-Mot, Somato-Motor; DorsAttn, Dorsal Attention; SalVentAttn, Salience-Ventral Attention; Cont, Control.

5.3.4. Higher-order graph results for intra-Default graph

5.3.4.1. Intra-Default graph connectivity results: absolute comparison

For absolute comparison (Fig. 5.6A), a greater number of connections were observed in the CP group compared to the HC group. Both groups exhibited primarily bilateral connectivity patterns. NBS identified a significant component of enhanced connectivity in the CP group ($P < 0.05$), comprising of 23 nodes and 36 edges and characterized by bilateral connections between frontal regions and other areas.

5.3.4.2. Intra-Default graph connectivity results: relative comparison

For relative comparison (Fig. 5.6B), the CP group continued to show denser connectivity patterns in both group-level and contrast graphs compared to the HC group. However, NBS analysis did not reveal any statistically significant differences between groups in the relative comparison.

Both comparison methods consistently revealed greater intra-Default connectivity in the CP group compared to HC participants at the group level. The absolute comparison method specifically identified a statistically significant

graph of enhanced bilateral connectivity in the CP group, while the relative comparison showed similar but non-significant trends.

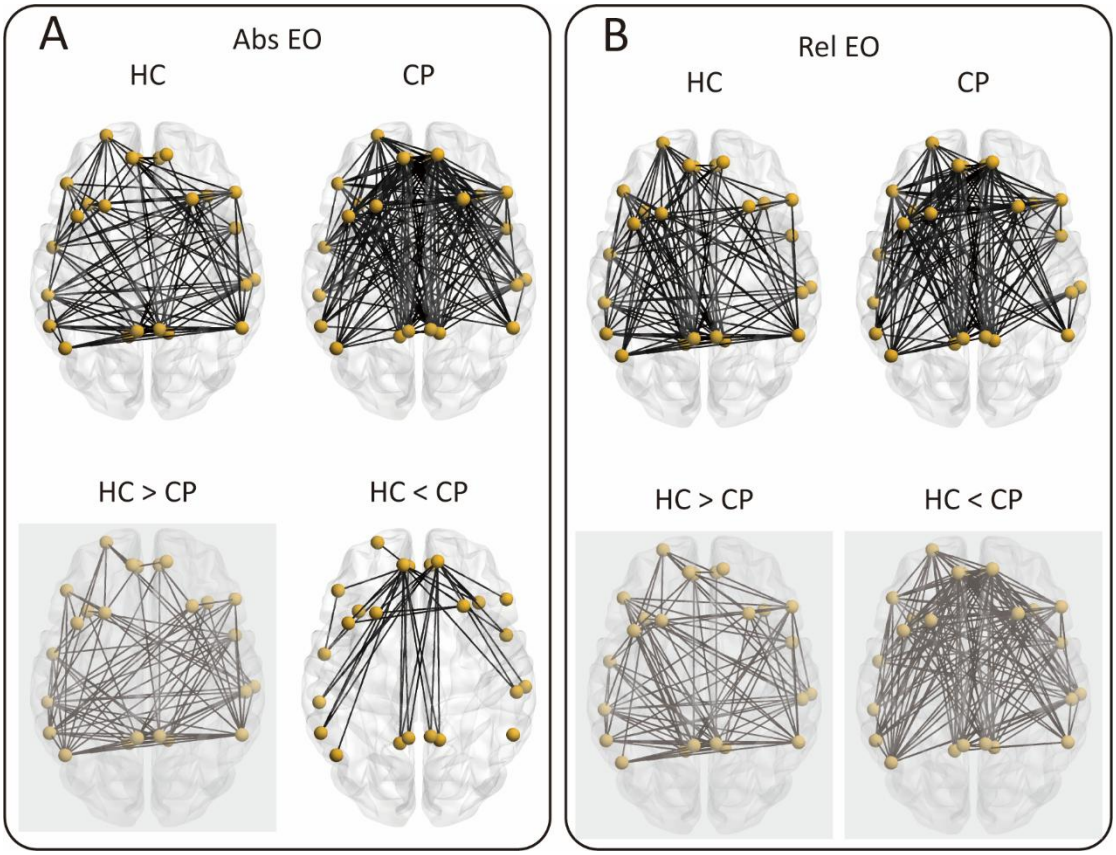

Figure 5.6. Higher-order intra- default graphs elicited in HC and CP groups using two comparison methods. (A) Group-level intra-network graphs for the default network (upper panel) and corresponding significant p-graph and *t*-graph ($t > 0$; shown in reduced opacity) were generated following NBS analysis between two groups (lower panel). (B) Similar to (A) but for the relative comparison. Both comparison methods consistently revealed greater intra-Default connectivity in the CP group compared to HC participants at the group level with significant graph identified in the absolute comparison but not the relative comparison. EO, eyes-open; Abs, absolute comparison; Rel, relative comparison; HC, healthy control group; CP, chronic pain patient group; NBS, network-based statistics.

5.3.4.3. Graph analysis results for intra-Default graph

No significant main effects of comparison method or interaction effects were found for intra-Default GNIs (Fig. 5.7). However, a significant main effect of group was identified for Geff. Post hoc analysis revealed greater Geff in the CP group than the HC group only in the relative comparison (t (64) = 2.20, P = 0.03), but not the absolute comparison (t (64) = 1.65, P = 0.11).

Detailed ANOVA statistics and post-hoc comparisons are provided in Table 5.2.

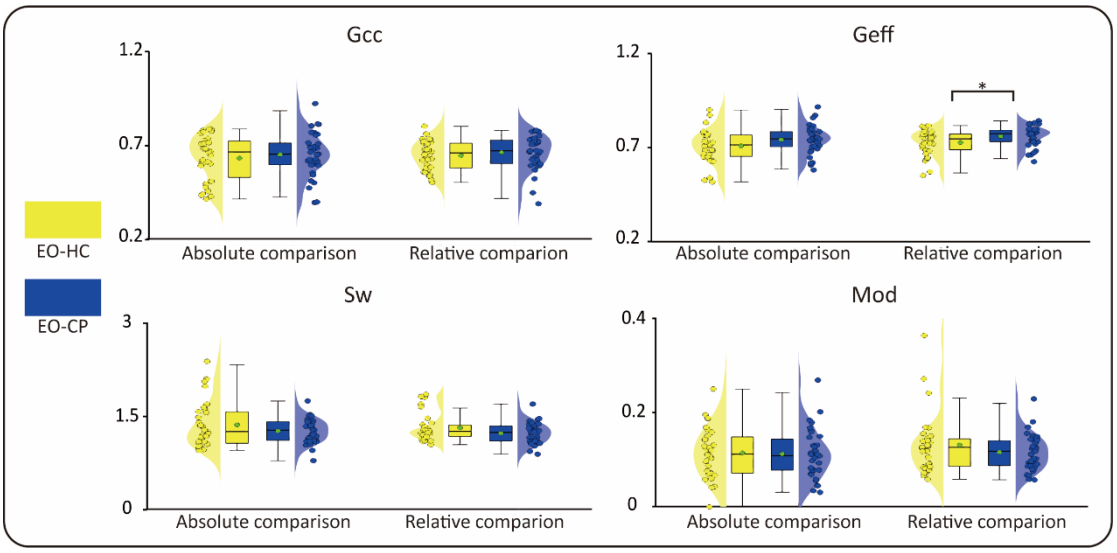

Figure 5.7. Graph analysis results for EO conditions in HC and CP groups using two comparison methods for intra-Default graphs. Violin plots with overlaid scatter and box plots show the results of two-way mixed ANOVA with Bonferroni correction for post hoc comparisons of four GNIs across the EO-HC (yellow) and EO-CP (blue) conditions and two comparison methods. A green-filled circle with a black edge denotes the mean value for each group. EO, eyes-open; HC, healthy control group; CP, chronic pain patient group; GNIs, global network inferences; Gcc, global clustering coefficient; Geff, global efficiency; Sw, small-worldness; Mod, modularity. *P < .05.

5.3.5. Higher-order graph results for inter-network graph

5.3.5.1. Inter-network graph connectivity results: absolute comparison

For absolute comparison (Fig. 5.8A), the HC group exhibited a multi-network communication pattern in contrast graphs, though these findings did not survive statistical correction. In comparison, the CP group demonstrated a distinctive Control network (Cont)-centered connectivity profile, with connections observed between the Cont network and multiple other networks including SalVenAtten, DorsAtten, SomMot, Vis and Default networks.

5.3.5.2. Inter-network graph connectivity results: relative comparison

Relative comparison (Fig. 5.8B) revealed similar multi-network connectivity patterns in HC contrast graphs and Cont-centred pattern in CP contrast graphs. The CP group maintained the connections observed in the absolute comparison, with additional specific network connections emerging, including links between SalVenAtten-SomMot, SalVenAtten-Vis, and SomMot-Default.

Both comparison methods consistently identified distinctive inter-network connectivity patterns between groups. The CP group consistently exhibited a hub-like organisation centred on the Cont network across both methods. In contrast, the HC group demonstrated a more distributed, multi-network communication pattern.

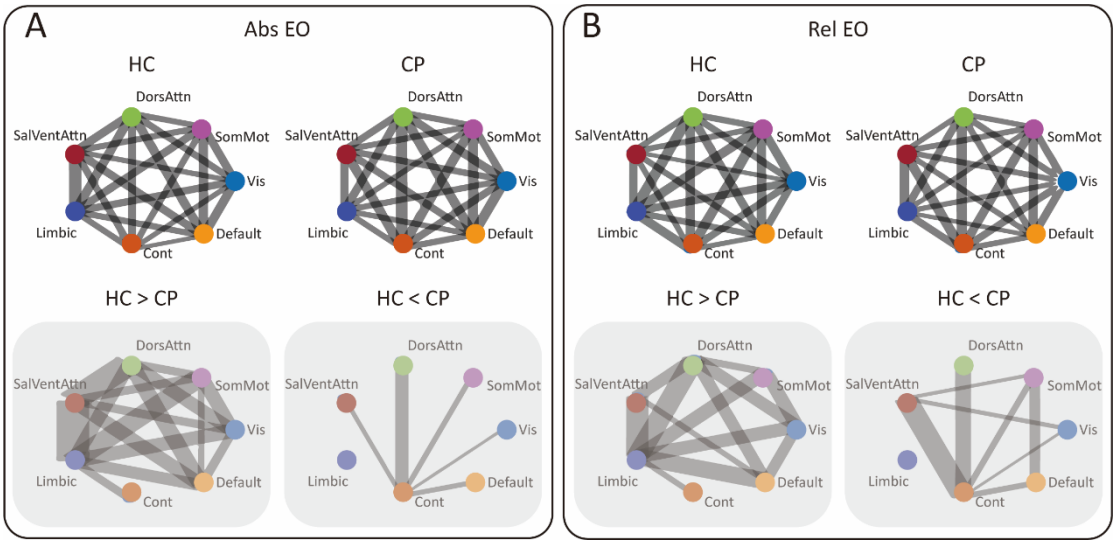

Figure 5.8. Higher-order inter-network graphs elicited by EO conditions in HC and CP groups using two comparison methods. (A) Group-level inter-network weighted graphs and corresponding *t*-graphs ($t > 0$; shown in reduced opacity) were generated following NBS analysis between groups. (B) Similar to (A) but for relative comparison. The stroke size of each connection indicates the edge weight, representing connectivity strength in the upper panels, whereas in the lower panels it represents the corresponding t-value. Both comparison methods consistently identified distinctive inter-network connectivity patterns, with CP group exhibited a Cont- centred pattern and the HC group demonstrated a more distributed, multi-network communication pattern. EO, eyes-open; HC, healthy control group; CP, chronic pain patient group; NBS, network-based statistics; Abs, absolute comparison; Rel, relative comparison.

5.3.5.3. Graph analysis results for inter-network graphs: edge betweenness centrality in absolute comparison

Consistent with the inter-network t-graph findings, edges with heightened Ebc were more prominent in HC contrast graphs compared to CP groups in the absolute comparison (Fig. 5.9A). The most distinctive edges in HC

contrasts included connections between Default-Cont and Default-Vis. Additionally, three edges linking DorsAttn with Limbic, Default, and Vis demonstrated notable betweenness centrality, along with Limbic-SalVentAtten.

The CP contrast similarly revealed a Cont-centred pattern, with prominent edges connecting Cont with Limbic, SalVentAtten, and Vis, supplemented by SalVentAtten-Default.

5.3.5.4. Graph analysis results for inter-network graphs: edge betweenness centrality in relative comparison

The relative comparison yielded consistent findings with the absolute method, showing larger Ebc in HC contrasts (Fig. 5.9B). Distinctive edges also included Default with DorsAttn and SomMot, along with additional links between SomMot and DorsAttn and Vis.

Similarly, the CP contrast graph emphasised the Cont network, demonstrating four edges connected with other networks.

The Ebc patterns demonstrated remarkable consistency between comparison methods, reinforcing the functional importance of the Cont in the CP group connectivity. Additionally, the Default network emerged as a distinctive feature in HC group connectivity across both comparison methods, characterised by multiple high Ebc edges with other networks.

5.3.5.5. Graph analysis results for inter-network graphs: local clustering coefficient

No statistically significant differences in local clustering coefficient (Lcc) were observed between the two groups across the networks examined, using either comparison methods (Fig. 5.9C).

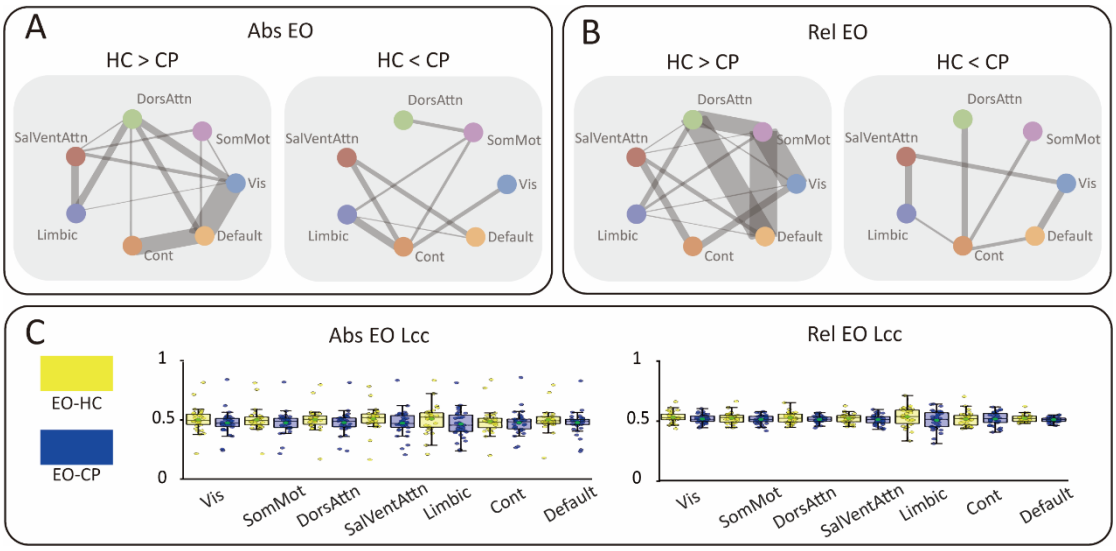

Figure 5.9. Results for local graph inferences analysis from inter-network graphs elicited by EO conditions in HC and CP groups using two comparison methods. (A) Ebc corresponded *t*-graphs generated following NBS in absolute comparison between two groups ($t > 0$; shown in reduced opacity). (B) Similar to (A) but for relative comparison. The stroke size of each connection represents the corresponding t-value for the Ebc graph contrasts. (C) Box plots illustrate the statistical analysis for Lcc by paired-sample *t*-test with FDR correction between groups for two comparison methods. The Ebc patterns demonstrated consistency between comparison methods, reinforcing the functional importance of the Cont network in the CP group, while the Default network emerged as a distinctive feature in the HC group. EO, eyes-open; HC, healthy control group; CP, chronic pain patient group; Ebc, Edge betweenness centrality; NBS, network-based statistics; Abs, absolute comparison; Rel, relative comparison; Vis, Visual; SomMot, Somato-Motor; DorsAttn, Dorsal Attention; SalVentAttn, Salience-Ventral Attention; Cont, Control.

5.3.5.6. Graph analysis results for inter-network graphs: global network inferences

Significant main effects of comparison methods (absolute vs. relative) were observed in both Gcc and Geff (Fig. 5.10) where post-hoc comparisons showed that the relative comparison significantly increased Gcc and Geff compared to the absolute comparison only in the CP group (Gcc: t (34) = 2.13, P = 0.04; Geff: t (34) = 2.00, P = 0.05) but not in the HC group (Gcc: t (30) = 1.06, P = 0.31; Geff: t (30) = 1.00, P = 0.32).

Detailed ANOVA statistics and post-hoc comparisons are provided in Table 5.2.

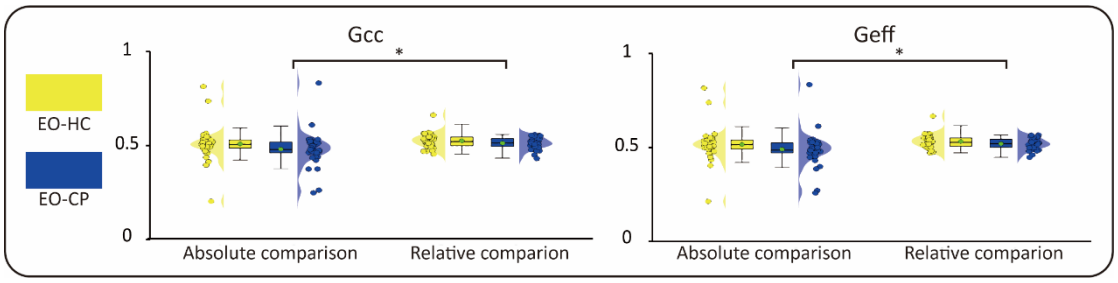

Figure 5.10. Graph analysis results for EO conditions in HC and CP groups using two comparison methods for inter-network graphs. Violin plots with overlaid scatter and box plots show the results of two-way mixed ANOVA with Bonferroni correction for post hoc comparisons of two GNIs across the EO-HC (yellow) and EO-CP (blue) conditions and two comparison methods. EO, eyes-open; HC, healthy control group; CP, chronic pain patient group; GNIs, global network inferences; Gcc, global clustering coefficient; Geff, global efficiency. *P < .05.

Table 5.2. **Statistical results for GNIs from EO conditions between HC and CP groups using two comparison methods (ANOVA and Post-hoc Comparisons).**

Graphs	GNIs	Effect	$F_{(1,64)}$	P	η_p^2	Post-hoc	T	$P_{Bonferroni}$	95% CI
sensor	Gcc	Comparison (Main)	26.58	<0.001	0.29	Abs > Rel (HC)	4.70	<0.001	[0.05, 0.14]
						Abs > Rel (CP)	2.53	0.01	[0.01, 0.09]
sensor	Geff	Comparison (Main)	8.05	0.01	0.11	Abs > Rel (HC)	2.86	0.01	[0.01, 0.03]
						Abs > Rel (CP): ns	1.29	0.21	[-0.01, 0.02]
sensor	Geff	Group (Main)	11.28	0.001	0.15	CP > HC (Abs)	3.17	<0.01	[0.01, 0.06]
						CP > HC (Rel)	3.27	<0.01	[0.02, 0.08]
sensor	Sw	Comparison (Main)	6.44	0.02	0.09	Abs > Rel (HC):ns	1.56	0.13	[-0.07, 0.57]
						Abs > Rel (CP)	2.05	0.05	[0.01, 0.61]
sensor	Sw	Group (Main)	15.46	<0.001	0.20	HC > CP (Abs)	3.34	0.001	[-0.37, 1.48]
						HC > CP (Rel)	3.84	<0.001	[0.47, 1.50]
sensor	Mod	Comparison (Main)	74.49	<0.001	0.54	Rel > Abs (HC)	6.80	<0.001	[-0.12, 0.31]
						Rel > Abs (CP)	6.20	<0.001	[0.02, 0.04]
sensor	Mod	Group (Main)	4.12	0.04	0.06	HC > CP (Abs):ns	0.23	0.08	[0.00, 0.03]
						HC > CP (Rel):ns	1.78	0.07	[0.00, 0.03]
source	Geff	Comparison (Main)	7.61	<0.01	0.11	Rel > Abs (HC):ns	1.50	0.20	[-0.01, 0.03]
						Rel > Abs (CP)	2.75	0.01	[0.01, 0.04]
source	Sw	Comparison (Main)	6.30	0.02	0.09	Abs > Rel (HC):ns	1.54	0.13	[-0.02, 0.17]
						Abs > Rel (CP)	2.02	0.05	[0.00, 0.18]
Intra-Default	Geff	Group (Main)	5.29	0.03	0.08	CP > HC (Abs):ns	1.65	0.11	[-0.01, 0.07]
						CP > HC (Rel)	2.20	0.03	[0.00, 0.06]
Inter-network	Gcc	Comparison (Main)	4.77	0.03	0.07	Rel > Abs (HC):ns	1.06	0.31	[-0.02, 0.05]
						Rel > Abs (CP)	2.13	0.04	[0.00, 0.06]
Inter-network	Geff	Comparison (Main)	4.45	0.04	0.07	Rel > Abs (HC):ns	1.00	0.32	[-0.02, 0.05]
						Rel > Abs (CP)	2.00	0.05	[0.00, 0.06]

Note. EO, eyes-open; HC, healthy control group; CP, chronic pain patient group; GNIs, global network inferences; Gcc, global clustering coefficients; Geff, global efficiency; Sw, small-worldness; Mod, modularity; Abs, absolute comparison; Rel, relative comparison.

5.3.6. Classification performance

The top three classification performances based on GNIs derived from all 18 graphs and their combination in EO condition for both comparison methods were presented in the Table 5.3. While permutation-based *P* values indicated statistically significant classifications, the prediction AUC-ROCs based on single comparison methods did not exceed 0.82.

Specifically, the relative comparison method achieved the highest AUC-ROC among single-method approaches, reaching 0.81 with 70% accuracy, while the absolute comparison yielded a maximum AUC-ROC of 0.74 with 71% accuracy. In contrast, feature combination from both absolute and relative comparisons significantly improved classification performance, achieving a peak AUC-ROC of 0.86 and 74% accuracy.

These results suggest that integrating both comparison methods can enhance the predictive performance of GNIs in classifying HC and CP groups for EO conditions.

Table 5.3. Classification performance for HC and CP groups based on GNIs across eighteen graphs and both comparison methods under EO conditions.

Comp	GNIs	AUC-ROC	ACC	Sensitivity	Specificity	P_{perm}
Abs	Abs_sensor+Abs_source+Abs_Default	0.74	71%	0.63	0.81	<0.001
Abs	Abs_sensor+Abs_source+Abs_Default+Abs_DorsAttn	0.72	68%	0.54	0.84	0.001
Abs	Abs_sensor+Abs_source+Abs_Default+Abs_inter	0.72	70%	0.63	0.77	0.002
Rel	Rel_sensor+Rel_SomMot+Rel_Cont	0.81	70%	0.63	0.77	<0.001
Rel	Rel_sensor+Rel_SomMot+Rel_Cont+inter_OC	0.80	73%	0.71	0.74	<0.001
Rel	Rel_sensor+source_OC+Rel_Cont+VIS_OC	0.80	73%	0.63	0.84	<0.001
Abs+Rel	Abs_source+Abs_Default+Abs_SA+Abs_inter+Rel_sensor+Rel_DorsAttn+Rel_SalVentAttn+Rel_Cont	0.86	74%	0.66	0.84	<0.001
Abs+Rel	Abs_source+Abs_Cont+Abs_DorsAttn+Abs_inter+Rel_sensor+Rel_DorsAttn+Rel_SalVentAttn+Rel_Cont	0.85	74%	0.63	0.87	<0.001
Abs+Rel	Abs_sensor+Abs_source+Abs_SomMot+Abs_SalVentAttn+Rel_sensor+Rel_source+Rel_Vis+Rel_DorsAttn+Rel_SalVentAttn+Rel_Cont+Rel_inter	0.85	74%	0.63	0.87	<0.001

Note. EO, eyes-open; HC, healthy control group; CP, chronic pain patient group; Comp, Comparison methods; Abs, absolute comparison; Rel, relative comparison; Vis, intra-Visual network; SomMot, intra-Somato-Motor network, DorsAttn, intra-Dorsal Attention network; SalVentAttn, intra-Salience-Ventral Attention network, Limbic, intra-Limbic network; Cont, intra-Control network; Default, intra-Default network; inter, inter-network; AUC-ROC, area under the receiver operating characteristic curve; ACC, accuracy; $P_{perm,}$ P value based on 1000 permutation.

5.4. Discussion for eyes-open condition in paired-state group

5.4.1. Representative connectivity patterns

Under the EO condition, significant graphs emerged for the CP contrast in the sensor space and for the intra-Default networks. The brain-wide sensor space graph, identified by both comparison methods, was characterised by larger bilateral connections, with a predominance in the right prefrontal regions. Additionally, a significant intra-Default graph was found in the CP contrast and showed a bilateral distribution and was observed only in the absolute comparison.

The significant brain-wide graph in the CP contrast is consistent with previous research illustrating increased resting EEG alpha power spectra in chronic neurogenic pain, with the most prominent contributions from electrodes in the frontal regions (Sarnthein et al., 2006). Similar overactivation in the alpha band has been observed in patients with persistent pain after breast cancer treatment (van den Broeke et al., 2013). Moreover, the significant intra-Default graph in CP contrast aligns with findings that Default showed increased coupling with pain-related regions in CP at rest (Baliki et al., 2014). Specifically, chronic pain may alter the normative functioning of the Default by weakening the mPFC's connection with posterior components of the Default whilst strengthening connectivity with the insula, suggesting a shift in pain modulation from sensory-processing to emotional-processing functions (Hashmi et al., 2013).

Although not surviving statistical correction, consistent trends in source-space results appeared across both comparison methods: a posterior connectivity pattern in the HC contrast and an anterior connectivity pattern in the CP contrast. This pattern of overactive, frontally-emphasised connectivity aligns with fMRI studies (Hashmi et al., 2013; Kucyi et al., 2014; Seminowicz & Moayedi, 2017), underscoring the role of frontal brain regions in chronic pain as being more critical for pain modulation and emotional evaluation than for sensory processing (Baliki et al., 2011; Baliki & Apkarian, 2015). The intra-Default graphs further revealed a greater number of connections in the CP contrast under the relative comparison.

Finally, inter-network graphs from both comparison methods indicated multi-network connectivity in the HC contrast, with the Default network showing connections of high topological importance (high edge betweenness centrality). In contrast, the CP was characterised by a shift in critical network pathways, with the highest centrality edges localised within the Cont network, highlighted consistently in the inter-network and Ebc graphs across both comparison methods. This altered connectivity profile is reminiscent of findings linking the Cont and amygdala, which is most exaggerated in patients with the greatest pain catastrophising, representing a shared neural basis for cognitive/emotional changes and distress symptoms in anxiety and chronic pain (Jiang et al., 2016).

5.4.2. Global network inferences and networks

Our findings demonstrate that the choice of comparison method (absolute vs. relative) substantially influenced GNIs across sensor space, source space, and inter-network graphs, highlighting the impact of baseline normalisation on these measures.

Importantly, distinct network functional inferences between the HC and CP groups also emerged in the sensor space and intra-Default graphs. In the sensor space graphs, the CP group consistently showed significantly higher Geff and lower Sw across both comparison methods. The increase in Geff in the CP group was further supported by the intra-Default graphs in the relative comparison. This observed increase in global integration was not aligned with some previous findings from fMRI research (Case et al., 2019; Mano et al., 2018), and EEG research in the beta band (Case et al., 2019) and gamma band (Ta Dinh et al., 2019). A potential explanation for this discrepancy lies in the network density; previous studies often used limited links (e.g., less than 30% density), whereas our analysis preserved half of the connectivity to maintain a biologically plausible value of small-worldness in our dataset. It is also noteworthy that a systematic review suggests that only three out of ten articles reported lower global efficiency in CP, while others reported no significant difference. Moreover, the significantly lower Sw we observed in CP was consistent with findings in neuropathic pain (Xin et al., 2024) from both functional (P. Zhang et al., 2021) and structural networks (P. Zhang et al., 2022), indicating the brain networks in CP was topologically more similar to random networks and less cost-efficient (Liao et al., 2017).

5.4.3. Network reorganisation

Group differences in functional network characteristics were evident in both brain-wide sensor space graphs and intra-Default graphs. The more extensive connectivity observed in the CP group across both comparison methods aligned with its higher global efficiency and reduced small-worldness. This finding is consistent with reported overactivation in the alpha band within regions

of the pain network, including: the anterior cingulate, anterior and posterior insula, parietal lobule, thalamus, somatosensory cortex, and dorsolateral prefrontal cortex (Prichep et al., 2018). This pattern aligns with the thalamocortical dysrhythmia model (Llinás et al., 2005). According to this model (Tu et al., 2020; Tu, Li, et al., 2023), abnormal nociceptive input would cause abnormal thalamic bursting, resulting in disinhibition of neighbouring structures and the generation of abnormal oscillations. Such overactivation might lead to enhanced functional integration but a disrupted relationship between functional segregation and integration, thereby leading to reduced small-worldness. Additionally, this greater functional integration was also reflected in the intra-Default graphs in the relative comparison, alongside a bilateral CP contrast distribution in the absolute comparison. This is consistent with observations in neuropathic chronic pain where increased alpha power has also been observed in MEG data within the Default network (Kisler et al., 2020).

5.4.4. Classification performance

Classification performance based on GNIs from all graphs in EO condition for HC and CP achieved the highest AUC-ROC of 0.86 and an accuracy of 74%, although models using a single comparison method did not exceed 0.82 AUC-ROC. Furthermore, the performance of models using only the relative comparison method was superior to those using the absolute method, particularly in terms of AUC-ROC. This suggests that combining both comparison methods enhances the predictive power of GNIs for classifying HC and CP groups under EO conditions. It also indicates that the choice of comparison method itself did not differ in its ability to classify the subject groups.

5.5. Results for eyes-closed condition in paired-state group

5.5.1. Brain-wide graph results in sensor space

5.5.1.1. Sensor space connectivity results: absolute comparison

Under the EC condition, the sensor space graph derived from the absolute comparison revealed distinct patterns for each group: the HC group exhibited a connectivity pattern distributed predominantly within the right hemisphere, whereas the CP group exhibited a densely connected, bilateral distribution (Fig. 5.11A). NBS analysis identified a significant component demonstrating greater connectivity in the CP group relative to the HC group, comprising 62 nodes and 1075 edges ($P < 0.001$). This graph in the CP contrast was bilaterally distributed, with a predominance of connections in the right prefrontal regions.

5.5.1.2. Sensor space connectivity results: relative comparison

Consistent with the findings from the absolute comparison, the relative comparison also showed a right-hemisphere dominant pattern for the HC group and a bilateral connectivity pattern for the CP group (Fig. 5.11B). NBS analysis similarly identified a significant graph of greater connectivity in the CP group, comprising 62 nodes and 1097 edges ($P < 0.001$). This graph shared the same overall bilateral distribution for the CP contrast, again demonstrating a right-hemisphere predominant trend in the prefrontal regions.

In summary, the group-level sensor space graphs from both comparison methods consistently revealed a right-hemisphere dominant pattern in the HC group, in contrast to a bilateral distribution in the CP group. Both methods identified a significant, large-scale graph of increased connectivity in the CP group, which was characterised by its bilateral nature and a predominant focus in the right prefrontal regions.

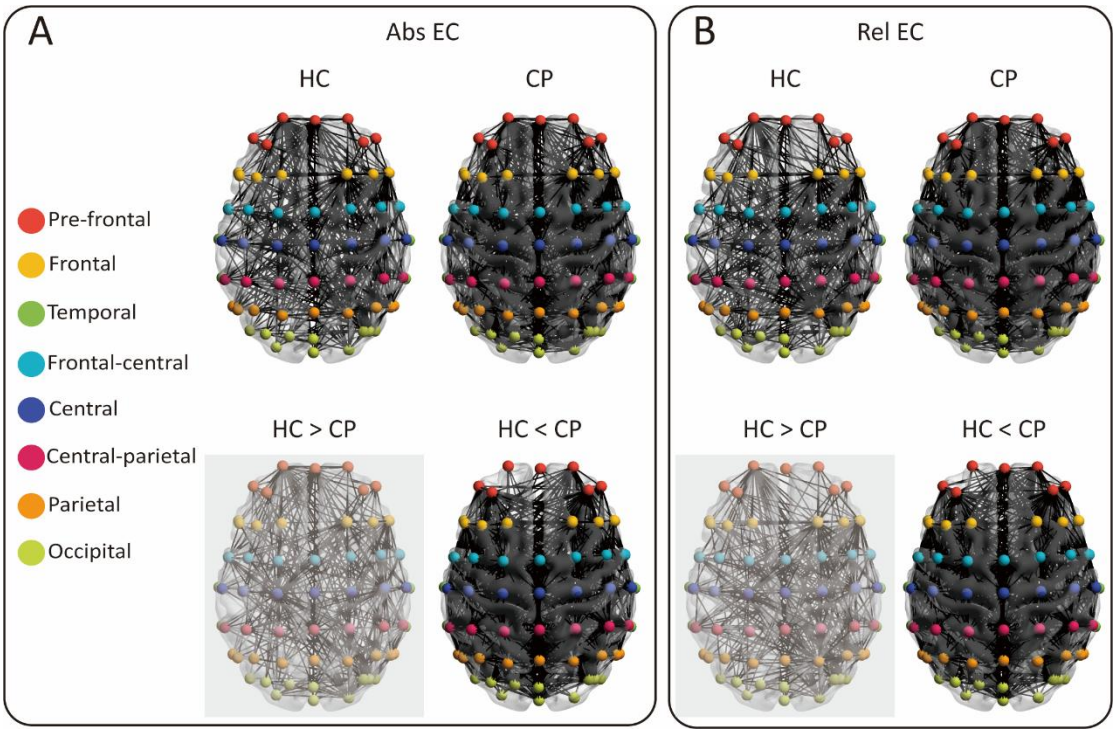

Figure 5.11. Graphs elicited by EC conditions in HC and CP groups using two comparison methods in sensor space. (A) Group-level functional connectivity graph for EC in both groups (first row). Sensors corresponding to different scalp regions (Prefrontal, Frontal, Temporal, Frontal-central, Central, Central-parietal, Parietal, and Occipital) were colour-labelled for visual distinction. Group difference connectivity patterns were identified using NBS and visualised as significant *p*-graphs and t-graphs in reduced opacity (second row). (B) Similar to (A) but for relative comparison. The group-level graphs from both comparison methods revealed a right-hemisphere dominance in the HC group,

in contrast to a bilateral distribution in the CP group. NBS analysis further identified a consistent bilateral connectivity pattern with right prefrontal predominance in the CP contrast across both methodologies. EC, eyes-closed; HC, healthy control group; CP, chronic pain patient group; NBS, network-based statistics; Abs, absolute comparison; Rel, relative comparison.

5.5.1.3. Sensor space graph analysis results

Significant main effects of comparison methods (absolute vs. relative) were observed across all four GNIs, whereas the significant main effect of group (HC vs. CP) were shown in GNIs except for Gcc (Fig. 5.12). For Gcc, post-hoc comparisons revealed significantly higher values in the absolute comparison than in the relative comparison for both the HC and CP groups (HC: t (30) = 4.00, $P < 0.001$; CP: t (34) = 2.16, $P = 0.03$).

Although functional integration (Geff) showed significant main effects for both factors, post-hoc comparisons for the comparison method did not reach significance. However, Geff was significantly higher in the CP group than in the HC group for both comparison methods (absolute comparison: t (64) = 3.92, $P < 0.01$; relative comparison: t (64) = 3.56, $P < 0.01$).

Small-worldness values were significantly higher in the absolute comparison than in the relative comparison for both groups (HC: t (30) = 2.82, $P < 0.01$; CP: t (34) = 2.73, $P < 0.01$). Furthermore, Sw was significantly increased in the HC group relative to the CP group under both comparison methods (absolute comparison: t (64) = 3.87, $P < 0.001$; relative comparison: t (64) = 4.02, $P < 0.001$).

Modularity was significantly larger in the relative comparison for both groups (HC: t (30) = 5.28, $P < 0.001$; CP: t (34) = 2.00, $P < 0.01$). Moreover,

while no significant difference between groups was found for the absolute comparison (t (64) = 1.42, P = 0.19) Mod values were significantly higher in the HC group than in the CP group for the relative comparison (t (64) = 3.00, P < 0.01).

Detailed ANOVA statistics and post-hoc comparisons are provided in Table 5.4.

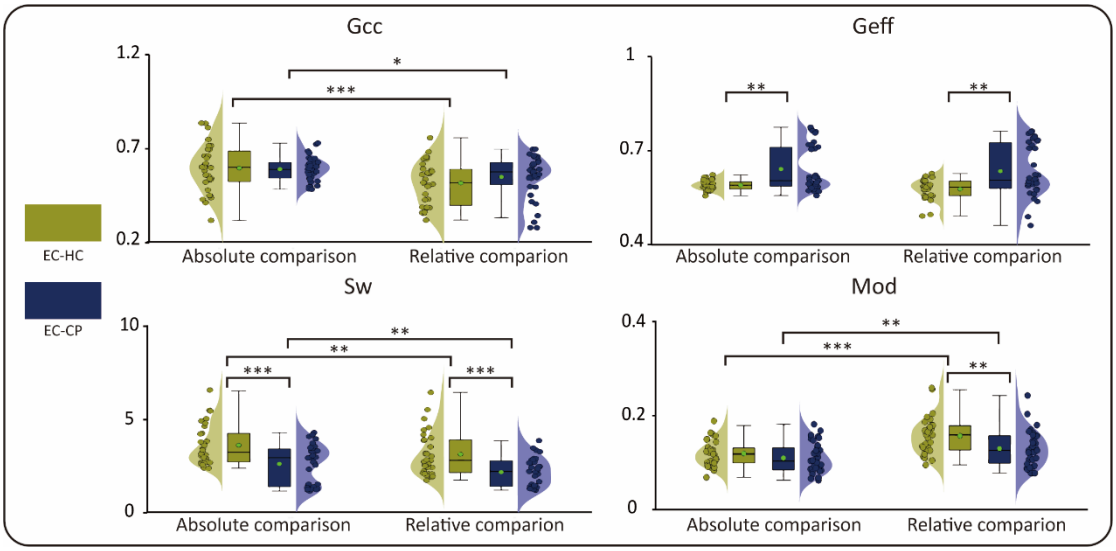

Figure 5.12. Graph analysis results for EC conditions in HC and CP groups using two comparison methods in sensor space. Violin plots with overlaid scatter and box plots show the results of two-way mixed ANOVA with Bonferroni correction for post hoc comparisons of four GNIs across the HC (dark yellow) and CP (dark blue) groups and two comparison methods. A green-filled circle with a black edge denotes the mean value for each group. EC, eyes-closed; HC, healthy control group; CP, chronic pain patient group; GNIs, global network inferences; Gcc, global clustering coefficient; Geff, global efficiency; Sw, small-worldness; Mod, modularity. *P < .05, **P < .01, ***P < .001.

5.5.2. Brain-wide graph results in source space

5.5.2.1. Source space connectivity results: absolute comparison

Group-level graphs for the absolute comparison revealed a bilateral distribution of connectivity in both the HC and CP groups under EC conditions (Fig. 5.13A). Although they did not survive statistical correction, the NBS analysis identified ipsilateral connectivity patterns in the t-graphs. Specifically, the HC contrast showed increased connectivity within the right hemisphere, with connections linking frontal to central regions, and interhemispheric connections between the right frontal and left parietal regions. In contrast, the CP contrast revealed more prominent connections within the left hemisphere, particularly involving central regions, and between the left central and right occipital regions.

5.5.2.2. Source space connectivity results: relative comparison

In the relative comparison, the group-level connectivity graphs exhibited patterns largely consistent with those observed in the absolute comparison, with both groups showing a bilaterally distributed, dense pattern of connections (Fig. 5.13B). The t-graphs for the HC contrast demonstrated bilateral edges linking anterior regions. Conversely, the CP contrast revealed a left-hemisphere-dominated distribution, with increased connectivity between left central regions and right occipital regions.

In summary, source space graphs from both comparison methods showed a bilateral, dense distribution of connections in both groups. The HC group displayed a right-frontal to left parietal distribution with right-hemisphere-

dominant connectivity in the absolute comparison, while a bilateral anterior distribution was revealed in the relative comparison. In contrast, the CP contrast showed greater consistency between comparison methods, exhibiting a left-hemisphere-dominant pattern in posterior regions, along with increased interhemispheric connectivity from left central to right occipital regions.

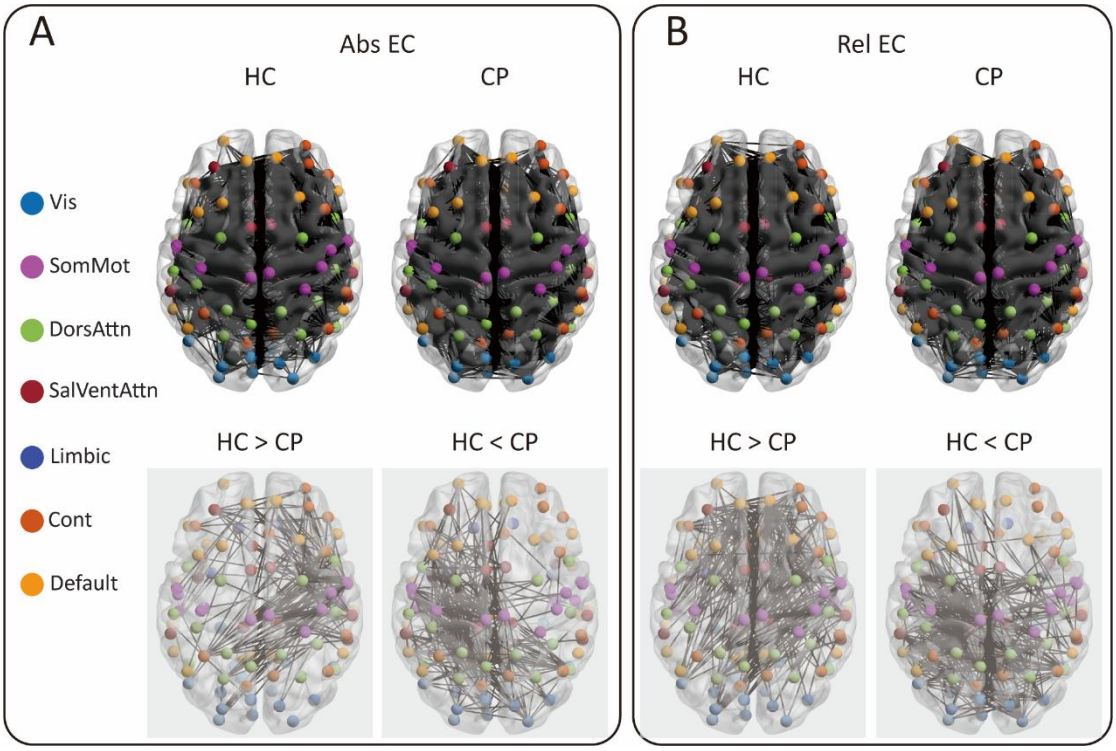

Figure 5.13. Graphs elicited by EC conditions in HC and CP groups using two comparison methods in source space. (A) Group-level functional connectivity matrices in absolute comparison for EC in HC and CP groups (first row) projected in source space for 100 pairs of brain regions organised into 7 different functional networks (Visual, Somato-motor, Dorsal Attention, Salience-Ventral Attention, Limbic, Control, and Default). The *t*-graphs (second row) constructed from connections with a t-value larger than 1.69 compared between conditions using NBS (shown in reduced opacity). (B) Similar to (A) but for relative comparison. The group-level graphs from both comparison methods revealed a bilaterally distributed, dense pattern of connections in both groups.

The HC group exhibited right-hemisphere-dominant connectivity in the absolute comparison, whereas the relative comparison revealed more anteriorly distributed bilateral connections. In contrast, the CP group demonstrated a consistent left-hemisphere-dominant pattern across both comparison methods. EC, eyes-closed; HC, healthy control group; CP, chronic pain patient group; NBS, network-based statistics; Abs, absolute comparison; Rel, relative comparison.

5.5.2.3. Source space graph analysis results

The significant main effect of comparison methods (absolute vs. relative) was only observed in Geff (Fig. 5.14). Specifically, Geff exhibited significant larger values in the relative comparison than the absolute comparison in both HC and CP groups (HC: t (30) = 2.29, P = 0.03; CP: t (34) = 2.00, P = 0.04). No other significant results were found in GNIs in source space graphs.

Detailed ANOVA statistics and post-hoc comparisons are provided in Table 5.4.

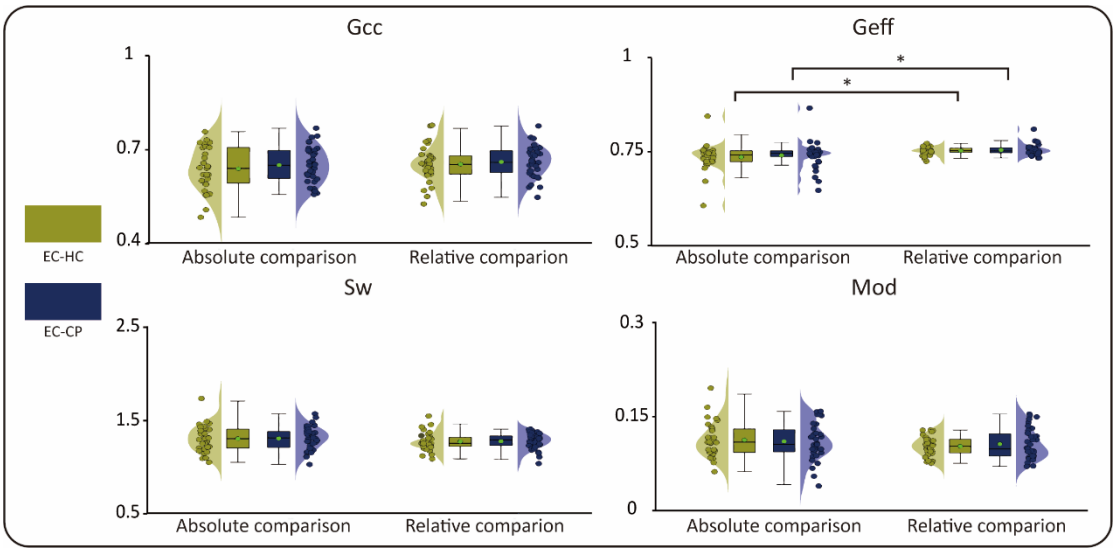

Figure 5.14. Graph analysis results for EC conditions in HC and CP groups using two comparison methods in source space. Violin plots with overlaid

scatter and box plots show the results of two-way mixed ANOVA with Bonferroni correction for post hoc comparisons of four GNIs across the HC (dark yellow) and CP (dark blue) conditions and two comparison methods. A green-filled circle with a black edge denotes the mean value for each group. EC, eyes-closed; HC, healthy control group; CP, chronic pain patient group; GNIs, global network inferences; Gcc, global clustering coefficient; Geff, global efficiency; Sw, small-worldness; Mod, modularity. *P < .05.

5.5.3. Intra- and inter-network connectivity strength

The only significant difference between groups was found in the SalVentAttn network with significantly larger connectivity strength in the HC group than CP group for intra-network connectivity strength in the absolute comparison (t (64) = 2.14, P = 0.04). No other significant results were found for intra- and inter-network connectivity strength in the EC conditions for both groups using the two comparison methods in source space (Fig. 5.15).

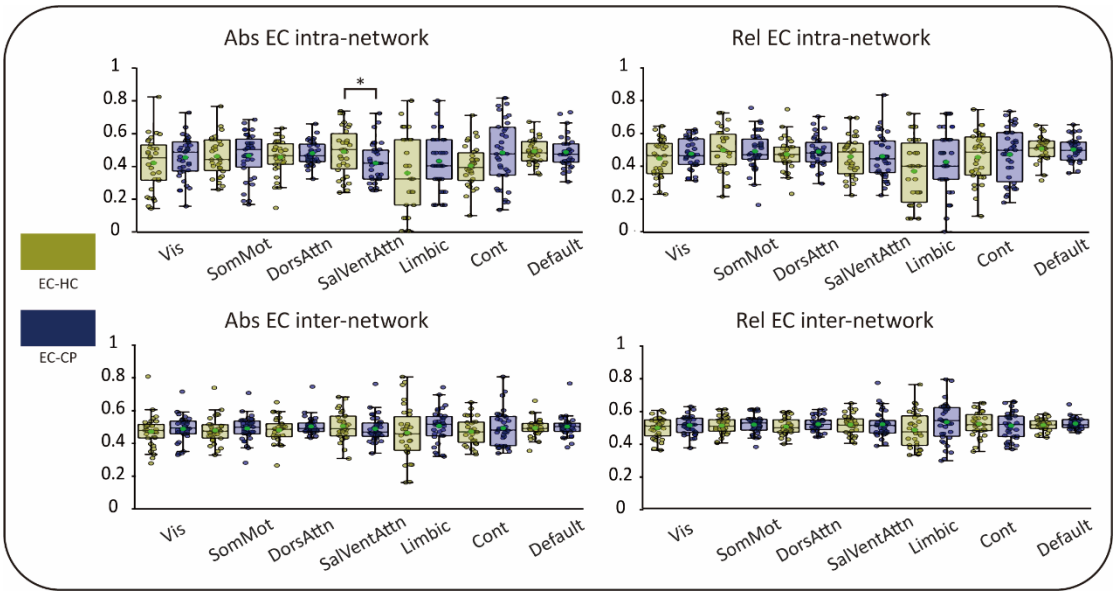

Figure 5.15. Intra-network and inter-network connectivity strength for EC conditions in HC and CP groups using two comparison methods in source

space. Box plots display intra- and inter-network mean connections were performed using a paired-sample *t*-test with FDR correction for two comparison methods in two groups. EC, eyes-closed; HC, healthy control group; CP, chronic pain patient group; Abs, absolute comparison; Rel, relative comparison; Vis, Visual; SomMot, Somato-Motor; DorsAttn, Dorsal Attention; SalVentAttn, Salience-Ventral Attention; Cont, Control. *$P < .05$.

5.5.4. Higher-order graph results for intra-Default graph

5.5.4.1. Intra-Default graph connectivity results: absolute comparison

In the absolute comparison (Fig. 5.16A), group-level intra-Default graphs exhibited dense connectivity patterns in both groups. Although no significant graph survived statistical correction, positive t-statistic graphs illustrated predominantly right-hemisphere connections in the HC group, whereas the CP group showed a left-hemisphere distribution of connection.

5.5.4.2. Intra-Default graph connectivity results: relative comparison

Relative comparison (Fig. 5.16B) similarly revealed densely connected distributions in both groups. While also not surviving statistical correction, this comparison demonstrated more extensively distributed bilateral connections in the HC contrast, compared to relatively sparse connectivity in the CP contrast.

In summary, for the intra-Default graphs, group-level graphs from both comparison methods consistently showed dense connectivity patterns in both groups. Although no statistically significant graphs were identified in the between-group comparisons, the absolute comparison revealed predominantly

ipsilateral distributions in both group contrasts, whereas the relative comparison showed more bilateral connectivity patterns.

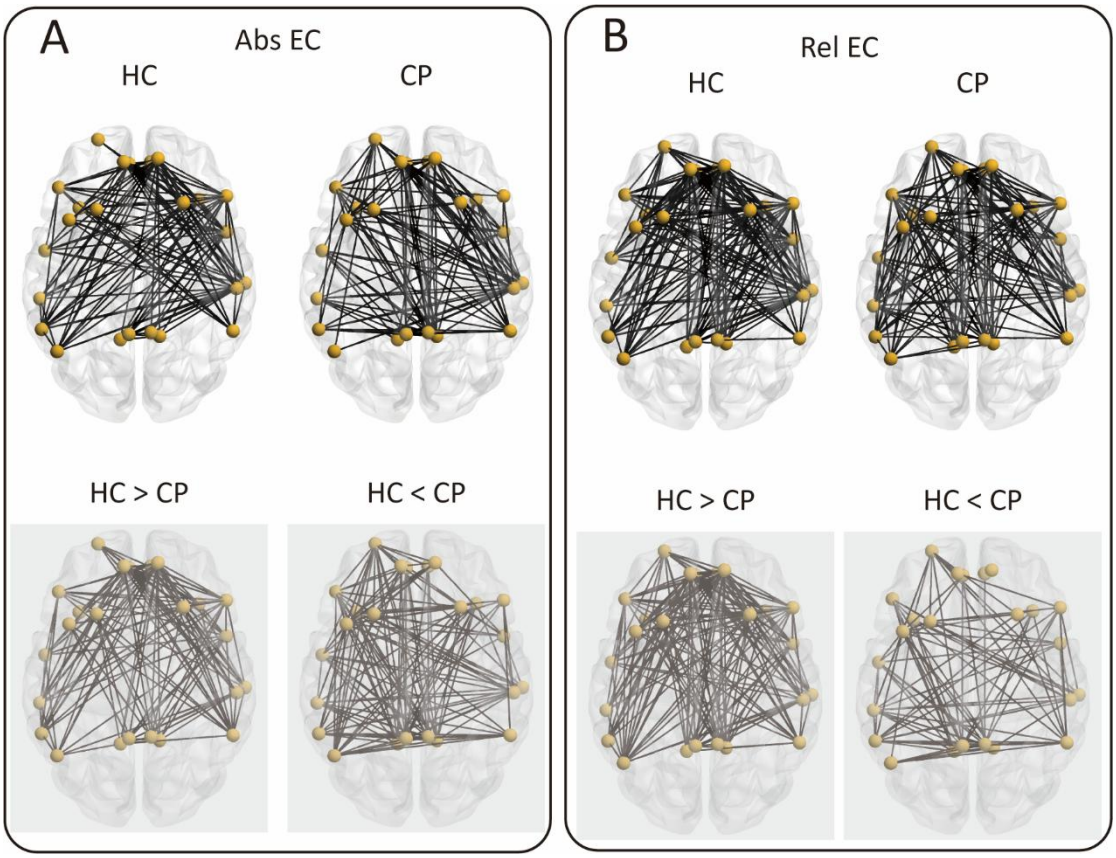

Figure 5.16. Higher-order intra- default graphs elicited by EC conditions in HC and CP groups using two comparison methods. (A) Group-level intra-network graphs for the default network and corresponding *t*-graphs ($t > 0$; shown in reduced opacity) were generated following NBS analysis in both groups. (B) Similar to (A) but for relative comparison. The group-level graphs from both comparison methods consistently showed dense connectivity patterns in both groups. Although no statistically significant graphs were identified, the absolute comparison revealed predominantly ipsilateral distributions in both group contrasts, whereas the relative comparison showed more bilateral connectivity patterns. EC, eyes-closed; HC, healthy control group; CP, chronic pain patient group; NBS, network-based statistics; Abs, absolute comparison; Rel, relative comparison.

5.5.4.3. Graph analysis results for intra-Default graph

Significant main effects of comparison methods (absolute vs. relative) were only observed in Geff and Sw (Fig. 5.17). Post-hoc comparisons revealed that the HC group exhibited significantly enhanced Geff and reduced Sw in the relative comparison (Geff: t (30) = 3.71, P < 0.01; Sw: t (30) = -2.00, P = 0.02). In contrast, no significant differences between comparison methods were found in the CP group (Geff: t (34) = 0.75, P = 0.48; Sw: t (34) = -0.44, P = 0.66). Furthermore, post-hoc analysis demonstrated significantly increased Geff in the HC group compared to the CP group specifically in the relative comparison (t (64) = 2.69, P = 0.01).

Detailed ANOVA statistics and post-hoc comparisons are provided in Table 5.4.

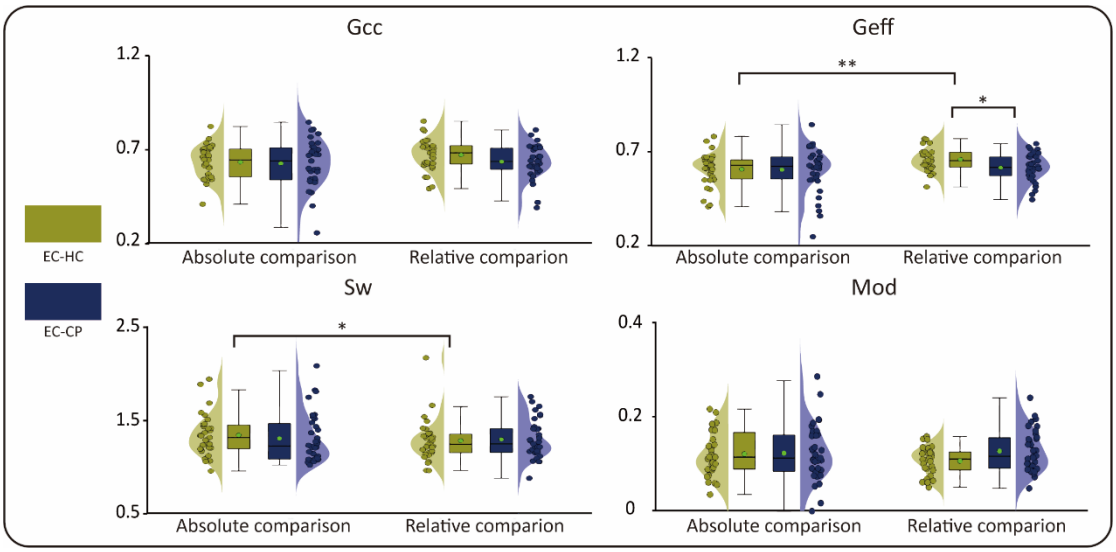

Figure 5.17. Graph analysis results for EC conditions in HC and CP groups using two comparison methods for intra-Default graphs. Violin plots with overlaid scatter and box plots show the results of two-way mixed ANOVA with Bonferroni correction for post hoc comparisons of four GNIs across the HC

(dark yellow) and CP (dark blue) groups and two comparison methods. A green-filled circle with a black edge denotes the mean value for each group. EC, eyes-closed; HC, healthy control group; CP, chronic pain patient group; GNIs, global network inferences; Gcc, global clustering coefficient; Geff, global efficiency; Sw, small-worldness; Mod, modularity. *P < .05, **P < .01.

5.5.5. Higher-order graph results for inter-network graph

5.5.5.1. Inter-network graph connectivity results: absolute comparison

In the absolute comparison (Fig. 5.18A), although no significant graph survived statistical correction, a connectivity pattern centred on the SalVentAttn network was observed in the HC contrast, while the CP contrast exhibited a multi-network connectivity pattern.

5.5.5.2. Inter-network graph connectivity results: relative comparison

The relative comparison (Fig. 5.18B) similarly did not reveal any statistically significant graphs. The HC contrast demonstrated an active connectivity pattern centred on the Cont network while the CP contrast again revealed a multi-network connectivity pattern.

In summary, although no significant graphs survived statistical corrections for the inter-network analyses, a consistent multi-network communication pattern emerged across both comparison methods in the CP contrast. Conversely, the HC contrast exhibited a SalVentAttn-dominated pattern in the absolute comparison and a Cont-dominated pattern in the relative comparison.

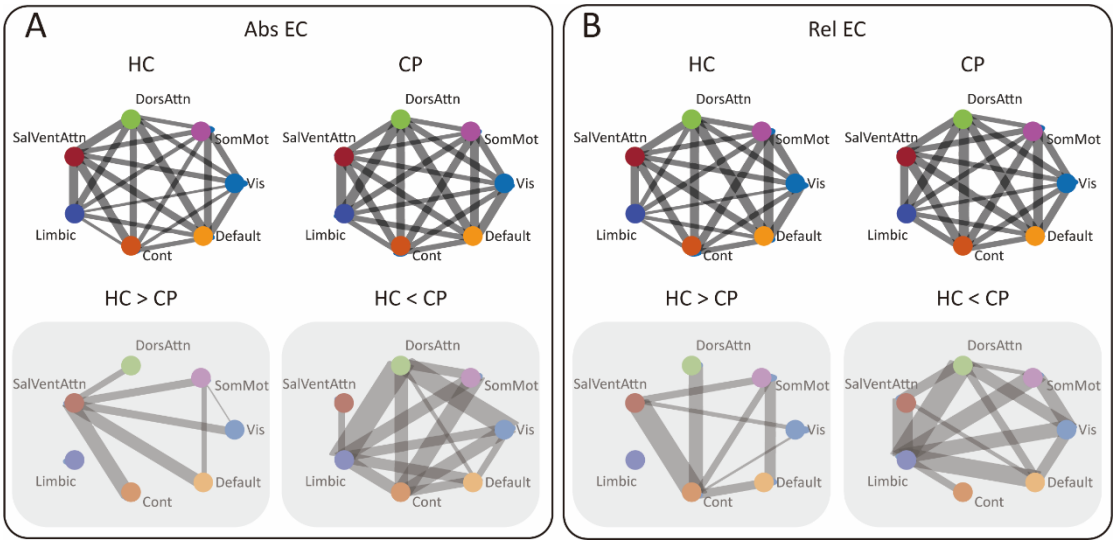

Figure 5.18. Higher-order inter-network graphs elicited by EC conditions in HC and CP groups using two comparison methods. (A) Group-level inter-network weighted graphs and corresponding *t*-graphs ($t > 0$; shown in reduced opacity) were generated following NBS analysis in two groups. (B) Similar to (A) but for relative comparison. The stroke size of each connection indicates the edge weight, representing connectivity strength in the upper panels, whereas in the lower panels it represents the corresponding t-value. Although no significant graphs survived statistical corrections for the inter-network analyses, a consistent multi-network communication pattern emerged across both comparison methods in the CP contrast. Conversely, the HC contrast exhibited a SalVentAttn-dominated pattern in the absolute comparison and a Cont-dominated pattern in the relative comparison. EC, eyes-closed; HC, healthy control group; CP, chronic pain patient group; NBS, network-based statistics; Abs, absolute comparison; Rel, relative comparison.

5.5.5.3. Graph analysis results for inter-network graphs: edge betweenness centrality in absolute comparison

For the absolute comparison (Fig. 5.19A), no significant graphs survived statistical correction. However, in the HC contrast, the SalVentAttn network held

several important edges, with SalVentAttn–Limbic and SalVentAttn–Cont connections showing distinctive importance. In the CP contrast, the Limbic, DorsAttn, and SomMot networks each maintained three key edges, which were shared among them.

5.5.5.4. Graph analysis results for inter-network graphs: edge betweenness centrality in relative comparison

In the relative comparison (Fig. 5.19B), the Default network emerged with several distinctive edges in the HC contrast, linking with the Cont, DorsAttn, SomMot, and Vis networks. In addition, Vis–DorsAttn connections showed prominent edge betweenness centrality. By contrast, the CP contrast revealed fewer connections in the relative Ebc graphs.

Across both comparison methods, no significant Ebc graphs were identified. Nonetheless, the Default network displayed distinctive edges in the HC contrast in the relative comparison, suggesting its potential importance in inter-network communication.

5.5.5.5. Graph analysis results for inter-network graphs: local clustering coefficient

No significant results were found in the Lcc comparison for the EC conditions between HC and CP groups, for both comparison methods (Fig. 5.19C).

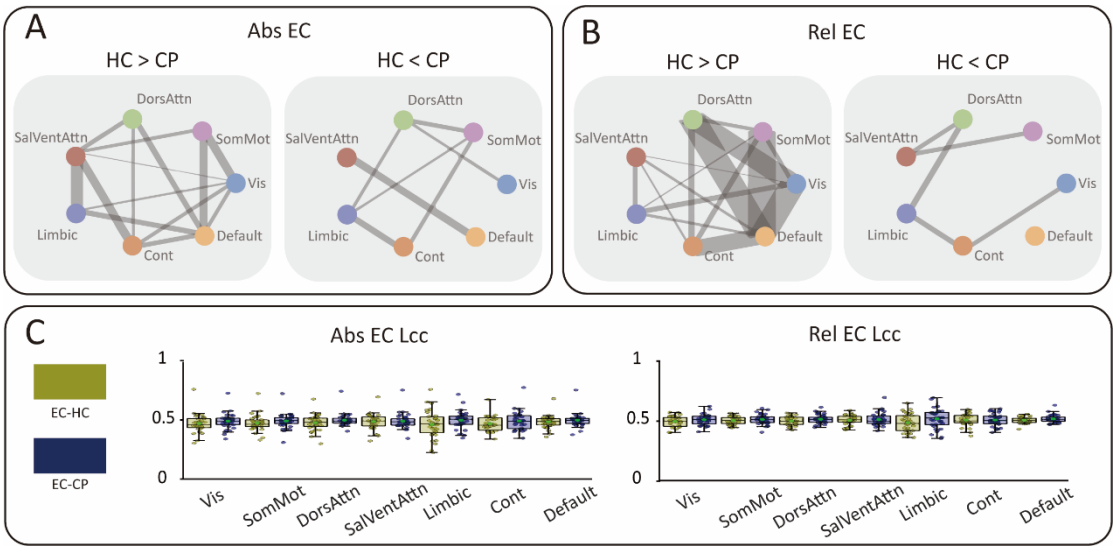

Figure 5.19. Results for local graph inferences analysis from inter-network graphs elicited by EC conditions in HC and CP groups using two comparison methods. (A) Ebc corresponded *t*-graphs generated following NBS ($t > 0$; shown in reduced opacity). (B) Similar to (A) but for relative comparison. The stroke size of each connection represents the corresponding t-value for the Ebc graph contrasts. (C) Box plots illustrate the statistical analysis for Lcc by paired-sample *t*-test with FDR correction between two groups for two comparison methods. The Ebc graphs revealed no significant graphs in both comparisons. Nonetheless, the Default network displayed distinctive edges in the HC contrast in the relative comparison. EC, eyes-closed; HC, healthy control group; CP, chronic pain patient group; Ebc, Edge betweenness centrality; NBS, network-based statistics; Abs, absolute comparison; Rel, relative comparison.

5.5.5.6. Graph analysis results for inter-network graphs: global network inferences

A significant main effect of comparison was observed for both Gcc and Geff in the inter-network graphs under EC conditions across both comparison

methods. However, no significant post-hoc differences were detected (Fig. 5.20).

Detailed ANOVA statistics and post-hoc comparisons are provided in Table 5.4.

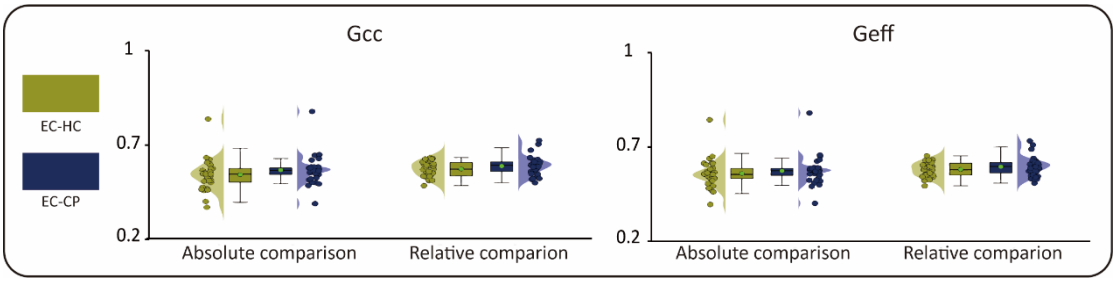

Figure 5.20. Graph analysis results for EC conditions HC and CP groups using two comparison methods for inter-network graphs. Violin plots with overlaid scatter and box plots show the results of two-way mixed ANOVA with Bonferroni correction for post hoc comparisons of two GNIs across the HC (dark yellow) and CP (dark blue) conditions and two comparison methods. EC, eyes-closed; HC, healthy control group; CP, chronic pain patient group; GNIs, global network inferences; Gcc, global clustering coefficient; Geff, global efficiency.

Table 5.4. **Statistical results for GNIs from EC conditions in HC and CP groups using absolute and relative comparison methods.**

Graphs	GNIs	Effect	$F_{(1,64)}$	P	η_p^2	Post-hoc Comparisons	T	$P_{Bonferroni}$	95% CI
sensor	Gcc	Comparison (Main)	18.94	<0.001	0.23	Abs > Rel (HC)	4.00	<0.001	[0.04, 0.12]
						Abs > Rel (CP)	2.16	0.03	[0.00, 0.08]
sensor	Geff	Comparison (Main)	4.62	0.04	0.07	Abs > Rel (HC):ns	1.86	0.06	[0.00, 0.03]
						Abs > Rel (CP): ns	1.29	0.29	[-0.01, 0.02]
sensor	Geff	Group (Main)	15.30	<0.001	0.19	CP > HC (Abs)	3.92	<0.01	[0.03, 0.08]
						CP > HC (Rel)	3.56	<0.01	[0.03, 0.08]
sensor	Sw	Comparison (Main)	15.38	<0.001	0.19	Abs > Rel (HC)	2.82	<0.01	[0.14, 0.83]
						Abs > Rel (CP)	2.73	<0.01	[0.12, 0.77]
sensor	Sw	Group (Main)	20.06	<0.001	0.24	HC > CP (Abs)	3.87	<0.001	[0.49, 1.53]
						HC > CP (Rel)	4.02	<0.001	[0.48, 1.45]
sensor	Mod	Comparison (Main)	37.30	<0.001	0.37	Rel > Abs (HC)	5.28	<0.001	[0.02, 0.05]
						Rel > Abs (CP)	2.00	<0.01	[0.01, 0.03]
sensor	Mod	Group (Main)	6.85	0.01	0.10	HC > CP (Abs):ns	1.42	0.19	[-0.01, 0.02]
						HC > CP (Rel)	3.00	<0.01	[0.01, 0.05]
source	Geff	Comparison (Main)	9.52	<0.01	0.13	Rel > Abs (HC)	2.29	0.03	[0.00, 0.03]
						Rel > Abs (CP)	2.00	0.04	[0.00, 0.03]
Intra-Default	Geff	Comparison (Main)	8.08	<0.01	0.11	Rel > Abs (HC)	3.23	<0.01	[0.02, 0.07]
						Rel > Abs (CP):ns	0.75	0.48	[-0.02, 0.03]
Intra-Default	Geff					HC > CP (Abs):ns	0.10	0.92	[-0.04, 0.04]
						HC > CP (Rel)	2.69	0.01	[0.01, 0.06]
Intra-Default	Sw	Comparison (Main)	4.31	0.04	0.06	Abs > Rel (HC)	2.00	0.02	[0.02, 0.16]
						Abs > Rel (CP):ns	0.44	0.66	[-0.05, 0.08]
Inter-network	Gcc	Comparison (Main)	5.86	0.02	0.08	Rel > Abs (HC):ns	2.00	0.06	[0.00, 0.05]
						Rel > Abs (CP):ns	1.42	0.15	[-0.01, 0.04]
Inter-network	Geff	Comparison (Main)	4.45	0.040	0.07	Rel > Abs (HC):ns	1.50	0.150	[-0.02, 0.04]
						Rel > Abs (CP):ns	1.22	0.20	[-0.01, 0.03]

Note. EC, eyes-closed; GNIs, global network inferences; Gcc, global clustering coefficients; Geff, global efficiency; Sw, small-world-ness; Mod, modularity; Abs, absolute comparison; Rel, relative comparison.

5.5.6. Classification performance

The top three classification performances based on GNIs across all graphs and their combinations in EC condition for both comparison methods, were presented in Table 5.5. Although permutation-based *P* values indicated statistically significant classifications, the prediction AUC-ROCs from single-method approaches did not exceed 0.82.

Among single methods, the absolute comparison achieved the highest performance, with an AUC-ROC of 0.81 and 71% accuracy, whereas the relative comparison reached a maximum AUC-ROC of 0.78 and 67% accuracy. In contrast, combining features from both absolute and relative comparisons substantially improved classification, yielding a peak AUC-ROC of 0.91 and 80% accuracy.

These findings suggest that integrating both comparison methods enhances the predictive power of GNIs for distinguishing between HC and CP groups under EC conditions.

Table 5.5. Classification performance for HC and CP groups based on GNIs across eighteen graphs and both comparison methods under EC conditions.

Comp	GNIs	AUC-ROC	ACC	Sensitivity	Specificity	P_{perm}
Abs	Abs_sensor+Abs_source+Abs_Vis+Abs_SomMot+Abs_Cont+Abs_inter	0.81	71%	0.57	0.87	0
Abs	Abs_sensor+Abs_DorsAttn+Abs_SalVentAttn+Abs_Cont+Abs_inter	0.79	70%	0.60	0.81	0
Abs	Abs_sensor+Abs_Vis+Abs_SomMot	0.79	74%	0.60	0.90	0
Rel	Rel_sensor+Rel_Default	0.78	67%	0.57	0.77	0
Rel	Rel_sensor+Rel_source+Rel_SomMot+Rel_DorsAttn+Rel_SalVentAttn+Rel_Default+Rel_inter	0.77	71%	0.63	0.81	0.001
Rel	Rel_sensor+Rel_DorsAttn+Rel_SalVentAttn+Rel_Cont	0.77	64%	0.57	0.71	0
Abs+Rel	Abs_sensor+Abs_DorsAttn+Abs_Default+Abs_inter+Rel_sensor+Rel_source+Rel_Vis+Rel_Cont+Rel_Default+Rel_inter	0.91	80%	0.69	0.94	0.00
Abs+Rel	Abs_sensor+Abs_DorsAttn+Abs_Default+Rel_sensor+Rel_source+Rel_Vis+Rel_Cont+Rel_Default+Rel_inter	0.90	79%	0.66	0.94	0.00
Abs+Rel	Abs_sensor+Abs_Cont+Abs_inter+Rel_SomMot+Rel_SalVentAttn+Rel_Default+Rel_inter	0.89	79%	0.69	0.90	0.00

Note. EC, eyes-closed; Comp, Comparison methods; Abs, absolute comparison; Rel, relative comparison; Vis, intra-Visual network; SomMot, intra-Somato-Motor network, DorsAttn, intra-Dorsal Attention network; SalVentAttn, intra-Salience-Ventral Attention network, Limbic, intra-Limbic network; Cont, intra-Control network; Default, intra-Default network; inter, inter-network; AUC-ROC, area under the receiver operating characteristic curve; ACC, accuracy; P_{perm}, P value based on 1000 permutation.

5.6. Discussion for eyes-closed condition in paired-state group

5.6.1. Representative connectivity patterns

Under the EC condition, significant graphs emerged exclusively for the CP contrast in the sensor space across both comparison methods. These graphs were characterized by densely connected bilateral patterns, with a predominance in the right prefrontal regions. This pattern replicates previous observations of alpha-band over-activation in widespread brain regions in chronic pain (Prichep et al., 2018).

Although not surviving statistical correction, consistent source-space results appeared across both methods, showing a right frontal to left parietal anterior connectivity in the HC contrast and a left-hemispheric dominant connectivity pattern extending from central to parietal regions in the CP contrast. In the inter-network graphs, the CP contrast exhibited multi-network connectivity across both methods. By contrast, in the HC, the SalVentAttn network appeared as a hub in the absolute comparison, while the Cont network emerged as a hub in the relative comparison, with the Default network displaying distinctive edges in the Ebc t-graphs. Additionally, intra-network connectivity strength for SalVentAttn was significantly greater in the HC group than in the CP group in the absolute comparison.

The SalVentAttn network is crucial for detecting salient stimuli and coordinating network switching to generate behavioural responses (Uddin, 2015). It is typically more active during exteroceptive states (e.g., EO resting-state), while the Default dominates during interoceptive states (e.g., EC resting-state)

(Costumero et al., 2020). Moreover, the SalVentAttn and Default are normally anticorrelated, and the SalVentAttn drives the switching between the Default network and Cont network (Goulden et al., 2014). Therefore, during the interoceptive EC state, the Default would be expected to be more active, with suppressed SalVentAttn activity. Contrary to this expectation, we observed significantly increased SalVentAttn intra-network connectivity strength and hub-like properties in the HC group compared to the CP group. This attenuated SalVentAttn connectivity may be related to an aberrant correlated pattern which was previously observed in chronic pain and thought to reflect a maladaptive cognitive state, suggesting a general overthinking of the constant pain for patients and activating the Default (Tu et al., 2019). Such network dysfunction is a recognised marker of disease severity across several neurological and psychiatric disorders (Hemington et al., 2016).

5.6.2. Global network inferences and networks

Comparison methods substantially influenced GNIs across all types of graphs, once again underscoring the impact of baseline normalisation.

Group differences in GNIs were observed in both the sensor space and intra-Default graphs. In the sensor space, the CP group consistently showed significantly higher Geff and lower Sw than the HC group across both comparison methods. Furthermore, decreased Mod was observed in the CP group only in the relative comparison. This finding aligns with previous research, highlighting a decrease in modularity with increased cognitive load (Kitzbichler et al., 2011; Vatansever et al., 2015). Collectively, these results indicate increased global functional integration and information efficiency in the CP group,

accompanied by reduced small-worldness and modularity, suggesting a shift towards a more randomised, less segregated network architecture (Liao et al., 2017).

In contrast, the intra-Default graph revealed significantly decreased Geff in the CP group, aligning with the fewer connectivity edges in the t-graph in the intra-Default graph, suggesting weaker information flow within the Default network, indicating a larger connectivity in the interoceptive state in the HC group compared to the CP group. Compared to the controversial results of intra-Default Geff in EO condition, this may indicate that the EC condition, which typically induces a broad multi-network reconfiguration with enhanced Default connectivity (Costumero et al., 2020; J. Han et al., 2023). is characterised by a failure of the CP brain to dynamically upregulate Default integration effectively.

5.6.3. Dynamic network reconfiguration

Under the EC condition, the CP group exhibited a distinct profile of maladaptive network reorganization. The significant sensor space graphs, associated with higher global efficiency but reduced small-worldness and modularity, point to a brain-wide shift towards a less specialised and more disorganised state. The significant reduction of intra-Default Geff in the CP further suggests insufficient information transfer within a network that is critical for interoceptive processing, which is typically enhanced during EC rest (Costumero et al., 2020; J. Han et al., 2023).

Concurrently, the SalVentAttn network, which is normally anticorrelated with the Default, showed significantly weaker intra-network connectivity in the CP group This finding, combined with the sparser connectivity observed in the intra-Default graphs for the CP contrast, points toward an abnormal loss of

anticorrelation between these two fundamental networks, a phenomenon also reported in other studies (Baliki et al., 2008; Hemington et al., 2016; Tu et al., 2019), and suggests a failure to properly segregate internal (Default) and external/salience (SalVentAttn) processing.

The transition from an EO to an EC state typically induces a broad network reconfiguration that enhances Default connectivity (Costumero et al., 2020; J. Han et al., 2023). Our results indicate that while the HC group leverages this shift to engage in a more structured dynamic with distinct network roles, the CP group relies on a less efficient, diffuse pattern of multi-network communication, reflecting an impaired dynamic reconfiguration between brain states.

In summary, during the interoceptive EC condition, the CP group exhibits an imbalanced brain architecture. This dysfunction is characterized by inefficient global integration (high Geff but low Sw/Mod), impaired within-network processing (low intra-Default Geff) and a breakdown in the normal competitive relationship between the Default and SalVentAttn networks.

5.6.4. Classification performance

Classification performance under EC conditions achieved an AUC-ROC above 0.91 and 80% accuracy when combining both comparison methods. The combined model substantially outperforms single-method approaches. This highlights the advantage of integrating comparison methods for robust group classification.

5.7. Classification performance from combined eyes-open and eyes-closed conditions

The top three classification performances based on GNIs from all graphs combining both EO and EC conditions for each single comparison method, are presented in Table 5.6.

Table 5.6. Classification performance for HC and CP groups based on GNIs across all eighteen graphs combined EO and EC conditions for single comparison methods.

Comp	GNIs	AUC-ROC	ACC	Sensitivity	Specificity	P_{perm}
Abs	EO_source+EO_SomMot+EO_Default+EO_DorsAttn+EC_sensor+EO_source_C+EC_SomMot+EC_SalVentAttn+EC_Cont+EC_Vis	0.91	80%	0.71	0.90	0
Abs	EO_source+EO_Default+EO_DorsAttn+EO_Vis+EO_inter+EC_sensor+EC_Cont+EO_DorsAttn_C+EC_Vis+EC_inter	0.90	80%	0.69	0.94	0
Abs	EO_source+EO_SomMot+EO_Default+EO_DorsAttn+EC_sensor+EO_source_C+EC_SomMot+EC_SalVentAttn+EC_Cont+EC_Vis+EC_inter	0.90	79%	0.71	0.87	0
Rel	EO_sensor+EO_source+EO_SomMot+EO_Default+EO_Cont+EO_inter+EC_Default+EC_DorsAttn	0.83	82%	0.74	0.90	0
Rel	EO_sensor+EO_source+EO_SomMot+EO_Default+EO_Cont+EO_inter+EC_Default+EC_DorsAttn+EC_inter	0.83	82%	0.74	0.90	0
Rel	EO_sensor+EO_source+EO_Default+EO_Cont+EO_inter+EC_sensor+EC_source+EC_Default+EC_Vis	0.83	79%	0.74	0.84	0

Note. EO, eyes-open; EC, eyes-closed; Comp, Comparison methods; Abs, absolute comparison; Rel, relative comparison; Vis, intra-Visual network; SomMot, intra-Somato-Motor network, DorsAttn, intra-Dorsal Attention network; SalVentAttn, intra-Salience-Ventral Attention network, Limbic, intra-Limbic network; Cont, intra-Control network; Default, intra-Default network; inter, inter-network; AUC-ROC., area under the receiver operating characteristic curve; ACC, accuracy; P_{perm}, P value based on 1000 permutation.

All selected classification models yielded significant permutation p-values. The accuracy was comparable between the two comparison methods: the third-best model achieved 79% accuracy, while the top two models for the absolute and relative comparisons reached 80% and 82% accuracy, respectively. A similar pattern was observed for sensitivity and specificity, with differences between the best-performing single-method models not exceeding 0.04. Specifically, maximum sensitivity reached 0.71 for the absolute comparison and 0.74 for the relative comparison, while maximum specificity was 0.94 for the absolute and 0.90 for the relative comparison. In contrast, the AUC-ROC values revealed a clearer distinction: models based on the absolute comparison consistently exceeded 0.90, whereas the best relative comparison model reached only 0.84.

These findings indicate that integrating data from both eye states enhances predictive performance compared to using single eye-state conditions within a given comparison method. While accuracy, sensitivity, and specificity metrics were similar between the absolute and relative methods, the superior AUC-ROC values suggest that the absolute comparison provides greater overall discriminative ability for distinguishing between groups.

5.8. Results for eyes-open and eyes-closed conditions in single-state group

5.8.1. Brain-wide graph results in sensor space

5.8.1.1. Sensor space connectivity results: eyes-open conditions

Under the EO condition, the sensor space graph derived from both groups yielded densely connected connectivity patterns (Fig. 5.21A). NBS analysis identified a significant graph demonstrating greater connectivity in the CP group relative to the HC group, comprising 62 nodes and 1086 edges (P < 0.001). This graph in the CP contrast was bilaterally distributed, with a predominance of connections in the right prefrontal regions.

5.8.1.2. Sensor space connectivity results: eyes-closed conditions

Consistent with the findings from the EO conditions, the EC conditions also showed a bilateral connectivity pattern for the HC and CP groups (Fig. 5.21B). NBS analysis similarly identified a significant graph of greater connectivity in the CP group, comprising 62 nodes and 677 edges (P < 0.01). This graph shared the same overall bilateral distribution for the CP contrast, again demonstrating a right-hemisphere predominant trend in the prefrontal regions.

In summary, the group-level sensor space graphs from both eye states consistently revealed a bilateral distribution in the HC and CP groups, and the significant graph was identified in the CP contrast with a large-scale bilateral connectivity pattern and a predominant focus in the right prefrontal regions.

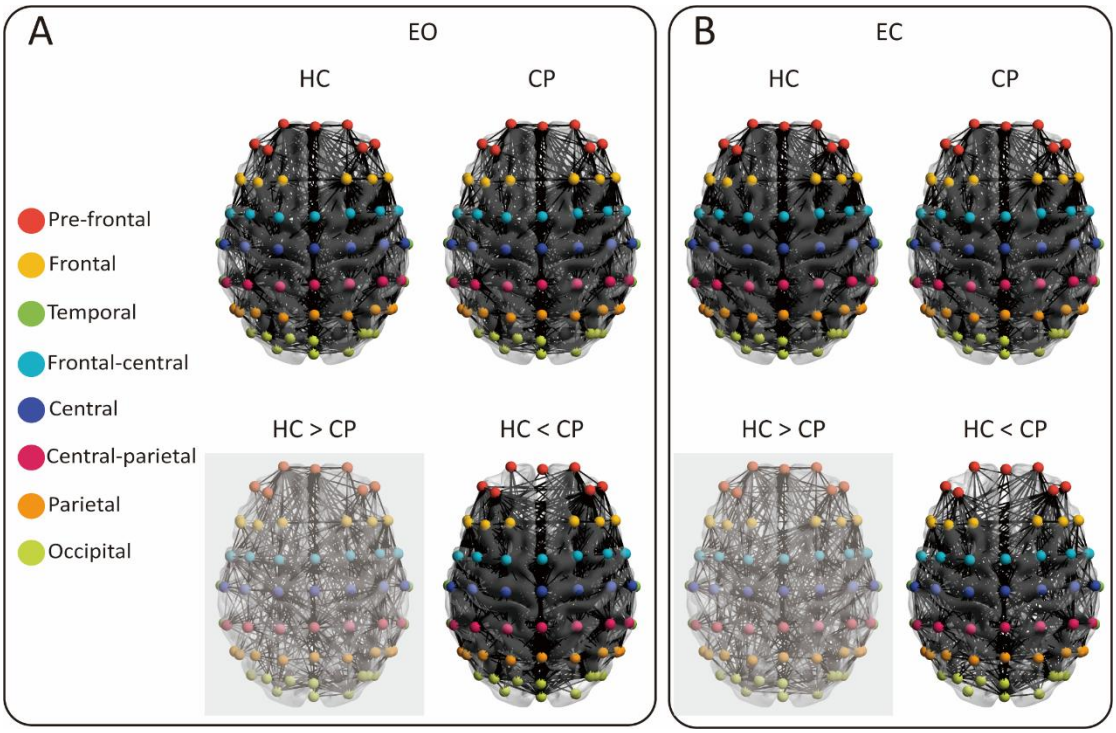

Figure 5.21. Graphs elicited by EO and EC conditions in HC and CP groups in sensor space. (A) Group-level functional connectivity graph for EO in both groups (first row). Sensors corresponding to different scalp regions (Pre-frontal, Frontal, Temporal, Frontal-central, Central, Central-parietal, Parietal, and Occipital) were colour-labelled for visual distinction. Group differenced connectivity patterns were identified using NBS and visualised as significant *p*-graphs or t-graphs with reduced opacity (second row). (B) Similar to (A) but for EC condition. The group-level sensor space graphs from both eye states consistently revealed bilateral distributions in both the HC and CP groups. A significant graph was identified in the CP contrast, characterized by large-scale bilateral connectivity with a predominant focus in the right prefrontal regions. EO, eyes-open; EC, eyes-closed; HC, healthy control group; CP, chronic pain patient group; NBS, network-based statistics.

5.8.1.3. Sensor space graph analysis results

No significant main effect of eye-state (EO vs. EC) was identified in the sensor space GNIs. However, a significant main effect of group (HC vs. CP) was observed across all four GNIs (Fig. 5.22).

The post-hoc comparisons revealed significantly higher values of Gcc, Sw, and Mod in the HC than in CP groups in EO conditions (Gcc: t (102) = 2.37, P = 0.02; Sw: t (102) = 4.59, P < 0.001; Mod: t (102) = 2.33, P = 0.03). Furthermore, EC conditions also showed significant larger values in these GNIs except for a non-significant Mod (Gcc: t (101) = 2.50, P = 0.02; Sw: t (101) = 2.93, P < 0.001; Mod: t (101) = 1.33, P = 0.18).

On the contrary, the CP group displayed larger Geff in both EO and EC conditions (EO: t (102) = 4.27, P < 0.001; EC: t (101) = 2.27, P = 0.02).

Detailed ANOVA statistics and post-hoc comparisons are provided in Table 5.7.

Notably, a bimodal distribution of Geff was observed in the CP group under both EO and EC conditions. To better characterise this distributional pattern, we performed an additional exploratory analysis. Detailed findings are reported in Section 5.10.

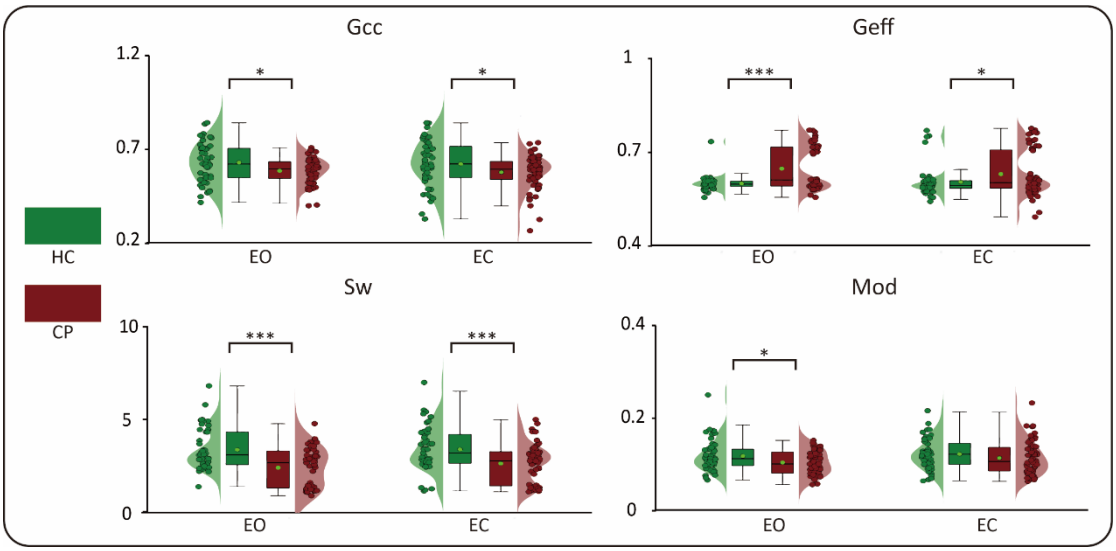

Figure 5.22. Graph analysis results for EO and EC conditions in HC and CP groups in sensor space. Violin plots with overlaid scatter and box plots show the results of two-way between-subjects ANOVA with Bonferroni correction for post hoc comparisons of four GNIs across the HC (dark green) and CP (dark red) groups and two comparison methods. A green-filled circle with a black edge denotes the mean value for each group. EO, eyes-open; EC, eyes-closed; HC, healthy control group; CP, chronic pain patient group; GNIs, global network inferences; Gcc, global clustering coefficient; Geff, global efficiency; Sw, small-worldness; Mod, modularity. *P < .05, ***P < .001.

Table 5.7. **Statistical results for GNIs from EO and EC conditions in HC and CP groups in the sensor space (ANOVA and Post-hoc Comparisons).**

Graphs	GNIs	Effect	*F*	*P*	η_p^2	Post-hoc Comparisons	*T*	$P_{Bonferroni}$	95% CI
sensor	Gcc	Group (Main)	11.59	<0.001	0.05	HC > CP (EO)	2.37	0.02	[0.01, 0.08]
						HC > CP (EC)	2.50	0.02	[0.01, 0.08]
sensor	Geff	Group (Main)	21.44	<0.001	0.09	CP > HC (EO)	4.27	<0.001	[0.03, 0.07]
						CP > HC (EC)	2.27	0.02	[0.00, 0.05]
sensor	Sw	Group (Main)	34.68	<0.001	0.14	HC > CP (EO)	4.59	<0.001	[0.55, 1.38]
						HC > CP (EC)	2.93	<0.001	[0.36, 1.16]
sensor	Mod	Group (Main)	6.45	0.01	0.03	HC > CP (EO)	2.33	0.03	[0.00, 0.03]
						HC > CP (EC): ns	1.33	0.18	[0.00, 0.02]

Note. EO, eyes-open; EC, eyes-closed; GNIs, global network inferences; Gcc, global clustering coefficients; Geff, global efficiency; Sw, small-worldness; Mod, modularity.

5.8.2. Brain-wide graph results in source space

5.8.2.1. Source space connectivity results: eyes-open condition

In the EO condition (Fig. 5.23A), group-level graphs for both the HC and CP groups revealed a bilateral distribution of connectivity. Although they did not survive statistical correction, the NBS analysis identified a pattern for the HC contrast characterised by connections within the left hemisphere's posterior regions. Conversely, the CP contrast revealed a pattern of bilateral connectivity predominantly located in anterior regions.

5.8.2.2. Source space connectivity results: eyes-closed condition

In the EC condition (Fig. 5.23B), the group-level connectivity graphs for both groups also exhibited a bilaterally distributed, dense pattern of connections. While not surviving statistical correction, the t-graphs for the HC contrast demonstrated a connectivity pattern linking the right frontal region to the left parietal region. Conversely, the CP contrast was characterised by a left-hemisphere-dominated distribution.

In summary, source space graphs across both eye states showed a bilaterally distributed, dense pattern of connections in both groups. Although not surviving statistical correction, distinct spatial patterns were suggested. The HC group displayed an ipsilateral posterior distribution in the left hemisphere during the EO condition, shifting to a right-frontal to left-parietal pattern in the EC condition. Conversely, the CP contrast showed a bilateral anterior distribution in the EO condition and a left-hemisphere-dominated pattern in the EC condition.

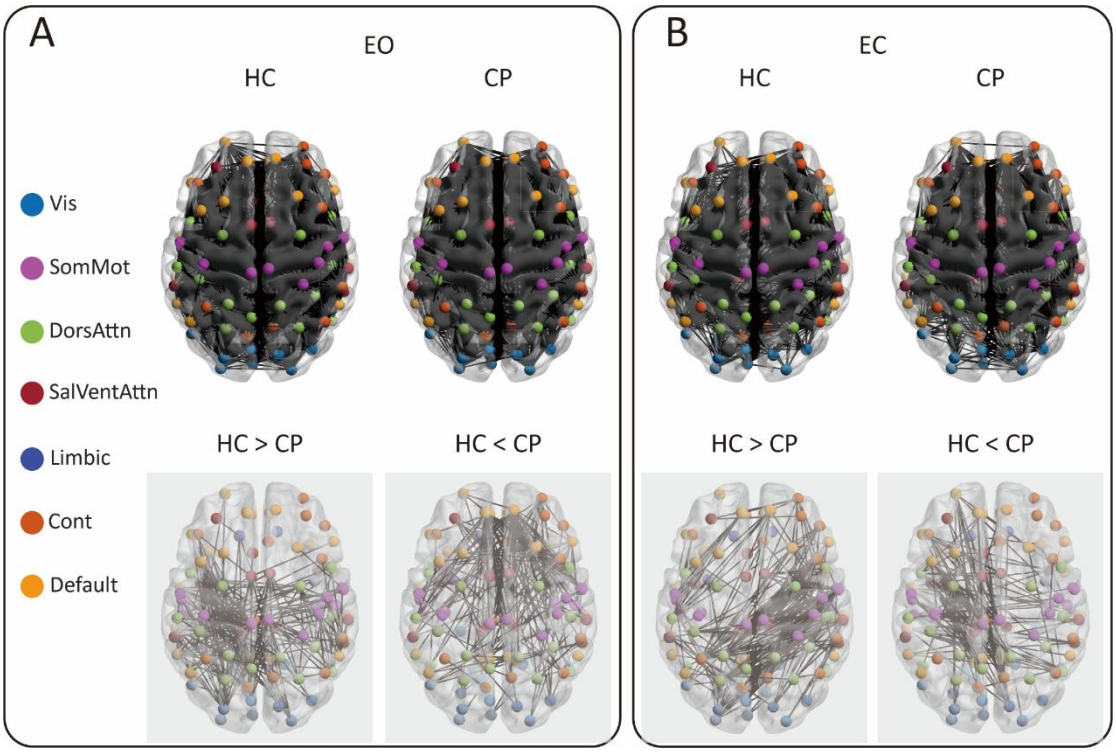

Figure 5.23. Graphs elicited by EO and EC conditions in HC and CP groups in source space. (A) Group-level functional connectivity matrices for EO in HC and CP groups (first row) projected in source space for 100 pairs of brain regions organised into 7 different functional networks (Visual, Somatomotor, Dorsal Attention, Salience-Ventral Attention, Limbic, Control, and Default). The *t*-graphs (second row) constructed from connections with a t-value larger than 1.66 compared between conditions using NBS (shown in reduced opacity). (B) Similar to (A) but for EC condition. The group-level graphs from both eye states showed a bilaterally distributed, dense pattern of connections in both groups. Although not surviving statistical correction, the HC group displayed an ipsilateral posterior distribution in the left hemisphere during the EO condition, shifting to a right-frontal to left-parietal pattern in the EC condition. Conversely, the CP contrast showed a bilateral anterior distribution in the EO condition and a left-hemisphere-dominated pattern in the EC condition. EO, eyes-open; EC, eyes-closed; HC, healthy control group; CP, chronic pain patient group; NBS, network-based statistics.

5.8.2.3. Source space graph analysis results

No significant results were found in the GNIs from the source space graphs for the EO and EC conditions between HC and CP groups (Fig. 5.24).

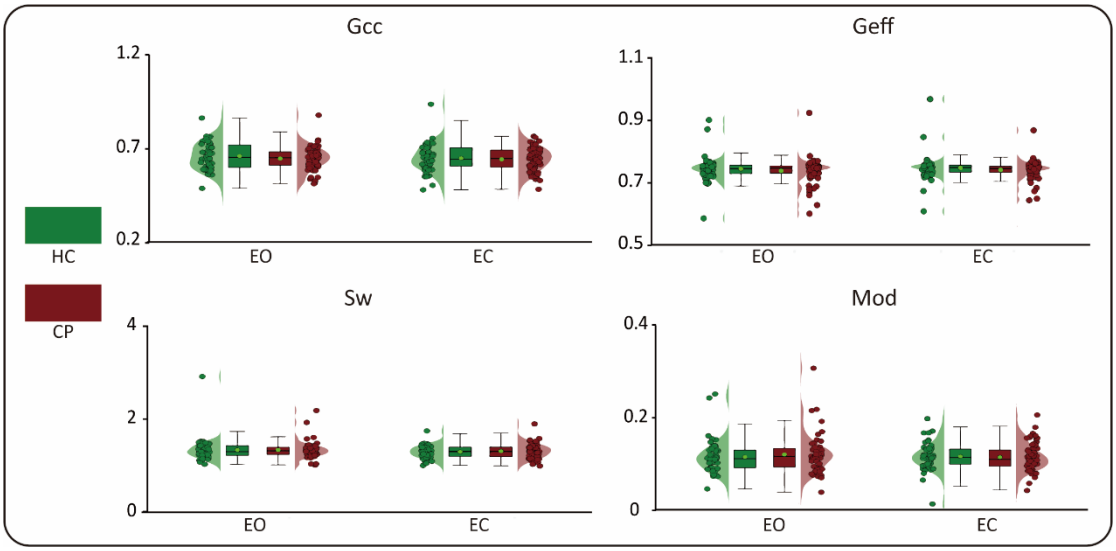

Figure 5.24. Graph analysis results for EO and EC conditions in HC and CP groups in source space. Violin plots with overlaid scatter and box plots show the results of two-way between-subjects ANOVA with Bonferroni correction for post hoc comparisons of four GNIs across the HC (dark green) and CP (dark red) conditions in two eye states. A green-filled circle with a black edge denotes the mean value for each group. EO, eyes-open; EC, eyes-closed; HC, healthy control group; CP, chronic pain patient group; GNIs, global network inferences; Gcc, global clustering coefficient; Geff, global efficiency; Sw, small-worldness; Mod, modularity.

5.8.3. Intra- and inter-network connectivity strength

No significant differences were found in intra- or inter-network connectivity strength for EO and EC conditions between HC and CP groups in source space (Fig. 5.25).

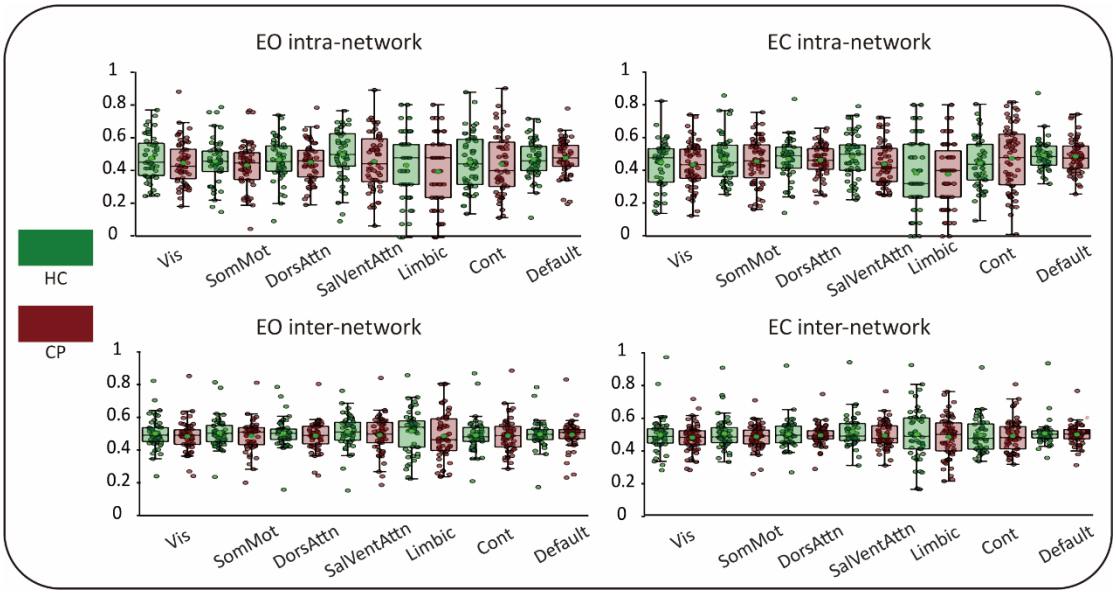

Figure 5.25. Intra-network and inter-network connectivity strength for EO and EC conditions in HC and CP groups in source space. Box plots display intra- and inter-network mean connections were performed using a paired-sample *t*-test with FDR correction for both eye states in two groups. EO, eyes-open; EC, eyes-closed; HC, healthy control group; CP, chronic pain patient group; Abs, absolute comparison; Rel, relative comparison; Vis, Visual; SomMot, Somato-Motor; DorsAttn, Dorsal Attention; SalVentAttn, Salience-Ventral Attention; Cont, Control.

5.8.4. Higher-order graph results for intra-Default graph

5.8.4.1. Intra-Default graph connectivity results: eyes-open condition

In the EO condition (Fig. 5.26A), group-level intra-Default graphs exhibited bilateral, dense connectivity patterns in both groups. Although no significant graph survived statistical correction, the positive t-statistic graphs illustrated a

more densely connected pattern in the CP group, whereas the HC contrast showed sparser connectivity patterns.

5.8.4.2. Intra-Default graph connectivity results: eyes-closed condition

In the EC condition (Fig. 5.26B), both groups similarly revealed bilaterally connected distributions. While also not surviving statistical correction, the analysis demonstrated more densely distributed bilateral connections in the CP contrast compared to the relatively sparse connectivity observed in the HC contrast.

In summary, for the intra-Default graphs, group-level graphs across both eye states consistently revealed dense bilateral connectivity patterns in both groups. Although no statistically significant graphs were identified in the between-group comparisons, the CP contrast was characterised by densely interconnected bilateral distributions in both conditions. In contrast, the HC contrast consistently exhibited sparser connectivity.

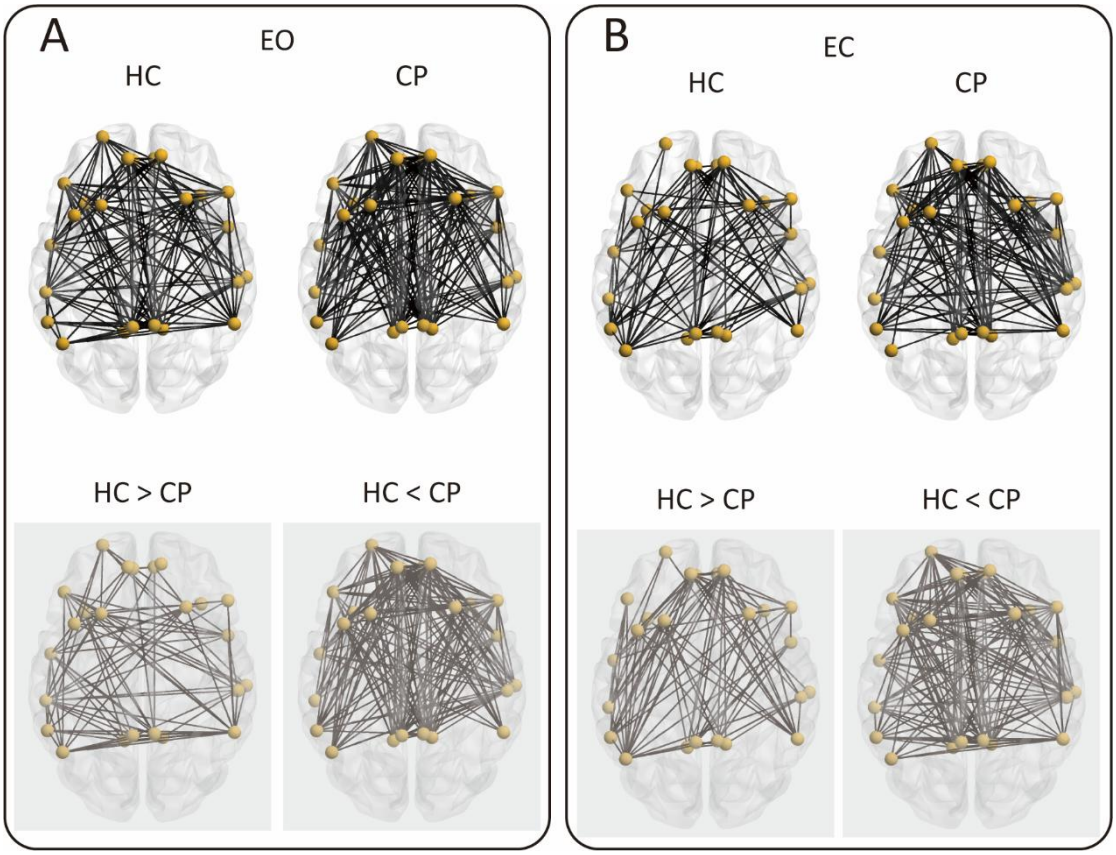

Figure 5.26. Higher-order intra- default graphs elicited by EO and EC conditions in HC and CP groups. (A) Group-level intra-network graphs for the default network and corresponding *t*-graphs ($t > 0$; shown in reduced opacity) were generated following NBS analysis for both groups in EO condition. (B) Similar to (A) but for EC condition. The group-level graphs across both eye states consistently revealed dense bilateral connectivity patterns in both groups. Although no statistically significant graphs were identified in the between-group comparisons, the CP contrast was characterised by densely interconnected bilateral distributions in both conditions, whereas the HC contrast consistently exhibited sparser connectivity. EO, eyes-open; EC, eyes-closed; HC, healthy control group; CP, chronic pain patient group; NBS, network-based statistics.

5.8.4.3. Graph analysis results for intra-Default graph

No significant results were found in the GNIs from the intra-Default graphs for the EO and EC conditions between HC and CP groups (Fig. 5.27).

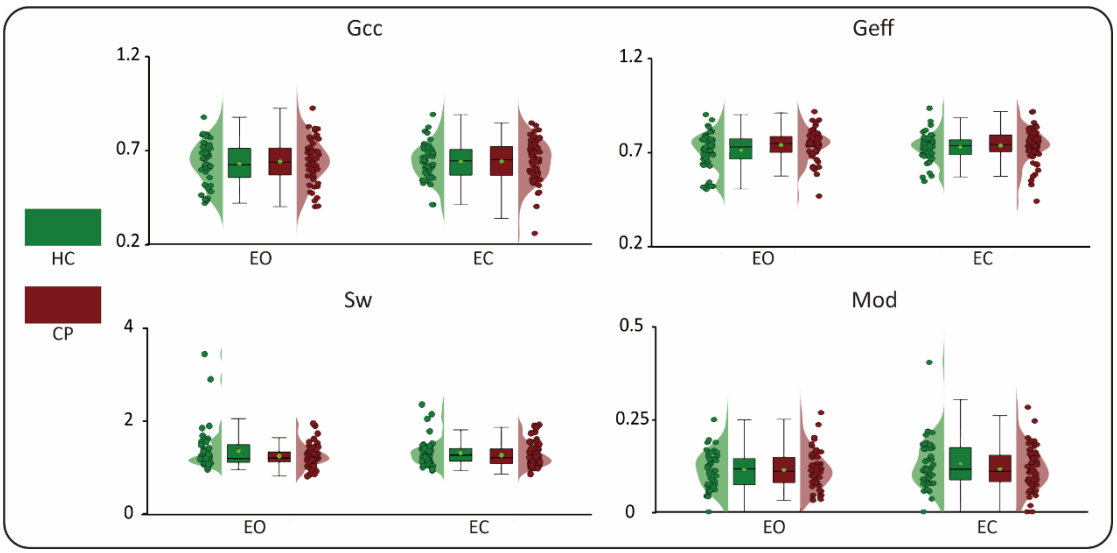

Figure 5.27. Graph analysis results for EO and EC conditions in HC and CP groups for intra-Default graphs. Violin plots with overlaid scatter and box plots show the results of two-way between-subjects ANOVA with Bonferroni correction for post hoc comparisons of four GNIs across the HC (dark green) and CP (dark red) groups in both eye states. A green-filled circle with a black edge denotes the mean value for each group. EO, eyes-open; EC, eyes-closed; HC, healthy control group; CP, chronic pain patient group; GNIs, global network inferences; Gcc, global clustering coefficient; Geff, global efficiency; Sw, small-worldness; Mod, modularity.

5.8.5. Higher-order graph results for inter-network graph

5.8.5.1. Inter-network graph connectivity results: eyes-open condition

In the EO condition (Fig. 5.28A), although no significant graph survived statistical correction, a multi-network communication pattern was observed in the HC contrast, while the CP contrast was characterised by a sparser connectivity pattern, predominantly centred on the Cont network.

5.8.5.2. Inter-network graph connectivity results: eyes-closed condition

In the EC condition (Fig. 5.28B), a similar pattern was observed, though no statistically significant graphs were revealed. The HC contrast also demonstrated a multi-network connectivity pattern, whereas the CP contrast showed a t-graph with sparse edges, again indicating a Cont-centred connectivity profile.

In summary, although no inter-network graphs survived statistical correction, a consistent pattern emerged across both eye states. The HC contrast was characterised by a multi-network communication pattern, while the CP contrast exhibited a sparser, Cont-dominated pattern in both conditions.

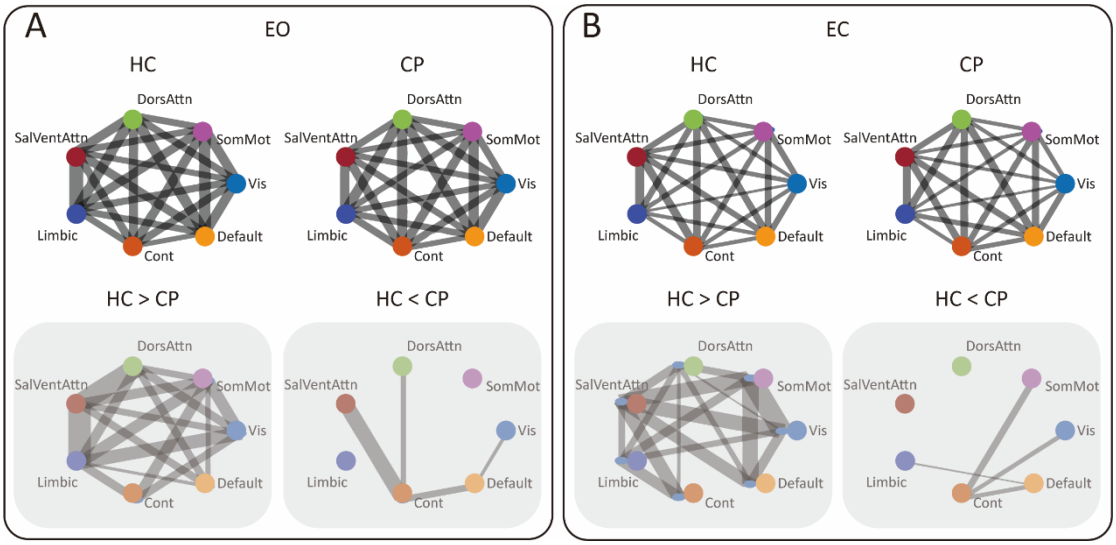

Figure 5.28. Higher-order inter-network graphs elicited by EO and EC conditions in HC and CP groups. (A) Group-level inter-network weighted graphs and corresponding *t*-graphs ($t > 0$; shown in reduced opacity) were generated following NBS analysis for two groups in EO condition. (B) Similar to (A) but in EC condition. The stroke size of each connection indicates the edge weight, representing connectivity strength in the upper panels, whereas in the lower panels it represents the corresponding t-value. Although no significant graphs survived statistical corrections for the inter-network analyses, a consistent multi-network communication pattern emerged across both eye states in the HC contrast. Conversely, the CP contrast exhibited exhibited a sparser, Cont-dominated pattern in both conditions. EO, eyes-open; EC, eyes-closed; HC, healthy control group; CP, chronic pain patient group; NBS, network-based statistics.

5.8.5.3. Graph analysis results for inter-network graphs: edge betweenness centrality in eyes-open condition

For the EO condition (Fig. 5.29A), no significant graphs survived statistical correction. However, t-graphs revealed in the HC contrast showed that the

DorsAttn network possessed several high-betweenness edges, with DorsAttn-Limbic and DorsAttn-Default Mode Network connections being particularly distinctive. The CP contrast was characterised by distinctive Cont-SalVentAttn and Default-Visual edges.

5.8.5.4. Graph analysis results for inter-network graphs: edge betweenness centrality in eyes-closed condition

In the EC condition (Fig. 5.29B), the Cont and Default network emerged with several distinctive high-betweenness edges in the HC contrast. Specifically, the Cont network demonstrated connections with the SalVentAttn, DorsAttn, and Default networks, while the Default network showed connections with the Limbic and SomMot. In the CP contrast, the Default-SalVentAttn edges were particularly prominent.

In summary, although no statistically significant graphs were identified, the Ebc graphs suggested distinct inter-network patterns. The Cont and Default networks exhibited distinctive edges in the CP contrast across both eye states. Conversely, in the HC contrast, the DorsAttn network displayed high-betweenness edges in the EO condition, whereas the Cont and Default networks assumed key integrative roles in the EC condition.

5.8.5.5. Graph analysis results for inter-network graphs: local clustering coefficient

No significant results were found in the Lcc comparison for the EO and EC conditions between HC and CP groups (Fig. 5.29C).

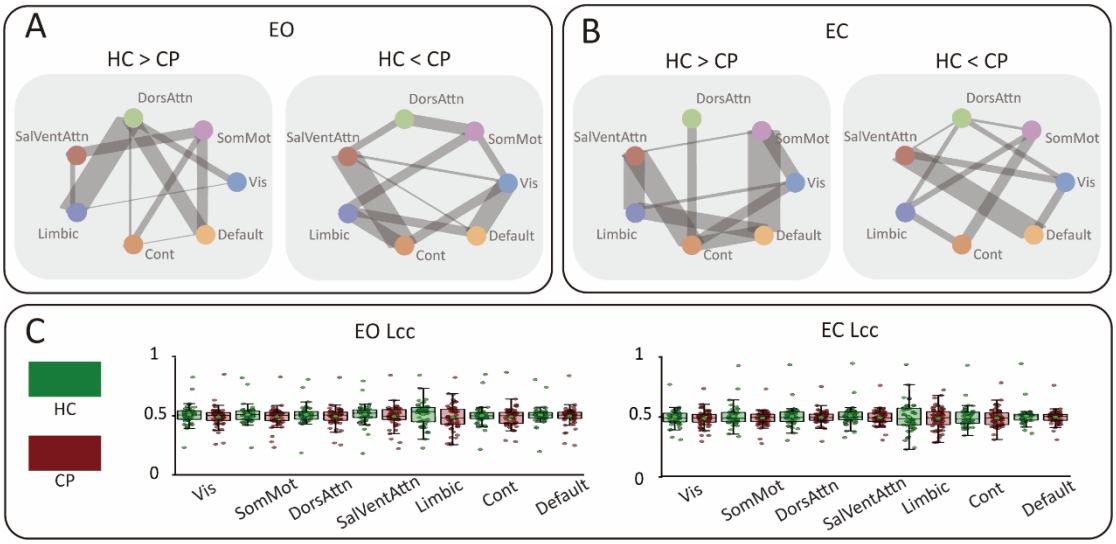

Figure 5.29. Results for local graph inferences analysis from inter-network graphs elicited by EO and EC conditions in HC and CP groups. (A) Ebc corresponded *t*-graphs for EO condition in both groups generated following NBS ($t > 0$; shown in reduced opacity). (B) Similar to (A) but for EC condition. The stroke size of each connection represents the corresponding t-value for the Ebc graph contrasts. (C) Box plots illustrate the statistical analysis for Lcc by paired-sample *t*-test with FDR correction between two groups for two eye states. Although no statistically significant graphs were identified, the Cont and Default networks exhibited distinctive edges in the CP contrast across both eye states. Conversely, in the HC contrast, the DorsAttn network displayed high-betweenness edges in the EO condition, whereas the Cont and Default networks assumed key integrative roles in the EC condition. EO, eyes-open; EC, eyes-closed; HC, healthy control group; CP, chronic pain patient group; Ebc, Edge betweenness centrality; NBS, network-based statistics.

5.8.5.6. Graph analysis results for inter-network graphs: global network inferences

No significant results were found in the GNIs from the inter-network graphs for the EO and EC conditions between HC and CP groups (Fig. 5.30).

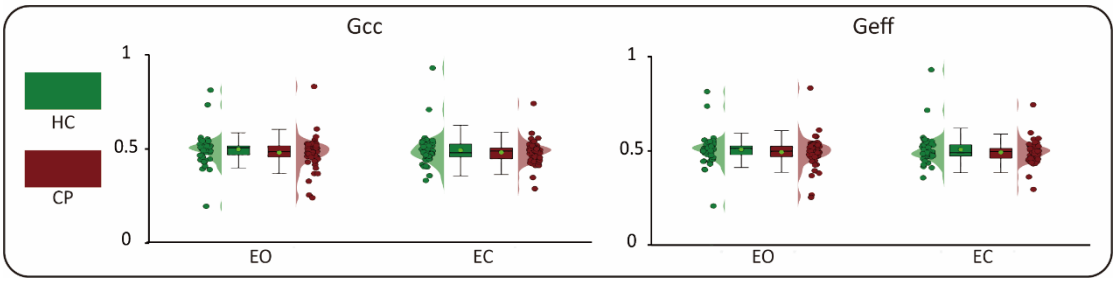

Figure 5.30. Graph analysis results for EO and EC conditions HC and CP groups for inter-network graphs. Violin plots with overlaid scatter and box plots show the results of two-way between-subjects ANOVA with Bonferroni correction for post hoc comparisons of two GNIs across the HC (dark green) and CP (dark red) conditions and two eye states. EO, eyes-open; EC, eyes-closed; HC, healthy control group; CP, chronic pain patient group; GNIs, global network inferences; Gcc, global clustering coefficient; Geff, global efficiency.

5.8.6. Classification performance

The top three classification performances based on GNIs across all nine graphs for their combinations from either EO or EC conditions were presented in Table 5.8. Although permutation-based *P* values indicated statistically significant classifications, the prediction AUC-ROCs did not exceed 0.80 for any single condition.

The highest performance achieved using the EO condition yielded an AUC-ROC of 0.79 with 75% accuracy, while the EC condition reached a maximum AUC-ROC of 0.78 with 74% accuracy. The similarity in these results indicates negligible difference in performance between the two states.

These findings suggest that the predictive utility of GNIs for distinguishing between HC and CP groups did not differ meaningfully between the EO and EC conditions.

Table 5.8. Classification performance for HC and CP groups based on GNIs across nine graphs under both EO and EC conditions.

Eye states	GNIs	AUC-ROC	ACC	Sensitivity	Specificity	P_{perm}
EO	sensor+source+Default+Cont	0.79	75%	0.64	0.86	0.00
	sensor+SM+Default+Vis+inter	0.77	70%	0.53	0.88	0.00
	sensor+source+Default+Cont+inter	0.77	72%	0.58	0.84	0.00
	sensor+source+SomMot+SalVentAttn+Cont+DorsAttn+Vis	0.78	74%	0.66	0.86	0.00
EC	sensor+source+SomMot+Cont+Default+Vis	0.76	71%	0.63	0.82	0.00
	sensor+source+SomMot+Cont+Default+Vis+inter	0.76	73%	0.66	0.82	0.00

Note. EO, eyes-open; EC, eyes-closed; Vis, intra-Visual network; SomMot, intra-Somato-Motor network, DorsAttn, intra-Dorsal Attention network; SalVentAttn, intra-Salience-Ventral Attention network, Limbic, intra-Limbic network; Cont, intra-Control network; Default, intra-Default network; inter, inter-network; AUC-ROC, area under the receiver operating characteristic curve; ACC, accuracy; P_{perm}, P value based on 1000 permutation.

5.9. Discussion for eyes-open and eyes-closed conditions in single-state group

5.9.1. Representative connectivity patterns

With a larger number of participants in each group, significant functional connectivity graphs emerged exclusively for the CP contrast in the sensor space under both conditions. These graphs were characterised by densely connected, bilateral patterns with right prefrontal predominance, replicating previous reports of alpha-band hyperactivation in chronic pain at a large brain scale, independent of eye-state (Prichep et al., 2018; Sarnthein et al., 2006; van den Broeke et al., 2013). This finding is consistent with the thalamocortical dysrhythmia model of chronic pain (Hughes & Crunelli, 2005; Llinás et al., 2005; Suffczynski et al., 2001; Tu et al., 2020).

Although not surviving statistical correction, consistent trends in intra-Default graphs indicated denser connectivity in the CP group across conditions. In inter-network graphs, the HC contrast exhibited a multi-network connectivity pattern, whereas the CP contrast was dominated by the Cont network. Furthermore, the Ebc graphs revealed a dual-hub pattern involving the Cont and Default networks in the CP contrast under both conditions. This heightened Cont network connectivity aligns with reports of aberrant functional coupling between the Cont network and amygdala, which is most pronounced in patients with high pain catastrophising (Jiang et al., 2016), representing a shared neural substrate for the cognitive-emotional disturbances common to both chronic pain and anxiety disorders (Kucyi & Davis, 2015; Ploner et al., 2017; Tracey et al., 2019; Wiech & Tracey, 2009).

5.9.2. Global network inferences and networks

Eye-state was found to have no significant impact on GNIs across graph types, whereas a significant group effect was observed in sensor space graphs. Specifically, both EO and EC conditions showed significantly greater global segregation and small-worldness in the HC group, alongside reduced global integration compared to the CP group. Significantly higher modularity was also observed in the HC group under the EO condition. These findings were consistent across both eye states, with the exception of no significant changes being found in the modularity in EC condition, suggesting the CP group exhibits altered global network characteristics that remain largely consistent across eye states during rest.

Importantly, this analysis revealed a significant decrease in Gcc in the CP group, consistent with a multicentre fMRI study (Mano et al., 2018). The combination of decreased functional segregation and increased integration, culminating in reduced small-worldness, indicates a shift toward a more randomised (Xin et al., 2024) and less cost-efficient network architecture (Liao et al., 2017).

5.9.3. Dynamic network reconfiguration

The CP group exhibited a profile of maladaptive network reorganisation characterised by reduced global segregation, increased global efficiency, and reduced small-worldness and modularity in sensor space. This pattern indicated a dysfunction in brain-wide connectivity, leaning towards a more random communication pattern (Xin et al., 2024). Although not surviving correction, trends suggested denser intra-Default connectivity in the CP group, alongside

distinctive Default-Vis connectivity in the EO condition and Default-SalVentAttn connectivity in the EC condition. Both patterns are aberrant; healthy Default typically shows enhanced connectivity with visual regions in EC (not EO) (Costumero et al., 2020; J. Han et al., 2023), and remains anticorrelated with the SalVentAttn network (Baliki et al., 2008; Hemington et al., 2016; Tu et al., 2019). This dysregulation suggests Default hyperexcitation, potentially reflecting a maladaptive overthinking for self-referential processing of the pain experience (Johansson et al., 2024).

The inter-network graphs showed a consistent dual-hub pattern involving the Default and Cont networks in the CP group, further implicating the Cont network in the pathophysiology of chronic pain. This finding is consistent with reports of exaggerated Cont-amygdala connectivity, particularly in patients with high pain catastrophising (Jiang et al., 2016).

In contrast, the HC group demonstrated significantly higher small-worldness, driven by increased segregation and decreased integration, reflecting an optimised, cost-efficient brain architecture. This was accompanied by a multi-network communication pattern across both eye states. The lack of such broad, flexible network engagement appears to be a characteristic deficit in CP, irrespective of eye-state.

5.9.4. Classification performance

Classification performance under both EO and EC conditions yielded AUC-ROCs with values not exceeding 0.80 and accuracy rates of up to 75%. Both conditions produced comparable results, highlighting the robust, yet similar, discriminatory power of GNIs across different states. This indicates that the discriminatory power of GNIs was robust and similar across both resting-state

conditions, suggesting that the ability to detect group differences is not dependent on a specific eye-state.

5.10. Additional analysis for single-state group global network inferences in sensor space

Given the bimodal distribution of Geff identified in the CP group across both EO and EC conditions, we performed an exploratory post-hoc clustering analysis to characterise subgroup differences. We applied k-means clustering with k = 2 to partition the CP group based on Geff values, in order to resolve the observed bimodal structure. Clustering results revealed that the subgroup exhibiting significantly higher Geff comprised only patients with chronic back pain (CBP), in both EO and EC conditions.

Based on this empirical clustering outcome, we formally subdivided the original CP group into two clinically distinct subgroups: CBP group for patients diagnosed with chronic back pain; whereas CP_O group for patients with other chronic pain conditions, including fibromyalgia (FM) and mixed chronic pain.

To examine group differences in sensor space GNIs across the full spectrum of participants, we conducted a one-way ANOVA with Bonferroni correction comparing all three subgroups alongside the healthy control (HC) group: HC, CBP, and CP_O for EO and EC condition, separately. This three-group comparison allowed us to test whether the elevated Geff observed in the k-means cluster represented a unique network phenotype specific to CBP, as distinct from other chronic pain phenotypes and healthy brain function.

5.10.1. Sensor space graph analysis results: further division for three groups

The significant main effect of group (HC, CBP, CP_O) was observed across all four GNIs in both EO and EC conditions (Fig. 5.31).

Post-hoc comparisons revealed significantly higher Gcc values in the HC group relative to the CP_O group in EC conditions (t (73) = 2.85, P = 0.02, 95% CI = [0.01, 0.11]). For Geff, highly significant group differences were detected in both EO and EC conditions, with the CBP subgroup showing markedly higher Geff than both HC and CP_O (EO: CBP > HC: t (70) = 24.24, P < 0.001, 95% CI = [0.12, 0.14]; CBP > CP_O: t (53) = 23.69, P < 0.001, 95% CI = [0.12, 0.15]; EC: CBP > HC: t (65) = 13.10, P < 0.001, 95% CI = [0.11, 0.16]; CBP > CP_O: t (42) = 14.70, P < 0.001, 95% CI = [0.12, 0.17]).

In contrast, Sw and Mod exhibited consistent patterns across EO and EC states, with significantly higher values in the HC and CP_O groups compared with the CBP subgroup. For Sw, HC > CBP (EO: t (70) = 10.09, P < 0.001, 95% CI = [1.59, 2.60]; EC: t (65) = 8.77, P < 0.001, 95% CI = [1.51, 2.70]) and CP_O > CBP (EO: t (53) = 8.46, P < 0.001, 95% CI = [1.35, 2.43]; EC: t (42) = 7.56, P < 0.001, 95% CI = [1.27, 2.47]). For Mod, HC > CBP (EO: t (70) = 5.57, P < 0.001, 95% CI = [0.02, 0.05]; EC: t (65) = 4.44, P < 0.001, 95% CI = [0.02, 0.06]) and CP_O > CBP (EO: t (53) = 5.40, P < 0.001, 95% CI = [0.02, 0.06]; EC: t (42) = 4.82, P < 0.001, 95% CI = [0.02, 0.06]).

Detailed one-way ANOVA statistics and post-hoc comparisons are provided in Table 5.9.

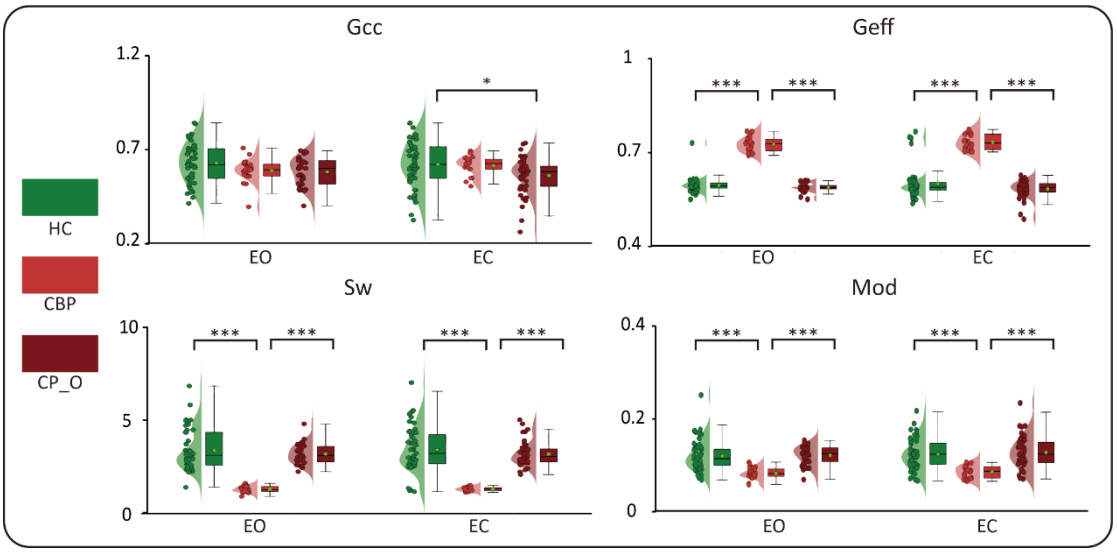

Figure 5.31. Graph analysis results for EO and EC conditions in HC and CP groups in sensor space. Violin plots with overlaid scatter and box plots show the results of one-way ANOVA with Bonferroni correction for post-hoc comparisons of four GNIs across three groups: healthy controls (HC, dark green), chronic back pain (CBP, red), and other chronic pain (CP_O, dark red) separately in two eye states. EO, eyes-open; EC, eyes-closed; HC, healthy control group; CBP, chronic back pain subgroup; CP_O, other chronic pain subgroup; GNIs, global network inferences; Gcc, global clustering coefficient; Geff, global efficiency; Sw, small-worldness; Mod, modularity.

Table 5.9. Statistical results for GNIs from EO and EC conditions in HC, CBP, and CP_O groups in the sensor space (ANOVA and Post-hoc Comparisons).

GNIs	Eye-state	*F*	*P*	η_p^2	Post-hoc Comparisons	*T*	$P_{Bonferroni}$	95% CI
Gcc	EO	3.47	0.04	0.06				
Gcc	EC	4.32	0.02	0.07	HC > CP_O	2.85	0.02	[0.01, 0.11]
Geff	EO	344.61	<0.001	0.87	CBP > HC	24.24	<0.001	[0.12, 0.14]
					CBP > CP_O	23.69	<0.001	[0.12, 0.15]
Geff	EC	110.54	<0.001	0.67	CBP > HC	13.10	<0.001	[0.11, 0.16]
					CBP > CP_O	14.70	<0.001	[0.12, 0.17]
Sw	EO	54.10	<0.001	0.52	HC > CBP	10.09	<0.001	[1.59, 2.60]
					CP_O > CBP	8.46	<0.001	[1.35, 2.43]
Sw	EC	28.68	<0.001	0.41	HC > CBP	8.77	<0.001	[1.51, 2.70]
					CP_O > CBP	7.56	<0.001	[1.27, 2.47]
Mod	EO	16.18	<0.001	0.26	HC > CBP	5.57	<0.001	[0.02, 0.05]
					CP_O > CBP	5.40	<0.001	[0.02, 0.06]
Mod	EC	12.51	<0.001	0.19	HC > CBP	4.44	<0.001	[0.02, 0.06]
					CP_O > CBP	4.82	<0.001	[0.02, 0.06]

Note. EO, eyes-open; EC, eyes-closed; HC, healthy control group; CBP, chronic back pain subgroup; CP_O, other chronic pain subgroup; GNIs, global network inferences; Gcc, global clustering coefficients; Geff, global efficiency; Sw, small-worldness; Mod, modularity; Abs, absolute comparison; Rel, relative comparison.

5.10.2. Discussion for sensor space graph analysis: further division for three groups

Exploratory k-means clustering and subsequent three-group ANOVA provided critical new insights into the heterogeneous network topology within the chronic pain cohort, clarifying how distinct clinical phenotypes exhibit divergent alpha-band network organisation in resting-state EEG. This analytical approach addresses a key limitation of prior studies that pooled heterogeneous chronic pain subtypes, which risked masking subtype-specific neurophysiological signatures.

Consistent with the bimodal distribution of Geff in the overall CP group, partitioning patients into CBP and CP_O subgroups revealed a highly specific and consistent network phenotype unique to CBP within the present sample. Across both EO and EC conditions, the CBP subgroup demonstrated markedly elevated global efficiency relative to both HC and the CP_O subgroup. This pronounced enhancement of global integration was accompanied by significantly reduced Sw and Mod in CBP compared with both HC and CP_O. These findings clarify that the increased global efficiency and network maladaptation previously reported in the overall chronic pain group were driven predominantly by the CBP subgroup within the present dataset, resolving the apparent heterogeneity within chronic pain populations in this study. Caution is warranted in generalising these patterns as uniquely specific to CBP, as the limited number of fibromyalgia patients included means we cannot exclude divergent topological profiles emerging with a larger, more representative fibromyalgia cohort in future research.

Parallels in the spectral domain strengthen this interpretation. McLain et al. (2025), analysing the same secondary dataset, reported that peak alpha frequency (PAF) differs significantly between CBP and widespread pain (including FM), with widespread pain associated with higher global PAF than CBP. Additionally, Cavaleri et al. (2025) validated in an independent dataset that participants with urologic chronic pelvic pain syndrome and widespread pain exhibited significantly lower global average PAF than those with localised pain. Given that our GNIs were derived from alpha-band EEG, it is unsurprising that these metrics similarly exhibit diagnosis-specific profiles, suggesting they may serve as complementary biomarkers alongside PAF for the clinical stratification of chronic pain subtypes within this sample.

These subgroup differences may be attributed to the underlying heterogeneity of chronic pain pathophysiological mechanisms. For instance, CBP patients exhibit significant alterations in global brain network topology, characterised by a prolonged characteristic path length alongside reduced clustering coefficient, global efficiency, and local efficiency, relative to HC (Liu et al., 2018). Further neuroimaging investigations have revealed distinct nodal network abnormalities in CBP patients, who display significantly higher mPFC/rACC nodal degree, efficiency, and betweenness than HC (Tu et al., 2019). Complementary fMRI research has additionally identified impaired global information transfer efficiency across functional brain networks as a key pathophysiological state underlying CBP (Tu et al., 2020). Moreover, augmented inter-network information transfer between the salience network and primary somatosensory cortex (S1) has been validated as a critical neural substrate, mediating the reallocation of attentional resources and affective encoding of nociceptive input in the

chronic pain state (J. Kim et al., 2019). Collectively, these findings support a model of maladaptive thalamocortical plasticity in CBP, wherein persistent afferent input drives hyper-connected, hyper-integrated network architecture at the expense of modular specialisation.

In contrast, the CP_O subgroup, comprising fibromyalgia and mixed chronic pain patients, retained a modular, well-segregated network structure broadly comparable to HC in the present analysis. Only Gcc distinguished CP_O from HC, and exclusively in the EC condition. This is consistent with fibromyalgia literature showing that structural network abnormalities in FM involve compromised segregation and integration (Tu, Wang, et al., 2023), and that FM is associated with disrupted PCC connectivity in the DMN and increased anterior insula connectivity in the salience network (Van Ettinger-Veenstra et al., 2019), rather than the global hyper-efficiency phenotype observed in CBP. A recent meta-analysis (Butry et al., 2025) confirmed lower local efficiency across chronic pain broadly, but our findings extend this by demonstrating that global network architecture remains unaltered in non-CBP chronic pain subtypes within this sample.

Crucially, subgroup differences were stable across EO and EC states, indicating that CBP-related network abnormalities reflect a trait-like neurophysiological marker rather than a state-dependent fluctuation. This cross-state consistency reinforces the potential diagnostic utility of Geff, Sw, and Mod as objective stratification tools.

From a clinical perspective, these results support a model in which localised nociceptive input in CBP drives large-scale network reorganisation, excessive functional integration and diminished modular specialisation, consistent

with maladaptive sensorimotor and frontoparietal plasticity. Fibromyalgia and mixed chronic pain, by contrast, appear to involve distinct pathophysiological mechanisms that spare global network architecture, implying that targeted neuromodulation strategies for CBP (e.g., targeting hyper-integrated networks) may not be applicable to other chronic pain subtypes, highlighting the need for personalised treatment approaches.

Methodologically, these findings underscore the importance of accounting for clinical heterogeneity in neuroimaging research. Pooling heterogeneous pain phenotypes risks masking subtype-specific network signatures and reducing cross-site reproducibility (Butry et al., 2025). Graph-theoretical metrics derived from resting-state alpha-band EEG, particularly Geff, Sw and Mod, demonstrate sufficient sensitivity to discriminate between closely related clinical subgroups, supporting their translational potential for objective patient stratification and neuromodulation targeting.

In summary, this additional analysis reveals that elevated global efficiency and reduced small-worldness and modularity represent a robust, state-independent network signature in CBP patients within this study. These findings refine our understanding of network dysfunction in chronic pain, emphasise the distinctive neuroplasticity profile associated with CBP, and provide empirically grounded support for stratifying chronic pain cohorts in future neuroscientific research and clinical neuromodulation applications.

5.11. Summary

This chapter examined brain network reorganisation in HC and CP groups during EO and EC resting-states, applying both absolute and relative

comparison methods in the paired-state (within-subject) analysis, and only the absolute comparison in the single-state (between-subject) analysis.

Our analyses revealed robust and consistent alpha band EEG reorganisation in chronic pain, characterised by widespread sensor-space overactivation and stable changes in global network topology. Specifically, the CP group demonstrated a persistent profile of increased global integration (higher Geff), decreased small-worldness and modularity across both resting-states. This consistent profile indicates a fundamental shift toward a less optimised, more randomised brain architecture in chronic pain, consistent with the thalamocortical dysrhythmia model of chronic pain (Hughes & Crunelli, 2005; Llinás et al., 2005; Suffczynski et al., 2001). This pattern is primarily driven by the CBP subgroup, while the CP_O subgroup (fibromyalgia and mixed chronic pain) retains a network architecture largely comparable to healthy controls, with only minor differences in global clustering coefficient observed exclusively in the EC condition within the present sample. These subgroup-specific network abnormalities arise from the heterogeneous pathophysiological mechanisms underlying distinct chronic pain phenotypes, with localised chronic back pain driving maladaptive thalamocortical plasticity, hyper-connected global networks, and lost modular specialisation (Tu et al., 2019, 2020).

We also found significantly decreased intra-Default global efficiency specifically and reduced SalVentAttn intra-network connectivity for CP group in the EC condition. This aligns with the aberrant loss of Default-SalVentAttn anticorrelation reported in chronic pain, thought to reflect a maladaptive cognitive state

focused on self-referential processing (Goulden et al., 2014; Johansson et al., 2024; Tu et al., 2019).

Divergent group differences emerged in intra-Default graphs. graphs from the paired-state analysis. In the EO condition, the CP group showed increased intra-Default Geff, whereas in the EC condition, they exhibited decreased intra-Default Geff. This eye-state-dependent dysregulation of the Default aligns with its known dynamicity (Costumero et al., 2020; J. Han et al., 2023), and highlights its abnormal reactivity in CP (Baliki et al., 2014). These nuanced Default findings were predominantly revealed by the relative comparison method, underscoring the impact of baseline normalisation.

Validation in the single-state group consistently reproduced the significant sensor-space GNI alterations and non-significant intra-Default findings. However, inter-network graphs differed, particularly in the EC condition, suggesting that EC may be a less stable state for characterising specific network communication mechanisms in chronic pain (Weng et al., 2020). Consequently, the EO condition may be more suitable for elucidating the specific network communication mechanisms disrupted in chronic pain. Moreover, the stability of subgroup differences across EO and EC states confirms that CBP-related network anomalies represent trait-like biomarkers rather than state-dependent fluctuations, strengthening their diagnostic value.

Finally, classification analysis demonstrated that the best performance for distinguishing groups was achieved by the paired-state group, either by combining GNIs from both EO and EC conditions (absolute comparison) or by integrating both comparison methods for the EC condition alone. Both models

achieved an AUC-ROC of 0.91 with 80% accuracy. This confirms that integrating information across states and methods enhances predictive power. The strong performance of the relative comparison in this between-subject context contrasts with its inferior performance for within-subject classification in Chapter 4, highlighting its context-dependent utility.

In conclusion, this investigation revealed widespread alpha-band overactivation in chronic pain patients during resting-states, marked by a consistent pattern of maladaptive brain network reorganisation. The core finding was a significantly larger brain-wide connectivity graph in the sensor space, accompanied by reduced global segregation, increased integration, and diminished small-worldness and modularity, indicating a shift toward a more randomised and less cost-efficient brain architecture across resting-states. This signature is strongly pronounced to CBP. Abnormal Default hyperactivation was evident not only in its internal connectivity but also in its altered communication with networks such as SalVentAttn and Cont, pointing to maladaptive crosstalk underlying self-referential overthinking and catastrophising in chronic pain. Methodologically, while both eye states were informative, the greater variability in EC results suggests the EO condition may be more reliable for exploring specific network mechanisms. Ignoring clinical heterogeneity by pooling distinct pain phenotypes risks masking subtype-specific network signatures and reducing reproducibility; graph-theoretical inferences from alpha-band EEG enable robust stratification of chronic pain subgroups. The relative comparison method demonstrated particular value in enhancing detection sensitivity through activity normalisation. Finally, classification performance using GNIs achieved excellent results, with the best performance (AUC-ROC = 0.91, 80% accuracy)

incorporating both absolute and relative comparison features. This robust performance strongly suggests that collecting data from both EO and EC conditions can significantly enhance the power of future diagnostic models in chronic pain. The novel contribution of this work is the identification of a core maladaptive network signature in chronic pain, stratified by clinical subtype and compounded by state-specific dysregulation, compounded by state-specific dysregulation, which provides a promising foundation for objective, network-based diagnosis.

Chapter 6

General discussion and conclusion

This chapter synthesises the principal findings and conclusions of the research programme. It critically examines how global network inferences serve as robust biomarkers of pain-related brain reorganisation across experimental and clinical pain states. The collective implications of the methodological and empirical advances are discussed, with particular emphasis on the comparative utility of analytical approaches and multimodal protocols. The chapter concludes by acknowledging the limitations of the current work and outlining clear directions for future research and clinical translation.

6.1. Summary of empirical findings

This thesis provides significant advances in understanding pain-related brain reorganisation across both experimental and clinical pain conditions through a systematic, multi-level analysis of functional connectivity and graph theory. A core empirical contribution is the identification that global network inferences (GNIs) derived from alpha-band oscillations can be validated as robust biomarkers capable of tracking neuroplastic adaptations across diverse contexts. Three consistent network signatures emerged:

(1) Tonic pain triggers an adaptive shift from functional segregation to integration.

(2) Post-stimulation rest induces a reconfiguration towards greater segregation and small-worldness.

(3) Chronic pain is characterised by a maladaptive state of increased integration and diminished small-worldness, a signature predominantly driven by the CBP subgroup.

The consistent GNI patterns observed across different pain conditions and analytical methods highlight their reliability as indicators of brain reorganisation, effectively bridging experimental models with clinical chronic pain. Finally, the established translational validity of these network measures, evidenced by superior predictive power in machine learning classifiers, paves the way for objective pain diagnostics and personalised therapeutic strategies.

The following sections detail the findings of each study to address the research questions and synthesise them into a unified framework.

6.1.1. Network reorganisation in tonic pain: from segregation to integration

This study investigated the neural dynamics of experimental tonic pain through EEG-based functional connectivity and graph theory.

6.1.1.1. Can functional connectivity and network topology differentiate between experimental tonic noxious hot from innocuous warm conditions?

Our findings suggest that both functional connectivity patterns and graph-theoretical measures successfully differentiated between noxious hot and innocuous warm conditions. The results revealed a brain-wide reorganisation characterised by a global shift from functional segregation to integration.

6.1.1.2. What is the neuronal mechanism, as revealed by our connectivity and graph analyses, underpin these pain-states?

The neuronal mechanism underpinning this pain-state difference may reflect a fundamental transition from intra- to inter-network communication, potentially mediated by thalamocortical circuits and GABAergic inhibition. The Somato-Motor network was identified as pivotal, shifting from a locally specialised processor during warmth to a global integrator during pain, a transition likely facilitated by rapidly increased synaptic plasticity. This reorganisation was quantified by a statistically significant reduction in the global clustering coefficient when intra-network connections were excluded.

6.1.1.3. Will the network inferences from graph-theory measurements provide accurate pain-state classification?

The translational potential of these network inferences is strongly supported. A machine learning model utilising these global network measures achieved AUC-ROC of 0.94 and accuracy of 86% in classifying pain states. Furthermore, their clinical relevance was underscored by how psychological traits modulated network topology: pain catastrophising amplified segregation and integration during pain, while anxiety was linked to reduced network differentiation during innocuous warmth.

In summary, this research provides compelling evidence that tonic pain is associated with a quantifiable reorganisation of large-scale brain dynamics. The robustness of these GNIs for classification and their modulation by psychological traits confirms their significant potential as objective biomarkers for pain states. The novel finding of this study is the quantification of a rapid, large-scale network shift during tonic pain, validated by robust classification and linked to individual psychological differences.

6.1.2. Tracking neuroplasticity: cross-state signatures of sensory stimulation

This study investigated the reconfiguration of resting-state brain networks following sensory stimulation, yielding clear answers to our core questions.

6.1.2.1. How does functional connectivity and network topology change from pre- to post-stimulation resting-states?

Both EEG-based functional connectivity and graph-theoretic network inferences successfully differentiated between pre- and post-stimulation resting-states. Analyses revealed significant differences in sensor-space graphs and showed a consistent post-stimulation increase in functional segregation and small-worldness alongside reduced modularity. Findings in EO suggested that pre-stimulation modularity was related to robust Default interactions, particularly between the Default and Vis, SomMot, and DorsAttn networks.

6.1.2.2. Do these time-dependent changes differ between eyes-open and eyes-closed resting-state conditions?

Time-dependent changes differed substantially between EO and EC conditions. While both states showed a general post-stimulation shift towards increased segregation, the specific reconfiguration patterns were state-dependent. EO restructured from a SalVentAttn-integrated state to a SomMot-Vis dual-hub architecture, whereas EC shifted from broad multi-network integration to a focused SalVentAttn-dominated state. Moreover, a significant decreased modularity intra-Default was found exclusively in the EO condition, suggesting that pre-stimulation modularity was related to robust Default interactions, particularly between the Default and Vis, SomMot, and DorsAttn networks.

6.1.2.3. What neuronal mechanisms underpin these post-stimulation changes?

The neuronal mechanism underpinning these changes is a stimulation-induced shift in the brain's functional architecture towards specialised,

segregated processing. This is characterised by a reorganisation of hub dominance and a strengthening of long-range, inter-hemispheric pathways, reflecting an optimisation for processing recent sensory experience. The increase in small-worldness and reduction in modularity further indicate a rebalancing towards efficient, specialised information processing.

6.1.2.4. Will the network inferences from graph-theory measurements validate these changes and demonstrate translational potential?

The translational potential of these graph-theory measurements is strongly validated. A machine learning model using GNIs achieved high classification accuracy for pre- versus post-stimulation states especially using features combined both EO and EC (AUC-ROC = 0.88, 81% accuracy, underscoring the sensitivity of this multimodal approach for detecting stimulation-induced neuroplasticity.

In summary, this study revealed that sensory stimulation induces a predictable reconfiguration of resting-state networks, characterised by a shift towards increased functional segregation and small-worldness. While the specific patterns were state-dependent, in another word, differing between EO and EC conditions, a unified signature of neuroplasticity was identified. Critically, a machine learning model combining features from both states achieved excellent classification (AUC-ROC = 0.88), underscoring the sensitivity of this multimodal approach. The novel contribution here is the identification of a unified, state-dependent signature of post-stimulation neuroplasticity, detectable with a multimodal EO/EC approach.

6.1.3. Chronic pain signatures: maladaptive network integration

This investigation into resting-state brain dynamics of chronic pain (CP) patients versus healthy controls (HC) yielded clear, affirmative answers to our primary research questions.

6.1.3.1. How do functional connectivity and network topology differ in resting-states between chronic pain patients and healthy controls?

Both EEG-based functional connectivity and graph-theoretic network inferences robustly differentiated CP from HC. The most consistent finding was a brain-wide overactivation in sensor-space connectivity in the CP group, alongside distinct alterations in intra- and inter-network communication, particularly involving the Default network.

6.1.3.2. Do these group differences vary between eyes-open and eyes-closed resting-state conditions?

Group differences varied by eye-state, revealing both stable and state-dependent maladaptive reorganisation. A core, state-independent signature of CP was identified: reduced global segregation, increased global integration, and diminished small-worldness and modularity, indicating a shift towards a less optimised, more random network architecture. Critically, this global signature is not uniform across chronic pain subtypes: it is exclusively observed in the CBP subgroup (excluding reduced segregation).

Divergent group differences emerged in intra-Default graphs: in the EO condition, the CP group showed increased intra-Default Geff, whereas in the EC condition, they exhibited decreased intra-Default Geff alongside

significantly lower connectivity strength within SalVentAttn. The EC condition points toward an abnormal loss of anticorrelation between these two fundamental networks, a phenomenon also reported in other chronic pain studies, suggests a failure to properly segregate internal (Default) and external/salience (SalVentAttn) processing.

6.1.3.3. What neuronal mechanisms underpin these group differences?

The neuronal mechanism is a widespread maladaptive reorganisation driven by chronic pain, with distinct pathophysiological substrates across subtypes: localised CBP characterised by thalamocortical dysrhythmia leading to global alpha-band overactivation, while fibromyalgia and mixed chronic pain involve region-specific network abnormalities without global hyper-integration. This disrupts the normal balance between functional segregation and integration, resulting in less specialised local processing and inefficient global communication.

6.1.3.4. Will the network inferences from graph-theory measurements validate for such group differences and therefore have translational potential?

The translational potential is strongly validated. Subgroup-stratified graph inferences, especially Geff, Sw, and Mod, enable reliable discrimination between CBP, CP_O, and HC, even across EO and EC states, confirming their value as trait-like biomarkers for pain subtype stratification.

Machine learning models using GNIs achieved excellent performance, with a top model combining EO and EC features achieving an AUC-ROC of

0.91 and 80% accuracy. This demonstrates that these network-based biomarkers hold significant promise for developing objective diagnostic tools for chronic pain.

In summary, this study identified a distinct, maladaptive signature of chronic pain, subtype-specific to CBP, marked by a pervasive shift towards a disorganised, hyper-integrated, yet less efficient brain architecture. This core dysfunction was consistent across both EO and EC resting-states, reflecting a stable trait-like marker rather than a state-dependent fluctuation, but was compounded by state-dependent failures, particularly a breakdown in Default network regulation during EC. The translational promise of these findings was cemented by a diagnostic model that achieved an AUC-ROC of 0.91 in classifying patients and controls, providing a robust, network-based tool for objective chronic pain diagnosis. The novel finding of this study is the identification of a core maladaptive network signature in CP, compounded by state-specific dysregulation, which forms a viable basis for objective diagnosis. The novel finding of this study is the identification of a core maladaptive network signature specific to CBP, distinct from other chronic pain subtypes and compounded by state-specific dysregulation, which forms a viable basis for objective, subtype-stratified diagnosis.

6.2. Consistent network biomarkers across pain conditions

Across all three studies, GNIs demonstrated consistent and reliable patterns, underscoring their potential as robust EEG-based biomarkers for pain-related brain dynamics. As summarised in Table 6.1, distinct GNI signatures

emerged consistently within each study, revealing a continuum of network dysfunction from tonic experimental pain to chronic clinical pain.

Notably, this continuum is further refined by pain chronicity and clinical subtype: adaptive network shifts in experimental tonic pain progress to maladaptive, subtype-specific persistence in chronic pain, with CBP exhibiting the most profound global network reorganisation.

Table 6.1. Significant GNIs shown across studies in all graphs.

Study	data type	Graph	Gcc	Geff	Sw	Mod
Study 1	tonic pain	sensor	Hot < Warm: both	Hot > Warm: Abs		Hot < Warm: Abs
		source	Hot < Warm: Rel	Hot > Warm: Abs	Hot < Warm: both	
		intra-SomMot	Hot < Warm: both			
		inter-network	Hot > Warm: Abs	Hot > Warm: Abs		
Study 2	resting EO	sensor	Post > Pre: Rel		Post > Pre: Rel	Post < Pre: Rel
		source				
		intra-Default				Post < Pre: Abs
		inter-network				
Study 2	resting EC	sensor	Post > Pre: Abs	Post < Pre: Abs	Post > Pre: Abs	Post < Pre: Abs
		source				
		intra-Default				
		inter-network				
Study 3	paired-EO	sensor		CP > HC: both	CP < HC: both	
		source				
		intra-Default		CP > HC: Rel		
		inter-network				
Study 3	paired-EC	sensor		CP > HC: both	CP < HC: both	CP < HC: Rel
		source				
		intra-Default		CP < HC: Rel		
		inter-network				
Study 3	single	sensor	CP < HC	CP > HC	CP < HC	CP < HC
		source				
		intra-Default				
		inter-network				

Note. Significant GNI patterns across Study 1 (tonic pain), Study 2 (post-stimulation rest), and Study 3 (chronic pain). GNIs, global network inferences; EO, eyes-open; EC, eyes-closed; Abs, absolute comparison; Rel, relative comparison; HC, healthy control group; CP, chronic pain patient group; Gcc, global clustering coefficients; Geff, global efficiency; Sw, small-worldness; Mod, modularity.

In Study 1 (tonic pain), GNIs revealed a characteristic pattern of increased global integration and decreased segregation during pain. Study 2 (post-stimulation rest) showed that sensory stimulation consistently induced increased functional segregation and small-worldness across different resting-states. Most notably, Study 3 (chronic pain) identified a stable maladaptive signature in patients, specifically the CBP subgroup, characterised by consistently increased global integration and decreased small-worldness across both eye states and analysis methods.

Crucially, these GNI patterns yield a direct bridge between experimental and clinical pain biomarkers. The consistent observation of increased integration (Geff), and reduced small-worldness (Sw) in both the tonic pain of healthy participants (Study 1) and the spontaneous brain state of CBP patients (Study 3) suggests a fundamental shared mechanism of disrupted network balance (Kastrati et al., 2022; Zheng et al., 2020). This pattern indicates a brain state overly biased towards global, diffuse information processing at the expense of specialised, efficient modular organisation. This contrasts sharply with the adaptive response seen in healthy post-stimulation rest (Study 2), which showed increased segregation and small-worldness, indicating a flexible return to an optimal network architecture (Arami & Komaki, 2022)..

The superior classification performance achieved using these measures further validates GNIs as generalisable biomarkers capable of identifying: 1) intra-subject pain states, 2) stimulation-induced neuroplasticity, and 3) inter-subject chronic pain conditions.

The clinical relevance of GNIs is further enhanced by their modulation by psychological traits in Study 1. Pain catastrophising amplified network segregation and integration during pain, while anxiety reduced these measures during innocuous stimulation, revealing clinically meaningful individual differences in pain processing.

In summary, GNIs demonstrate significant translational value, providing a quantifiable bridge connecting evoked pain states with spontaneous clinical pain conditions. They also enable stratification of clinically distinct chronic pain subtypes, resolving long-standing heterogeneity in pain neuroscience research. Critically, these GNI signatures were extractable across multiple contexts: during sensory stimulation, in pre-/post-stimulation resting-states, and in chronic pain populations, demonstrating their broad applicability for understanding pain-related brain reorganisation from a network neuroscience perspective. The novel contribution of this synthesis is the establishment of GNIs as a consistent, translatable metric that bridges distinct pain paradigms, from evoked states to spontaneous clinical conditions and enables objective subtyping of chronic pain.

6.2.1. Alpha-band oscillations in pain: from network mechanisms to biomarkers

Across all three studies, our findings demonstrate that large-scale brain reorganisation in both tonic and chronic pain conditions can be reliably captured through GNIs derived from alpha-band oscillatory activity measured using phase-based functional connectivity. These results align with the broader literature emphasising the central role of alpha dynamics in shaping cortical

network communication (Apkarian et al., 2011; Bak et al., 2021; Baliki & Apkarian, 2015).

Alpha-band oscillations are widely understood as a network-level gating mechanism regulating the flow of neural information. This gating may operate through two complementary processes. At the large-scale network level, alpha-phase synchronisation modulates information transfer between distant cortical nodes (Palva & Palva, 2007), whereas locally, fluctuations in alpha amplitude influence neuronal excitability and sensory gain control (Romei et al., 2008). As a fundamental thalamocortical rhythm (Lőrincz et al., 2009), alpha oscillations are thought to gate sensory input during early processing stages; for instance, alpha-band event-related desynchronisation (ERD) during tonic pain reflects selective filtering of incoming nociceptive information and suppression of irrelevant sensory input (Jensen & Mazaheri, 2010; Peng et al., 2015).

Beyond sensory gating, alpha oscillations also play a key role in higher-order, pulvino-cortical networks involved in top-down cognitive control. These networks support long-range synchronisation between cortical areas, facilitating attentional allocation, expectation, and cognitive modulation of sensation (Klimesch, 2012; Saalmann et al., 2012). This duality is consistent with hierarchical predictive processing frameworks, in which lower-frequency oscillations (alpha/beta) carry predictive feedback signals, while higher-frequency gamma oscillations relay feedforward prediction errors (Bastos et al., 2012).

The communication-through-coherence (CTC) theory (Fries, 2005, 2015) offers a compelling explanation for how alpha-phase alignment enables flexible coordination among neural populations, supporting stable long-range

communication channels. Recent findings, however, suggest that macroscale alpha coherence may not require synchronous excitatory spiking; rather, it may emerge from coordinated inhibitory activity in GABAergic interneuron circuits (Pesaran et al., 2018; Schneider et al., 2021).

Our results strongly position alpha-band functional connectivity as a biomarker of pain-related network dynamics. They further establish alpha-band GNIs as sensitive tools for discerning pathophysiologically distinct chronic pain subtypes, beyond simple case–control discrimination. They are consistent with evidence from recent large-scale analyses showing that phase-based alpha connectivity captures network-level reorganisation that cannot be inferred from activation magnitudes alone (Bott et al., 2025). Moreover, empirical interventions manipulating alpha-phase synchrony using neurostimulation techniques (Ahn et al., 2019; X. Li et al., 2025; Peng et al., 2023), underscore the causal relevance of alpha-mediated communication pathways.

Finally, insights from network-informed neuromodulation strategies in other neurological disorders, particularly those involving large-scale network disruption, provide a conceptual foundation for future pain interventions. Developments in state-dependent stimulation, multifocal and subcortical targeting, individualised electric-field modelling, and accelerated modulation protocols (Rektorová et al., 2025), highlight the translational potential of our findings. By identifying subtype-specific maladaptive alpha-band network signatures through GNIs in chronic pain, our work opens promising avenues for next-generation neuromodulation treatments aimed at restoring healthy brain network organisation in pain management.

6.3. Methodological considerations

6.3.1. Analytical approach in comparison methods

Our analysis revealed that the choice between absolute and relative comparison methods significantly influenced the detection of connectivity patterns, network inferences, and subsequent machine learning performance across all three studies.

Connectivity Patterns: At the group level, source-space and intra-network graphs demonstrated greater similarity between comparison methods than sensor-space graphs across all studies. While distinctive patterns emerged in sensor-space analyses, particularly in the EO condition of Study 2, condition contrasts consistently aligned between comparison methods. This consistency demonstrates the robustness of identified condition effects and underscores the complementary value of employing both approaches for comprehensive brain network characterisation. Notably, relative comparisons tended to emphasise inter-hemispheric and posterior connectivity, while absolute comparisons proved more sensitive for capturing time effects, especially in EC conditions in Default network of Study 2.

Network Inferences: We consistently observed main effects of comparison methods across analyses, with the most frequent significant GNI differences appearing in sensor space. Mixed results emerged, with both methods showing unique advantages. In group comparisons, relative comparisons exclusively revealed certain differences, particularly nuanced findings such as the eye-state-dependent dysregulation of the Default network in chronic pain

patients. This highlights a critical methodological insight: baseline resting-state normalisation in relative comparisons reduces inter-subject variability in intrinsic connectivity, thereby unmasking condition-specific network reorganisation that may be obscured in absolute comparisons.

Classification Performance: Comparative analysis revealed context-dependent advantages for each method. In tonic pain, absolute comparisons demonstrated superior classification performance, suggesting stronger potential as translational biomarkers due to their direct association with general neurophysiological states. For pre- and post-stimulation states, a hybrid approach proved most effective: combining methods enhanced predictive power in EO conditions, while EC conditions relied entirely on absolute comparisons. In chronic pain classification, relative comparisons excelled for EO states, while EC conditions benefited most from method integration.

These findings support a strategic application framework: relative comparisons excel for mechanistic investigations where normalisation reduces inter-subject variability, particularly in EO conditions and for understanding specific network interactions. Conversely, absolute comparisons show stronger performance for biomarker discovery and diagnostic applications, especially in EC conditions. The integration of both methods, combined with multimodal (EO+EC) data collection, represents the most powerful approach for comprehensive pain state classification, achieving excellent performance (AUC-ROC up to 0.91) that bridges experimental and clinical pain domains.

6.3.2. Multimodal assessment: open and closed eye states

Our analyses indicate that while eye-state significantly modulates functional connectivity patterns, fundamental signatures of pain processing maintain consistency across both EO and EC conditions. This consistency manifests in both intra-subject responses to stimulation and inter-subject chronic pain conditions, affirming the robustness of GNIs as biomarkers of pain-related brain reorganisation. Furthermore, the stability of CBP-specific network abnormalities across EO and EC confirms their status as trait-like markers rather than state-dependent fluctuations.

Intra-subject responses: Both EO and EC conditions exhibited increased functional segregation and small-worldness following sensory stimulation, though distinct reconfiguration patterns emerged. EO conditions demonstrated a transition from Salience/Ventral Attention network-driven integration to Somato-Motor-Visual dual-hub segregation, indicating enhanced specialised sensory processing (Costumero et al., 2020; J. Han et al., 2023; Lou et al., 2024). Conversely, EC conditions shifted from broad multi-network integration to focused Salience/Ventral Attention network dominance, suggesting consolidation toward internally-directed processing (Agcaoglu et al., 2019; Costumero et al., 2020; J. Han et al., 2023).

Inter-Subject Responses: In chronic pain populations, both EO and EC conditions revealed consistent maladaptive reorganisation characterised by increased integration, and diminished small-worldness and modularity. This profile is exclusive to CBP; CP_O patients show no such global changes, preserving network architecture near HC levels. This persistent profile indicates a fundamental shift toward less optimised brain architecture, aligning with

thalamocortical dysrhythmia models (Hughes & Crunelli, 2005; Llinás et al., 2005; Suffczynski et al., 2001; Tu et al., 2020). EO conditions proved more reliable for characterising specific network communication mechanisms, while EC conditions revealed state-specific dysfunctions in Default network regulation.

Classification Performance: For intra-subject classification, combining both eye states yielded superior discriminative power, with peak performance (AUC-ROC = 0.88, 81% accuracy) achieved through integrated EO-EC features under absolute comparison. Enhanced performance with added intra-network features confirms that both global and network-specific connectivity contribute to accurate brain state discrimination. For inter-subject classification in chronic pain, optimal performance (AUC-ROC = 0.91, 80% accuracy) was achieved either by combining GNIs from both EO and EC conditions (absolute comparison) or by integrating both comparison methods for EC conditions alone.

These findings support a strategic methodological approach of EO conditions appear optimal for mechanistic investigations of network interactions, while combined EO-EC protocols enhance diagnostic classification. Multimodal EO+EC data collection is particularly critical for reliable chronic pain subtyping, as it strengthens the reproducibility of subtype-specific network signatures. The consistent GNI patterns across eye states validate their utility as stable biomarkers, with absolute comparisons demonstrating particular strength for translational applications. Future research should leverage multimodal eye-state protocols to maximise both mechanistic understanding and diagnostic precision in pain conditions.

6.4. Limitations and future directions

Before presenting the specific limitations and future research avenues, it is important to acknowledge that the current study, while offering novel insights into pain-related network reorganisation, is not without methodological and analytical constraints. These limitations do not undermine the principal findings but instead highlight areas where further refinement, validation, and methodological expansion are required. By outlining these considerations, we aim to provide a balanced interpretation of our results and to clarify the conceptual and practical foundations for subsequent research in this field.

6.4.1. Limitations of EEG source-level results and multi-modal validation

A key limitation of the present study concerns EEG-derived source-level analyses, which are constrained by the inherently low spatial resolution of the EEG modality. EEG signals undergo volume conduction (Schoffelen & Gross, 2009) and spatial smearing (Dominguez et al., 2007) across the scalp, resulting in uncertainty in source localisation and reduced precision when mapping functional connectivity to discrete cortical and subcortical regions. This spatial blurring compromises the interpretability of source-level network nodes and edges, as neighbouring neural sources may be conflated or mislocalised, thereby weakening the anatomical specificity of the observed network effects, where it is often referred to as signal leakage (Lai et al., 2018).

To mitigate this limitation and strengthen the anatomical validity of EEG-based network biomarkers, future research should undertake direct cross-modal comparisons between EEG source-level findings and fMRI functional

connectivity data within the same cohort of pain patients. fMRI provides high spatial resolution and precise localisation of deep brain structures, enabling validation, refinement and anatomical anchoring of EEG source-level network results (Nguyen et al., 2016). Moreover, simultaneous EEG-fMRI acquisition permits complementary analysis of temporal dynamics (captured by EEG) and spatial precision (afforded by fMRI), allowing a more comprehensive characterisation of pain-associated network dysfunction and validating the generalisability of EEG-derived network biomarkers across imaging modalities (Warbrick, 2022).

6.4.2. Specificity of alpha oscillations

A further notable limitation lies in the limited specificity of alpha oscillations as a pain-selective biomarker, given that alpha-band activity is modulated by a wide range of cognitive, attentional and sensory processes unrelated to pain. Alpha oscillations are suppressed by sustained attention (Klimesch, 2012), visual engagement (Peylo et al., 2021), working memory (Wianda & Ross, 2019) and motor preparation (Deiber et al., 2012), whilst being enhanced during relaxed wakefulness (Kalauzi et al., 2012), mind wandering (Compton et al., 2019) and sensory suppression (Foxe & Snyder, 2011). Such non-specificity implies that the alpha-band network alterations observed here may partly reflect general cognitive or attentional differences between groups, rather than arising exclusively from pain-related neural processing (Sadaghiani & Kleinschmidt, 2016). Although the study adopted resting-state recordings to minimise task-related confounding factors, residual fluctuations in arousal, attentional allocation and internal cognitive processing may still drive alpha-band variability,

hindering definitive attribution of observed effects to pain pathophysiology (Apkarian et al., 2011; Bak et al., 2021; Baliki & Apkarian, 2015).

Future work should improve the specificity of alpha-band pain biomarkers by integrating alpha-band analyses with other spectral markers (e.g., theta, beta, gamma), which are also implicated in nociceptive processing (J. A. Kim & Davis, 2021). By integrating these multiple frequency bands into a unified analytical framework, the diagnostic specificity of the resulting biomarker panel can be further enhanced. Beyond boosting specificity, this multi-band approach also serves a critical purpose: it helps mitigate confounding influences driven by non-pain-related cognitive variability, which has previously complicated the interpretation of alpha-band findings in pain research.

6.4.3. Statistical limitations in functional connectivity

The primary limitation of this research concerns the statistical robustness of our connectivity findings. Our inference on the connectivity patterns is primarily drawn from thresholded graphs (t-graphs), with only a limited number of significant probability-based graphs (p-graphs). This scarcity of statistically significant connectivity graphs following multiple comparisons correction constrains the strength of our network-level interpretations. This limitation is particularly relevant for subgroup analyses, where smaller sample sizes may reduce statistical power. Future studies should address this limitation through larger sample sizes and multi-dataset validation to enhance statistical power and improve the detection of reproducible network alterations across chronic pain subtypes.

6.4.4. Potential overfitting in classification model

Our feature selection approach warrants careful consideration regarding potential overfitting. While our theory-driven inclusion of all GNI features was designed to test their collective biomarker potential, the performance improvements observed with additional features may reflect overfitting rather than inherent predictive power. The current study did not implement formal feature selection techniques, which means that the enhanced classification performance with combined comparison methods or eye states could be artificially inflated. Crucially, the improved classification performance observed when merging data from EO and EC conditions to integrate complementary information may also arise from overfitting to the training dataset, rather than a genuine gain in biomarker generalisability.

Future work should incorporate rigorous feature selection methods such as Kullback-Leibler Divergence analysis to distinguish genuinely informative features from redundant ones. This is especially important for translating subtype-specific biomarkers into clinically feasible diagnostic tools.

6.4.5. External validation of pain biomarkers

While the current study shows strong classification performance for GNI-based biomarkers in the analysed sample, external validation in fully independent cohorts is essential to confirm clinical applicability and generalisability. All chronic pain findings derive from a single dataset; biomarker performance may decline in populations with differing demographics, pain comorbidities or medications. Without external replication, these biomarkers lack robustness for

routine clinical translation, as sensitivity and specificity may not extend beyond the original setting.

The current work identifies a consistent, core maladaptive network signature in chronic pain, while also uncovering clinically meaningful heterogeneity across chronic pain subtypes. Accordingly, external validation must examine two key points: first, whether the identified network profiles can be reliably mapped to distinct chronic pain subtypes; second, whether the core GNI signatures maintain stability across different pain subtypes and testing conditions.

Future research should prioritise prospective external validation across multiple independent research centres and diverse clinical environments (Bott et al., 2025). Participant recruitment should cover well-defined chronic pain subtypes, demographically matched healthy controls, and clinical control groups with other neurological or psychiatric disorders to ensure discriminant validity. Evaluating biomarker performance in large-scale, multicentre cohorts will help confirm the phenotypic stability of network signatures, refine optimal diagnostic cut-off thresholds, and establish normative reference ranges necessary for formal clinical implementation (Ahmad & Barkana, 2025; L. B. Zhang et al., 2024). Furthermore, longitudinal validation is essential to determine whether these biomarkers can dynamically track fluctuations in pain severity, predict individual treatment responsiveness, and monitor disease progression over time (Seminowicz et al., 2020). These steps are critical to translating resting-state EEG-derived global network metrics into clinically actionable tools that support objective stratification, targeted neuromodulation, and personalised management strategies for chronic pain.

6.4.6. Future directions

While our findings establish a foundational model of pain-related network dynamics, several important directions emerge for future investigation that directly address all aforementioned limitations and consolidate methodological, analytical, and clinical progress. Future studies should first develop comprehensive multi-modal analytical frameworks integrating simultaneous EEG-fMRI to resolve EEG source localisation uncertainty and signal leakage, moving beyond exclusive alpha-band focus to incorporate theta, beta, and gamma oscillations within a unified multi-band spectral model that reduces non-pain cognitive confounders and enhances biomarker specificity.

To address the statistical power limitation associated with the fibromyalgia subgroup is a top priority. Future research should recruit a larger and more representative cohort of fibromyalgia patients to rigorously examine whether the observed network signature is specific to CBP or whether distinct topological patterns emerge in fibromyalgia when analysed with an adequate sample size. This step will resolve current ambiguities regarding subtype-specific network profiles and improve the generalisability of findings across the full spectrum of chronic pain phenotypes.

To strengthen statistical robustness of functional connectivity results, future work must adopt larger sample sizes, multi-dataset replication, and improved multiple-comparison procedures, especially for chronic pain subgroup analyses. For classification modelling, rigorous feature selection methods should be implemented to eliminate overfitting, isolate predictive GNI features, and support clinical translation of subtype-specific biomarkers.

External and longitudinal validation stands as a central priority: future research must conduct prospective, multi-centre validation across independent cohorts, diverse clinical settings, and clinical control groups to verify the generalisability, discriminant validity, and phenotypic stability of GNI network signatures; longitudinal designs will clarify whether these biomarkers track pain severity, predict treatment response, and monitor disease progression, enabling clinically actionable stratification, targeted neuromodulation, and personalised chronic pain care.

Moreover, since we have already found that psychological traits modulate GNIs in distinct, clinically relevant ways in the tonic pain study, future studies will also need to systematically explore the corresponding pain-related psychological traits across well-defined chronic pain subtypes for a better understanding of inter-subject variability in pain processing. This is essential for building a more sensitive, specific, and generalisable biomarker to support personalised therapeutic interventions. Translational research will link subtype-specific network signatures to targeted neuromodulation and intervention strategies, bridging network neuroscience and clinical practice.

Translating these findings to clinical applications requires further validation, including large-scale, multi-centre studies accounting for real-world complexities (e.g., co-morbidities, medication effects, pain duration differences). Priority should go to prospective cohort studies validating GNI-based subtyping for predicting treatment outcomes, alongside developing practical real-time pain assessment tools. Additionally, integrating network-based biomarkers with emerging interventions, exploring how identified subtype-specific signatures

guide neuromodulation or predict treatment responsiveness, will be key to delivering biologically informed, individualised pain therapies.

6.5. Conclusion and research contributions

This research programme offers compelling evidence for robust and recurrent network-level signatures across pain states, characterised by distinct patterns of functional segregation and integration. Our findings demonstrate that experimental tonic pain leads to decreased segregation and increased integration, while sensory stimulation elicits a reconfiguration towards greater segregation and enhanced small-worldness during subsequent rest. Most notably, chronic back pain patients exhibit a unique maladaptive signature of increased integration, and diminished small-worldness that remains evident across eye states.

Critically, we identified a fundamental progression in network organisation across pain conditions: from the adaptive reconfiguration following tonic stimulation to the subtype-specific maladaptive persistence observed in chronic pain. This progression provides a network-based framework for understanding pain chronification, with GNIs serving as potential biomarkers for monitoring this transition and stratifying distinct chronic pain subtypes. Caution is warranted in generalisation, as the limited number of fibromyalgia patients included means we cannot exclude divergent topological profiles emerging with a larger, more representative fibromyalgia cohort in future research.

This work demonstrates strong translational potential, as evidenced by outstanding classification performance across diverse pain conditions: our models achieved AUC-ROC = 0.94 for distinguishing tonic noxious from

innocuous stimulation, an AUC-ROC = 0.88 for differentiating pre- and post-stimulation states, and an AUC-ROC = 0.91 for classifying chronic pain patients versus healthy controls. This robust performance across multiple pain paradigms validates the clinical potential of network-based biomarkers.

Our methodological advances in comparison strategies and eye-state protocols provide a solid foundation for future pain neuroscience research, while the consistent GNI patterns observed across both experimental and clinical pain conditions establish a foundation for developing objective diagnostic tools and personalised therapeutic interventions. Crucially, these maladaptive network signatures are uniquely specific to CBP, underscoring the biological uniqueness of CBP-related neuroplasticity and the necessity of subgroup stratification in clinical research.

The novel contribution of this thesis is the identification of a fundamental, progressive reconfiguration in brain network organisation, from adaptive changes following tonic stimulation to subtype-specific maladaptive persistence in chronic pain, thereby establishing a network-based framework for understanding pain chronification and clinical heterogeneity. This framework is supported by validated EEG-derived alpha-band global network biomarkers with strong translational potential for stratified, objective diagnosis, personalised treatment and targeted neuromodulation.

Bibliography

1. Achard, S., & Bullmore, E. (2007). Efficiency and cost of economical brain functional networks. *PLoS Computational Biology*, *3*(2), e17.
2. Adamovich, T., Zakharov, I., Tabueva, A., & Malykh, S. (2022). The thresholding problem and variability in the EEG graph network parameters. *Scientific Reports*, *12*(1). https://doi.org/10.1038/s41598-022-22079-2
3. Agcaoglu, O., Wilson, T. W., Wang, Y., Stephen, J., & Calhoun, V. D. (2019). Resting state connectivity differences in eyes open versus eyes closed conditions. *Human Brain Mapping*, *40*(8), 2488–2498. https://doi.org/10.1002/hbm.24539
4. Ahmad, B., & Barkana, B. D. (2025). Pain and the Brain: A Systematic Review of Methods, EEG Biomarkers, Limitations, and Future Directions. *Neurology International*, *17*(4), 46. https://doi.org/10.3390/neurolint17040046
5. Ahn, S., Prim, J. H., Alexander, M. L., McCulloch, K. L., & Fröhlich, F. (2019). Identifying and Engaging Neuronal Oscillations by Transcranial Alternating Current Stimulation in Patients With Chronic Low Back Pain: A Randomized, Crossover, Double-Blind, Sham-Controlled Pilot Study. *The Journal of Pain*, *20*(3), 277.e1-277.e11. https://doi.org/10.1016/j.jpain.2018.09.004
6. Alain, C., Arnott, S. R., Hevenor, S., Graham, S., & Grady, C. L. (2001). “What” and “where” in the human auditory system. *Proceedings of the National Academy of Sciences*, *98*(21), 12301–12306.

7. Alhajri, N., Boudreau, S. A., & Graven-Nielsen, T. (2022). Angular gyrus connectivity at alpha and beta oscillations is reduced during tonic pain—Differential effect of eye state. *Neuroimage Clin*, *33*, 102907. https://doi.org/10.1016/j.nicl.2021.102907
8. Alhajri, N., Boudreau, S. A., & Graven-Nielsen, T. (2023). Decreased Default Mode Network Connectivity Following 24 Hours of Capsaicin-induced Pain Persists During Immediate Pain Relief and Facilitation. *The Journal of Pain*, *24*(5), 796–811. https://doi.org/10.1016/j.jpain.2022.12.004
9. Alhajri, N., Boudreau, S. A., Mouraux, A., & Graven-Nielsen, T. (2023). Pain-free default mode network connectivity contributes to tonic experimental pain intensity beyond the role of negative mood and other pain-related factors. *Eur J Pain*, *27*(8), 995–1005. https://doi.org/10.1002/ejp.2141
10. Alshelh, Z., Marciszewski, K. K., Akhter, R., Di Pietro, F., Mills, E. P., Vickers, E. R., Peck, C. C., Murray, G. M., & Henderson, L. A. (2018). Disruption of default mode network dynamics in acute and chronic pain states. *NeuroImage: Clinical*, *17*, 222–231. https://doi.org/10.1016/j.nicl.2017.10.019
11. Apkarian, A. V., Bushnell, M. C., Treede, R., & Zubieta, J. (2005). Human brain mechanisms of pain perception and regulation in health and disease. *European Journal of Pain*, *9*(4), 463–463. https://doi.org/10.1016/j.ejpain.2004.11.001
12. Apkarian, A. V., Hashmi, J. A., & Baliki, M. N. (2011). Pain and the brain: Specificity and plasticity of the brain in clinical chronic pain. *PAIN,*

Biennial Review of Pain, *152*(3, Supplement), S49–S64. https://doi.org/10.1016/j.pain.2010.11.010

13. Arami, M., & Komaki, A. (2022). Reciprocal Interaction of Pain and Brain: Plasticity-induced Pain, Pain-induced Plasticity, and Therapeutic Targets. *CNS & Neurological Disorders - Drug Targets*, *22*. https://doi.org/10.2174/1871527322666221102141002
14. Avena-Koenigsberger, A., Misic, B., & Sporns, O. (2018). Communication dynamics in complex brain networks. *Nature Reviews Neuroscience*, *19*(1), 17–33. https://doi.org/10.1038/nrn.2017.149
15. Bak, M. S., Park, H., & Kim, S. K. (2021). Neural Plasticity in the Brain during Neuropathic Pain. *Biomedicines*, *9*(6), 624. https://doi.org/10.3390/biomedicines9060624
16. Baliki, M. N., & Apkarian, A. V. (2015). Nociception, Pain, Negative Moods, and Behavior Selection. *Neuron*, *87*(3), 474–491. https://doi.org/10.1016/j.neuron.2015.06.005
17. Baliki, M. N., Baria, A. T., & Apkarian, A. V. (2011). The Cortical Rhythms of Chronic Back Pain. *The Journal of Neuroscience*, *31*(39), 13981–13990. https://doi.org/10.1523/JNEUROSCI.1984-11.2011
18. Baliki, M. N., Geha, P. Y., Apkarian, A. V., & Chialvo, D. R. (2008). Beyond Feeling: Chronic Pain Hurts the Brain, Disrupting the Default-Mode Network Dynamics. *The Journal of Neuroscience*, *28*(6), 1398–1403. https://doi.org/10.1523/jneurosci.4123-07.2008
19. Baliki, M. N., Mansour, A. R., Baria, A. T., & Apkarian, A. V. (2014). Functional Reorganization of the Default Mode Network across Chronic

Pain Conditions. *PLoS ONE*, *9*(9), e106133. https://doi.org/10.1371/journal.pone.0106133

20. Barabási, D. L., Bianconi, G., Bullmore, E., Burgess, M., Chung, S., Eliassi-Rad, T., George, D., Kovács, I. A., Makse, H., Nichols, T. E., Papadimitriou, C., Sporns, O., Stachenfeld, K., Toroczkai, Z., Towlson, E. K., Zador, A. M., Zeng, H., Barabási, A.-L., Bernard, A., & Buzsáki, G. (2023). Neuroscience Needs Network Science. *The Journal of Neuroscience*, *43*(34), 5989–5995. https://doi.org/10.1523/jneurosci.1014-23.2023
21. Bastos, A. M., Usrey, W. M., Adams, R. A., Mangun, G. R., Fries, P., & Friston, K. J. (2012). Canonical Microcircuits for Predictive Coding. *Neuron*, *76*(4), 695–711. https://doi.org/10.1016/j.neuron.2012.10.038
22. Bhargava, A. (1986). On the Theory of Testing for Unit Roots in Observed Time Series. *The Review of Economic Studies*, *53*(3), 369–384. https://doi.org/10.2307/2297634
23. Bott, F. S., Zebhauser, P. T., Hohn, V. D., Turgut, Ö., May, E. S., Tiemann, L., Gil Ávila, C., Heitmann, H., Nickel, M. M., Day, M. A., Adhia, D. B., Ashar, Y. K., Wager, T. D., Granovsky, Y., Yarnitsky, D., Jensen, M. P., Gross, J., & Ploner, M. (2025). Exploring electroencephalographic chronic pain biomarkers: A mega-analysis. *eBioMedicine*, *120*, 105955. https://doi.org/10.1016/j.ebiom.2025.105955
24. Brandes, U. (2001). A faster algorithm for betweenness centrality*. *The Journal of Mathematical Sociology*, *25*(2), 163–177. https://doi.org/10.1080/0022250x.2001.9990249

25. Brockwell, P. J., & Davis, R. A. (Eds). (2002). Stationary Processes. In *Introduction to Time Series and Forecasting* (pp. 45–82). Springer. https://doi.org/10.1007/0-387-21657-X_2

26. Bullmore, E., & Sporns, O. (2009). Complex brain networks: Graph theoretical analysis of structural and functional systems. *Nature Reviews Neuroscience*, *10*(3), 186–198. https://doi.org/10.1038/nrn2575

27. Butry, L., Thomä, J., Elsenbruch, S., Icenhour, A., Rehmann, R., Enax-Krumova, E., & Schlaffke, L. (2025). Brain network properties in chronic pain—A systematic review and meta-analysis of graph-based connectivity metrics. *Frontiers in Neuroscience*, *19*. https://doi.org/10.3389/fnins.2025.1672542

28. Buzsáki, G. (2006). *Rhythms of the Brain*. Oxford University Press. https://doi.org/10.1093/acprof:oso/9780195301069.001.0001

29. Cao, F.-L., Xu, M., Gong, K., Wang, Y., Wang, R., Chen, X., & Chen, J. (2019). Imbalance Between Excitatory and Inhibitory Synaptic Transmission in the Primary Somatosensory Cortex Caused by Persistent Nociception in Rats. *The Journal of Pain*, *20*(8), 917–931. https://doi.org/10.1016/j.jpain.2018.11.014

30. Case, M., Shirinpour, S., Vijayakumar, V., Zhang, H., Datta, Y., Nelson, S., Pergami, P., Darbari, D. S., Gupta, K., & He, B. (2019). Graph theory analysis reveals how sickle cell disease impacts neural networks of patients with more severe disease. *NeuroImage: Clinical*, *21*, 101599. https://doi.org/10.1016/j.nicl.2018.11.009

31. Cavaleri, R., McLain, N. J., Heindel, M., Schrepf, A., Rodriguez, L. V., & Kutch, J. J. (2025). Peak alpha frequency is related to the degree of

widespread pain, but not pain intensity or duration, among people with urologic chronic pelvic pain syndrome. *PAIN Reports*, *10*(2), e1251. https://doi.org/10.1097/PR9.0000000000001251

32. Chen, Z. S. (2021). Decoding pain from brain activity. *Journal of Neural Engineering*, *18*(5), 051002. https://doi.org/10.1088/1741-2552/ac28d4
33. Cohen, M. X. (2014). *Analyzing neural time series data: Theory and practice*. MIT press.
34. Cohen, S. P., Vase, L., & Hooten, W. M. (2021). Chronic pain: An update on burden, best practices, and new advances. *The Lancet*, *397*(10289), 2082–2097. https://doi.org/10.1016/S0140-6736(21)00393-7
35. Compton, R. J., Gearinger, D., & Wild, H. (2019). The wandering mind oscillates: EEG alpha power is enhanced during moments of mind-wandering. *Cognitive, Affective, & Behavioral Neuroscience*, *19*(5), 1184–1191. https://doi.org/10.3758/s13415-019-00745-9
36. Corbetta, M., & Shulman, G. L. (2002). Control of goal-directed and stimulus-driven attention in the brain. *Nature Reviews Neuroscience*, *3*(3), 201–215. https://doi.org/10.1038/nrn755
37. Costumero, V., Bueichekú, E., Adrián-Ventura, J., & Ávila, C. (2020). Opening or closing eyes at rest modulates the functional connectivity of V1 with default and salience networks. *Scientific Reports*, *10*(1), 9137. https://doi.org/10.1038/s41598-020-66100-y
38. Davis, K. D., Aghaeepour, N., Ahn, A. H., Angst, M. S., Borsook, D., Brenton, A., Burczynski, M. E., Crean, C., Edwards, R., Gaudilliere, B., Hergenroeder, G. W., Iadarola, M. J., Iyengar, S., Jiang, Y., Kong, J.-T., Mackey, S., Saab, C. Y., Sang, C. N., Scholz, J., … Pelleymounter, M.

A. (2020). Discovery and validation of biomarkers to aid the development of safe and effective pain therapeutics: Challenges and opportunities. *Nature Reviews Neurology*, *16*(7), 381–400. https://doi.org/10.1038/s41582-020-0362-2

39. Deiber, M.-P., Sallard, E., Ludwig, C., Ghezzi, C., Barral, J., & Ibanez, V. (2012). EEG alpha activity reflects motor preparation rather than the mode of action selection. *Frontiers in Integrative Neuroscience*, *6*. https://doi.org/10.3389/fnint.2012.00059
40. Delorme, A., & Makeig, S. (2004). EEGLAB: an open source toolbox for analysis of single-trial EEG dynamics including independent component analysis. *Journal of Neuroscience Methods*, *134*(1), 9–21.
41. Dominguez, L. G., Wennberg, R., Velazquez, J. L., & Guevara Erra, R. (2007). Enhanced measured synchronization of unsynchronized sources: Inspecting the physiological significance of synchronization analysis of whole brain electrophysiological recordings. *International Journal of Physical Sciences*, *2*, 305–317.
42. Dowman, R., Rissacher, D., & Schuckers, S. (2008). EEG indices of tonic pain-related activity in the somatosensory cortices. *Clin Neurophysiol*, *119*(5), 1201–1212. https://doi.org/10.1016/j.clinph.2008.01.019
43. Eldabe, S., Obara, I., Panwar, C., & Caraway, D. (2022). Biomarkers for Chronic Pain: Significance and Summary of Recent Advances. *Pain Research and Management*, *2022*, 1–6. https://doi.org/10.1155/2022/1940906

44. Farmer, M. A., Baliki, M. N., & Apkarian, A. V. (2012). A dynamic network perspective of chronic pain. *Neuroscience Letters*, *520*(2), 197–203.
45. Feng, L., Li, H., Cui, H., Xie, X., Xu, S., & Hu, Y. (2021). Low Back Pain Assessment Based on Alpha Oscillation Changes in Spontaneous Electroencephalogram (EEG). *Neural Plasticity*, *2021*, 1–11. https://doi.org/10.1155/2021/8537437
46. Fonov, V. S., Evans, A. C., McKinstry, R. C., Almli, C. R., & Collins, D. L. (2009). Unbiased nonlinear average age-appropriate brain templates from birth to adulthood. *NeuroImage*, *47*, S102.
47. Foxe, J. J., & Snyder, A. C. (2011). The Role of Alpha-Band Brain Oscillations as a Sensory Suppression Mechanism during Selective Attention. *Frontiers in Psychology*, *2*. https://doi.org/10.3389/fpsyg.2011.00154
48. Fries, P. (2005). A mechanism for cognitive dynamics: Neuronal communication through neuronal coherence. *Trends in Cognitive Sciences*, *9*(10), 474–480. https://doi.org/10.1016/j.tics.2005.08.011
49. Fries, P. (2015). Rhythms for Cognition: Communication through Coherence. *Neuron*, *88*(1), 220–235. https://doi.org/10.1016/j.neuron.2015.09.034
50. Furman, A. J., Meeker, T. J., Rietschel, J. C., Yoo, S., Muthulingam, J., Prokhorenko, M., Keaser, M. L., Goodman, R. N., Mazaheri, A., & Seminowicz, D. A. (2018). Cerebral peak alpha frequency predicts individual differences in pain sensitivity. *NeuroImage*, *167*, 203–210. https://doi.org/10.1016/j.neuroimage.2017.11.042
51. Furman, A. J., Prokhorenko, M., Keaser, M. L., Zhang, J., Chen, S., Mazaheri, A., & Seminowicz, D. A. (2020). Sensorimotor Peak Alpha

Frequency Is a Reliable Biomarker of Prolonged Pain Sensitivity. *Cerebral Cortex*, *30*(12), 6069–6082. https://doi.org/10.1093/cercor/bhaa124

52. Gagniuc, P. A. (2017). *Markov Chains: From Theory to Implementation and Experimentation*. John Wiley & Sons.
53. Gil Ávila, C., Bott, F. S., Tiemann, L., Hohn, V. D., May, E. S., Nickel, M. M., Zebhauser, P. T., Gross, J., & Ploner, M. (2023). DISCOVER-EEG: an open, fully automated EEG pipeline for biomarker discovery in clinical neuroscience. *Scientific Data*, *10*(1), 613.
54. Goldman, D. (1950). The clinical use of the “average” reference electrode in monopolar recording. *Electroencephalography and Clinical Neurophysiology*, *2*(1–4), 209–212.
55. Goulden, N., Khusnulina, A., Davis, N. J., Bracewell, R. M., Bokde, A. L., McNulty, J. P., & Mullins, P. G. (2014). The salience network is responsible for switching between the default mode network and the central executive network: Replication from DCM. *NeuroImage*, *99*, 180–190. https://doi.org/10.1016/j.neuroimage.2014.05.052
56. Granot, M., Weissman-Fogel, I., Crispel, Y., Pud, D., Granovsky, Y., Sprecher, E., & Yarnitsky, D. (2008). Determinants of endogenous analgesia magnitude in a diffuse noxious inhibitory control (DNIC) paradigm: Do conditioning stimulus painfulness, gender and personality variables matter? *PAIN®*, *136*(1–2), 142–149.
57. Gusnard, D. A., & Raichle, M. E. (2001). Searching for a baseline: Functional imaging and the resting human brain. *Nature Reviews Neuroscience*, *2*(10), 685–694. https://doi.org/10.1038/35094500

58. Han, J., Zhou, L., Wu, H., Huang, Y., Qiu, M., Huang, L., Lee, C., Lane, T. J., & Qin, P. (2023). Eyes-Open and Eyes-Closed Resting State Network Connectivity Differences. *Brain Sciences*, *13*(1), 122. https://doi.org/10.3390/brainsci13010122

59. Han, Q., Wang, H., Lu, X., Li, Y., Guo, Y., Zhao, X., Feng, Y., & Hu, L. (2025). Preoperative resting-state electrophysiological signals predict acute but not chronic postoperative pain. *European Journal of Pain*, *29*(1), e4757. https://doi.org/10.1002/ejp.4757

60. Hashmi, J. A., Baliki, M. N., Huang, L., Baria, A. T., Torbey, S., Hermann, K. M., Schnitzer, T. J., & Apkarian, A. V. (2013). Shape shifting pain: Chronification of back pain shifts brain representation from nociceptive to emotional circuits. *Brain*, *136*(9), 2751–2768. https://doi.org/10.1093/brain/awt211

61. Heitmann, H., Gil Ávila, C., Nickel, M. M., Ta Dinh, S., May, E. S., Tiemann, L., Hohn, V. D., Tölle, T. R., & Ploner, M. (2022). Longitudinal resting-state electroencephalography in patients with chronic pain undergoing interdisciplinary multimodal pain therapy. *Pain*, *163*(9), e997–e1005. https://doi.org/10.1097/j.pain.0000000000002565

62. Hemington, K. S., Wu, Q., Kucyi, A., Inman, R. D., & Davis, K. D. (2016). Abnormal cross-network functional connectivity in chronic pain and its association with clinical symptoms. *Brain Struct Funct*, *221*(8), 4203–4219. https://doi.org/10.1007/s00429-015-1161-1

63. Hu, L., & Iannetti, G. D. (2016). Painful Issues in Pain Prediction. *Trends in Neurosciences*, *39*(4), 212–220. https://doi.org/10.1016/j.tins.2016.01.004

64. Huang, S., Wakaizumi, K., Wu, B., Shen, B., Wu, B., Fan, L., Baliki, M. N., Zhan, G., Apkarian, A. V., & Huang, L. (2019). Whole-brain functional network disruption in chronic pain with disk herniation. *Pain*, *160*(12), 2829–2840.

65. Hughes, S. W., & Crunelli, V. (2005). Thalamic Mechanisms of EEG Alpha Rhythms and Their Pathological Implications. *The Neuroscientist*, *11*(4), 357–372. https://doi.org/10.1177/1073858405277450

66. Iannetti, G. D., Hughes, N. P., Lee, M. C., & Mouraux, A. (2008). Determinants of Laser-Evoked EEG Responses: Pain Perception or Stimulus Saliency? *Journal of Neurophysiology*. (world). https://doi.org/10.1152/jn.00097.2008

67. Iannetti, G. D., & Mouraux, A. (2010). From the neuromatrix to the pain matrix (and back). *Experimental Brain Research*, *205*(1), 1–12. https://doi.org/10.1007/s00221-010-2340-1

68. Jackman, J. S., Bell, P. G., Van Someren, K., Gondek, M. B., Hills, F. A., Wilson, L. J., & Cockburn, E. (2023). Effect of hot water immersion on acute physiological responses following resistance exercise. *Frontiers in Physiology*, *14*. https://doi.org/10.3389/fphys.2023.1213733

69. Jao, T., Vértes, P. E., Alexander-Bloch, A. F., Tang, I.-N., Yu, Y.-C., Chen, J.-H., & Bullmore, E. T. (2013). Volitional eyes opening perturbs brain dynamics and functional connectivity regardless of light input. *NeuroImage*, *69*, 21–34. https://doi.org/10.1016/j.neuroimage.2012.12.007

70. Jensen, O., & Mazaheri, A. (2010). Shaping functional architecture by oscillatory alpha activity: Gating by inhibition. *Frontiers in Human Neuroscience*, *4*, 186.

71. Jiang, Y., Oathes, D., Hush, J., Darnall, B., Charvat, M., Mackey, S., & Etkin, A. (2016). Perturbed connectivity of the amygdala and its subregions with the central executive and default mode networks in chronic pain. *PAIN*, *157*(9), 1970. https://doi.org/10.1097/j.pain.0000000000000606

72. Johansson, E., Xiong, H.-Y., Polli, A., Coppieters, I., & Nijs, J. (2024). Towards a Real-Life Understanding of the Altered Functional Behaviour of the Default Mode and Salience Network in Chronic Pain: Are People with Chronic Pain Overthinking the Meaning of Their Pain? *Journal of Clinical Medicine*, *13*(6), 1645. https://doi.org/10.3390/jcm13061645

73. Kalauzi, A., Vuckovic, A., & Bojić, T. (2012). EEG alpha phase shifts during transition from wakefulness to drowsiness. *International Journal of Psychophysiology*, *86*(3), 195–205. https://doi.org/10.1016/j.ijpsycho.2012.04.012

74. Kaplan, A. Ya., Fingelkurts, A. A., Fingelkurts, A. A., Borisov, S. V., & Darkhovsky, B. S. (2005). Nonstationary nature of the brain activity as revealed by EEG/MEG: Methodological, practical and conceptual challenges. *Signal Processing*, *85*(11), 2190–2212. https://doi.org/10.1016/j.sigpro.2005.07.010

75. Kastrati, G., Thompson, W. H., Schiffler, B., Fransson, P., & Jensen, K. B. (2022). Brain network segregation and integration during painful thermal stimulation. *Cerebral Cortex*, *32*(18), 4039–4049. https://doi.org/10.1093/cercor/bhab464

76. Keitel, A., Keitel, C., Alavash, M., Bakardjian, K., Benwell, C. S. Y., Bouton, S., Busch, N. A., Criscuolo, A., Doelling, K. B., Dugue, L., Grabot,

L., Gross, J., Hanslmayr, S., Klatt, L.-I., Kluger, D. S., Learmonth, G., London, R. E., Lubinus, C., Martin, A. E., … Kotz, S. A. (2025). *Brain rhythms in cognition—Controversies and future directions* (arXiv:2507.15639). arXiv. https://doi.org/10.48550/arXiv.2507.15639

77. Kim, H., Mawla, I., Lee, J., Gerber, J., Walker, K., Kim, J., Ortiz, A., Chan, S.-T., Loggia, M. L., & Wasan, A. D. (2020). Reduced tactile acuity in chronic low back pain is linked with structural neuroplasticity in primary somatosensory cortex and is modulated by acupuncture therapy. *NeuroImage*, *217*, 116899.
78. Kim, J. A., & Davis, K. D. (2021). Neural Oscillations: Understanding a Neural Code of Pain. *The Neuroscientist*, *27*(5), 544–570. https://doi.org/10.1177/1073858420958629
79. Kim, J., Loggia, M. L., Cahalan, C. M., Harris, R. E., Beissner, F., Garcia, R. G., Kim, H., Barbieri, R., Wasan, A. D., & Edwards, R. R. (2015). The somatosensory link in fibromyalgia: Functional connectivity of the primary somatosensory cortex is altered by sustained pain and is associated with clinical/autonomic dysfunction. *Arthritis & Rheumatology*, *67*(5), 1395–1405.
80. Kim, J., Loggia, M. L., Edwards, R. R., Wasan, A. D., Gollub, R. L., & Napadow, V. (2013). Sustained deep-tissue pain alters functional brain connectivity. *Pain*, *154*(8), 1343–1351. https://doi.org/10.1016/j.pain.2013.04.016
81. Kim, J., Mawla, I., Kong, J., Lee, J., Gerber, J., Ortiz, A., Kim, H., Chan, S.-T., Loggia, M. L., Wasan, A. D., Edwards, R. R., Gollub, R. L., Rosen, B. R., & Napadow, V. (2019). Somatotopically specific primary

somatosensory connectivity to salience and default mode networks encodes clinical pain. *Pain*, *160*(7), 1594–1605. https://doi.org/10.1097/j.pain.0000000000001541

82. Kim, W., Kim, S. K., & Nabekura, J. (2017). Functional and structural plasticity in the primary somatosensory cortex associated with chronic pain. *Journal of Neurochemistry*, *141*(4), 499–506. https://doi.org/10.1111/jnc.14012
83. Kisler, L. B., Kim, J. A., Hemington, K. S., Rogachov, A., Cheng, J. C., Bosma, R. L., Osborne, N. R., Dunkley, B. T., Inman, R. D., & Davis, K. D. (2020). Abnormal alpha band power in the dynamic pain connectome is a marker of chronic pain with a neuropathic component. *NeuroImage: Clinical*, *26*, 102241. https://doi.org/10.1016/j.nicl.2020.102241
84. Kitzbichler, M. G., Henson, R. N. A., Smith, M. L., Nathan, P. J., & Bullmore, E. T. (2011). Cognitive Effort Drives Workspace Configuration of Human Brain Functional Networks. *The Journal of Neuroscience*, *31*(22), 8259–8270. https://doi.org/10.1523/JNEUROSCI.0440-11.2011
85. Klimesch, W. (2012). Alpha-band oscillations, attention, and controlled access to stored information. *Trends in Cognitive Sciences*, *16*(12), 606–617. https://doi.org/10.1016/j.tics.2012.10.007
86. Koessler, L., Maillard, L., Benhadid, A., Vignal, J. P., Felblinger, J., Vespignani, H., & Braun, M. (2009). Automated cortical projection of EEG sensors: Anatomical correlation via the international 10–10 system. *NeuroImage*, *46*(1), 64–72.
87. Kong, J., Jensen, K., Loiotile, R., Cheetham, A., Wey, H. Y., Tan, Y., Rosen, B., Smoller, J. W., Kaptchuk, T. J., & Gollub, R. L. (2013).

Functional connectivity of the frontoparietal network predicts cognitive modulation of pain. *Pain*, *154*(3), 459–467. https://doi.org/10.1016/j.pain.2012.12.004

88. Krukow, P., Rodríguez-González, V., Kopiś-Posiej, N., Gómez, C., & Poza, J. (2024). Tracking EEG network dynamics through transitions between eyes-closed, eyes-open, and task states. *Scientific Reports*, *14*(1), 17442. https://doi.org/10.1038/s41598-024-68532-2
89. Kucyi, A., & Davis, K. D. (2015). The dynamic pain connectome. *Trends in Neurosciences*, *38*(2), 86–95.
90. Kucyi, A., & Davis, K. D. (2017). The Neural Code for Pain: From Single-Cell Electrophysiology to the Dynamic Pain Connectome. *The Neuroscientist*, *23*(4), 397–414. https://doi.org/10.1177/1073858416667716
91. Kucyi, A., Moayedi, M., Weissman-Fogel, I., Goldberg, M. B., Freeman, B. V., Tenenbaum, H. C., & Davis, K. D. (2014). Enhanced medial prefrontal-default mode network functional connectivity in chronic pain and its association with pain rumination. *The Journal of Neuroscience: The Official Journal of the Society for Neuroscience*, *34*(11), 3969–3975. https://doi.org/10.1523/JNEUROSCI.5055-13.2014
92. Kuner, R., & Flor, H. (2017). Structural plasticity and reorganisation in chronic pain. *Nature Reviews Neuroscience*, *18*(1), 20–30. https://doi.org/10.1038/nrn.2016.162
93. Kutch, J. J., Labus, J. S., Harris, R. E., Martucci, K. T., Farmer, M. A., Fenske, S., Fling, C., Ichesco, E., Peltier, S., Petre, B., Guo, W., Hou, X., Stephens, A. J., Mullins, C., Clauw, D. J., Mackey, S. C., Apkarian, A. V., Landis, J. R., Mayer, E. A., & Network, for the M. R. (2017).

Resting-state functional connectivity predicts longitudinal pain symptom change in urologic chronic pelvic pain syndrome: A MAPP network study. *PAIN*, *158*(6), 1069. https://doi.org/10.1097/j.pain.0000000000000886

94. Lai, M., Demuru, M., Hillebrand, A., & Fraschini, M. (2018). A comparison between scalp- and source-reconstructed EEG networks. *Scientific Reports*, *8*(1), 12269. https://doi.org/10.1038/s41598-018-30869-w
95. Latora, V., & Marchiori, M. (2001). Efficient behavior of small-world networks. *Physical Review Letters*, *87*(19), 198701.
96. Lee, J.-J., Kim, H. J., Čeko, M., Park, B., Lee, S. A., Park, H., Roy, M., Kim, S.-G., Wager, T. D., & Woo, C.-W. (2021). A neuroimaging biomarker for sustained experimental and clinical pain. *Nature Medicine*, *27*(1), 174–182. https://doi.org/10.1038/s41591-020-1142-7
97. Lee, J.-J., Lee, S., Lee, D. H., & Woo, C.-W. (2022). Functional brain reconfiguration during sustained pain. *eLife*, *11*. https://doi.org/10.7554/elife.74463
98. Lenoir, D., Cagnie, B., Verhelst, H., & De Pauw, R. (2021). Graph Measure Based Connectivity in Chronic Pain Patients: A Systematic Review. *Pain Physician*, *24*(7), E1037–E1058.
99. Lenoir, D., Willaert, W., Coppieters, I., Malfliet, A., Ickmans, K., Nijs, J., Vonck, K., Meeus, M., & Cagnie, B. (2020). Electroencephalography During Nociceptive Stimulation in Chronic Pain Patients: A Systematic Review. *Pain Medicine*, *21*(12), 3413–3427. https://doi.org/10.1093/pm/pnaa131

100. Li, H., Li, X., Wang, J., Gao, F., Wiech, K., Hu, L., & Kong, Y. (2022). Pain-related reorganization in the primary somatosensory cortex of patients with postherpetic neuralgia. *Human Brain Mapping*, *43*(17), 5167–5179. https://doi.org/10.1002/hbm.25992

101. Li, L., Di, X., Zhang, H., Huang, G., Zhang, L., Liang, Z., & Zhang, Z. (2022). Characterization of whole-brain task-modulated functional connectivity in response to nociceptive pain: A multisensory comparison study. *Hum Brain Mapp*, *43*(3), 1061–1075. https://doi.org/10.1002/hbm.25707

102. Li, X., Jin, R., Lu, X., Zhan, Y., Jiang, N., & Peng, W. (2025). Alpha transcranial alternating current stimulation modulates pain anticipation and perception in a context-dependent manner. *Pain*, *166*(5), 1157–1166. https://doi.org/10.1097/j.pain.0000000000003452

103. Liao, X., Vasilakos, A. V., & He, Y. (2017). Small-world human brain networks: Perspectives and challenges. *Neuroscience & Biobehavioral Reviews*, *77*, 286–300. https://doi.org/10.1016/j.neubiorev.2017.03.018

104. Liu, J., Zhang, F., Liu, X., Zhuo, Z., Wei, J., Du, M., Chan, Q., Wang, X., & Wang, D. (2018). Altered small-world, functional brain networks in patients with lower back pain. *Science China Life Sciences*, *61*(11), 1420–1424. https://doi.org/10.1007/s11427-017-9108-6

105. Llinás, R., Urbano, F. J., Leznik, E., Ramírez, R. R., & Van Marle, H. J. F. (2005). Rhythmic and dysrhythmic thalamocortical dynamics: GABA systems and the edge effect. *Trends in Neurosciences*, *28*(6), 325–333. https://doi.org/10.1016/j.tins.2005.04.006

106. Lloyd, D. M., Wittkopf, P. G., Arendsen, L. J., & Jones, A. K. P. (2020). Is Transcranial Direct Current Stimulation (tDCS) Effective for the Treatment of Pain in Fibromyalgia? A Systematic Review and Meta-Analysis. *The Journal of Pain*, *21*(11–12), 1085–1100. https://doi.org/10.1016/j.jpain.2020.01.003

107. Lor, C. S., Zhang, M., Karner, A., Steyrl, D., Sladky, R., Scharnowski, F., & Haugg, A. (2023). Pre- and post-task resting-state differs in clinical populations. *NeuroImage : Clinical*, *37*, 103345. https://doi.org/10.1016/j.nicl.2023.103345

108. Lőrincz, M. L., Kékesi, K. A., Juhász, G., Crunelli, V., & Hughes, S. W. (2009). Temporal Framing of Thalamic Relay-Mode Firing by Phasic Inhibition during the Alpha Rhythm. *Neuron*, *63*(5), 683–696. https://doi.org/10.1016/j.neuron.2009.08.012

109. Lou, W., Li, X., Jin, R., & Peng, W. (2024). Time-varying phase synchronization of resting-state functional magnetic resonance imaging reveals a shift toward self-referential processes during sustained pain. *Pain*, *165*(7), 1493–1504. https://doi.org/10.1097/j.pain.0000000000003152

110. Makovac, E., Dipasquale, O., Jackson, J. B., Medina, S., O'Daly, O., O'Muircheartaigh, J., de Lara Rubio, A., Williams, S. C. R., McMahon, S. B., & Howard, M. A. (2020). Sustained perturbation in functional connectivity induced by cold pain. *European Journal of Pain*, *24*(9), 1850–1861. https://doi.org/10.1002/ejp.1633

111. Mano, H., Kotecha, G., Leibnitz, K., Matsubara, T., Sprenger, C., Nakae, A., Shenker, N., Shibata, M., Voon, V., Yoshida, W., Lee, M.,

Yanagida, T., Kawato, M., Rosa, M. J., & Seymour, B. (2018). Classification and characterisation of brain network changes in chronic back pain: A multicenter study. *Wellcome Open Research*, *3*, 19. https://doi.org/10.12688/wellcomeopenres.14069.2

112. Mano, H., & Seymour, B. (2015). Pain: A Distributed Brain Information Network? *PLoS Biology*, *13*(1), e1002037. https://doi.org/10.1371/journal.pbio.1002037

113. May, E. S., Butz, M., Kahlbrock, N., Hoogenboom, N., Brenner, M., & Schnitzler, A. (2012). Pre- and post-stimulus alpha activity shows differential modulation with spatial attention during the processing of pain. *NeuroImage*, *62*(3), 1965–1974. https://doi.org/10.1016/j.neuroimage.2012.05.071

114. McLain, N., Cavaleri, R., & Kutch, J. (2025). Peak alpha frequency differs between chronic back pain and chronic widespread pain. *European Journal of Pain*, *29*(3), e4737. https://doi.org/10.1002/ejp.4737

115. Modares-Haghighi, P., Boostani, R., Nami, M., & Sanei, S. (2021). Quantification of pain severity using EEG-based functional connectivity. *Biomedical Signal Processing and Control*, *69*, 102840.

116. Mouraux, A., Diukova, A., Lee, M. C., Wise, R. G., & Iannetti, G. D. (2011). A multisensory investigation of the functional significance of the “pain matrix”. *NeuroImage*, *54*(3), 2237–2249. https://doi.org/10.1016/j.neuroimage.2010.09.084

117. Mussigmann, T., Bardel, B., & Lefaucheur, J.-P. (2022). Resting-state electroencephalography (EEG) biomarkers of chronic neuropathic

pain. A systematic review. *NeuroImage*, *258*, 119351. https://doi.org/10.1016/j.neuroimage.2022.119351

118. Newman, M. E. (2004). Fast algorithm for detecting community structure in networks. *Physical Review E—Statistical, Nonlinear, and Soft Matter Physics*, *69*(6), 066133.

119. Newman, M. E. (2006). Modularity and community structure in networks. *Proceedings of the National Academy of Sciences*, *103*(23), 8577–8582.

120. Nguyen, T., Potter, T., Nguyen, T., Karmonik, C., Grossman, R., & Zhang, Y. (2016). EEG Source Imaging Guided by Spatiotemporal Specific fMRI: Toward an Understanding of Dynamic Cognitive Processes. *Neural Plasticity*, *2016*, 4182483. https://doi.org/10.1155/2016/4182483

121. Nickel, M. M., May, E. S., Tiemann, L., Schmidt, P., Postorino, M., Ta Dinh, S., Gross, J., & Ploner, M. (2017). Brain oscillations differentially encode noxious stimulus intensity and pain intensity. *NeuroImage*, *148*, 141–147. https://doi.org/10.1016/j.neuroimage.2017.01.011

122. Nickel, M. M., Ta Dinh, S., May, E. S., Tiemann, L., Hohn, V. D., Gross, J., & Ploner, M. (2020). Neural oscillations and connectivity characterizing the state of tonic experimental pain in humans. *Human Brain Mapping*, *41*(1), 17–29. https://doi.org/10.1002/hbm.24784

123. Nir, R.-R., Sinai, A., Moont, R., Harari, E., & Yarnitsky, D. (2012). Tonic pain and continuous EEG: Prediction of subjective pain perception by alpha-1 power during stimulation and at rest. *Clinical Neurophysiology*, *123*(3), 605–612. https://doi.org/10.1016/j.clinph.2011.08.006

124. O'Neill, G. C., Tewarie, P., Vidaurre, D., Liuzzi, L., Woolrich, M. W., & Brookes, M. J. (2018). Dynamics of large-scale electrophysiological networks: A technical review. *NeuroImage*, *180*, 559–576. https://doi.org/10.1016/j.neuroimage.2017.10.003

125. Onnela, J.-P., Saramäki, J., Kertész, J., & Kaski, K. (2005). Intensity and coherence of motifs in weighted complex networks. *Physical Review E*, *71*(6), 065103. https://doi.org/10.1103/PhysRevE.71.065103

126. Oostenveld, R., Fries, P., Maris, E., & Schoffelen, J.-M. (2011). FieldTrip: Open source software for advanced analysis of MEG, EEG, and invasive electrophysiological data. *Computational Intelligence and Neuroscience*, *2011*(1), 156869.

127. Ortiz, E., Stingl, K., Münßinger, J., Braun, C., Preissl, H., & Belardinelli, P. (2012). Weighted phase lag index and graph analysis: Preliminary investigation of functional connectivity during resting state in children. *Computational and Mathematical Methods in Medicine*, *2012*(1), 186353.

128. Palva, S., & Palva, J. M. (2007). New vistas for α-frequency band oscillations. *Trends in Neurosciences*, *30*(4), 150–158. https://doi.org/10.1016/j.tins.2007.02.001

129. Peng, W., Babiloni, C., Mao, Y., & Hu, Y. (2015). Subjective pain perception mediated by alpha rhythms. *Biological Psychology*, *109*, 141–150.

130. Peng, W., Hu, L., Zhang, Z., & Hu, Y. (2014). Changes of spontaneous oscillatory activity to tonic heat pain. *PloS One*, *9*(3), e91052.

131. Peng, W., Zhan, Y., Jin, R., Lou, W., & Li, X. (2023). Aftereffects of alpha transcranial alternating current stimulation over the primary sensorimotor cortex on cortical processing of pain. *PAIN*, *164*(6), 1280. https://doi.org/10.1097/j.pain.0000000000002814

132. Pesaran, B., Vinck, M., Einevoll, G. T., Sirota, A., Fries, P., Siegel, M., Truccolo, W., Schroeder, C. E., & Srinivasan, R. (2018). Investigating large-scale brain dynamics using field potential recordings: Analysis and interpretation. *Nature Neuroscience*, *21*(7), 903–919. https://doi.org/10.1038/s41593-018-0171-8

133. Peylo, C., Hilla, Y., & Sauseng, P. (2021). Cause or consequence? Alpha oscillations in visuospatial attention. *Trends in Neurosciences*, *44*(9), 705–713. https://doi.org/10.1016/j.tins.2021.05.004

134. Pfannmoller, J., & Lotze, M. (2019). Review on biomarkers in the resting-state networks of chronic pain patients. *Brain Cogn*, *131*, 4–9. https://doi.org/10.1016/j.bandc.2018.06.005

135. Pfannmöller, J., Strauss, S., Langner, I., Usichenko, T., & Lotze, M. (2019). Investigations on maladaptive plasticity in the sensorimotor cortex of unilateral upper limb CRPS I patients. *Restorative Neurology and Neuroscience*, *37*(2), 143–153.

136. Phillips, C. J. (2009). The Cost and Burden of Chronic Pain. *Reviews in Pain*, *3*(1), 2–5. https://doi.org/10.1177/204946370900300102

137. Pinheiro, E. S. D. S., Queirós, F. C. D., Montoya, P., Santos, C. L., Nascimento, M. A. D., Ito, C. H., Silva, M., Nunes Santos, D. B., Benevides, S., Miranda, J. G. V., Sá, K. N., & Baptista, A. F. (2016). Electroencephalographic Patterns in Chronic Pain: A Systematic Review of the

Literature. *PLOS ONE*, *11*(2), e0149085. https://doi.org/10.1371/journal.pone.0149085

138. Ploner, M., & May, E. S. (2018). Electroencephalography and magnetoencephalography in pain research—Current state and future perspectives. *Pain*, *159*(2), 206–211. https://doi.org/10.1097/j.pain.0000000000001087

139. Ploner, M., Sorg, C., & Gross, J. (2017). Brain Rhythms of Pain. *Trends in Cognitive Sciences*, *21*(2), 100–110. https://doi.org/10.1016/j.tics.2016.12.001

140. Ploner, M., & Tiemann, L. (2021). Exploring Dynamic Connectivity Biomarkers of Neuropsychiatric Disorders. *Trends in Cognitive Sciences*, *25*(5), 336–338. https://doi.org/10.1016/j.tics.2021.03.005

141. Polanía, R., Nitsche, M. A., & Ruff, C. C. (2018). Studying and modifying brain function with non-invasive brain stimulation. *Nature Neuroscience*, *21*(2), 174–187. https://doi.org/10.1038/s41593-017-0054-4

142. Prichep, L. S., Shah, J., Merkin, H., & Hiesiger, E. M. (2018). Exploration of the Pathophysiology of Chronic Pain Using Quantitative EEG Source Localization. *Clinical EEG and Neuroscience*, *49*(2), 103–113. https://doi.org/10.1177/1550059417736444

143. Qi, R., Ke, J., Schoepf, U. J., Varga-Szemes, A., Milliken, C. M., Liu, C., Xu, Q., Wang, F., Zhang, L. J., & Lu, G. M. (2016). Topological Reorganization of the Default Mode Network in Irritable Bowel Syndrome. *Molecular Neurobiology*, *53*(10), 6585–6593. https://doi.org/10.1007/s12035-015-9558-7

144. Raja, S. N., Carr, D. B., Cohen, M., Finnerup, N. B., Flor, H., Gibson, S., Keefe, F. J., Mogil, J. S., Ringkamp, M., Sluka, K. A., Song, X.-J., Stevens, B., Sullivan, M. D., Tutelman, P. R., Ushida, T., & Vader, K. (2020). The revised International Association for the Study of Pain definition of pain: Concepts, challenges, and compromises. *Pain*, *161*(9), 1976–1982. https://doi.org/10.1097/j.pain.0000000000001939

145. Rektorová, I., Pupíková, M., Fleury, L., Brabenec, L., & Hummel, F. C. (2025). Non-invasive brain stimulation: Current and future applications in neurology. *Nature Reviews Neurology*, 1–18. https://doi.org/10.1038/s41582-025-01137-z

146. Romei, V., Brodbeck, V., Michel, C., Amedi, A., Pascual-Leone, A., & Thut, G. (2008). Spontaneous Fluctuations in Posterior α-Band EEG Activity Reflect Variability in Excitability of Human Visual Areas. *Cerebral Cortex*, *18*(9), 2010–2018. https://doi.org/10.1093/cercor/bhm229

147. Rubinov, M., Kötter, R., Hagmann, P., & Sporns, O. (2009). Brain connectivity toolbox: A collection of complex network measurements and brain connectivity datasets. *NeuroImage*, *47*, S169.

148. Rubinov, M., & Sporns, O. (2010). Complex network measures of brain connectivity: Uses and interpretations. *NeuroImage*, *52*(3), 1059–1069. https://doi.org/10.1016/j.neuroimage.2009.10.003

149. Saalmann, Y. B., Pinsk, M. A., Wang, L., Li, X., & Kastner, S. (2012). Pulvinar regulates information transmission between cortical areas based on attention demands. *Science (New York, N.Y.)*, *337*(6095), 753–756. https://doi.org/10.1126/science.1223082

150. Sadaghiani, S., & Kleinschmidt, A. (2016). Brain Networks and α-Oscillations: Structural and Functional Foundations of Cognitive Control. *Trends in Cognitive Sciences*, *20*(11), 805–817. https://doi.org/10.1016/j.tics.2016.09.004

151. Salomons, T. V., Iannetti, G. D., Liang, M., & Wood, J. N. (2016). The “Pain Matrix” in Pain-Free Individuals. *JAMA Neurology*, *73*(6), 755–756. https://doi.org/10.1001/jamaneurol.2016.0653

152. Santarnecchi, E., Galli, G., Polizzotto, N. R., Rossi, A., & Rossi, S. (2014). Efficiency of weak brain connections support general cognitive functioning. *Human Brain Mapping*, *35*(9), 4566–4582. https://doi.org/10.1002/hbm.22495

153. Sarnthein, J., Stern, J., Aufenberg, C., Rousson, V., & Jeanmonod, D. (2006). Increased EEG power and slowed dominant frequency in patients with neurogenic pain. *Brain*, *129*(1), 55–64. https://doi.org/10.1093/brain/awh631

154. Schaefer, A., Kong, R., Gordon, E. M., Laumann, T. O., Zuo, X.-N., Holmes, A. J., Eickhoff, S. B., & Yeo, B. T. (2018). Local-global parcellation of the human cerebral cortex from intrinsic functional connectivity MRI. *Cerebral Cortex*, *28*(9), 3095–3114.

155. Schneider, M., Broggini, A. C., Dann, B., Tzanou, A., Uran, C., Sheshadri, S., Scherberger, H., & Vinck, M. (2021). A mechanism for inter-areal coherence through communication based on connectivity and oscillatory power. *Neuron*, *109*(24), 4050-4067.e12. https://doi.org/10.1016/j.neuron.2021.09.037

156. Schoffelen, J., & Gross, J. (2009). Source connectivity analysis with MEG and EEG. *Human Brain Mapping*, *30*(6), 1857–1865. https://doi.org/10.1002/hbm.20745

157. Seminowicz, D. A., Bilska, K., Chowdhury, N. S., Skippen, P., Millard, S. K., Chiang, A. K. I., Chen, S., Furman, A. J., & Schabrun, S. M. (2020). A novel cortical biomarker signature for predicting pain sensitivity: Protocol for the PREDICT longitudinal analytical validation study. *PAIN Reports*, *5*(4), e833. https://doi.org/10.1097/PR9.0000000000000833

158. Seminowicz, D. A., & Davis, K. D. (2007). Interactions of pain intensity and cognitive load: The brain stays on task. *Cerebral Cortex (New York, N.Y.: 1991)*, *17*(6), 1412–1422. https://doi.org/10.1093/cercor/bhl052

159. Seminowicz, D. A., & Moayedi, M. (2017). The Dorsolateral Prefrontal Cortex in Acute and Chronic Pain. *The Journal of Pain*, *18*(9), 1027–1035. https://doi.org/10.1016/j.jpain.2017.03.008

160. Sitaram, R., Ros, T., Stoeckel, L., Haller, S., Scharnowski, F., Lewis-Peacock, J., Weiskopf, N., Blefari, M. L., Rana, M., Oblak, E., Birbaumer, N., & Sulzer, J. (2017). Closed-loop brain training: The science of neurofeedback. *Nature Reviews Neuroscience*, *18*(2), 86–100. https://doi.org/10.1038/nrn.2016.164

161. Spielberger, C. D., Gonzalez-Reigosa, F., Martinez-Urrutia, A., Natalicio, L. F. S., & Natalicio, D. S. (2017). The State-Trait Anxiety Inventory. *Revista Interamericana de Psicología/Interamerican Journal of Psychology*, *5*(3 & 4). https://doi.org/10.30849/rip/ijp.v5i3

162. Spisak, T., Kincses, B., Schlitt, F., Zunhammer, M., Schmidt-Wilcke, T., Kincses, Z. T., & Bingel, U. (2020). Pain-free resting-state functional brain connectivity predicts individual pain sensitivity. *Nature Communications*, *11*(1). https://doi.org/10.1038/s41467-019-13785-z

163. Sporns, O. (2013). Network attributes for segregation and integration in the human brain. *Current Opinion in Neurobiology*, *23*(2), 162–171. https://doi.org/10.1016/j.conb.2012.11.015

164. Sporns, O., & Honey, C. J. (2006). Small worlds inside big brains. *Proceedings of the National Academy of Sciences*, *103*(51), 19219–19220.

165. Suffczynski, P., Kalitzin, S., Pfurtscheller, G., & Lopes Da Silva, F. H. (2001). Computational model of thalamo-cortical networks: Dynamical control of alpha rhythms in relation to focal attention. *International Journal of Psychophysiology*, *43*(1), 25–40. https://doi.org/10.1016/S0167-8760(01)00177-5

166. Sullivan, M. J. L., Bishop, S. R., & Pivik, J. (1995). The Pain Catastrophizing Scale: Development and validation. *Psychological Assessment*, *7*(4), 524–532. https://doi.org/10.1037/1040-3590.7.4.524

167. Ta Dinh, S., Nickel, M. M., Tiemann, L., May, E. S., Heitmann, H., Hohn, V. D., Edenharter, G., Utpadel-Fischler, D., Tölle, T. R., Sauseng, P., Gross, J., & Ploner, M. (2019). Brain dysfunction in chronic pain patients assessed by resting-state electroencephalography. *Pain*, *160*(12), 2751–2765. https://doi.org/10.1097/j.pain.0000000000001666

168. Torta, D. M., Legrain, V., Mouraux, A., & Valentini, E. (2017). Attention to pain! A neurocognitive perspective on attentional modulation

of pain in neuroimaging studies. *Cortex*, *89*, 120–134. https://doi.org/10.1016/j.cortex.2017.01.010

169. Tracey, I., Woolf, C. J., & Andrews, N. A. (2019). Composite Pain Biomarker Signatures for Objective Assessment and Effective Treatment. *Neuron*, *101*(5), 783–800. https://doi.org/10.1016/j.neuron.2019.02.019

170. Tsay, R. S. (2005). *Analysis of Financial Time Series*. John Wiley & Sons.

171. Tu, Y., Cao, J., Bi, Y., & Hu, L. (2021). Magnetic resonance imaging for chronic pain: Diagnosis, manipulation, and biomarkers. *Science China Life Sciences*, *64*(6), 879–896. https://doi.org/10.1007/s11427-020-1822-4

172. Tu, Y., Fu, Z., Mao, C., Falahpour, M., Gollub, R. L., Park, J., Wilson, G., Napadow, V., Gerber, J., Chan, S.-T., Edwards, R. R., Kaptchuk, T. J., Liu, T., Calhoun, V., Rosen, B., & Kong, J. (2020). Distinct thalamocortical network dynamics are associated with the pathophysiology of chronic low back pain. *Nature Communications*, *11*(1). https://doi.org/10.1038/s41467-020-17788-z

173. Tu, Y., Jung, M., Gollub, R. L., Napadow, V., Gerber, J., Ortiz, A., Lang, C., Mawla, I., Shen, W., Chan, S. T., Wasan, A. D., Edwards, R. R., Kaptchuk, T. J., Rosen, B., & Kong, J. (2019). Abnormal medial prefrontal cortex functional connectivity and its association with clinical symptoms in chronic low back pain. *Pain*, *160*(6), 1308–1318. https://doi.org/10.1097/j.pain.0000000000001507

174. Tu, Y., Li, Z., Zhang, L., Zhang, H., Bi, Y., Yue, L., & Hu, L. (2023). Pain-preferential thalamocortical neural dynamics across species. *Nature Human Behaviour*, *8*(1), 149–163. https://doi.org/10.1038/s41562-023-01714-6

175. Tu, Y., Tan, A., Bai, Y., Hung, Y. S., & Zhang, Z. (2016). Decoding Subjective Intensity of Nociceptive Pain from Pre-stimulus and Post-stimulus Brain Activities. *Frontiers in Computational Neuroscience*, *10*. https://doi.org/10.3389/fncom.2016.00032

176. Tu, Y., Wang, J., Li, Z., Xiong, F., & Gao, F. (2023). Topological alterations in white matter structural networks in fibromyalgia. *Neuroradiology*, *65*(12), 1737–1747. https://doi.org/10.1007/s00234-023-03225-7

177. Uddin, L. Q. (2015). Salience processing and insular cortical function and dysfunction. *Nature Reviews Neuroscience*, *16*(1), 55–61. https://doi.org/10.1038/nrn3857

178. Valentini, E., Halder, S., McInnerney, D., Cooke, J., Gyimes, I. L., & Romei, V. (2022). Assessing the specificity of the relationship between brain alpha oscillations and tonic pain. *NeuroImage*, *255*, 119143.

179. Valentini, E., Halder, S., & Romei, V. (2024). The independence and predictivity of resting pain-free slow alpha frequency as a biomarker of pain: A reply to Mazaheri et al. *NeuroImage*, *296*, 120681. https://doi.org/10.1016/j.neuroimage.2024.120681

180. van den Broeke, E. N., Wilder-Smith, O. H. G., van Goor, H., Vissers, K. C. P., & van Rijn, C. M. (2013). Patients with Persistent Pain after Breast Cancer Treatment Show Enhanced Alpha Activity in

Spontaneous EEG. *Pain Medicine*, *14*(12), 1893–1899. https://doi.org/10.1111/pme.12216

181. Van Der Miesen, M. M., Lindquist, M. A., & Wager, T. D. (2019). Neuroimaging-based biomarkers for pain: State of the field and current directions. *PAIN Reports*, *4*(4), e751. https://doi.org/10.1097/pr9.0000000000000751

182. Van Ettinger-Veenstra, H., Lundberg, P., Alföldi, P., Södermark, M., Graven-Nielsen, T., Sjörs, A., Engström, M., & Gerdle, B. (2019). Chronic widespread pain patients show disrupted cortical connectivity in default mode and salience networks, modulated by pain sensitivity. *Journal of Pain Research*, *Volume 12*, 1743–1755. https://doi.org/10.2147/JPR.S189443

183. Vanneste, S., & De Ridder, D. (2021). Chronic pain as a brain imbalance between pain input and pain suppression. *Brain Communications*, *3*(1), fcab014. https://doi.org/10.1093/braincomms/fcab014

184. Vatansever, D., Menon, D. K., Manktelow, A. E., Sahakian, B. J., & Stamatakis, E. A. (2015). Default Mode Dynamics for Global Functional Integration. *Journal of Neuroscience*, *35*(46), 15254–15262. https://doi.org/10.1523/JNEUROSCI.2135-15.2015

185. Vigotsky, A. D., Iannetti, G. D., & Apkarian, A. V. (2024). Mental state decoders: Game-changers or wishful thinking? *Trends in Cognitive Sciences*, *28*(10), 884–895. https://doi.org/10.1016/j.tics.2024.06.004

186. Vinck, M., Oostenveld, R., Van Wingerden, M., Battaglia, F., & Pennartz, C. M. (2011). An improved index of phase-synchronization for

electrophysiological data in the presence of volume-conduction, noise and sample-size bias. *NeuroImage*, *55*(4), 1548–1565.

187. Vittersø, A. D., Halicka, M., Buckingham, G., Proulx, M. J., & Bultitude, J. H. (2022). The sensorimotor theory of pathological pain revisited. *Neuroscience & Biobehavioral Reviews*, *139*, 104735.

188. Vries, M. de, Wilder-Smith, O. H., Jongsma, M. L., Broeke, E. N. van den, Arns, M., Goor, H. van, & Rijn, C. M. van. (2013). Altered resting state EEG in chronic pancreatitis patients: Toward a marker for chronic pain. *Journal of Pain Research*. (world). https://www.tandfonline.com/doi/abs/10.2147/JPR.S50919

189. Wang, H., Guo, Y., Tu, Y., Peng, W., Lu, X., Bi, Y., Iannetti, G. D., & Hu, L. (2023). Neural processes responsible for the translation of sustained nociceptive inputs into subjective pain experience. *Cerebral Cortex*, *33*(3), 634–650. https://doi.org/10.1093/cercor/bhac090

190. Wang, K., Chen, Y., Huang, S., Liu, H., & Wu, W. (2021). Attention Bias to Pain Words Comes Early and Cognitive Load Matters: Evidence from an ERP Study on Experimental Pain. *Neural Plasticity*, *2021*, 9940889. https://doi.org/10.1155/2021/9940889

191. Warbrick, T. (2022). Simultaneous EEG-fMRI: What Have We Learned and What Does the Future Hold? *Sensors*, *22*(6), 2262. https://doi.org/10.3390/s22062262

192. Watts, D. J., & Strogatz, S. H. (1998). Collective dynamics of 'small-world'networks. *Nature*, *393*(6684), 440–442.

193. Weng, Y., Liu, X., Hu, H., Huang, H., Zheng, S., Chen, Q., Song, J., Cao, B., Wang, J., Wang, S., & Huang, R. (2020). Open eyes and

closed eyes elicit different temporal properties of brain functional networks. *NeuroImage*, *222*, 117230. https://doi.org/10.1016/j.neuroimage.2020.117230

194. Wianda, E., & Ross, B. (2019). The roles of alpha oscillation in working memory retention. *Brain and Behavior*, *9*(4), e01263. https://doi.org/10.1002/brb3.1263

195. Wiech, K., & Tracey, I. (2009). The influence of negative emotions on pain: Behavioral effects and neural mechanisms. *NeuroImage*, *47*(3), 987–994. https://doi.org/10.1016/j.neuroimage.2009.05.059

196. Woo, C.-W., & Wager, T. D. (2015). Neuroimaging-based biomarker discovery and validation. *Pain*, *156*(8), 1379–1381. https://doi.org/10.1097/j.pain.0000000000000223

197. Xia, M., Wang, J., & He, Y. (2013). BrainNet Viewer: A network visualization tool for human brain connectomics. *PloS One*, *8*(7), e68910.

198. Xin, H., Yang, B., Jia, Y., Qi, Q., Wang, Y., Wang, L., Chen, X., Li, F., Lu, J., & Chen, N. (2024). Graph Metrics Reveal Brain Network Topological Property in Neuropathic Pain Patients: A Systematic Review. *Journal of Pain Research*, *Volume 17*, 3277–3286. https://doi.org/10.2147/JPR.S483466

199. Zalesky, A., Cocchi, L., Fornito, A., Murray, M. M., & Bullmore, E. D. (2012). Connectivity differences in brain networks. *NeuroImage*, *60*(2), 1055–1062.

200. Zalesky, A., Fornito, A., & Bullmore, E. T. (2010). Network-based statistic: Identifying differences in brain networks. *NeuroImage*, *53*(4), 1197–1207.

201. Zebhauser, P. T., Heitmann, H., May, E. S., & Ploner, M. (2024). Resting-state electroencephalography and magnetoencephalography in migraine–a systematic review and meta-analysis. *The Journal of Headache and Pain*, *25*(1). https://doi.org/10.1186/s10194-024-01857-5

202. Zebhauser, P. T., Hohn, V. D., & Ploner, M. (2023). Resting-state electroencephalography and magnetoencephalography as biomarkers of chronic pain: A systematic review. *Pain*, *164*(6), 1200–1221. https://doi.org/10.1097/j.pain.0000000000002825

203. Zhang, K. L., Yuan, H., Wu, F. F., Pu, X. Y., Liu, B. Z., Li, Z., Li, K. F., Liu, H., Yang, Y., & Wang, Y. Y. (2021). Analgesic Effect of Non-invasive Brain Stimulation for Neuropathic Pain Patients: A Systematic Review. *Pain and Therapy*, *10*(1), 315–332. https://doi.org/10.1007/s40122-021-00252-1

204. Zhang, L. B., Chen, Y. X., Li, Z. J., Geng, X. Y., Zhao, X. Y., Zhang, F. R., Bi, Y. Z., Lu, X. J., & Hu, L. (2024). Advances and challenges in neuroimaging-based pain biomarkers. *Cell Reports Medicine*, *5*(10), 101784. https://doi.org/10.1016/j.xcrm.2024.101784

205. Zhang, P., Jiang, Y., Liu, G., Han, J., Wang, J., Ma, L., Hu, W., & Zhang, J. (2021). Altered brain functional network dynamics in classic trigeminal neuralgia: A resting-state functional magnetic resonance imaging study. *The Journal of Headache and Pain*, *22*(1), 147. https://doi.org/10.1186/s10194-021-01354-z

206. Zhang, P., Wan, X., Ai, K., Zheng, W., Liu, G., Wang, J., Huang, W., Fan, F., Yao, Z., & Zhang, J. (2022). Rich-club reorganization and related network disruptions are associated with the symptoms and severity in classic trigeminal neuralgia patients. *NeuroImage: Clinical*, *36*, 103160. https://doi.org/10.1016/j.nicl.2022.103160

207. Zheng, W., Woo, C.-W., Yao, Z., Goldstein, P., Atlas, L. Y., Roy, M., Schmidt, L., Krishnan, A., Jepma, M., Hu, B., & Wager, T. D. (2020). Pain-Evoked Reorganization in Functional Brain Networks. *Cerebral Cortex*, *30*(5), 2804–2822. https://doi.org/10.1093/cercor/bhz276

208. Zhu, K., Chang, J., Zhang, S., Li, Y., Zuo, J., Ni, H., Xie, B., Yao, J., Xu, Z., Bian, S., Yan, T., Wu, X., Chen, S., Jin, W., Wang, Y., Xu, P., Song, P., Wu, Y., Shen, C., … Dong, F. (2024). The enhanced connectivity between the frontoparietal, somatomotor network and thalamus as the most significant network changes of chronic low back pain. *NeuroImage*, *290*, 120558. https://doi.org/10.1016/j.neuroimage.2024.120558